NASA/TP– 20240007991

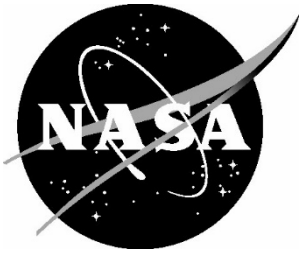

Characterization of NUW-LHT-5M, A Lunar Highland Simulant

Douglas L. Rickman
Jacobs ESSCA/NASA Marshall Space Flight Center, Huntsville, AL

P. Douglas Archer, Jr. and Rostislav N. Kovtun
Jacobs JETSII/Johnson Space Center, Houston, Texas

Martin Barmatz
Jet Propulsion Laboratory, California Institute of Technology, California

Matt Creedon
Washington Mills, Niagara Falls, New York

Brandon Dotson, Kerri Donaldson Hanna, Jared M. Long-Fox, and Catherine Millwater
University of Central Florida, Orlando, Florida

Michael R. Effinger
Marshall Space Flight Center, Huntsville, Alabama

Ronald M. Hutcheon
Microwave Properties North, Deep River Ontario, Canada

Yong-Rak Kim
Texas A&M University, College Station, Texas

Austin Patridge and Alan Whittington
University of Texas at San Antonio, Texas

July 2024

NASA STI Program Report Series

Holly Shulman
Blue Star Advanced Manufacturing, LLC, Belmont New York

Ryan P. Wilkerson
Los Alamos National Laboratory, Los Alamos, New Mexico

NASA STI Program Report Series

Since its founding, NASA has been dedicated to the advancement of aeronautics and space science. The NASA scientific and technical information (STI) program plays a key part in helping NASA maintain this important role.

The NASA STI program operates under the auspices of the Agency Chief Information Officer. It collects, organizes, provides for archiving, and disseminates NASA's STI. The NASA STI program provides access to the NTRS Registered and its public interface, the NASA Technical Reports Server, thus providing one of the largest collections of aeronautical and space science STI in the world. Results are published in both non-NASA channels and by NASA in the NASA STI Report Series, which includes the following report types:

- TECHNICAL PUBLICATION. Reports of completed research or a major significant phase of research that present the results of NASA Programs and include extensive data or theoretical analysis. Includes compilations of significant scientific and technical data and information deemed to be of continuing reference value. NASA counterpart of peer-reviewed formal professional papers but has less stringent limitations on manuscript length and extent of graphic presentations.

- TECHNICAL MEMORANDUM. Scientific and technical findings that are preliminary or of specialized interest, e.g., quick release reports, working papers, and bibliographies that contain minimal annotation. Does not contain extensive analysis.

- CONTRACTOR REPORT. Scientific and technical findings by NASA-sponsored contractors and grantees.

- CONFERENCE PUBLICATION. Collected papers from scientific and technical conferences, symposia, seminars, or other meetings sponsored or co-sponsored by NASA.

- SPECIAL PUBLICATION. Scientific, technical, or historical information from NASA programs, projects, and missions, often concerned with subjects having substantial public interest.

- TECHNICAL TRANSLATION. English-language translations of foreign scientific and technical material pertinent to NASA's mission.

Specialized services also include organizing and publishing research results, distributing specialized research announcements and feeds, providing information desk and personal search support, and enabling data exchange services.

For more information about the NASA STI program, see the following:

- Access the NASA STI program home page at http://www.sti.nasa.gov

.

NASA/TP– 20240007991

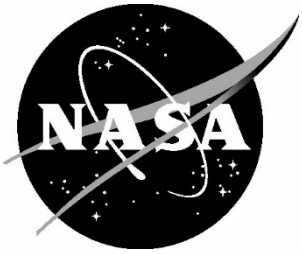

Characterization of NUW-LHT-5M, A Lunar Highland Simulant

Douglas L. Rickman
Jacobs ESSCA/NASA Marshall Space Flight Center, Huntsville, AL

P. Douglas Archer, Jr. and Rostislav N. Kovtun
Jacobs JETSII/Johnson Space Center, Houston, Texas

Martin Barmatz
Jet Propulsion Laboratory, California Institute of Technology, California

Matt Creedon
Washington Mills, Niagara Falls, New York

Brandon Dotson, Kerri Donaldson Hanna, Jared M. Long-Fox, and Catherine Millwater
University of Central Florida, Orlando, Florida

Michael R. Effinger
Marshall Space Flight Center, Huntsville, Alabama

Ronald M. Hutcheon
Microwave Properties North, Deep River Ontario, Canada

National Aeronautics and
Space Administration

Marshall Spce Flight Center
Huntsville, Alabama

July 2024

Yong-Rak Kim
Texas A&M University, College Station, Texas

Austin Patridge and Alan Whittington
University of Texas at San Antonio, Texas

Holly Shulman
Blue Star Advanced Manufacturing, LLC, Belmont New York

Ryan P. Wilkerson
Los Alamos National Laboratory, Los Alamos, New Mexico

National Aeronautics and
Space Administration

Marshall Spce Flight Center
Huntsville, Alabama

July 2024

Available from:

NASA STI Program / Mail Stop 050
NASA Langley Research Center
Hampton, VA 23681-2199

Characterization of NUW-LHT-5M, A Lunar Highland Simulant

Douglas L. Rickman[1]*, P. Douglas Archer, Jr.[2], Martin Barmatz[3], Matt Creedon[4], Kerri Donaldson Hanna[5], Brandon Dotson[6], Michael R. Effinger[7], Jared M. Long-Fox[8], Ron Hutcheon[9], Yong-Rak Kim[10], Rostislav Kovtun[11], Catherine Millwater[12], Austin Patridge[13], Holly Shulman[14], Alan Whittington[15], Ryan P. Wilkerson[16]

1 Jacobs ESSCA, Marshall Space Flight Center, Huntsville AL, 35812
2,Jacobs JETSII, NASA Johnson Space Center, Houston, TX 77058
3 Jet Propulsion Laboratory, California Institute of Technology, CA 91109
4 Washington Mills, Niagara Falls, NY 14302
5,6,8,12 University of Central Florida, Orlando, FL 32816
7 NASA Marshall Space Flight Center, Huntsville AL, 35812
9 Microwave Properties North, #325 Wylie Road, Deep River Ontario K0J1P0, Canada
10 Texas A&M University, College Station, TX 77843
13,15 The University of Texas at San Antonio, TX 78249
14 Blue Star Advanced Manufacturing, LLC, Belmont NY, 14813
16 Los Alamos National Laboratory, Los Alamos NM, 87545

1 douglas.l.rickman@nasa.gov
4 mcreedon@washingtonmills.com
5 Kerri.DonaldsonHanna@ucf.edu
8 jared.long-fox@ucf.edu
10 yong-rak.kim@tamu.edu
11 rostislav.n.kovtun@nasa.gov
14 drhollyshulman@gmail.com
15 alan.whittington@utsa.edu

* *Corresponding author.*
douglas.l.rickman ORCID: 0000-0003-3409-2882

Abstract

A new simulant of the lunar highlands regolith, NUW-LHT-5M, was designed by NASA and manufactured by Washington Mills. The simulant was based on Apollo 16 data and is a member of the NU-LHT-series. NASA's Marshall Space Flight Center and Johnson Space Center have already purchased 3 metric tons of the simulant for advanced engineering work. In support of engineering uses of the simulant, we provided measurements of the simulant including: mineral abundance and composition, liberation, X-ray fluorescence (XRF), ferrous iron, carbon, sulfur, 60 element inductively coupled plasma (ICP), loss on ignition, particle size, both 2D and 3D particle shape, specific surface area, shear, cohesion, internal friction, helium pycnometry, minimum index density, tap density, magnetic susceptibility, cryogenic and high temperature permittivity, visible and near-infrared (VNIR) and middle infra-red spectroscopy (MIR), differential scanning calorimetry (DSC), viscosity, thermal diffusivity, thermal conductivity, thermal gravimetric analysis (TGA), evolved gas analysis (EGA), and spark sintering. For the crystalline components the design of the simulant called for two rocks from the Stillwater Complex, Montana: 17.6 wt% norite, 37.7% anorthosite, and 4.7 wt% olivine from an unspecified commercial source. The other 40% of the simulant was a high calcium (An100), vesicular glass that Washington Mills made specifically for the simulant. Fabrication and quality control processes for both the glass and the simulant are described. Importantly, most of the graphs and tables presented herein provide values for both the new simulant and data for the older NASA mare simulant, JSC-1A. Finally, we discussed the current limitations of NUW-LT-5M and most other lunar regolith simulants to replicate the lunar material.

Table of Contents

1. Introduction

Prior to 2006, lunar simulants were, in almost all cases, patterned after regolith samples returned from the lunar mare by Apollo 11, 12, 14, 15 and 17. Because of the mare target, simulants could be reasonably made from single terrestrial sources, resulting in many simulants from multiple nations. Prominent examples at the time included FJS-1 (Takeda et al., 2006, Kanamori et al., 2006), the JSC-1 and materials patterned after it (McKay et al., 1994, Carter, 2005, Hill et al., 2007), and MLS-1A (Weiblen and Gordon, 1988, Weiblen et al., 1990). These sources were uniformly basaltic and frequently contained volcanic ash. Production of analogous simulants was done in several nations, such as Germany, China, and Korea (Engelschiøn et al., 2020, Zheng, et al., 2008, Byung-Hyun, 2015).

In 2006, the National Aeronautics and Space Administration (NASA) collaborated with the United States Geological Survey (USGS) to develop the technology needed to make a simulant of the lunar highland regolith. This effort was a collaboration among Stephen Wilson, and Douglas B. Stoeser, both USGS Central Region Mineral Resources scientists, and Douglas L. Rickman of NASA. Features that were deemed important in the final simulant included: (1) glass of a composition essentially the same as the bulk crystalline composition, (2) as high a Ca/(Ca+Na) ratio in the plagioclase as practical, (3) minimal primary non-lunar mineralogy, such as quartz, and secondary minerals generated by weathering, metamorphism, and hydrothermal processes. The latter can contain problematic amounts of H_2O or OH^-, carbonates, sulfates, zeolites, and clays. There were also practical requirements, specifically: (1) legal access, (2) shipping costs, (3) availability of total mass, (4) road access, (5) availability of heavy equipment, and (6) logistical support. The intent of the effort was to show where to obtain the crystalline feedstocks, manufacture the glass, mill, mix, characterize, distribute, and document in detail how a highland simulant in useful quantities could feasibly be made. It was immediately apparent that a highland simulant would be more challenging to make than a mare simulant, as there was no recognized single rock on Earth with appropriate mineralogical characteristics that also contained glass.

The result of this multiyear effort was the development of a series of highland simulants designated the NU-LHT-series (NASA USGS—Lunar Highland Type), publications documenting their design, manufacture (Stoeser and Wilson, 2007, Wilson and Stoeser, 2009, Stoeser et al., 2010, Rickman et al., 2011, Rickman et al., 2013), and methodology for comparative analysis of simulants versus lunar materials (Schrader et al, 2009). Lacking technology to simulate space weathering, these simulants were intended to emulate immature lunar samples. Most of the crystalline feedstocks in the simulants were taken from zones in the Stillwater Complex in Nye, MT, with the active and generous cooperation of the Stillwater Mining Company. Various other feeds, such as commercially purchased olivine, pyrite, ilmenite, fluor-apatite, and synthetic whitlockite (β-Tri-Calcium Phosphate) were used in at least one of the simulants in the series. Glass was made by Mike Weinstein at Zybek in Boulder, CO using electric arc fusion from the sandy waste produced in the mine's milling process. Also, a high-quality agglutinate and a breccia were made (Weinstein et al., 2012). None of the highest quality simulants in the series was produced beyond the point of demonstrating it could be done and to obtain production cost estimates, all less than 1000 kg.

The opportunity to draw upon lessons learned from the NU-LHT-series is timely now that NASA is strongly focused on a return to the Moon (NASA, 2020). For this, substantial amounts of simulant from the NU-LHT-series are needed. Out of the NU-LHT-series, NU-LHT-2M was used as the starting point to create a simpler version in the series, NUW-LHT-5M. Compared to -2M the new simulant was to have a glass even closer to the average Apollo 16 composition, more total glass, and not include added trace minerals (Rickman et al., 2022). Originally to be named NU-LHT-5M, the name has subsequently been changed to NUW-LHT-5M in recognition of the fabricator, including the glass: Washington Mills, Niagara Falls, NY.

An underlying philosophy guiding the work was, that to be useful, lunar simulants must be considered engineering materials. We therefore provide extensive characterization of NUW-LHT-5M, a highland simulant, and for comparison on JSC-1A, a widely used mare simulant, without attempting to discuss the numerous engineering applications of the data.

2. Significance to NASA

NASA's requirement to have sustaining operations and human presence on the Moon effectively requires in situ resource utilization (ISRU) for resources, construction, and outfitting of lunar infrastructure (Werkheiser et al., 2023). To accomplish this on the Moon, development of the manufacturing hardware and procedures technology must be done on Earth using lunar simulants, as there was not a sufficient volume of returned regolith from the Apollo missions. Technology development and experiments using lunar simulants will also reduce risk and increase the likelihood of successful missions on the Moon. There were multiple processes being pursued to accomplish NASA's engineering objectives; some of the processes involved melting or sintering. Therefore, having an accurate glass amount and composition, which affect melt temperatures, was important. This aspect was missing from historical and existing simulants in the U.S. To solve this, and the problem of obsolescence of previous simulants, it was decided to strategically partner with existing industry that had capabilities to make the glass and complete simulant alongside their existing products, using the same infrastructure. This was in contrast with either the government making it, or a business creating a new product line. The resulting new simulant is NUW-LHT-5M. The NU-LHT series was arguably the best historical highland simulants for multiple reasons, (e.g., appropriate glass, high (Ca/Ca+Na) ratio, attention to minimizing non-lunar minerals, inclusion of appropriate (Mg,Fe) silicates, and the presence of various trace minerals). By improving the glass composition and abundance to match the NU-LHT-2M basic simulant design, and removing the four trace minerals, NASA has a higher fidelity simulant that suits its application/lunar processing needs (ISECG, 2021). It can also be provided in large quantities, on a continuous or sporadic basis with consistent quality controls. For the reasons above, it was expected to become a standard for many ISRU application developments, especially those involving high-temperature processing. Currently, NASA has ordered 3.0 metric tons of the simulant. 1,452 kg will be used by the Moon to Mars Planetary Additive Construction Technology project at Marshall Space Flight Center (MSFC). Of that, 840 kg will be used in the giant V20 vacuum chamber; 60 kg will go for Alfred University and/or Blue Star Manufacturing for microwave testing; 560 kg has gone to the company ICON for testing with laser-based construction. 489 kg went to Johnson Space Center (JSC). 1,059 kg is being used in the new, large, thermal and radiation vacuum chamber named Planetary, Lunar, and Asteroid Natural Environments Testbed (PLANET) (Hayward et al., 2023).

3. Manufacturing

The simulant is manufactured by Washington Mills Electro Minerals, Niagara Falls, NY (WM) (Creedon et al., 2023) (use of company names shall not be construed as endorsements; they are provided for the purpose of completeness of information). See also the Appendix A. The primary crystalline feedstocks, donated by Stillwater mine, were from company property; these were handpicked rocks from surface exposures of anorthite and norite in the Stillwater Complex, near Nye, MT. The respective coordinates were 45.39665, -109.88634 and 45.39006, -109.89307. On the map of Geraghty 2013, the units are labeled Anorthosite, (AZIII), and Norite Zone I, (NZI). The norite and anorthosite were provided by NASA/MSFC from stockpiles used to make other members of the NU-LHT-series. In addition, a commercially available olivine from Turkey was used as part of the feedstock. The glass was batch-fabricated in-house by WM, using commercial oxides fused in a graphite-lined crucible, and then water-quenched. The glass product was a mixture of solid glass and low-density, friable, vesicular granules exhibiting minor variation due to imperfect mixing of the raw oxides, Figure 3.1. There were also very small amounts of metallic iron as spheres and highly irregular fragments emulating lunar meteoritic iron.

During development of the manufacturing process, Washington Mills produced and delivered two test batches of the simulant, termed as "Test 1" and "Test 2". The former was a 2-kg run and the second was a 20-kg run. Primary production was nearly complete on the first major run at the time of this writing. While there was no change of design between tests, the possibility that changes of unknown nature due to manufacturing processes might exist that cannot be eliminated. Unless otherwise noted, all the samples used for the work reported here were from Test 2. While the authors explicitly recognized that every production run is expected to have differences at some level, the authors feel that these were currently substantially less than the differences with other simulants.

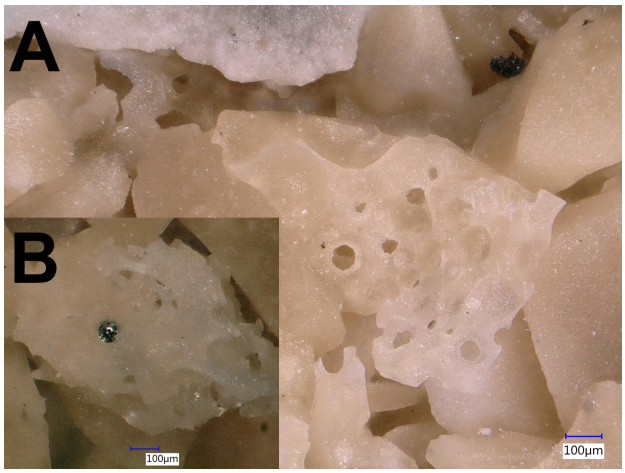

Figure 3.1. A. - Detail of NUW-LHT-5M glass after heating in vacuum to 1300°C, which emphasizes some features. Compositional variation shows as color variation; compare upper left with center. Multiple vesicles are visible in the particle at center and elsewhere. A black cluster of ~20 µm spheres of metallic iron is in the upper right. B.- Inset. Glass foam with Fe^0 sphere. Photos by M. Petkov.

3.1 Process Monitoring

During production, WM monitored particle size distribution (PSD) and elemental abundance frequently to assure product consistency.

The PSD limits were guided by the Carrier, 2003, values required by the design. Given the particle size range, this required measurements using two different techniques. Sieving, according to American Society for Testing and Materials standard C136, was used for the coarser particles using a RoTap RX-29 sieve shaker. Finer particles were measured using a Microtrac S3500 Particle Size Analyzer system. Merging of the two datasets was done using a logic developed for the purpose by WM. As the various feedstocks have different milling characteristics, they were separately

crushed in a roll mill and then individually ball-milled before being blended in a V-Blender. PSD data were taken at several phases of the process, sufficient to confirm product quality. As expected, the data showed there are acceptable variation between production runs; therefore, for uses that will be highly sensitive to PSD, thorough sampling and analysis on the material as received is suggested.

While the simulant was designed predominately based on mineralogy, the elemental analysis provided a quick and relatively easy way to monitor production. This has been especially important because of the application of batch-processing through the graphite electric-arc furnace was novel, and some details of the production have been challenging. For many users the most obvious place this can be seen was in the Fe content of the final simulant. Because of the reducing environment in the furnace, Test 1 and Test 2 generated more metallic iron than desired, much of which dropped out of the simulant during further processing, leaving the simulant deficient in total Fe. Data given in Table 4.4, XRF, showed the Fe deficiency has now been largely corrected.

4. Composition of the Simulant

4.1 Mineralogy

The mineralogy was extremely important in a lunar simulant. The mineralogy is extremely important, as it dictates many engineering properties and subsequent processes used for resource utilization. To obtain the statistically valid, necessary mineralogy data, the simulant team at MSFC has previously used automated mineralogy analysis generated by QEMSCAN® systems (Schrader et al., 2008, Schrader, 2009). Here we report multiple mineralogical and chemical analyses done by Australian Laboratory Services Canada Ltd. (ALS), Kamloops, BC, on NUW-LHT-5M, Table 4.1, and major minerals versus grain size, which is distinct from particle size, Figure 4.1. For the full ALS report on the simulant, see Appendix B.

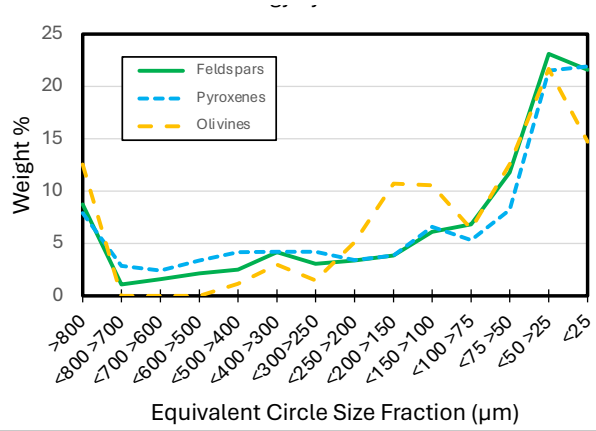

Figure 4.1. Mineralogy, excluding glass, versus grain size for NUW-LHT-5M. Grain size was computed from the measured area of a mineral in the plain of section, which was then converted to a circle of equivalent area. Note the changes in scaling along the X axis. Feldspars includes all plagioclases, K-feldspar, epidote and clinozoisite. Pyroxenes includes both pyroxenes and amphibole. Grain sizing maybe overestimated due to coarse particle effects.

Based on sieve data, ALS divided the 210-g aliquot of provided simulant into three subsamples, roughly equal by mass. The subsamples size boundaries, determined by sieve and mass, were >106 µm, >38 µm & <106 µm, and <38 µm. As is common in geochemical analyses related to mining, a total value for the simulant was also reported under the label "Head". Doing size-limited measurements demonstrated there are, as expected, various biases in the simulant as a function of particle size. The mineralogy data were acquired using a QEMSCAN (Pirrie and Rollinson, 2011, Ayling et al., 2012, Bell et al., 2020), from planar sections through unsorted particles

Table 4.1 Mineralogy by sieve bin. Glass is not included. Collectively, these minerals make up 60% of the simulant. Other minerals are known to be present, but were not abundant enough to be dependably identified with the technique used. Notes: (1) 'Elemental Iron\Iron Oxides' includes Steel and may include Magnetite, Hematite and Goethite/Limonite. (2) 'Plagioclase feldspars' includes Epidote(?) and Clinozoisite. (3) 'Pyroxenes' includes Clinopyroxenes and Orthopyroxenes. (4) 'Micas' includes Biotite/Phlogopite and Muscovite. (5) 'Carbonates' includes Calcite, Ankerite/Dolomite and Magnesite. (6) 'Others' includes Sphene (Titanite), Rutile/Anatase, Epidote(?), Serpentine, Sulfide Minerals, Apatite, Spinel and unresolved mineral species.

Mineral	Mineral Assays, wt%			
	>106µm	<106>38µm	<38µm	Total
Fe0/Fe oxides	0.07	0.09	0.29	0.16
Quartz	0.41	0.60	0.73	0.58
Bytownite	78.9	84.6	81.2	81.3
Albite	0.46	0.35	0.63	0.49
K-Feldspar	0.01	0.02	0.13	0.06
Pyroxenes	11.2	7.78	7.97	9.11
Amphibole	0.83	0.76	2.62	1.45
Olivine	4.61	3.91	2.88	3.80
Chlorite	2.13	0.91	1.62	1.61
Talc	0.14	0.13	0.30	0.20
Micas	0.12	0.09	0.20	0.14
Carbonates	0.06	0.07	0.11	0.08
Kaolinite (clay)	0.03	0.02	0.08	0.04
Others	1.03	0.63	1.29	1.02
Total	100	100	100	100

held by epoxy. Particle counts were so large (Schrader et al., 2008) in each that statistical stability was good, and detection limits can reasonably reach the 0.05% range and lower. In these analyses, glass was ignored, as it was a separate, idealized constituent. In lunar samples, this should not be done.

The minerology of the simulant was dominated by the anorthosite and norite rocks from Stillwater. While the major minerals in these rocks were bytownite, enstatite, and augite or diopside, the minor and trace minerals were more complex (Boudreau, 2016, Aird et al., 2017). These minor/trace minerals included species such as sulfides, magnetite, ilmenite, both greenschist-grade and high-temperature alteration assemblages, and multiple other species. Some of these can be considered "lunar" while others, such as albite, biotite, calcite, clays, clinozoisite, epidote, hornblende, phlogopite, quartz, and stilbite, are either rarely or never lunar and are thus potentially detrimental to use in a lunar simulant. Minimizing the abundance of unwanted minerals was the reason the Stillwater feedstocks used in the simulant were handpicked. Available data showed their total abundance of non-lunar minerals in the simulant, as suggested by loss on ignition (LOI), X-ray diffraction (XRD), QEMSCAN, and analysis for silicosis risk, was probably between 4 to 5 weight percent. The abundance of individual species was generally below 1 wt%; only hornblende was frequently detectable by XRD. It should be noted that in contrast to the Merriam Crater feedstock used in multiple simulants including JSC-1A, there was suspicion the non-lunar minerals in NUW-LHT-5M were not concentrated on the perimeters of simulant particles. There was a tendency for the non-lunar minerals to concentrate in the fines, <38 µm.

ALS also determined the Ca/(Ca+Na) ratio at eight points in the plagioclase grains. The average value was an unexpectedly high 89. This was slightly higher than the published data would suggest (Boudreau, 2016). The Mg/(Mg+Fe) and the Ca/(Ca+Mg+Fe) values for the orthopyroxene and the clinopyroxene grains were 0.79, 0.03 and 0.75, 0.49 respectively. These values agreed well with work done by the USGS (Rickman et al., 2011).

Table 4.2. Liberation by sieve bin of four major mineral groups, as observed in a plane of section through the simulant. "Feld," or feldspar, includes all plagioclase, K-feldspar, and what may be epidote-clinozoisite family minerals. "Px," or pyroxene, includes both clino- and orthopyroxenes and amphiboles. "Ol," or olivine, includes the Turkish olivine added to the mix, as well as the minimal olivines in the Stillwater feedstocks. "Others" in this table includes such minerals as quartz, calcite, micas, and talc. Glass is ignored in this analysis. "Liberated" means that a particle is mono-mineralic in the plane of section through the simulant, as opposed to two or more minerals in non-liberated particles. See text for additional information.

Part A

Status	>106µm				<106 >38µm			
	Feld	Px	Ol	Other	Feld	Px	Ol	Other
Liberated	29.9	18.2	39.7	0.5	27.0	15.1	22.8	1.7
Binary - Feld		8.5	0.0	22.3		2.0	0.0	12.9
Binary - Px	1.6		2.5	2.3	0.2		3.8	2.0
Binary - Ol	0.0	1.3		0.3	0.0	1.5		0.4
Binary - OGn	2.1	2.4	0.9		1.1	1.9	0.9	
Multiphase	1.9	11.5	1.3	13.0	0.2	1.8	0.8	1.3
Total	35.5	41.8	44.5	38.4	28.6	22.2	28.3	18.3

Status	<38µm				Mineral Liberation, 2D			
	Feld	Px	Ol	Other	Feld	Px	Ol	Other
Liberated	34.3	27.2	22.9	24.1	91.3	60.5	85.4	26.3
Binary - Feld		4.2	0.3	13.9		14.7	0.3	49.1
Binary - Px	0.5		1.8	3.3	2.3		8.1	7.5
Binary - Ol	0.0	0.6		0.3	0.0	3.3		1.0
Binary - OGn	1.0	2.3	0.6		4.2	6.6	2.5	
Multiphase	0.1	1.6	1.6	1.7	2.2	14.9	3.7	16.1
Total	35.9	36.0	27.2	43.3	100	100	100	100

Part B

	Proportion by Weight-2D				Composition of Grains			
	Feld	Px	Ol	Other	Feld	Px	Ol	Other
Liberated	74.7	6.4	3.2	1.0	100	100	100	100
Binary - Feld		1.6	0.0	1.9		45	60	35
Binary - Px	1.9		0.3	0.3	55		47	29
Binary - Ol	0.0	0.4		0.0	40	53		29
Binary - Other	3.5	0.7	0.1		65	71	71	
Multiphase	1.8	1.6	0.1	0.6	44	38	3	15
Average	81.8	10.6	3.8	3.8	93	68	46	33

An interesting clue to the oxidation level of the Stillwater rocks during their formation was the detection of elemental iron inside the bytownite. The grains, as seen in a scanning electron microscope (SEM), were approximately 1 µm in size. Their composition was confirmed using a Bruker X Flash 5030 detector.

4.2 Liberation

As mineral beneficiation on the Moon is of substantial interest, ALS performed a liberation analysis on NUW-LHT-5M, Table 4.2. To the author's knowledge, these basic data have never previously been acquired on either lunar samples or lunar simulants. The lack of data on lunar material restricts interpretation of these data to qualitative interpretations. This type of data is essential to any ISRU-related work on mineral beneficiation, i.e., concentration of selected minerals.

Because (1) the simulant was made from few, relatively simple feedstocks, (2) the interest was in the major minerals, and (3) the particles had relatively simple shapes, (see below), interpretation of the data was straightforward. Most of the particles in the simulant were monomineralic (i.e.: liberated). Based on informal examination of several thin sections of lunar regolith, this may not

be true for the lunar material. Data in Table 4.2 Part A showed 35.5% by particle count of all feldspar were in the >106 μm size range; 29.9% of all feldspars were both in the >106 μm range and liberated, while 1.6% of the feldspars in that size range were locked with pyroxene. Of all the feldspars, 91.3 were liberated. In this part of the table, 0.0 indicated these mineral pairs were not observed in sufficient abundance to be statistically significant. In Part B of the table, which was by mass fraction, 81.8 wt% of the simulant was feldspar, of which 1.9 wt% was locked with pyroxene. Of that 1.9 wt%, 55% of a particle was feldspar on average and 45% was pyroxene. In the multiphase particles, on average 44% of the particle was feldspar, 38% was pyroxene, etc. In Part B composition values of "0"represented values <2%, and "100" represented values >95%. The liberation data are also broken out to show where the elements were. Al, Ca, Fe, Mg, Si were in liberated or locked particles. This is “deportment.” See the file B for relevant data.

The liberation results were a direct consequence of the feedstocks used to make the simulant: most of the olivine was added as a nearly pure phase, there was no glass in the mineral feedstocks, and the synthetic glass essentially lacked crystalline components at the scale of analysis, so glass can be ignored, as shown in Table 4.2. The grain sizes of the minerals in the feedstocks were close to the coarsest particle size in Test 2, ~1 mm. To make the smaller particles in the simulant, liberation was highly probable.

Given the interest in recovery of Fe and Ti in their various deportments from lunar material, data such as shown here would be extremely useful. With such data in hand for both Apollo samples and simulants, the relevance of various ISRU tests using terrestrial materials could be evaluated.

4.3 Mineralogy Accuracy

Mineralogy by systems like the QEMSCAN use elemental abundance at a point to assign mineral identity. The limitation of measurements from a plane of section view were overcome by analysis of a massive number of particles. Therefore, in principle, the mineralogy measured by QEMSCAN should closely approximate the elemental abundances, as given in the following section, found by analytical techniques that were intended not to be sensitive to mineralogy. There were, of course, limitations to ideality, but the comparison shown in Table 4.3 indicated the degree of closure in these analyses. There were many details behind such a table, discussion of which is beyond the scope of this paper.

Table 4.3. Comparison of elemental abundances computed from the QEMSCAN data versus direct measurements.

Method	Al	Ca	Fe	K	Mg	Na	Si
Chemical	13.7	10.2	2.3	<0.1	4.6	0.7	21.6
QEMSCAN	14.5	11.2	2.2	<0.1	3.8	0.8	20.8

4.4 Chemistry

A significant range of chemistry data was obtained on the simulant: inductively coupled plasma (ICP), Ferrous Fe, C, S, and X-ray fluorescence (XRF). LOI was also measured. Most of the data reported here were from ALS, and Alan Whittington and Austin Patridge both of the University of Texas, San Antonio, (UTSA). Data for comparison were dominantly from Steve Wilson of the USGS. The ALS and USGS data were from commercial labs, that use certified standards.

4.4.1 X-ray fluorescence

For more than 100 years geologists have used the convention of expressing major element abundances as weight % oxides, even though for the most part the oxides do not exist in the

Table 4.4. XRF for major elements in wt.% for NUW-LHT-5M Test 2 and other simulant materials. Values are the totals of each cation expressed as an oxide. Key: ALS—ALS Metallurgy Services, UTSA—University of Texas San Antonio, USGS—United States Geological Survey, WM—Washington Mills. BCR-2 is an analytical standard. Notes: (1) ALS used standards AMIS0788 and BCS-516. Process code ME-XRF26. (2) Whittington & Parsapoor, 2022. (3) NU-LHT-4M is the average of 16 samples. (4) Average of material delivered to ICON in 2023–2024, which is being used for the current production.

			Al2O3	CaO	Cr2O3	Fe2O3	K2O	MgO	MnO	Na2O	P2O5	SiO2	TiO2
ALS (1)	Head		26.08	14.55	0.08	3.42	0.04	7.67	0.04	1.02	<0.01	46.80	0.29
	>106µm		25.06	14.10	0.09	4.02	0.04	8.40	0.05	0.88	<0.01	46.07	0.32
	>38µm <106µm		25.73	14.35	0.08	3.19	0.04	7.72	0.04	0.93	<0.01	46.63	0.29
	<38um		26.79	14.55	0.09	2.77	0.06	6.95	0.04	1.10	<0.01	46.40	0.27
UTSA	NUW-LHT-5M	Glass	27.60	16.61	-	3.56	0.00	6.08	0.04	0.00	0.02	45.54	0.58
		Test 1	25.73	14.56	-	3.25	0.05	7.73	0.05	0.86	0.02	46.90	0.28
		Test 2	25.83	14.63	-	3.21	0.04	7.75	0.05	0.80	0.02	46.94	0.28
	JSC-1A		16.07	9.93	-	12.54	0.80	8.83	0.19	3.06	0.65	46.71	1.78
	JSC-1A (2)		15.02	10.42	-	11.61	0.82	9.01	0.18	2.70	0.66	47.71	1.59
USGS	NU-LHT-1M		24.00	13.60	0.12	4.91	0.09	8.66	0.08	1.42	<0.01	47.30	0.34
	NU-LHT-2M		24.50	13.60	0.10	4.15	0.09	8.37	0.07	1.46	0.06	47.00	0.39
	NU-LHT-4M (3)		23.59	12.96	0.11	4.78	0.16	8.74	0.07	1.50	0.10	47.47	0.41
	BP-1		16.00	10.20	<0.01	12.00	1.01	6.65	0.17	3.36	0.39	46.30	2.10
	JSC-1A		16.40	10.00	0.01	12.70	0.83	8.72	0.19	3.19	0.70	46.80	1.84
	LCATS-1		9.29	12.90	0.07	12.00	0.92	16.90	0.18	2.84	0.64	36.40	3.19
	OB-1		16.80	9.71	0.02	13.10	0.71	5.84	0.19	2.53	0.29	49.70	1.54
	Stillwater An		30.90	15.80	<0.01	1.32	0.06	1.05	0.02	2.13	<0.01	47.60	0.05
	GreenSpar		30.60	14.70	<0.01	0.49	0.22	0.17	0.01	2.49	0.01	51.00	0.03
	BCR-2		13.50	7.18	<0.01	13.90	1.78	3.64	0.20	3.12	0.35	54.20	2.29
WM	NUW-LHT-5M (4)		26.79	14.08	0.01	4.31	-	6.35	0.05	0.08	0.01	47.83	0.52

rock; in lunar samples the major elements are in silicate minerals. A common way to measure the elemental abundances is using XRF.

The major differences between the highland simulant NUW-LHT-5M and the mare simulant JSC-1A can be seen in Table 4.4. Highland regolith has more Al and Ca and less Fe than mare regolith. JSC-1A also intentionally had a higher Ti content because it was intended to mimic some of the Ti-rich Apollo samples, but there is a deeper use for these data. Al, Ca, and Na are primarily carried in the mineral plagioclase or their derived glass. The ratio of Ca/(Ca+Na), termed the An number, is very important for the melting temperature of the simulant. Higher An values have higher melt temperatures. Also, K and Na affected various properties of the melt, such as viscosity. Simulants normally inherit their An value only from their feedstocks. In this respect the Stillwater Complex has a slightly higher An compared to Merriam Crater, AZ, the source for JSC-1A; the -5M glass had a much higher An value, which made it a superior lunar simulant in this respect compared to JSC-1A.

The table clearly demonstrates that Test 1 and Test 2 had less Fe than the design specified. Changes to production methods enabled Washington Mills to raise the Fe closer to the target.

Table 4.5. FeO and Fe2O3 in wt% for NUW-LHT-5M Test 2 and other simulant materials. The measurements by UTSA also give the ±2σ estimate and the values measured for the standards they used. BIR-1A and BCR-2 are analytical standards. The NU-LHT-4M value is the average of 16 samples. ALS: ALS Metallurgy Services, UTSA: University of Texas San Antonio, USGS: United States Geological Survey.

			FeO	±2σ	Fe2O3	±2σ
ALS	NUW-LHT-5M	Head	2.80	-	-	-
		>106µm	3.33	-	-	-
		>38µm <106µm	2.79	-	-	-
		<38µm	2.16	-	-	-
UTSA	NUW-LHT-5M	HQ Glass	3.69	0.21	0	-
		HQ Glass	4.01	0.23	0	-
		Test 1	3.34	0.19	0	-
		Test 2	3.41	0.20	0	-
		Test 2	3.22	0.19	0	-
	JSC-1A		8.75	0.51	2.59	0.14
	JSC-1A		8.11	0.47	3.28	0.18
	USGS BIR-1a		9.63	0.56	1.64	0.09
	USGS BIR-1a		8.81	0.51	1.87	0.10
	BIR-1a Certified Values		8.34	0.10	2.06	0.10
USGS	NU-LHT-4M(1)		2.73	-	-	-
	NU-LHT-2M		2.06	-	-	-
	NU-LHT-1M		2.33	-	-	-
	BP-1		6.80	-	-	-
	OB-1		8.74	-	-	-
	JSC-1A		8.49	-	-	-
	LCATS-1		6.93	-	-	-
	Stillwater An		0.78	-	-	-
	GreenSpar		0.22	-	-	-
	BCR-2		10.60	-	-	-

though contamination during mining should usually be considered a possibility. Inorganic C in simulants commonly exists as a carbonate mineral, frequently calcite. As organic C and carbonate minerals are not found on the Moon, and they have properties that are distinctly non-lunar, avoiding all carbon in a simulant is desirable. S can be found in various types of terrestrial minerals, of those the sulfides are also found on the Moon, e.g., troilite, FeS. Other mineral groups containing S, such as sulfates, though common on Earth are not found on the Moon; therefore, if S is a concern, its nature in the simulant should be investigated. Information about C and S abundance in Apollo 16 samples can be found in Des Marais,1978.

4.4.2 Ferrous Iron, Carbon, and Sulfur

Ferrous Fe was measured by titration and was given in Table 4.5. The total values of reduced iron in NUW-LHT-5M reflected the low total Fe, ~3.2 wt% in the Test 2 batch, while its reduced Fe are a high proportion of the total Fe, ~90%. This is substantially higher than that of JSC-1A, 74%, or any other simulant measured in this work, which range from ~60% to 74%. The high value was strongly driven by the reducing environment in the glass production.

Total C and total S were measured by combustion using a Laboratory Equipment Corporation (LECO) instrument, Table 4.6. As the surface of the Moon has very little carbon, lower values in simulants were desirable. The major carrier of C in simulants was inherited from the feedstock, where approximately half was organic and half was inorganic. The organic sources in simulants are generally not known,

Table 4.6. Total carbon (C) and total sulfur (S) in wt.% for NUW-LHT-5M and several simulant materials.

		C	S
ALS	NUW-LHT-5M	0.05	0.02
USGS	NU-LHT-1M	0.03	0.01
	NU-LHT-2M	0.04	0.037
	NU-LHT-4M	0.04	0.05
	BP-1	0.54	0.015
	JSC-1A	0.04	0.011
	LCATS-1	0.82	0.06
	OB-1	0.06	<0.005
	Stillwater An	0.03	0.006
	GreenSpar	0.08	0.015
	BCR-2	0.02	0.035

4.4.3 ICP

Inductively coupled plasma (ICP) analyses were performed on four simulants made using Stillwater source rocks, one each for the simulants BP-1, OB-1, LCATS-1, and JSC-1A. Two anorthosites were also analyzed, Table 4.7. The analysis of NUW-LHT-5M was done by ALS, the other analyses were done under contract for the USGS as directed by Steve Wilson. There are currently three primary sources for anorthosites used in lunar highland simulants: Stillwater, MT, an anorthosite produced in Greenland, and one produced from the Shawmere Complex of Ontario. ICP values for the first two are included here.

For the most part variations in the data were dominated by the nature of the source rocks used to make the simulants, but here are a few points of interest: Several of the differences between NUW-LHT-5M vs. NU-LHT-2M or NU-LHT-4M were presumably dominated by the source of the glasses used. In -5M the glass was made from commercially available oxides. In -2M and -4M the glass was made by melting the mill sand produced as a waste product by the removal of the sulfide minerals carrying the Pt values from the ore. This was clearly seen in elements related to the Stillwater ore system, such a Cr, Cu, Ni, Pb, S, and Zn. Nd and related elements have been examined in some detail. The recipe for both -2M and -4M included the addition of very small amounts of apatite, purchased as naturally occurring, pure mineral. The apatite used in -4M was also analyzed and found to be very high in Nd and other rare earth elements, at levels many orders of magnitude higher than the Stillwater materials. Mass balance suggested this was sufficient to account for differences between -4M and -5M. Because apatites for -2M and -4M were purchased at different times, there were also differences between these simulants. Finally, there were two production runs of NU-LHT-4M. Unlike all the other data presented herein, there were differences in the ICP values between the two batches (which were intended to be identical) demonstrating the sensitivity of the simulants to variations in the feedstocks.

4.4.4 LOI

LOI values from three sources are presented in Table 4.8. LOI were measured by heating a sample in a furnace to a high temperature (i.e., 900 °C to 1000 °C). This was normally done in the ambient atmosphere. Sample weights were measured before and after heating.

The LOI of simulants must be interpreted with caution. Besides removal of H_2O on the outer surface of particles, it also included devolatilization reactions during mineralogical changes. It can also include weight gain due to oxidation of the simulant. The magnitude of each of these processes could not be recovered from LOI alone. Measurement of weight loss in this paper, as well (Wilkerson, 2023) demonstrated that most of the LOI in the tested simulants was due to removal of H_2O. Such H_2O, which was from genetic sources not related to the H_2O associated with permanently shadowed craters (Colaprete et al., 2010), is non-lunar to a large extent, though not completely, non-lunar.

Although interpretation of LOI values in simulants can be problematic, some useful information can be found in Table 4.8. Loss-gain in NUW-LHT-5M glass, as expected, was effectively 0. The large weight losses in LCATS-1, BP-1, and Stillwater anorthosite were a clear indication that non-lunar minerals in these materials were a substantial part of the material. Which in turn suggested that use of a high-temperature bake out (Wilkerson et al., 2023) might be useful for some users of these materials.

Table 4.7. ICP for NUW-LHT-5M, 8 simulants, and 2 anorthosites. BCR-2 is a USGS geochemical analytical standard. NU-LHT-4M #1 is the average of 15 samples. Stillwater Anorthosite is the average of 2 samples.

Source	Simulant	Ag	Al	As	B	Ba	Be	Bi	Ca	Cd	Ce	Co
		ppm	%	ppm	ppm	ppm	ppm	ppm	%	ppm	ppm	ppm
ALS	NUW-LHT-5M	0.23	9.97	<0.2	-	20.00	0.07	0.10	10.35	0.03	1.18	15.90
USGS	NU-LHT-1M	<1	13.10	<5	<10	27.90	<5	<0.1	10.20	<0.2	19.70	33.30
	NU-LHT-2M	<1	13.30	<5	<10	25.70	<5	<0.1	10.30	<0.2	11.90	28.60
	NU-LHT-4M #1	<1	12.65	<5	<10	164.13	<5	<0.1	9.61	<0.2	826.67	64.57
	NU-LHT-4M #2	<1	12.80	<5	<10	111.00	<10	0.10	9.56	<0.2	474.00	48.00
	BP-1	<1	8.72	<5	<10	509.00	<5	<0.1	7.52	<0.2	51.60	44.30
	JSC-1A	<1	9.08	<5	11.00	880.00	<5	<0.1	7.42	<0.2	99.90	50.10
	LCATS-1	<1	5.14	<5	40.00	795.00	<5	<0.1	9.55	<0.2	90.10	65.60
	OB-1	<1	9.30	<5	27.00	246.00	<5	<0.1	7.32	<0.2	20.90	41.30
	Stillwater An	<1	16.70	<5	<10	31.10	<5	<0.1	11.80	<0.2	1.20	5.45
	GreenSpar	<1	16.60	<5	<10	139.00	<5	<0.1	11.00	<0.2	3.40	1.30
	BCR-2	<1	7.15	<5	<10	666.00	<5	<0.1	5.16	0.20	51.80	36.70

Source	Simulant	Cr	Cs	Cu	Dy	Er	Eu	Fe	Ga	Gd	Ge	Hf
		ppm	ppm	ppm	ppm	ppm	ppm	%	ppm	ppm	ppm	ppm
ALS	NUW-LHT-5M	369.00	<0.05	25.40	0.18	0.15	0.07	2.22	10.60	0.13	0.15	1.00
USGS	NU-LHT-1M	864.00	0.10	39.00	0.34	0.27	0.15	3.64	12.90	0.28	<1	2.00
	NU-LHT-2M	741.00	<0.1	28.00	0.45	0.22	0.15	3.13	11.40	0.26	1.00	<1
	NU-LHT-4M #1	744.07	0.19	94.53	0.62	0.36	0.24	3.55	44.48	0.69	1.43	7.07
	NU-LHT-4M #2	696.00	0.10	64.00	0.51	0.27	0.24	3.23	31.00	0.61	1.00	4.00
	BP-1	99.00	0.40	43.00	4.44	2.22	1.67	8.76	18.90	5.51	1.00	4.00
	JSC-1A	120.00	0.30	61.00	4.90	2.48	2.21	9.31	23.70	6.34	2.00	4.00
	LCATS-1	482.00	0.40	47.00	5.34	2.00	2.56	8.82	19.70	7.51	2.00	6.00
	OB-1	141.00	0.90	217.00	4.75	3.03	1.53	9.61	21.30	4.73	1.00	3.00
	Stillwater An	37.50	<0.1	20.50	0.21	0.12	0.23	0.99	14.65	0.16	<1	<1
	GreenSpar	<10	<0.1	5.00	0.07	0.05	0.20	0.36	15.60	0.12	<1	<1
	BCR-2	11.00	1.00	15.00	6.32	3.53	2.11	9.90	23.50	6.52	2.00	5.00

Source	Simulant	Ho	In	K	La	Li	Lu	Mg	Mn	Mo	Na	Nb
		ppm	ppm	%	ppm	ppm	ppm	%	ppm	ppm	%	ppm
ALS	NUW-LHT-5M	0.03	0.01	<0.01	0.50	1.70	0.02	4.25	357.0	2.63	0.67	3.50
USGS	NU-LHT-1M	0.09	<0.2	0.09	2.80	<10	0.05	5.10	644.0	<2	1.13	4.10
	NU-LHT-2M	0.05	<0.2	0.08	1.90	<10	<0.05	4.91	570.0	11.00	1.16	4.80
	NU-LHT-4M #1	0.13	<0.2	0.15	77.89	<10	0.06	5.11	542.4	5.53	1.20	3.65
	NU-LHT-4M #2	0.14	<0.2	0.12	46.10	<10	<0.05	4.68	528.0	3.00	-	3.40
	BP-1	0.86	<0.2	0.91	24.40	11.00	0.30	3.79	1350.0	<2	-	26.40
	JSC-1A	0.95	<0.2	0.75	49.40	<10	0.28	5.16	1500.0	<2	-	40.30
	LCATS-1	0.86	<0.2	0.83	42.80	28.00	0.20	10.10	1460.0	2.00	-	62.00
	OB-1	1.01	<0.2	0.64	8.20	<10	0.38	3.41	1560.0	<2	-	1.90
	Stillwater An	<0.05	<0.2	0.06	0.70	<10	<0.05	0.62	153.0	<2	-	0.10
	GreenSpar	<0.05	<0.2	0.19	1.60	<10	<0.05	0.09	59.0	<2	-	0.30
	BCR-2	1.38	<0.2	1.55	24.00	<10	0.51	2.03	1540.0	251.00	-	11.10

Table 4.7. continued

Source	Simulant	Nd	Ni	P	Pb	Pr	Rb	Re	S	Sb	Sc	Se
		ppm	ppm	ppm	ppm	ppm	ppm	ppm	%	ppm	ppm	ppm
ALS	NUW-LHT-5M	0.50	247.00	20.00	2.20	0.12	<0.1	<0.002	<0.01	0.98	4.00	3.00
USGS	NU-LHT-1M	1.40	348.00	<0.01	<5	0.46	2.10	<0.02	0.20	0.50	12.00	<5
	NU-LHT-2M	1.30	345.00	0.02	<5	0.35	2.00	<0.02	0.20	<0.1	11.00	<5
	NU-LHT-4M #1	26.23	444.00	0.04	12.47	7.82	4.11	<0.02	0.20	0.46	11.00	<5
	NU-LHT-4M #2	15.60	377.00	0.03	9.00	4.49	3.30	<0.02	0.20	0.30	10.00	<5
	BP-1	26.50	60.00	0.18	<5	6.39	14.10	<0.02	0.10	<0.1	19.00	<5
	JSC-1A	45.50	107.00	0.33	8.00	11.50	10.00	<0.02	0.10	<0.1	28.00	<5
	LCATS-1	44.40	403.00	0.30	<5	11.30	24.00	<0.02	0.20	0.40	19.00	<5
	OB-1	16.70	73.00	0.14	6.00	3.17	13.90	<0.02	0.10	0.30	35.00	<5
	Stillwater An	0.70	29.50	<0.01	<5	0.14	0.65	<0.02	0.20	0.50	<5	<5
	GreenSpar	1.20	7.00	<0.01	<5	0.35	4.70	<0.02	0.20	<0.1	<5	<5
	BCR-2	28.10	10.00	0.15	11.00	6.88	45.00	<0.02	0.10	0.80	31.00	<5

Source	Simulant	Si	Sm	Sn	Sr	Ta	Tb	Te	Th	Ti	Tl	Tm
		%	ppm	ppm	ppm	ppm	ppm	ppm	ppm	%	ppm	ppm
ALS	NUW-LHT-5M	-	0.12	0.70	88.0	0.15	0.02	<0.05	0.11	0.16	<0.02	0.02
USGS	NU-LHT-1M	24.40	0.20	<1	118.0	<0.5	0.06	<0.5	0.30	0.20	<0.5	0.06
	NU-LHT-2M	24.00	0.30	<1	118.0	<0.5	0.05	<0.5	0.70	0.24	<0.5	<0.05
	NU-LHT-4M #1	24.15	0.83	2.20	145.8	0.65	0.11	<0.5	1.91	0.25	<0.5	0.06
	NU-LHT-4M #2	23.50	0.60	1.00	134.0	<0.5	0.11	<0.5	1.90	0.24	<0.5	0.06
	BP-1	23.20	6.40	2.00	805.0	2.70	0.80	<0.5	2.90	1.26	<0.5	0.31
	JSC-1A	23.90	7.70	1.00	978.0	3.40	0.88	<0.5	6.20	1.12	<0.5	0.36
	LCATS-1	18.60	8.60	3.00	1010.0	6.10	1.03	<0.5	5.30	1.95	<0.5	0.23
	OB-1	25.30	4.80	2.00	391.0	<0.5	0.78	<0.5	1.30	0.94	<0.5	0.44
	Stillwater An	24.50	0.10	<1	163.0	<0.5	<0.05	<0.5	<0.1	0.03	<0.5	<0.05
	GreenSpar	26.40	0.10	<1	293.0	<0.5	<0.05	<0.5	0.30	0.02	<0.5	<0.05
	BCR-2	26.60	6.20	2.00	346.0	1.20	1.09	<0.5	6.00	1.36	<0.5	0.54

Source	Simulant	U	V	W	Y	Yb	Zn	Zr
		ppm	ppm	ppm	ppm	ppm	ppm	ppm
ALS	NUW-LHT-5M	0.30	29.00	0.40	1.10	0.13	22.00	31.70
USGS	NU-LHT-1M	0.12	46.00	<1	2.20	0.30	28.00	96.30
	NU-LHT-2M	0.09	38.00	<1	2.10	0.20	22.00	9.70
	NU-LHT-4M #1	0.26	45.47	7.67	5.60	0.40	213.00	316.33
	NU-LHT-4M #2	0.20	42.00	4.00	5.10	0.40	71.00	179.00
	BP-1	0.95	195.00	<1	22.60	2.20	93.00	169.00
	JSC-1A	1.48	246.00	7.00	23.20	2.20	103.00	154.00
	LCATS-1	1.57	240.00	<1	22.40	1.40	100.00	230.00
	OB-1	0.44	409.00	7.00	25.40	2.90	112.00	91.20
	Stillwater An	<0.05	19.00	3.00	1.10	0.10	5.00	2.15
	GreenSpar	<0.05	<5	1.00	0.50	<0.1	7.00	13.50
	BCR-2	1.71	405.00	<1	32.50	3.50	128.00	182.00

Table 4.8. Loss on ignition, in wt. loss %, for NUW-LHT-5M Test 1 and Test 2, and other simulant materials. A negative value indicates weight gain.

			wt%	±2σ	n
ALS	NUW-LHT-5M	Head	0.26	-	1
		>106µm	0.23	-	1
		>38µm <106µm	0.20	-	1
		<38um	0.66	-	1
UTSA	NUW-LHT-5M	Glass	-0.04	0.187	4
		Test 1	0.58	0.132	3
		Test 2	0.44	0.028	4
	JSC-1A		-0.57	0.026	3
USGS	NU-LHT-1M		0.54	-	1
	NU-LHT-2M		1.08	-	1
	NU-LHT-4M		0.88	-	16
	BP-1		2.33	-	1
	JSC-1A		<0.01	-	1
	LCATS-1		5.34	-	1
	OB-1		0.19	-	1
	Stillwater Anorthosite		1.47	-	2
	GreenSpar		0.72	-	1
	BCR-2		0.10	-	1

The oxidation problem was recognized in the value measured by UTSA for JSC-1A, as the sample gained weight during heating. This result agreed with the work reported in Street et al., 2010. The LOI for the NUW-LHT-5M glass was effectively equal to 0, which was expected given the method of its fabrication and composition. The lower values for -5M vs. the other NU-LHT-series reflected the high glass content of -5M. The Stillwater anorthosite, which has veins of hydrothermal alteration, contributed approximately 90% of the LOI values for that series; and the volatile-bearing phases in -5M were concentrated in the finer fractions.

5. Silicosis Risk

Silicosis is an uncurable, potentially fatal disease caused by the inhalation of "silica" (SiO_2) particles (IARC Working Group, 2012). To be dangerous, silica phases must reach the alveoli of the lungs. To do this, the particles generally must be <10 µm in diameter, which is referred to as the respirable fraction. Accordingly, the relative mass of candidate phases below <10 µm should be known. A sample of NUW-LHT-5M was analyzed for the presence of quartz, cristobalite, and tridymite, which were the relevant phases in this simulant. Because simulants may be further sieved or milled by users, the total abundance of the candidate phases should be known for the bulk material. For this study DCM Science Laboratory, Appendix C, measured the total abundance and the abundance of quartz that was less than 10 µm. In NUW-LHT-5M cristobalite and tridymite were not found, due to the geologic environment of the Stillwater rocks used. The total quartz was found to be ~0.85 wt% and the respirable quartz to be 0.13 wt%. A full survey of the abundance of known risk species for multiple simulants may be found in Slabic et al., 2024. Because silicosis risk is only partially dependent on the abundance of minerals of concern, users are advised to consult with their industrial hygienist for their individual risk evaluation.

6. Particle Size

Representative PSDs for NUW-LHT-5M were given in Figure 6.1. Included were a variety of measurements by different methods and different organizations. The MSFC measurements were made using dynamic image analysis (DIA), using the same system as Wilkerson et al., 2024. Washington Mills used both a laser diffractometry analysis (LDA) system by Microtrac, as well as a sieving devise by RoTap. National Institute of Standards and Technology (NIST) and ALS both used sieving. Anton Paar, GmbH, measurements use a DIA system. The multiple measurements were done in recognition of the difficulty of determining a "true" size distribution for such a material (Abbireddy and Clayton, 2009; Dinis and Castilho, 2012).

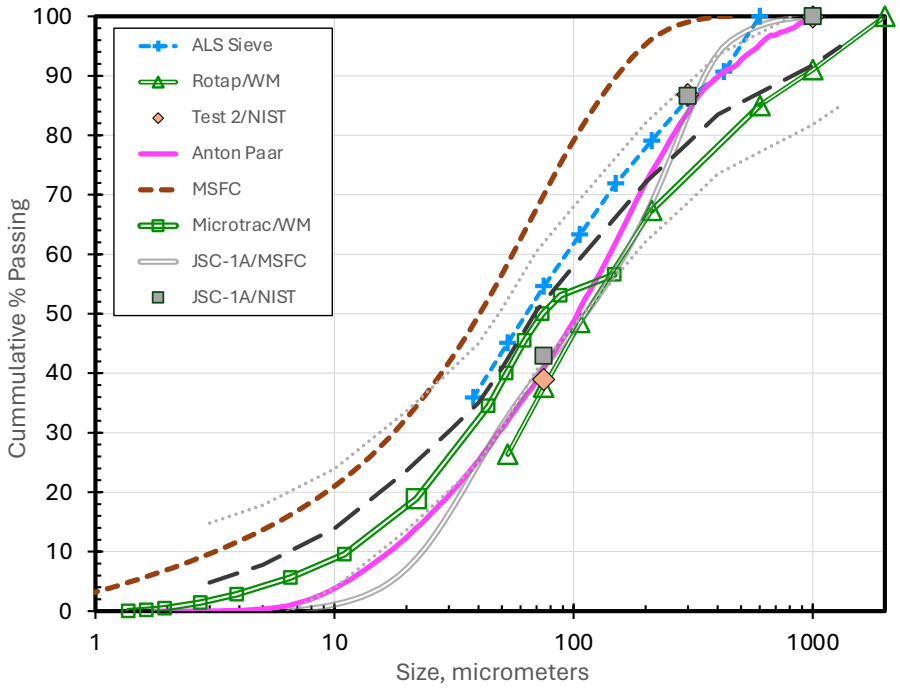

Figure 6.1. Particle size distribution, as cumulative wt%, for NUW-LHT-5M. All of the values are for -5M Test 2 except for the JSC-1A, and values by Washington Mills. Carrier's (2003) average distribution, dark grey, long dashed, and the ± 1 standard deviation, light grey, dotted, are also shown. For Apollo 16 particle size data see Butler et al. (1973). See the text for discussion.

We suggest some material-specific factors contribute to the difficulty in this case. Lunar simulants commonly and intentionally span at least three orders of magnitude in particle size. As demonstrated in Section 7, the particle shapes vary significantly and as a function of size. Also, as shown in Figure 4.1 and Table 4.1, the simulant particle composition was not consistent as a function of either particle or grain size. Few analytical techniques can cover such variations with uniform accuracy. The result of these, and presumably other factors, were clearly seen in the two measurements of the same material by Washington Mills, one from sieving and the other from LDA. We also noted there was the difficulty of obtaining a representative sample in a material that was prone to sorting. How these, or other factors, contributed to the difference values reported here is unknown. That a single lab can be consistent was demonstrated by the observation that Anton Paar measured both Test 1, not shown, and Test 2; one plot fell almost on top of the other.

As previously noted, Washington Mills actively monitored production of the simulant. One of the results of the work on Test 2, and a new analysis of the Graf, 1993 data was a shift in the target upper size range to include 1 – 2 mm. The WM values reported in the figure are from a recent, large delivery which post-date the recent design change in maximum particle size and the measurements made on the Test 2 samples. To maintain composition across the increased range, the grinding of all feedstocks, including the synthetic glass, was altered. As an unwanted consequence, the ~8 wt% of simulant >1 mm now includes ~0.6 wt% (0.05 wt% of total) glass rods which can be several mm long. Given how readily the simulant sorts, these glass rods can be seen more readily than their actual abundance would suggest.

The authors examined the difference between -5M and JSC-1A more carefully in Figure 6.2. A bimodal distribution has been observed in other simulants (Long-Fox et al. 2023), and it may be present in at least some lunar samples (Schrader et al., 2009). We offer three possible sources for

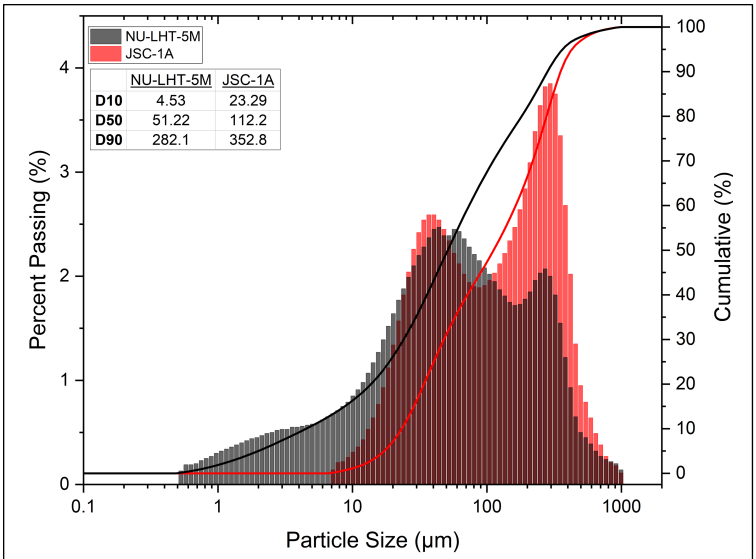

Figure 6.2. Particle size distribution, as percent passing, of NUW-LHT-5M and JSC-1A. See the text for discussion.

bimodal distributions. Various major minerals in the simulants and the lunar materials have different resistance to breaking; Table 4.1 hints at this. This could be a factor even though the reduction processes for simulants and lunar regolith are quite different. Selected portions of a simulant may also be re-milling to increase or decrease the abundance of particular particle size (Long-Fox and Britt, 2023). Without a size classification element in a milling circuit, such as a cyclone separator as used in ore processing, a bimodal distribution was a likely result. Finally, if a simulant is made from multiple feedstocks which are ground separately, as was -5M, the PSD of the mixture is the addition of all the separate PSDs. We did not offer a final explanation for the distributions observed here.

7. Particle Shape

7.1 2D

The shape of the particles in NUW-LHT-5M have been measured at MSFC using the same equipment and analyzed using the methods reported in Rickman and Lowers (2012) and improved in Wilkerson et al. (2024). For this study 3.41 million particles of -5M were measured and the JSC-1A data from 2.69 million particles used by Wilkerson et al. were reused. Figure 7.1 showed differences, in each of four size ranges, between the particle shapes of -5M and JSC-1A. Particles with more complex outlines have lower form factor (FF) values. Particles that were more elongated have lower aspect ratio (AR) values. As reference, a sphere plots at 1,1 on the graph. The amplitude of each population reflected its relative abundance out of the total simulant.

The strong tendency for most particles to be close to the ellipse line and have width/length values between 0.55 and 0.85 was characteristic of both Apollo samples and lunar regolith simulants. The simple curves in the >100 µm range were due to the few particles in that size range. Their placement in AR–FF space indicated the coarser particles had more complex shapes than finer particles but had a similar range of aspect ratios. The high degree of scatter in the 100–50 µm range was also a characteristic of a relatively low sample count. The apparent difference in the distribution of complex particles existed between the <10 µm and the 50–10 µm sub-populations is interesting. Given the pixel resolution in this study is 0.078 µm/pixel, with a minimum number of pixels per particle set to 123, the observed difference was real and unexplained. Additional plots of -5M shape data may be found in Appendix D.

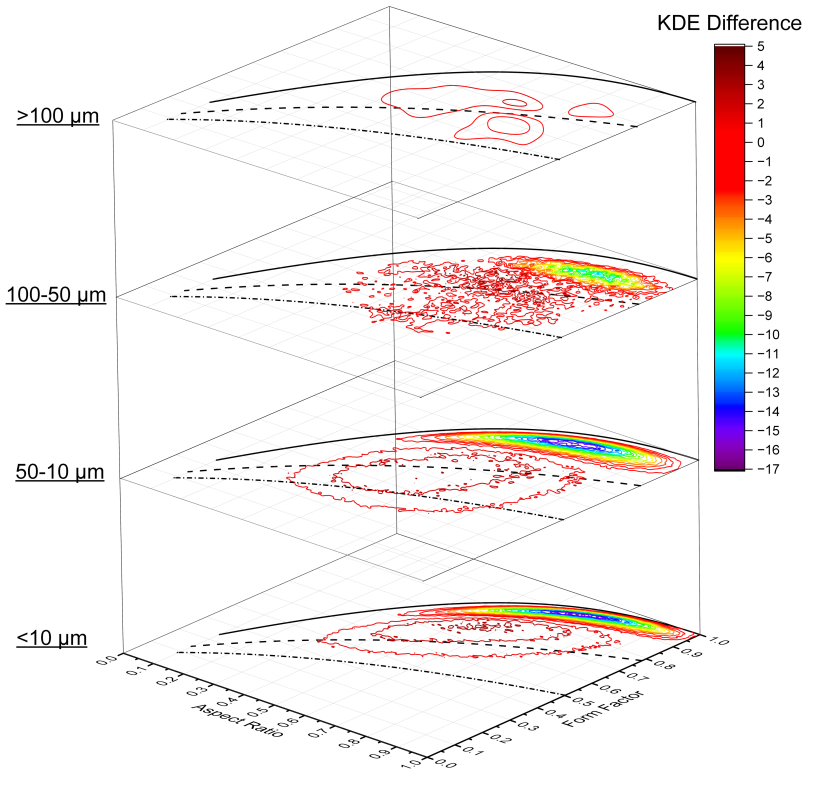

Figure 7.1. Difference between the 2D particle shape distribution of NUW-LHT-5M minus that of JSC-1A as a function of particle size, Form Factor (FF) and Aspect Ratio (AR). The solid line marks all possible ellipses, which are the maximum FF a shape can have in this space. The dash line is for all rectangles. The dash-dot line is for rectangles with whose perimeters have been lengthened 25% (Rickman and Lowers, 2012). If there are more NUW-LHT-5M particles at a given FF – AR location than there are JSC-1A particles, the boundary line's color moves into the reds. Data are particle count.

7.2 3D

3D measurements were made of NUW-LHT-5M and JSC-1A using an X-ray computed tomography process. Methods used are given in the Appendix E. For this paper the simulants were subdivided into three size ranges: >300 µm, 75–300 µm, <75 µm.

The voxel resolution, total mass, and number of particles in each size range for both simulants were shown in Table 7.1. Based on the analysis of Goguen et al. (in review), the particle count was sufficient to give analysis statistical robustness. Combining Table 7.1 data with the pycnometric data in Table 10.1 volume percent could be computed.

Our approach to analysis follows Garboczi (2011), and Garboczi and Hrabe, 2020. Three measures, in µm, were used: length (L), width (W), thickness (T), of each particle. Length was the greatest dimension; thickness was the shortest dimension (Garboczi, 2011); L, W, and T were mutually orthogonal. From these the ratios L/T, W/T, and L/W for -5M and JSC-1A can be examined as functions of particle size. Figure 7.2 showed the data for these ratios as functions of the sieve bins and simulant. It was interesting to note the lines for -5M were concave down and the lines for JSC-1A were concave up. The data in Figure 7.3 revealed the -5M particles were significantly less equant than the JSC-1A particles, as expected from the size of the

Table 7.1. Particles count, #, and % of total sample weight for the 3 sieved sample ranges used in the 3D measurements. Also given are the voxel resolutions used for each measurement. The minimum number of voxels accepted for a particle was 8×8×8.

Sieved Range	JSC-1A			NUW-LHT-5M		
	Resolution	Mass %	# particles analyzed	Resolution	Mass %	# particles analyzed
<75 µm	0.9 µm	42.9	33209	0.9 µm	38.9	53343
75 - 300 µm	3.5 µm	43.7	14773	3.5 µm	47.9	26723
>300 µm	16 µm	13.4	3703	12 µm	13.1	3537

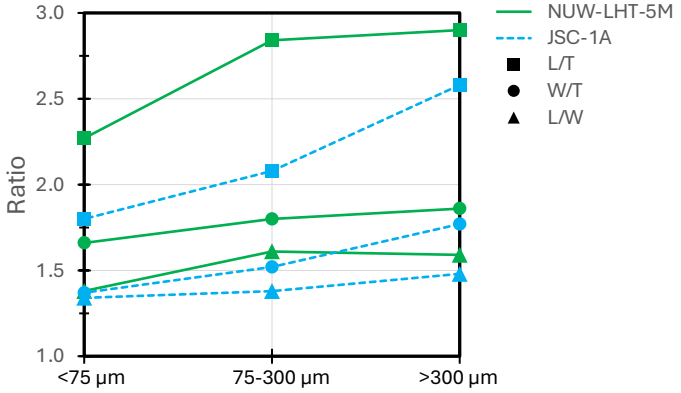

Figure 7.2. Variation in average ratios of Length, Width, and Thickness of NUW-LHT-5M and JSC-1A for three splits sieved for size.

crystalline components in the respective feedstocks. Also, there was a consistent pattern for all three ratios to increase in value as particle size decreases.

With the available data it was possible to reconstruct a complete volume-weighted fraction for each simulant (see the Appendix E.) Figure 7.4 showed the difference between the two simulants volume-weighted PSDs, as a function of W. Conceptually, this plot could be compared to Figure 6.2 and Figure 7.1. Visual examination showed such comparisons are not simple. In addition to the confusion of different scaling, the three sets of measurements were made for different technologies. A single explanation covering all three datasets was beyond the scope of this paper. Figure 7.5 showed the average value of L/T decreases with increasing W, with different, though similar, behavior between JSC-1A and NUW-LHT-5M. Using the full W size range was different than using just the binned averages in Table 7.1, but even in the table it was clear that L/T and W/T decreased as particle size increased.

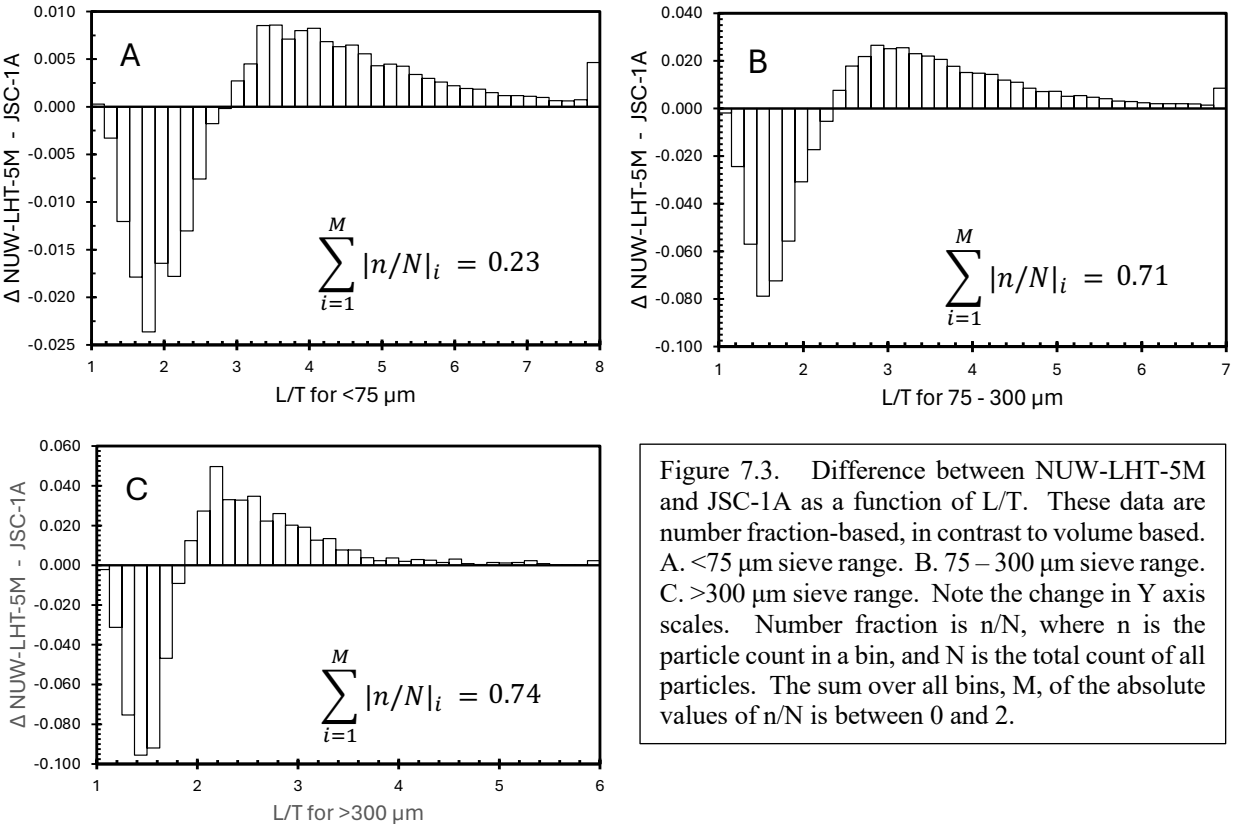

Figure 7.3. Difference between NUW-LHT-5M and JSC-1A as a function of L/T. These data are number fraction-based, in contrast to volume based. A. <75 µm sieve range. B. 75 – 300 µm sieve range. C. >300 µm sieve range. Note the change in Y axis scales. Number fraction is n/N, where n is the particle count in a bin, and N is the total count of all particles. The sum over all bins, M, of the absolute values of n/N is between 0 and 2.

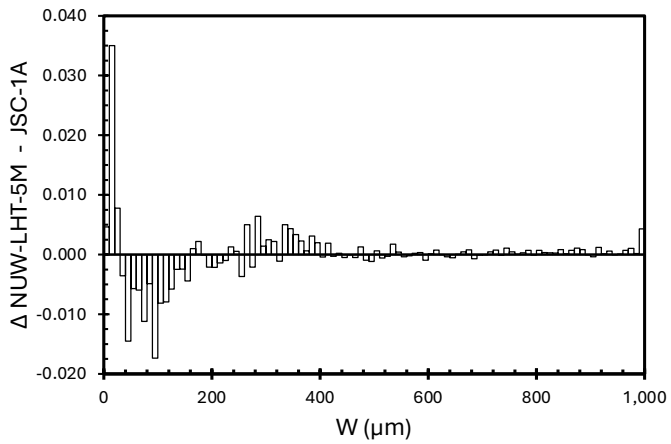

Figure 7.4. Difference of NUW-LHT-5M minus JSC-1A, between their volume-weighted particle size distributions, in terms of W. Values of W > 1000 are combined in the last interval.

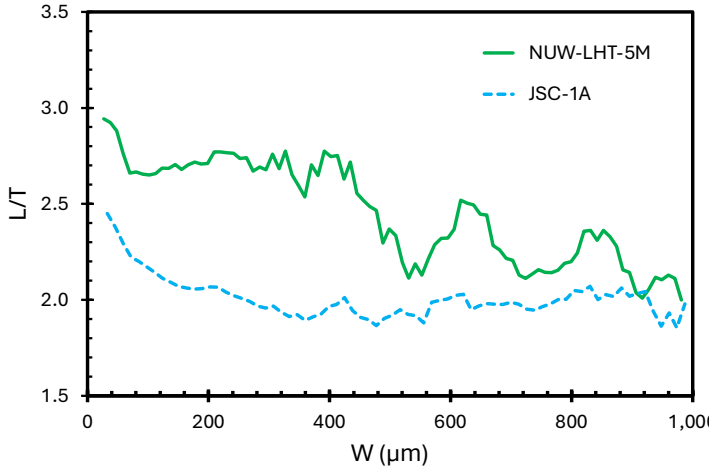

Figure 7.5. Volume weighted length divided by thickness, L/T, versus width, W, for NUW-LHT-5M and JSC-1A. Values of W > 1000 are truncated. Raw data have been smoothed by a moving 5 wide window.

Table 7.2. Average percents of void volume and fraction of particles with a void by sieve bin. A void is a cavity completely internal to

	JSC-1A		NUW-LHT-5M	
	Voids	Particles	Voids	Particles
<75 µm	0.42	19.8	0.27	8.9
75 - 300 µm	0.26	36.8	0.05	7.5
>300 µm	0.37	63.9	0.11	18.7

The CT data were used to examine voids internal to the particles, in contrast to porosity between the particles; Table 7.2 presents a summary of the results. Over the three size ranges JSC-1A simulant has relatively uniform volume of voids, averaged over all porous particles, not all particles. The uncertainty in each average value was at least half the reported value. In contrast the percentage of particles that have measured voids sharply decreased with size, which indicated the pores are relatively large compared to 300+ µm. In smaller particles the original large voids appeared as scalloped edges. The NUW-LHT-5M particles followed the same trend but with much smaller average void space and a much lower percentage of porous particles in each size class. Based on section images of JSC-1A, the voids were in the volcanic glass. In -5M the voids were believed to be restricted to the synthetic glass. The genesis of the former was a violent, volcanic eruption. The latter was a synthetic glass. Combining the void data with the data in Table 7.1 could generate an estimate of the total number of particles or the percent of the mass having voids in each simulant. Additional results are in Appendix E.

8. Specific Surface Area

The Brunauer-Emmett-Teller (BET) method of measurement of specific surface area was used to measure NUW-LHT-5M and these data are presented in Table 8.1. There are two observations from this data that suggested users of these values should be cautious. First, the data in the table for JSC-1A showed significant, unexplained scatter. Six samples of JSC-1A have been measured by three different organizations with results ranging from 1.01 to 2.00 without apparent pattern.

Table 8.1. Specific surface area by BET of NUW-LHT-5M, multiple simulants, and Apollo samples. Stony Brook data from Kaur et al, 2016. Apollo data from Cadenhead et al. (1977). (1) Sample baked out per Wilkerson et al., 2023. (2) Sample as received. JSC-1A-MT4 and JSC-1A-MT8 are out of proof samples retained from the 1-ton production lots of the simulant. JSC-1A AGGL was processed by Orbitec to add a synthetic agglutinate-like fraction (Gustafson et al. 2007). The BET for untreated NUW-LHT-5M at Alfred University is stated as being 0.7340 ± 0.0082 m^2/g.

Alfred	NUW-LHT-5M (1)	0.46
	NUW-LHT-5M (2)	0.73
	JSC-1A (1)	1.007
	JSC-1A (2)	1.3653
JSC	NU-LHT-1M	0.6505
	NU-LHT-2M	1.2996
	NU-LHT-4M	1.1683
	NU-LHT-4M	1.1094
	JSC-1A	1.2473
Stony Brook	NU-LTH-1M	1.366
	NU-LTH-2M	1.402
	NU-LTH-2M	0.94
	JSC-1A	1.323
	JSC-1A-MT4	2.002
	JSC-1A-MT8	1.633
	JSC-1A AGGL	0.802
	JSC-1A <10 µm	6.062
Apollo	10084	0.59
	12033	~0.02
	12070	0.57
	14003	0.51
	14163, 111	0.21
	14259	0.61
	15101, 68	0.65
	15301	0.68
	15401	0.48
	15401	0.40
	61221	0.78
	61241	0.72
	63321	0.43
	63341	0.42
	74220	0.42
	74220	0.46
	75081	0.50

Substantial variation was also seen in measurements of three NU-LHT-2M samples, ranging from 0.94 to 1.40. We conjected the variation in BET may be indicative of the problem of sorting in the simulants. Particles varying in size, shape, or density when in a fluid and gravity field will sort with vibration; all three factors existed in both simulants and lunar samples on Earth. Many users of simulant are accustomed to opening containers of simulant and seeing obvious particle segregation (Fig. 3 of Rickman et al., 2013). The scatter may also be due to the relatively low values of the measurement. Assuming the simulants, as produced, do not actually have the range of specific surface area (SSA) indicated by the measurements, additional care may be needed to obtain measurements with accuracy matching claimed precision.

Further, work by Catherine Lynch and Megan Elliot, Alfred University students, demonstrated the SSA of at least JSC-1A was very sensitive to high-temperature baking, Figure 8.1. Their values showed a drop in BET from 1.00 to approximately 0.2 from heating to ~800 °C, see also Wilkerson et al. (2023). It was concluded the heat treatment was altering non-lunar phases in the simulant to more lunar-like characteristics, bringing JSC-1A's BET values into line with Apollo samples. This paper added two points for -5M, one at 20 °C and one at 750 °C following our standard bake out protocol, per Wilkerson et al. (2023). Following the interpretation that a part of the BET values for JSC-1A derives from non-lunar minerals, in this case derived from weathering of the Merriam Crater feedstock, a process that removes these secondary minerals will lower the SSA. Acknowledging the hazard of interpreting just two data points, this may also explain the behavior of NUW-LHT-5M. It is believed -5M has a lower amount of non-lunar minerals than JSC-1A. Therefore, all other things being equal, the -5M starting SSA should be lower than that of JSC-1A and it should not be affected as much by the heating.

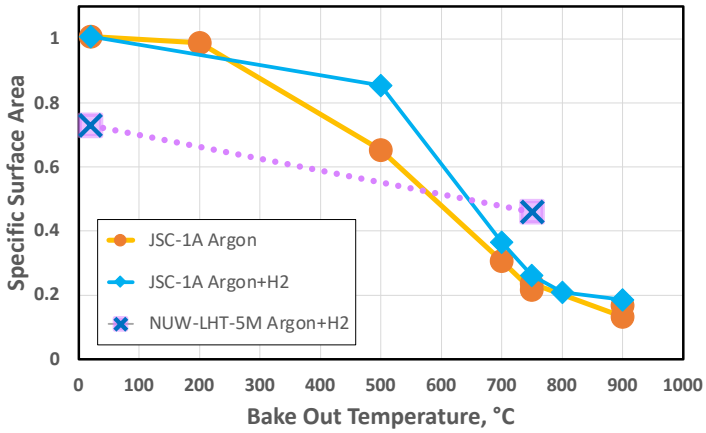

Figure 8.1. Specific surface area measured by BET versus baking procedure. "Argon" or "Argon+H2" refers to the flowing gas used during heating.

9. Shear, Cohesion, Angle of Internal Friction

The shear strength (σ_s) of the lunar regolith and its simulants was a key contributing factor to the net geomechanical properties of the material. The shear strength of the lunar regolith was driven by the PSD, particle morphology, and mineralogy and impacts the trafficability, bearing capacity, excavation mechanics, and flow characteristics of the lunar regolith. A common model used to quantify the shear strength of geologic materials is the Mohr-Coulomb Failure Criterion, a model that linearly relates normal stress (σ_n) to shear strength using the cohesion (c) and angle of internal friction (ϕ) as linear parameters. In turn cohesion and angle of internal friction are common inputs to computational models that simulate the mechanical behavior of rock and regolith.

Methods were given in the Appendix G.

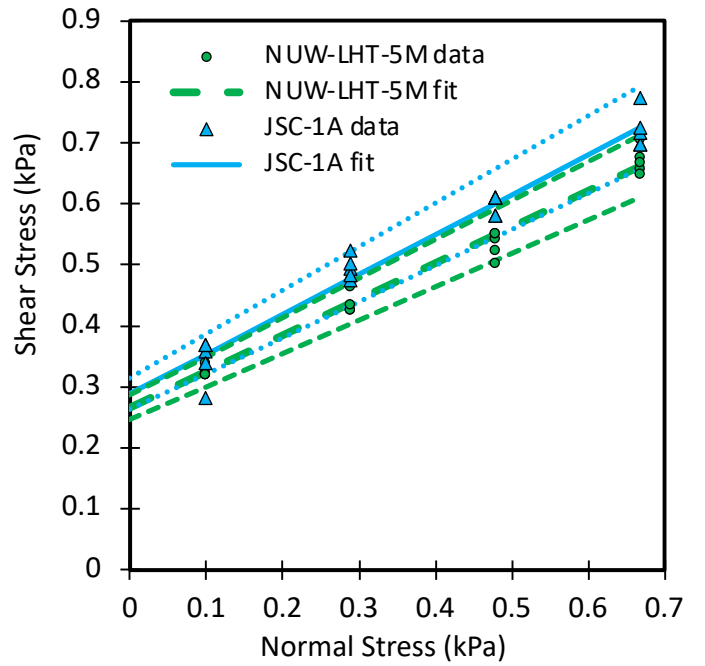

Figure 9.1. Shear strength and Mohr-Coulomb analysis of NUW-LHT-5M Test 1 at a nominal density of 1.265 g/cm^3 compared to JSC-1A at 1.480 g/cm^3. ±95% confidence levels for fits shown.

The results of linear regression analysis performed on the direct shear data from testing NUW-LHT-5M Test 1 according to the Mohr-Coulomb Failure Criterion were shown graphically in Figure 9.1. This analysis of NUW-LHT-5M Test 1 was to find the best-fit values of c and ϕ, along with their 95% uncertainties gives $c = 0.266 \pm 0.020$ kPa and $\phi = 30.69 \pm 2.68°$ with $R^2 = 0.975$. The average density of the simulant over the 20 total tests was 1.265 ± 0.0002 g/cm^3 (95% confidence). The results of the direct shear testing of NUW-LHT-5M Test 1 were shown graphically with the Mohr-Coulomb linear fit and 95% confidence intervals in Figure 9.1.

Estimates of the cohesion and angle of internal friction of lunar regolith

given by the Surveyor and Apollo models in Carrier et al. (1991) were both very slightly higher than those of NUW-LHT-5M Test 1 measured here, though the direct shear tests performed as part of this work were done at a low relative density and the shear strength of NUW-LHT-5M Test 1 will only increase at higher relative densities. It is expected that the cohesion and angle of internal friction ranges of NUW-LHT-5M Test 1 will overlap well with lunar estimates and measurements as density during testing is increased. The range of cohesion and angle of internal friction of lunar samples given by Carrier et al. (1972) envelop the corresponding parameter estimates given here, further indicating that NUW-LHT-5M Test 1 aligns well with the strength of lunar regolith samples. Work is ongoing to characterize the shear strength as a function of density so this assumption will be quantitatively evaluated when the relevant data are collected and analyzed (Dotson et al., 2023).

The cohesion and angle of internal friction of the standard lunar regolith simulant, JSC-1A were well-characterized and have wide ranges of values for both parameters. Cohesion estimates for JSC-1A generally fell between 0.1 to 2.5 kPa depending on sample density and methods used (McKay et al., 1994; Schrader et al., 2010). The angle of internal friction reported with these estimates of cohesion varied from 41.0° to 48.8°. It should be noted that the JSC-1 family of simulants are composed of basaltic cinders, meaning that they are better suited to serve as mare simulants. Whereas, NUW-LHT-5M Test 1 is a highlands simulant with different mineralogy than a basaltic mare simulant, and therefore, with different physical properties.

10. Densities

10.1 He Pycnometry Density

Density, ignoring pore space between particles, of the NUW-LHT-5M has been measured using helium (He) pycnometry, Table 10.1. Values ranged between 2.81 and 2.838 kg/m^3. This compared to 2.90 kg/m^3 for JSC-1A and 2.89 kg/m^3 for NU-LHT-4M. The high-glass, low-Fe content and the vesicular nature of the glass were presumed to account for -5M's slightly lower values. As noted above, specific surface area can be sensitive to the thermal history of a simulant. It is conjectured, this may be also true for pycnometry values.

10.2 Bulk, or Minimum Index Density

Table 10.1. Density in kg/m^3, using helium, for NUW-LHT-5M and JSC-1A. UTSA measurements were done after drying the samples at least 18 hours at 110 °C. 10 to 155 iterations of each measurement were made. (1) As received. (2) Baked per Wilkerson et al. (2023).

UTSA	NUW-LHT-5M HQ Glass	2731
	NUW-LHT-5M [Test 1]	2824
	NUW-LHT-5M [Test 2]	2813
	JSC-1A	2895
Alfred	NUW-LHT-5M (1)	2838
	NUW-LHT-5M (2)	2842

Herein bulk density is the minimum density, $\boldsymbol{\rho}_{\min}$, which can be achieved by "raining" the material into the vessel. Conceptually, this measurement included both the void between particles and within particles, if any. The measurement can be sensitive to the handling history of a sample. Values for this measure for NUW-LHT-5M were given in Table 10.2. The -5M values were significantly lower than those of JSC-1A and even -4M. This may be a combination of the geometry of the particles, vesicles in the synthetic glass, mineralogical, and elemental differences between the simulants.

10.3 Tap Density

Tap density was measured by filling a graduated cylinder, then measuring sample height within the cylinder after a

Table 10.2. Bulk density (minimum index density) in g/cm^3 for NUW-LHT-5M, NU-LHT-4M, and JSC-1A. (1) Alfred University date measured after a single tap to the containing cylinder. (2) Baked per Wilkerson et al. (2023).

UCF	NUW-LHT-5M	1.264
Alfred (1)	NUW-LHT-5M	1.25
	NUW-LHT-5M (2)	1.32
	NU-LHT-4M	1.42
	NU-LHT-4M (2)	1.36
	JSC-1A	1.52
	JSC-1A (2)	1.52
JSC	NUW-LHT-5M	1.27 - 1.30
UTEP	NU-LHT-4M	1.522
	JSC-1A	1.6

given number of mechanical tapes to the cylinder. As the number of taps increased, the packing in the sample increased. Measurements for tap density, as a function of the number of taps, for NUW-LHT-5M, NU-LHT-4M, and JSC-1A were given in Table 10.3. Those values may be compared to density measured by He pycnometry. The table also gave the densities of simulant after baking the simulant to 750 °C (Wilkerson et al., 2023). For this table a theoretical density, the inverse of porosity as used by geologists, was defined as 100 x (measured/pycnometric).

The table showed very modest changes in pycnometric density as a function of simulant composition. In contrast the difference in the measured densities at the beginning were significant, and, that difference disappeared as vibrations settles the simulants. We suggested this pattern has to do with the relative abundance of particles with higher Form Factors, as seen in NUW-LHT-5M and NU-LHT-4M compared to JSC-1A (Figure 7.1 and Wilkerson et al., 2024).

Table 10.3. Tap density (g/cm^3) and porosity (%) of NUW-LHT-5M, NU-LHT-4M, and JSC-1A following taps to the enclosing cylinder. (1) As received. (2) Baked per Wilkerson et al. (2023). Theoretical is 100 × (measured bulk density divided by pycnometric value).

Simulant Heat Treatment	Tap Count ->	1		3,000		6,000		9,000	
	Pycnometric	Measured Bulk	Theoretical	Measured Bulk	Porosity	Measured Bulk	Porosity	Measured Bulk	Porosity
JSC-1A (1)	2.90	1.52	52.4	1.99	68.6	2.04	70.3	-	-
JSC-1A (2)	2.97	1.52	51.2	2.01	67.7	2.05	69.0	-	-
NU-LHT-4M (1)	2.89	1.42	49.1	2.01	69.6	2.07	71.6	-	-
NU-LHT-4M (2)	2.93	1.36	46.4	1.95	66.6	2.00	68.3	-	-
NUW-LHT-5M (1)	2.838	1.25	44.0	1.95	68.7	-	-	1.99	70.1
NUW-LHT-5M (2)	2.842	1.32	46.4	1.93	67.9	-	-	1.97	69.3

11. Magnetic Susceptibility

Four ten-gram splits of NUW-LHT-5M were each measured three times, measuring both low and high frequency conditions using a Bartington Magnetic Susceptibility Meter MS2B/MS3 system for a total of 24 values, Table 11.1. Following Rochette et al. (2010), the values were corrected based on measured bulk density and expressed here as logχ MS, with χ in 10^{-9} m^3 kg^{-1}. The NUW-LHT-5M values ranged from 2.871–3.027. The values given in Rochette et al. (2010) for lunar regolith samples were about 4.4, though other groups of data fall around the -5M values.

Table 11.1. Magnetic susceptibility of NUW-LHT-5M, NU-LHT-4M, NU-LHT-4M, and JSC-1A, and Apollo soils. Magnetic susceptibility values are in logχ, in 10^{-9} m^3 kg^{-1}, with the average, standard deviation (s.d.), number of samples (N), and number of subsamples (n). Apollo soils data from Rochette et al. (2010).

	Mean	s.d.	N	n
NUW-LHT-5M	2.92	0.06	4	24
NU-LHT-4M	2.86	0.01	3	18
NU-LHT-2M	3.03	0.01	3	18
JSC-1A	3.37	0.01	3	18
Apollo Soils	4.39	0.20	18	18

12. Dielectrics

12.1 Low Temperature

The NUW-LHT-5M permittivity and permeability data were published in Barmatz et al. (2023). For comparison, data for JSC-1A, NU-LHT-4M, the glass used in -5M, and Stillwater anorthosite and pyroxenite were included in that paper. A principle finding of this work was heating this simulant purely by microwaves, and by extension the lunar highland regolith, was difficult to achieve within the temperature range 23 °C to 250 °C. The data also demonstrated that permittivity was sensitive to the bulk density of the material.

12.2 High Temperature Permittivity

Figure 12.1 showed the real and imaginary parts of the permittivity (ε' and ε" respectively), and Figure 12.2 showed the half power depth (HPD) and loss tangent (tanδ = ε"/ε') of NUW-LHT-5M and JSC-1AC. The real part of the permittivity, ε', reflected the polarization, which is a sum of many mechanisms such as space charge and ionic polarization. The imaginary part (loss factor) captures the effect of charge currents and the timelag of polarization mechanisms, which led to volumetric heating. It was clear in Figure 12.1 that JSC-1AC, a mare simulant, had greater polarization and greater dielectric loss than NUW-LHT-5M, a highland simulant. It could be understood intuitively that, as a material heated and absorbed microwaves more vigorously, the penetration depth decreased, as indicated in Figure 12.2, the ratio of the loss factor to polarization, Figure 12.2, was also a useful way to compare materials. However, the primary data needed for modeling was ε' and ε". A thorough analysis of dielectric properties at temperatures needed for understanding microwave heating of a series of highlands simulants will be presented in a follow-on publication to work performed by Barmatz et. al. (2023).

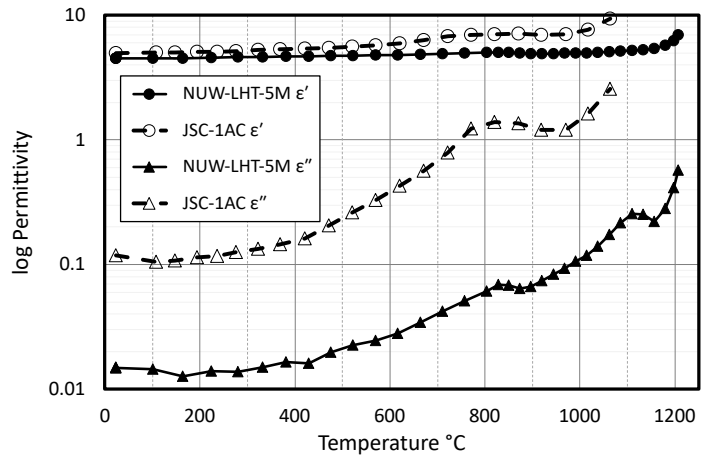

Figure 12.1. ε′ and ε″ at 2466 MHz for NUW-LHT-5M and JSC-1AC versus temperature during heating. The permittivity axis uses a log scale. Heating was terminated close to the temperature at which permittivity values began to change rapidly, interpreted as the beginning of melting. Compare with data in Section 14. Markers are on measured points. Values during cooling plot above the curves given, demonstrating presumably permanent change (particle fusion) was done to the simulant. Density of -5M started at 2.09g/cc and ended at 2.2g/cc. JSC-1AC started at 2.09g/cc and ended at 2.19g/cc.

Understanding of these data was assisted by coordination with the data in Section 14.1. At a material-dependent temperature, both ε′ and ε″ rapidly increased. Physically, this was due to melting of the crystallized glass and of the crystalline rock components.

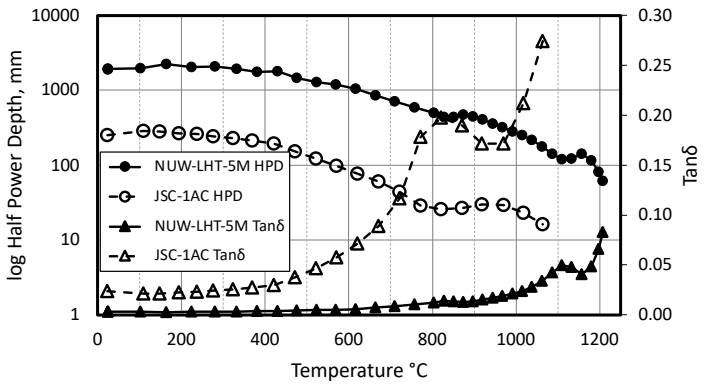

Figure 12.2. Log of Half Power Depth (HPD) and tanδ at 2466 MHz for NUW-LHT-5M and JSC-1AC versus temperature during heating. Markers are on measured points. HPD is depth in millimeters. JSC-1A is the coarse variant of the JSC-1A products (Gustafson, 2009).

Therefore, several important conclusions were drawn from these data. First, the utility of microwave heating of a simulant patterned after Apollo 16 material was problematic until the material's temperature rose significantly above lunar surface norm. Second, at some point the HPD dropped rapidly; therefore, without adequate thermal feedback and control, further energy input could lead to run-away conditions. Third, as the HPD was considered sensitive to the iron content of the simulant, new dielectric data may be desired for the currently produced -5M, which had higher iron than the Test 2 material.

The full reports of dielectric measurements made by Microwave Properties North for each material were included in the Appendix H as "S 12.2 JSC-1AC.doc" and "S 12.2 NUW-LHT-5M.docx". Each of these reports gave color photographs of the simulant after the heating and -5M before heating.

13. Spectroscopy

Methods used to obtain the spectroscopy data were given in the Appendix I.

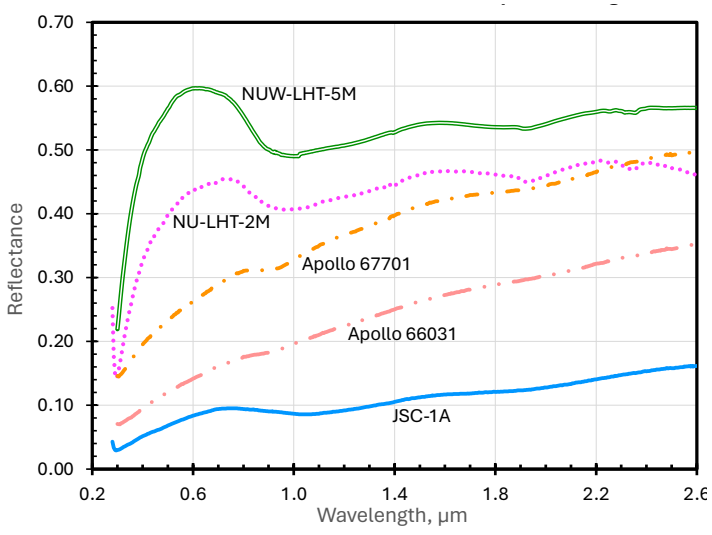

Figure 13.1. VNIR reflectance spectra in µm of NU-LHT-5M, JSC-1A and bulk Apollo highland regolith samples 66031 (I_s/FeO = 102; mature) and 67701 (I_s/FeO = 39; immature), all measured in RELAB.

The visible and near-infrared (VNIR) reflectance spectrum of NU-LHT-5M (Figure 13.1) had diagnostic absorption bands near 1.0 and 2.0 µm indicative of low-Ca pyroxene (orthopyroxene). The 1.0 µm was wider likely due to the presence of plagioclase, which had a diagnostic absorption band near 1.25 µm. These VNIR spectral features were consistent with spectra from the Moon's anorthositic highlands as seen in remote sensing observations of the Moon and in laboratory reflectance measurements of Apollo bulk regolith samples returned from the Moon. Observed differences between the VNIR reflectance spectra of NUW-LHT-

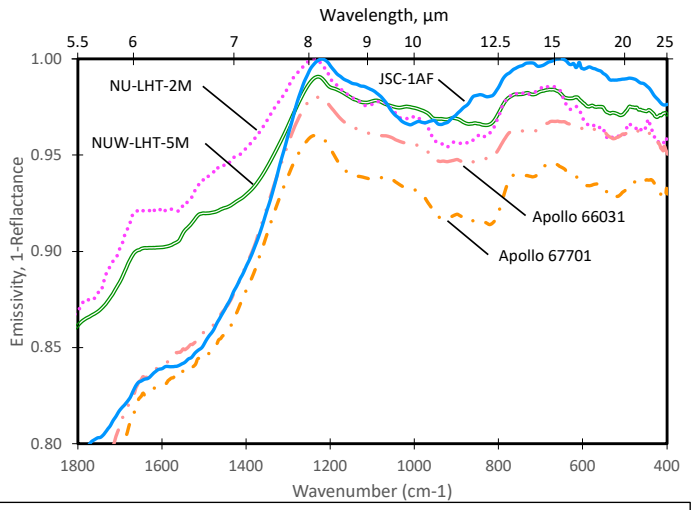

Figure 13.2. MIR reflectance spectrum in µm of NUW-LHT-5M, NU-LHT-2M, JSC-1AF measured in RELAB plotted as emissivity (1 – reflectance). Emissivity spectra of bulk Apollo highland regolith samples 66031 (I_s/FeO = 102; mature) and 67701 (I_s/FeO = 39; immature) measured in ALEC (Donaldson Hanna et al., 2017). NUW-LHT-5M was measured by RELAB. NU-LHT-2M and JSC-1AF are from Martin et al. (2012).

5M and Apollo regolith samples 66031 and 67701 were due to the presence of space weathering products (i.e., nanophase and microphase Fe and agglutinates). As seen in the spectra of two regolith samples of different maturities (66031 is a mature regolith with I_s/FeO = 102 and 67701 was an immature regolith with I_s/FeO = 39), when a regolith experienced increasing amounts of space weathering the VNIR spectra were changed in three main ways: (1) the overall reflectance (albedo) was reduced, (2) the slope of the spectrum became redder, and (3) the diagnostic absorption bands became reduced. Thus, the NU-LHT-5M spectrum was similar to the regolith sample that had experienced little to no space weathering, consistent with the original design of the NU-LHT-series.

The mid-infrared (MIR) reflectance spectrum of NU-LHT-5M (Figure 13.2) had diagnostic spectral features similar to features observed in MIR emissivity spectra of Apollo regolith samples 66031 and 67701 measured under ambient atmospheric and temperature conditions (Donaldson Hanna et al., 2017). The emissivity maximum observed near 1,200 cm^{-1} in all the spectra was the Christiansen feature (CF), which had been shown to be indicative of bulk composition (Conel, 1969). While the shape of the CF was different between the Apollo regolith samples and the NU-LHT-5M, the position of the maximum was similar. The CF shape difference between the Reflectance Experiment Laboratory (RELAB) biconical reflectance spectrum and the ambient emissivity spectra was likely due to the difference in measurement techniques, as only hemispherical reflectance spectra were known to be directly comparable to emissivity spectra. The other observed spectral features (i.e., the minima) related to the fundamental molecular vibration bands and the transparency feature (e.g., Salisbury and Walter, 1989) were also observed at similar positions when comparing the NH-LHT-5M and Apollo regolith sample spectra. This suggested the makeup of the simulant was similar to mineralogical makeup of the anorthositic highlands. We did observe differences in the slope between ~1,800 to 1,300 cm^{-1} and the depths of the vibration bands and transparency features. However, these differences were easily related to effects of particle size, albedo, or porosity.

Spectral comparisons can also be made to other lunar regolith simulants. The VNIR reflectance spectra of both NU-LHT-2M and NUW-LHT-5M were similar to one another with diagnostic absorption bands near 1.0 µm and 2.0 µm, indicative of low-Ca pyroxene and plagioclase. The only difference was albedo, with NU-LHT-5M having a higher albedo than NU-LHT-2M. In

contrast, the 1.0 µm band in the JSC-1A were at longer wavelengths suggesting a high-Ca pyroxene composition. Additionally, the JSC-1A spectra were lower albedo than the NU-LHT-2M and NU-LHT-5M and had lower spectral contrast in the 1.0 and 2.0 µm bands. At MIR wavelengths, the positions of the CF and the fundamental vibration bands (~1,100–900 cm^{-1} and ~750–400 cm^{-1}) in NUW-LHT-5M were at similar wavelengths to those in NU-LHT-2M, demonstrating the similarities in bulk composition between the two simulants. Two key differences were at higher frequencies (> 1,300 cm^{-1}) and near 850 cm^{-1}. Both of which were related to differences in PSD, suggesting the aliquot of NU-LHT-5M was composed of a greater abundance of finer particulates than the NU-LHT-2M aliquot. The diagnostic MIR spectral features observed in the JSC-1AF spectrum were at different wavelengths than features in the spectra of NU-LHT-5M and NU-LHT-2M, highlighting the differences in composition between the simulants.

14. Melt Properties

The behavior of lunar regolith at high temperatures was important to various proposed ISRU-related processes, such as oxygen recovery, construction, and metals extraction. Therefore, for process development and system technology development, it would be desirable to understand the thermal behavior of NUW-LHT-5M at temperatures approaching and exceeding liquidus.

Methods used to obtain data in this section were given in Appendix J. Also see Patridge et al., 2024 for more information.

14.1 Differential Scanning Calorimetry

Differential scanning calorimetry (DSC) data, apparent heat capacity ($Jg^{-1}K^{-1}$) against temperature for -5M and the glass used in the simulant, and data for JSC-1A were given in Figure 14.1. These, and other data, were acquired on heating and cooling at 30 °C/minute. The apparent heat capacity consisted of the "sensible" heat required to make atoms vibrate more at higher temperatures and the latent heat of phase transitions, such as exothermic crystallization and endothermic melting. In the figure

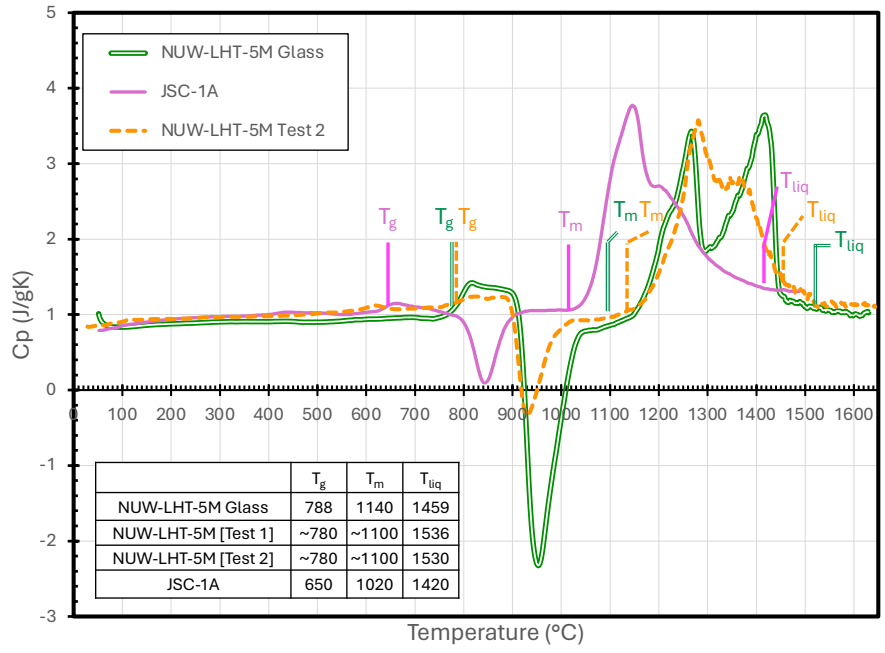

	T_g	T_m	T_{liq}
NUW-LHT-5M Glass	788	1140	1459
NUW-LHT-5M [Test 1]	~780	~1100	1536
NUW-LHT-5M [Test 2]	~780	~1100	1530
JSC-1A	650	1020	1420

Figure 14.1. DSC transformation temperatures. The glass transitions, Tg, melting onset, Tm, and liquidus, Tliq, for NUW-LHT-5M and its glass. JSC-1A data from Whittington and Parsapoor, 2022.

endothermic processes were positive, so heat capacities were normally positive. A negative apparent heat capacity meant the sample is releasing more heat by exothermic crystallization than was required to heat it (i.e., it was spontaneously heating) a process known as recalescence (Whittington and Sehlke, 2021). The approximate values of major thermal transition features were also shown for each material.

At ~620 °C -5M showed a weak endothermic peak, probably due to decomposition of one or more volatile-bearing phases within the simulant. As expected from the chemistry, the glass in highland simulant went through the glass transition, T_g, at a significantly higher temperature than the mare simulant. Above the glass transition, the liquid component of each simulant underwent crystallization, resulting in an exothermic trough in the apparent C_P curve. The now mostly to fully crystalline simulant began melting at T_m, which again was much higher for both -5M and its glass component than for JSC-1A. Over the melting interval, between T_m and the liquidus T_{liq}, the large endothermic peaks represented the latent heat of fusion. Both the -5M and JSC-1A simulants showed strong peaks with high-temperature shoulders, probably representing melting of newly-formed crystals followed by melting of larger crystals that were present in the simulants to begin with. The simulants have compositional differences between their glass components and the crystalline mineralogy, just as lunar agglutinate glasses have a different bulk composition to the crystalline mineralogy associated with them (Baker et al., 2020). The strongly bimodal melting pattern of the -5M glass suggested that two different crystal populations grew during heating. The heights of these peaks and the values of T_g, T_m, and T_{liq} would all be lower if determined at lower heating rates, but the latent heat of melting should be similar.

When the melted -5M material was quench-cooled and remelted, the second stage glass began and ended crystallization ~ 75 °C hotter than the original glass. One possible reason for this may be impurities, such as small metallic iron particles in the original glass, providing nuclei for crystallization on first heating. These nuclei would be completely melted into the glass on heating to 1,650 °C. The lack of significant nuclei in the quenched product was demonstrated by the lack of DSC features as it cooled. The heating data for remelted -5M and the remelted -5M glass were very different. There was a remarkable difference in behavior for relatively small changes in composition. Collectively, the DSC data provided additional insight into the high-temperature dielectric data.

Additional DSC features of NUW-LHT-5M and its glass were shown in Appendix J Figures I1 and J2.

14.2 Viscosity

Viscosity data were fitted to the Vogel-Fulcher-Tammann (VTF) equation (Vogel, 1921) of the form $\log \eta = A + B/(T\text{-}C)$ where viscosity, η, is in Pas and T is in K (Table 14.1). The best fit equations and root mean squared deviations were also given.

Table 14.1. Viscosity fitted to the Vogel-Fulcher-Tammann equation for NUW-LHT-5M, -5M glass, and JSC-1A. JSC-1A fit includes data at 925 °C < T < 990 °C

	log η	number	rmsd
NUW-LHT-5M Glass	-2.92 + 3162/(*T*-881.4)	8	0.01
NUW-LHT-5M Test 1	-3.05 + 4442/(*T*-631.8)	26	0.02
NUW-LHT-5M Test 2	-2.17 + 2555/(*T*-910.9)	16	0.01
JSC-1A	-3.86 + 4460/(*T*-644.8)	29	-

Although the VFT fits for Test 1 and Test 2, the two tests have different numerical coefficients, and the

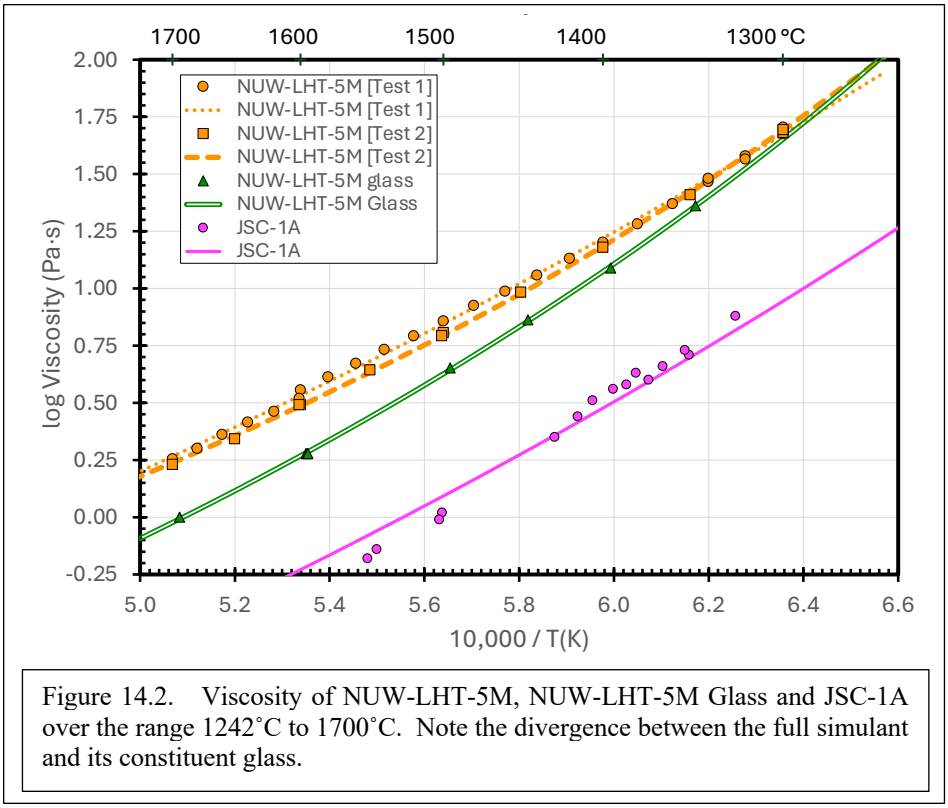

Figure 14.2. Viscosity of NUW-LHT-5M, NUW-LHT-5M Glass and JSC-1A over the range 1242˚C to 1700˚C. Note the divergence between the full simulant and its constituent glass.

resulting curves were generally within 0.06 log units (equivalent to a 15% difference in viscosity) (Figure 14.2). The molten NUW-LHT-5M was more viscous than its constituent glass at all temperatures measured, by 0.25 log units at 1,700 ˚C and by ~0.1 log units at 1,350 ˚C (equivalent to differences of ~75 and 25% in viscosity, respectively). The molten NUW-LHT-5M was substantially more viscous than JSC-1A by about 0.75 log units (equivalent to more than a factor of five difference in viscosity) across the entire measurement range. This is unsurprising because JSC-1A was a basaltic material, i.e. lower silicon content, and better suited to simulate mare than highlands compositions.

14.3 Thermal Diffusivity and Conductivity

Thermal diffusivity was determined for NUW-LHT-5M glass after it had been remelted at 1,650 °C and quenched (Figure 14.3). Based on three glass disks the best-fit average value of thermal diffusivity of D (mm^2s^{-1}) = 13.96 $T^{-0.6003}$ + 3.172 x 10^{-4} T, where T was in K. The range of values measured at a given temperature was always 0.02 mm^2s^{-1} or less, and the root mean square deviation between the equation and the average measurement at each temperature was less than 0.002 mms^{-1}.

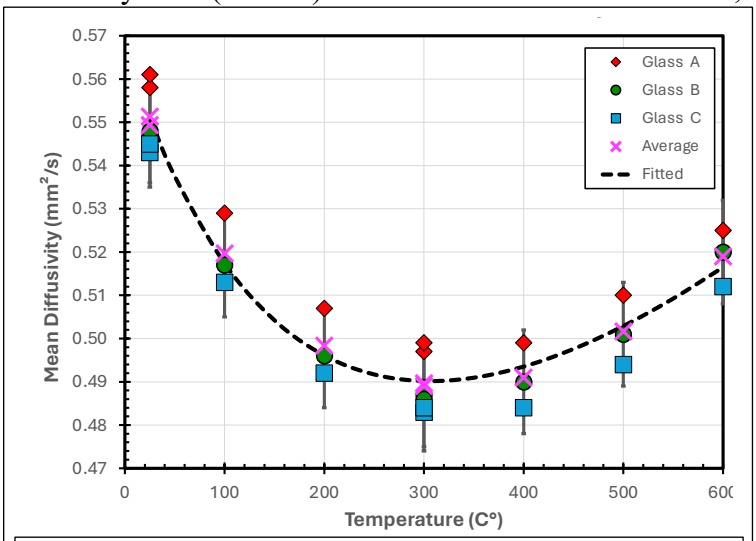

Figure 14.3. Thermal diffusivity of 3 samples of glass made from NUW-LHT-5M.

Thermal conductivity of the glass was calculated at each temperature as the product $k = D\rho C_P$. We calculated k for each temperature at which D was measured, using density adjusted for temperature, assuming a density of 2,753 kgm^{-3} at 298 °K with a volumetric thermal expansion coefficient of 1.53 x 10^{-5}

$^{\circ}K^{-1}$ and heat capacity equation described above. The calculated values of *k* were then fitted with the following equation:

$$k\ (Wm^{-1}K^{-1}) = 1.130 + 3.84x10^{-4}\ T - 7.16x10^{-3}\ T^{-2} + 0.141\ T^{-0.5},$$

where *T* was in K (RMSD = 0.003 $Wm^{-1}K^{-1}$). This equation was only valid up to the glass transition, above which the thermal diffusivity and conductivity of feldspathic and basaltic liquids was usually lower than for glass of the same composition (Hofmeister et al. 2009; Sehlke et al. 2020).

15. Thermal Gravimetric and Evolved Gas Analysis

When lunar regolith simulants were heated to a significant range and a number of volatiles can be evolved, the LOI section above (Wilkerson et al., 2023; Petkov and Voecks, 2023). A significant percentage of these volatiles were assumed to be non-lunar in nature. Thermogravimetry, Evolved Gas Analysis, and Differential Scanning Calorimetry analyses were done on NUW-LHT-5M to characterize its evolving volatiles.

These tests heated the simulant to 1,400 °C in a 30 mbar He atmosphere, evolving ~1 wt%; by which point the samples had melted. This temperature was substantially higher than temperatures used to obtain the LOI values reported herein, 0.25–0.6 wt%; probably because LOI measurements heat to ~1,000 °C in terrestrial atmosphere.

Analysis of gas evolution from NU-LHT-4M and JSC-1A has shown the processes involved to be complex and little understood. Given the use of the same Stillwater rocks as -4M, this was also true for -5M. Here we assumed m/z 18 is H_2O and m/z 44 is CO_2. What we provided here was an initial evaluation of our results. The primary volatile released was H_2O, with a low temperature peak (150 °C). This was likely due to adsorbed water, then multiple high-temperature peaks between 600–1,050 °C that could have resulted from dehydroxylation of clays or various non-lunar minerals present in small amounts. The candidate mineralogy included talc, sericite serpentine, and clinozoisite, all of which were known to be present in the Stillwater Complex. Of the simulant materials measured, H_2O was the most common and abundant species. There was also a CO_2 peak around 600 °C, which may be consistent with the decomposition of calcite, $CaCO_3$, or dolomite, $CaMg(CO_3)_2$, both of which were reported from the Stillwater rocks used to make the simulant (Boudreau, 2016) and Table 4.1.

The overall behavior was similar to JSC-1A, with one notable difference: JSC-1A had its primary CO_2 peak around 650 °C, in addition to peaks at lower temperature similar to NUW-LHT-5M. The higher temperature peak could be from calcium carbonate decomposition or a more crystallized Ca/Mg carbonate.

The Appendix K included plots of m/z 18, 28, 32, and 44 values.

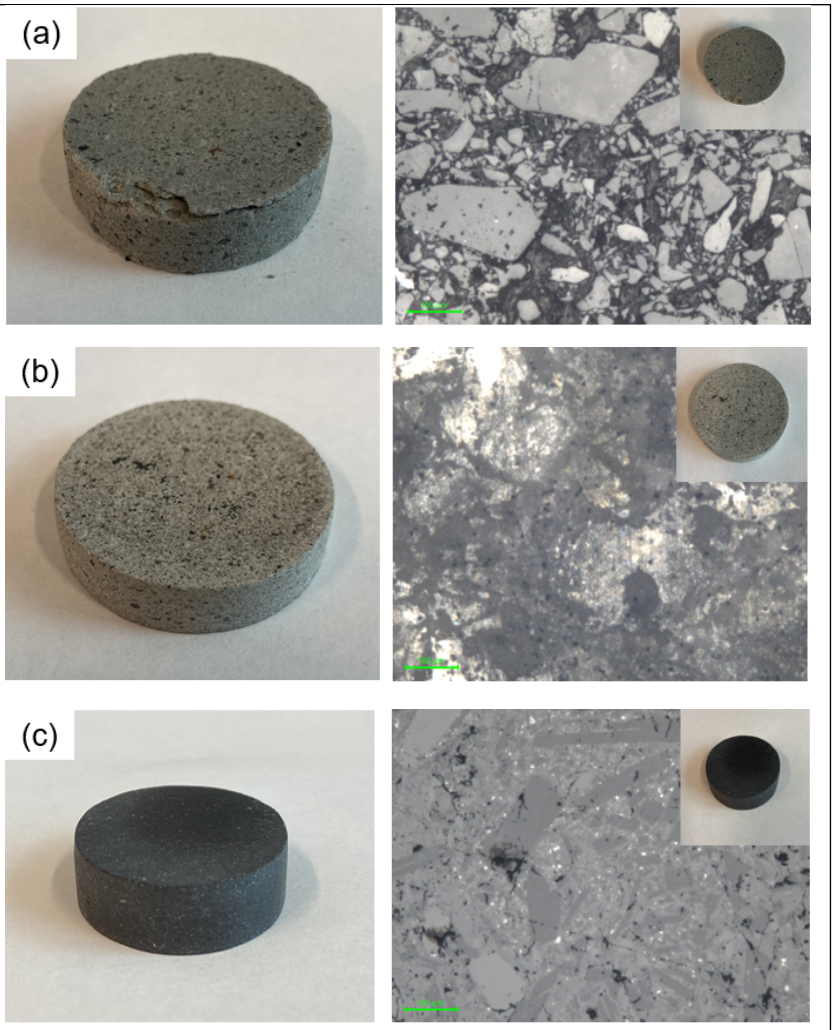

Figure 16.1. Spark Plasma Sintered specimens and resulting optical microscope images. (a) NUW-LHT-5M processed at 800 °C. (b) NUW-LHT-5M processed at 1,000 °C. (c) JSC-1A processed at 800 °C. Microscope image scales are 100 µm.

16. Spark Plasma Sintering

The spark plasma sintering (SPS) method has been used to densify ceramic and metallic materials. Unlike conventional sintering processes, SPS employs a pulse electric current, an applied uniaxial pressure, and a rapid heating rate in a vacuum atmosphere to sinter ceramic or metal powders. Potentially, it could provide many advantages due to the combined effect of electric field and applied pressure, such as high heating (as high as 1,000 ºC /min) and cooling rates, short processing times (i.e., minutes), low sintering temperatures, and a high density of sintered products (nearly 100% theoretical density). For examples see Munir et al. (2006), Santanach et al. (2011), and Guillon et al. (2014). The SPS method has been applied to several lunar regolith simulants (Zhang et al. 2020, 202l; Phuah et al. 2020; Jeon and Kim 2024).

Results presented in Figure 16.1 indicated that NUW-LHT-5M sintered at 1,000 °C and JSC-1A sintered at 800 °C were successful with a clean surface, which demonstrates that the necessary densification was achieved. The NUW-LHT-5M at 800 °C presented thin plate-shaped horizontal cracks normal to the direction of uniaxial pressure. Regarding NUW-LHT-5M cases, as the sintering temperature increased from 800 °C to 1,000 °C, scanning electron microscopic images presented a more homogeneous matrix which might be related to phase changes. In addition, JSC-1A and NUW-LHT-5M specimens showed different microstructures related to the different mineralogical compositions. Appendix L includes detailed methods and relevant references to the SPS.

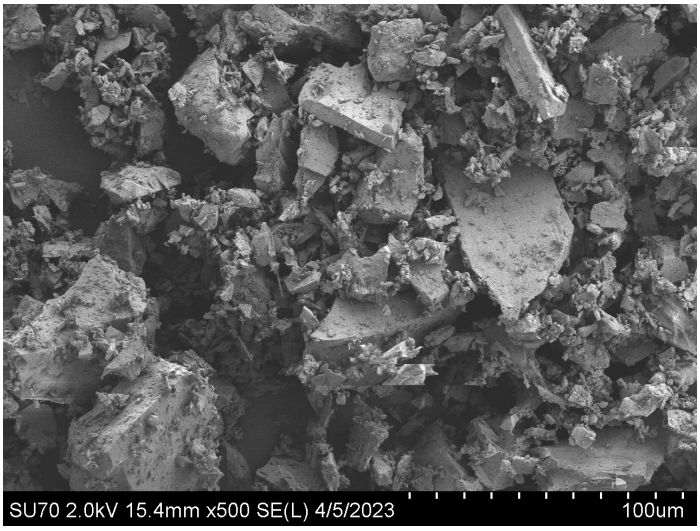

Figure 17.1. Manufacturer's SEM image of simulant after drying.

17. Scanning Electron Microscopy

In normally handled simulant, we have observed that larger particles of JSC-1A normally have many smaller particles weakly adhering. This can readily be seen by reflected light microscopy, as well as SEM images made of unmounted material. The adhesion appeared to be stronger after drying or baking of the simulant. As seen in Figure 17.1, such adhesion also occurred in NUW-LHT-5M. The significance of this behavior will depend on the nature of the simulant's use. For example, sieved particles may have more fines than expected.

18. Discussion

Throughout this paper we did not attempt to offer explanations for the data presented. For example, the subtleties of interpretation, explanation of physical processes, limitations to accuracy, and relationships with other data were not the purview herein. In part this is because such points, while necessary in the long run, were primarily of great interests to scientists and topic specialists. Rather, we have chosen conciseness and utility for the general user at the acknowledged risks inherent in ignoring such details.

Tests of NUW-LHT-5M revealed a quality lunar highlands simulant was available for proving out technology development of ISRU, supporting construction, and outfitting of a lunar economy, especially applications that involve high-temperature processing.

18.1 Sampling Error

We remarked multiple times herein that NUW-LHT-5M was prone to sorting. As demonstrated by Figure 3 of Rickman et al. (2013), this was not unique to -5M. The senior author has seen sorting in all simulants examined for it. For planetary simulants sorting can be a significant contributor to the general problem of potentially inadequate sample mass (Rawle, 2015 and references there in). While sampling error was a commonly understood problem in the mining industry, it may not be adequately appreciated by those working with lunar simulants. Insidiously, unless homogenized prior to correctly done sampling, any simulant aliquot would likely to be biased; and, once permanently separated, there would be no way for the aliquot to recover the original mixture. This added an unknown amount of potential error to measurements of the simulant. As a practical matter sampling error was normally ignored, effectively assuming it to be of minor importance. There was a lack of data and technique to do otherwise.

18.2 Limitations to Lunar Simulants

Lunar simulants, in particular highland simulants, have a number of common shortfalls in perfectly reproducing lunar norms. For example NUW-LHT-5M, as with all highland simulants we have studied, did not reproduce the grain size distributions found in lunar materials. There were no commercially available sources for the correct, mixed mineralogy and possessing either particle or grain sizes matching lunar norms. The crystal sizes in the terrestrial sources for the mineralogy used in highland lunar simulants (e.g., Stillwater, Greenland, and Shawmere) were measured in millimeters, not microns. One consequence was simulants cannot replicate the liberation behavior that will occur in lunar material. Producers of highland simulants have, appropriately, chosen to target reproduction of the bulk mineralogy, without attempting to replicate grain sizes. It appears that if grain size in the particles is important for some application, such as mineral beneficiation, efforts to make fully synthetic mineralogy will be needed (Weinstein et al., 2012; Cooper et al., 2023). Synthesis of the plagioclase has proven to be relatively easy, in sharp contrast to synthesizing the pyroxenes without unwanted phases.

Related to crystalline sizes, simulants also did not reproduce what geologists refer to as "texture." The term included all aspects of spatial distributions, either 2D or 3D. A well-known example was the difficulty of making particles that fully reproduced lunar agglutinates, see Figure 11b of Wilkerson et al., 2024). Shattering of particles, common in lunar samples, was problematic to create in simulants. Particles in the size range of 20 μm, with complex grain structures were common in lunar samples, but not readily created for simulants.

Because the geologic origins of the rocks were different, in finer details the mineralogy of simulants did not match that of the lunar templates. To illustrate, the simulants frequently have quartz and pyrite at abundance levels that were too high. The reverse was also true; the lunar mineralogy (Papike et al., 1991) included species, such as maskelynite and armalcolite, that were not found in the feedstocks used to make simulants. In like manner to the minor and trace minerals, if the trace elements in a simulant reproduce a desired abundance it is largely fortuitous.

Finally, the inability to reproduce space weathering in useful amounts sets limits on the spectroscopic accuracy of simulants (Figures 13.1 and 13.2). It also affected the geologic variable known as the maturity index (Morris, 1978). When checked, JSC-1A was found to be very different than lunar samples in this respect. Presumably, this would be also true of -5M.

All of these features limited the accuracy of a simulant and for the most part were out of reach for demonstrated technology. The engineering significance of these differences were, to a large extent, hard to judge. This mades it problematic for a producer to invest in technology development if there would be no clear need. The hope is that the simulants currently available are "good enough" to get us safely and productively onto the Moon.

19. Acknowledgments

The authors of this work gladly acknowledge the leadership of Dr. Douglas Benjamin Stoeser (decd.), formerly of the USGS in the design of the first simulants in the NU-LHT-series. We also acknowledge the role of Dr. Stephen Wilson, USGS retired, for leading and doing the work of

grinding, milling, mixing, and early characterizations of all NU-LHT-series members, save that of -5M. They shared the vision and knew how to make it reality.

We gratefully recognize the active cooperation and labor generously donated by Sibanye-Stillwater over multiple years, without which NASA's efforts to create these simulants would not have been possible. The authors appreciate the funding provided by NASA's Space Technology Mission Directorate via the MMPACT project to develop this material.

The senior author personally thanks his wife, Pamela, and granddaughter, Sophia, for the substantial reading, editing, and organization work they have done on this paper, which enabled the author to circumvent handicaps due to a brain hemorrhage.

20. References

Abbireddy, Chandra O. R., and Chris R. I. Clayton. “A Review of Modern Particle Sizing Methods.” *Proceedings of the ICE - Geotechnical Engineering* 162, no. GE4 (January 2009): 193–201. https://doi.org/10.1680/geng.2009.162.4.193.

Aird, Hannah M., Katherine M. Ferguson, Malia L. Lehrer, and Alan E. Boudreau. “A Study of the Trace Sulfide Mineral Assemblages in the Stillwater Complex, Montana, USA.” *Mineralium Deposita* 52, no. 3 (March 2017): 361–82. https://doi.org/10.1007/s00126-016-0664-x.

Ayling, Bridget F, Peter Rose, E. Zenach, Peter S Drakos, and Susan Petty. “QEMSCAN° (Quantitative Evaluation of Minerals by Scanning Electron Microscopy): Capability and Application to Fracture Characterization in Geothermal Systems.” In *Thirty-Seventh Workshop on Geothermal Reservoir Engineering*, Vol. SGP-TR-194, 2012. https://pangea.stanford.edu/ERE/pdf/IGAstandard/SGW/2012/Ayling.pdf.

Baker, A. E., B. L. Jolliff, C. N. Yasanayake, B. W. Denevi, and S. J. Lawrence. “Lunar Agglutinate Glass Compositions and Comparison to Soil Grain-Size Fractions,” 1321. Virtual, 2020. https://ui.adsabs.harvard.edu/abs/2020LPI....51.1321B.

Barmatz, Martin, David Steinfeld, Jonathan Batres, Hsin-Yi Hao, Douglas Rickman, and Holly Shulman. “Microwave Permittivity and Permeability Measurements on Lunar Simulants at Low Temperatures.” *Advances in Space Research*, 2023, S0273117723006890. https://doi.org/10.1016/j.asr.2023.08.041.

Bell, S K, K H Joy, J F Pernet-Fisher, and M E Hartley. “QEMSCAN as a Method of Semi-Automated Crystal Size Distribution Analysis: Insights from Apollo 15 Mare Basalts.” *Journal of Petrology* 61, no. 4 (October 18, 2020): egaa047. https://doi.org/10.1093/petrology/egaa047.

Boudreau, Alan E. “The Stillwater Complex, Montana – Overview and the Significance of Volatiles.” *Mineralogical Magazine* 80, no. 4 (June 2016): 585–637. https://doi.org/10.1180/minmag.2016.080.063.

Butler, J. C., G. M. Greene, and E. A. King Jr. “Grain Size Frequency Distributions and Modal Analyses of Apollo 16 Fines.” *Lunar and Planetary Science Conference Proceedings* 4 (January 1, 1973): 267.

Byung-Hyun, Ryu. “Basic Study for a Korean Lunar Simulant (KLS-1) Development,” 2015. http://ocean.kisti.re.kr/downfile/volume/kgts/GJBGC4/2015/v31n7/GJBGC4_2015_v31n7_53.pdf.

Cadenhead, D. A., M. G. Brown, D. K. Rice, and J. R. Stetter. “Some Surface Area and Porosity Characterizations of Lunar Soils.” In *Proc. 8th Lunar Sci. Conf.*, Volume 1. (A78-41551 18-91):1291–1303. Houston, TX: Pergamon Press, Inc., 1977. http://adsabs.harvard.edu/abs/1977LPSC....8.1291C.

Carrier, W. David III. “Particle Size Distribution of Lunar Soil.” *Journal of Geotechnical and Geoenvironmental Engineering* 129, no. 10 (2003): 956. https://doi.org/10.1061/(ASCE)1090-0241(2003)129:10(956).

Carrier, David, Leslie G. Bromwell, and Torrence Martin. “Strength and Compressibility of Returned Lunar Soil,” 3:3223–34. Houston, TX: Geochemica et Cosmochemica Acta, 1972. https://adsabs.harvard.edu/full/1972LPSC....3.3223C.

Carrier, W. David III, G. R. Olhoeft, and Wendell Mendell. “Physical Properties of the Lunar Surface.” In *Lunar Sourcebook: A User’s Guide to the Moon*, edited by Grant Heiken, David Vaniman, and Bevan. M. French, 522:475–594. New York, NY: Cambridge University Press, 1991. http://www.lpi.usra.edu/publications/books/lunar_sourcebook/pdf/Chapter09.pdf.

Carter, James L., McKay, David, Allen, Carlton C., and Taylor Lawrence A. “NEW LUNAR ROOT SIMULANTS: JSC-2 (JSC-1 CLONE) AND JSC-3.” In *Book of Abstracts, The Lunar Regolith Simulant Materials Workshop*, 10. Huntsville, AL, 2005.

Cooper, Howard, Holly Shulman, Douglas Rickman, Jennifer Edmunson, and Michael Effinger. “Synthesis of Simulated Lunar Highland Minerals.” In *Lunar and Planetary Science Conference #54*. The Woodlands, TX: LPI, 2023. https://www.hou.usra.edu/meetings/lpsc2022/pdf/1441.pdf.

Colaprete, Anthony, Peter H Schultz, Jennifer Heldmann, Diane H. Wooden, Mark Shirley, Kimberly Ennico, Brendan Hermalyn, et al. “Detection of Water in the LCROSS Ejecta Plume.” *Science* 330, no. 6003 (October 2010): 463–68. https://doi.org/10.1126/science.1186986.

Conel, James E. “Infrared Emissivities of Silicates: Experimental Results and a Cloudy Atmosphere Model of Spectral Emission from Condensed Particulate Mediums.” *Journal of Geophysical Research* 74, no. 6 (March 15, 1969): 1614–34. https://doi.org/10.1029/JB074i006p01614.

Creedon, Matthew, Tara Linneman, Douglas L. Rickman, and Michael R. Effinger. “Development of a New Lunar Highland Regolith Simulant NUW-LHT-5M.” Presented at the Lunar Surface Innovation Consortium, Johns Hopkins Applied Physics Lab, April 24, 2023. https://lsic.jhuapl.edu/Events/Agenda/index.php?id=380.

Des Marais, D. J. “Carbon, Nitrogen and Sulfur in Apollo 15, 16 and 17 Rocks.” In *Lunar and Planetary Science Conference (9th), March 13-17*, 2451–67. Houston, Texas, 1978. http://adsabs.harvard.edu/abs/1978LPSC....9.2451D.

Dinis, P., and A. Castilho. “Integrating Sieving and Laser Data To Obtain Bulk Grain-Size Distributions.” *Journal of Sedimentary Research* 82, no. 9 (October 12, 2012): 747–54. https://doi.org/10.2110/jsr.2012.62.

Donaldson Hanna, K. L., B. T. Greenhagen, W. R. Patterson III, C. M. Pieters, J. F. Mustard, N. E. Bowles, D. A. Paige, T. D. Glotch, and C. Thompson (2017), Effects of varying environmental conditions on emissivity spectra of bulk lunar soils: Application to Diviner thermal infrared observations of the Moon, Icarus, 283, 326-342.

Dotson, B., Sargeant, H., Millwater, C., Easter, P., Sanchez Valencia, D., Long-Fox, J., Britt, D., and Metzger, P. (2023), “New Insights into the Physical Properties of Regolith”, *54th Lunar and Planetary Science Conference*, Houston, TX, USA, March 13-17, 2023.

Engelschiøn, V. S., S. R. Eriksson, A. Cowley, M. Fateri, A. Meurisse, U. Kueppers, and M. Sperl. “EAC-1A: A Novel Large-Volume Lunar Regolith Simulant.” *Scientific Reports* 10, no. 1 (March 25, 2020): 1–9. https://doi.org/10.1038/s41598-020-62312-4.

Hofmeister, Anne M., Alan G. Whittington, and Maik Pertermann. “Transport Properties of High Albite Crystals, near-Endmember Feldspar and Pyroxene Glasses, and Their Melts to High Temperature.” *Contributions to Mineralogy and Petrology* 158, no. 3 (2009): 381–400. https://doi.org/10.1007/s00410-009-0388-3.

Garboczi, Edward J. “Three Dimensional Shape Analysis of JSC-1A Simulated Lunar Regolith Particles.” *Powder Technology* 207, no. 1–3 (February 2011): 96–103. https://doi.org/10.1016/j.powtec.2010.10.014.

Garboczi, E.J., and N. Hrabe. “Particle Shape and Size Analysis for Metal Powders Used for Additive Manufacturing: Technique Description and Application to Two Gas-Atomized and Plasma-Atomized Ti64 Powders.” *Additive Manufacturing* 31 (2020): 100965. https://doi.org/10.1016/j.addma.2019.100965.

Geraghty, Ennis. “Geologic Map of the Stillwater Complex within the Beartooth Mountains Front Laramide Triangle Zone, South-Central Montana.” Geologic map, print on demand 21 pages, 1 sheet, 1:48,000. Open-File Report 645. Montana Bureau of Mines and Geology, 2013. https://ngmdb.usgs.gov/Prodesc/proddesc_100917.htm.

Goguen, J., A. Sharits, A. Chiaramonti, T. Lafarge, E.J. Garboczi, Three-dimensional characterization of particle size, shape, and internal porosity for Apollo 11 and Apollo 14 lunar regolith and JSC-1A lunar regolith soil simulant, Icarus in review.

Graf, John C. *Lunar Soils Grain Size Catalog*. NASA Reference Publication 1265. NASA, 1993. https://ntrs.nasa.gov/api/citations/19930012474/downloads/19930012474.pdf.

Guillon, Olivier, Jesus Gonzalez-Julian, Benjamin Dargatz, Tobias Kessel, Gabi Schierning, Jan Räthel, and Mathias Herrmann. “Field-Assisted Sintering Technology/Spark Plasma Sintering: Mechanisms, Materials, and Technology Developments.” *Advanced Engineering Materials* 16, no. 7 (2014): 830–49. https://doi.org/10.1002/adem.201300409.

Gustafson, Robert J. “JSC-1A Lunar Regolith Simulant: Availability and Characterization.” In *Lunar Regolith Simulant Workshop, March 17-20*. Huntsville, AL, 2009. http://isru.msfc.nasa.gov/lib/workshops/2009/03_JSC-1A_Lunar_RegSimulant_Update_BGustafson.pdf.

Gustafson, Robert J., Brant C. White, Marty Gustafson, and J. Fournelle. “Development of High-Fidelity Lunar Regolith Simulants with Agglutinates.” Huntsville, AL: NASA/MSFC, 2007. https://www.nasa.gov/sites/default/files/atoms/files/day1_12_orbitec_agglutinate_bgustafson.pdf

Hayward, Erin G., Mary Nehls, Todd Schneider, Patrick Lynn, Peter Bertone, and Jason Vaughn. “Designing the PLANET Chamber for Lunar Environment Ground Testing.” In *AIAA SCITECH 2023 Forum*. National Harbor, MD & Online: American Institute of Aeronautics and Astronautics, 2023. https://doi.org/10.2514/6.2023-2468.

Hill, Eddy, Michael J. Mellin, Bill Deane, Yang Liu, and Lawrence A. Taylor. “Apollo Sample 70051 and High- and Low-Ti Lunar Soil Simulants MLS-1A and JSC-1A: Implications for Future Lunar Exploration.” *Journal of Geophysical Research* 112, no. E2 (February 2007): 1–11. https://doi.org/10.1029/2006JE002767.

IARC Working Group on the evaluation of carcinogenic risks to Humans. A Review of Human Carcinogens. Part C: Arsenic, Metals, Fibres, and Dusts/ IARC Working Group on the Evaluation of Carcinogenic Risks to Humans (2009: Lyon, France). Vol. Vol. 100C. IARC Monographs on the Evaluation of Carcinogenic Risks to Humans. Lyons, France: International Agency for Research on Cancer, 2012. http://monographs.iarc.fr/ENG/Monographs/vol68/.

International Space Exploration Coordination Group (ISECG). “In-Situ Resource Utilization Gap Assessment Report,” April 21, 2021. https://www.globalspaceexploration.org/wordpress/wp-content/uploads/2021/04/ISECG-ISRU-Technology-Gap-Assessment-Report-Apr-2021.pdf.

Jeon, Kyu, and Yong-Rak Kim. “Spark Plasma Sintering of NUW-LHT-5M Lunar Highland Simulant: Effect of Sintering Temperature on Physical, Mechanical, and Microstructural Properties.” In *2024 ASCE Earth & Space Conference*, 8. Miami, FL, 2024.

Kanamori, Hiroshi, Kai Matsui, Akira Miyahara, and Shigeru Aoki. “Development of New Lunar Soil Simulants in Japan.” Colorado School of Mines, 2006.

Kaur, Jasmeet, Douglas Rickman, and Martin A. Schoonen. “Reactive Oxygen Species (ROS) Generation by Lunar Simulants.” *Acta Astronautica* 122 (May 1, 2016): 196–208. https://doi.org/10.1016/j.actaastro.2016.02.002.

Long-Fox, Jared M., and Daniel T. Britt. “Characterization of Planetary Regolith Simulants for the Research and Development of Space Resource Technologies.” *Frontiers in Space Technologies* 4 (September 27, 2023): 1255535. https://doi.org/10.3389/frspt.2023.1255535.

Long-Fox, Jared M., Zoe A. Landsman, Parks B. Easter, Catherine A. Millwater, and Daniel T. Britt. “Geomechanical Properties of Lunar Regolith Simulants LHS-1 and LMS-1.” *Advances in Space Research* 71, no. 12 (2023): 5400–5412. https://doi.org/10.1016/j.asr.2023.02.034.

McKay, David S., James L. Carter, Walter W. Boles, Carlton C. Allen, and Judith Haley Allton. “JSC-1: A New Lunar Soil Simulant.” In *Space 94 (4th)*, edited by Rodney G. Galloway and Stanley Lokaj, 857–66. Albuquerque, NM: American Society of Civil Engineers, 1994. http://www.lpi.usra.edu/lunar/strategies/jsc_lunar_simulant.pdf.

Martin, Dayl J.P., Kerri L. Donaldson Hanna, Katherine H. Joy, and Jeffrey J. Gillis-Davis. “A Petrological and Spectral Characterisation of the NU-LHT-2M Lunar Highlands Regolith Simulant in Preparation for the PROSPECT Test Campaign.” *Planetary and Space Science* 221 (October 2022): 105561. https://doi.org/10.1016/j.pss.2022.105561.

Morris, Richard V. “The Surface Exposure (Maturity) of Lunar Soils - Some Concepts and Is/FeO Compilation.” In *Lunar and Planetary Science Conference (9th), March 13-17*, 2287–97. Houston, Texas: LPI, 1978.

Morrison, Aaron A., Michael Zanetti, Christopher W. Hamilton, Einat Lev, Catherine D. Neish, and Alan G. Whittington. “Rheological Investigation of Lunar Highland and Mare Impact Melt Simulants.” *Icarus* 317 (January 1, 2019): 307–23. https://doi.org/10.1016/j.icarus.2018.08.001.

Munir, Z. A., U. Anselmi-Tamburini, and M. Ohyanagi. “The Effect of Electric Field and Pressure on the Synthesis and Consolidation of Materials: A Review of the Spark Plasma Sintering Method.” *Journal of Materials Science* 41, no. 3 (2006): 763–77. https://doi.org/10.1007/s10853-006-6555-2.

NASA. “Artemis Plan: NASA’s Lunar Exploration Program Overview.” NASA Publication. NASA HQ, September 2020. https://www.nasa.gov/sites/default/files/atoms/files/artemis_plan-20200921.pdf.

Papike, J. J., Lawrence A. Taylor, and S. B. Simon. “Lunar Minerals.” In *Lunar Sourcebook: A User’s Guide to the Moon*, edited by Grant Heiken, David Vaniman, and Bevan. M. French, 121–82. Cambridge University Press, 1991. http://www.lpi.usra.edu/publications/books/lunar_sourcebook/pdf/Chapter05.pdf.

Patridge, Austin, Alan Whittington, Aaron Morrison, Douglas L Rickman, and John E Gruener. “Thermophysical Characterization of NUW-LHT-5M Lunar Highland Simulant.” In *Lunar and Planetary Science Conference*. The Woodlands, Texas, 2024. https://www.hou.usra.edu/meetings/lpsc2024/pdf/2553.pdf and https://ntrs.nasa.gov/api/citations/20240002849/downloads/Patridge_LPSC_Poster_2553_4%20Edited.pdf

Petkov, Mihail P., and Gerald E. Voecks. “Characterization of Volatiles Evolved during Vacuum Sintering of Lunar Regolith Simulants.” *Ceramics International*, 2023, S0272884223017649. https://doi.org/10.1016/j.ceramint.2023.06.178.

Phuah, Xin Li, Han Wang, Bruce Zhang, Jaehun Cho, Xinghang Zhang, and Haiyan Wang. “Ceramic Material Processing Towards Future Space Habitat: Electric Current-Assisted Sintering of Lunar Regolith Simulant.” *Materials* 13, no. 18 (September 17, 2020): 4128. https://doi.org/10.3390/ma13184128.

Pirrie, Duncan, and Gavyn K. Rollinson. “Unlocking the Applications of Automated Mineral Analysis.” *Geology Today* 27, no. 6 (2011): 226–35. https://doi.org/10.1111/j.1365-2451.2011.00818.x.

Rawle, Alan F. “Representative Sampling – Another Cinderella of Particle Size Analysis.” *Procedia Engineering* 102, New Paradigm of Particle Science and Technology Proceedings of The 7th World Congress on Particle Technology (2015): 1707–13. https://doi.org/10.1016/j.proeng.2015.01.306.

Rickman, Douglas L., and Heather A. Lowers. “Particle Shape and Composition of NU-LHT-2M.” NASA Technical Memorandum TM-2012-217458. MSFC, Huntsville, AL: NASA/Marshall Space Flight Center, 2012. https://ntrs.nasa.gov/api/citations/20120011878/downloads/20120011878.pdf.

Rickman, Douglas L., Douglas B. Stoeser, W. M. Benzel, Christian M. Schrader, and Jennifer E. Edmunson. “Notes on Lithology , Mineralogy , and Production for Lunar Simulants.” *NASA TM*, no. 2011–216454 (2011): 64. https://ntrs.nasa.gov/citations/20110007112.

Rickman, Douglas L., Stephen A. Wilson, Michael A. Weinstein, Douglas B. Stoeser, and Jennifer E. Edmunson. “On the Manufacture of Lunar Regolith Simulants.” *NASA TM* TM-2013-2174 (2013): 74. https://ntrs.nasa.gov/citations/20140003177.

Rickman, D. L., H. Shulman, M. Creedon, and M. R. Effinger. “Design of NU-LHT-5M and -6M, Lunar Highland Simulants.” In *53rd Lunar and Planetary Science Conference*, Abstract #1146. Houston: Lunar and Planetary Institute, 2022. https://www.hou.usra.edu/meetings/lpsc2022/pdf/1146.pdf.

Rochette, P., J. Gattacceca, A.V. Ivanov, M.A. Nazarov, and N.S. Bezaeva. “Magnetic Properties of Lunar Materials: Meteorites, Luna and Apollo Returned Samples.” *Earth and Planetary Science Letters* 292, no. 3–4 (2010): 383–91. https://doi.org/10.1016/j.epsl.2010.02.007.

Salisbury, John W., and Louis S. Walter. “Thermal Infrared (2.5–13.5 Mm) Spectroscopic Remote Sensing of Igneous Rock Types on Particulate Planetary Surfaces.” *Journal of Geophysical Research: Solid Earth* 94, no. B7 (July 10, 1989): 9192–9202. https://doi.org/10.1029/JB094iB07p09192.

Santanach, J. Gurt, A. Weibel, C. Estournès, Q. Yang, Ch. Laurent, and A. Peigney. “Spark Plasma Sintering of Alumina: Study of Parameters, Formal Sintering Analysis and Hypotheses on the Mechanism(s) Involved in Densification and Grain Growth.” *Acta Materialia* 59, no. 4 (2011): 1400–1408. https://doi.org/10.1016/j.actamat.2010.11.002.

Schrader, Christian M. “Overview of the Figure of Merit Analyses for Simulants and the Fit-to-Use Matrix.” In *2009 Regolith Simulant Workshop*, 17. Marshall Space Flight Center, Huntsville, Alabama, 2009. https://www.nasa.gov/sites/default/files/atoms/files/07_simusersguide_foms_matrix_cschrader.pdf.

Schrader, Christian M., Douglas L. Rickman, Carole A. Mclemore, John C. Fikes, Stephen A. Wilson, Douglas B. Stoeser, Alan R. Butcher, and Pieter W. S. K. Botha. “Extant and Extinct Lunar Regolith Simulants: Modal Analyses of NU-LHT-1M and -2m, OB-1, JSC-1, JSC-1A and -1AF, FJS-1, and MLS-1.” In *Planetary and Terrestrial Mining Sciences Symposium (5th), June 9-11*. Toronto, Canada: NORCAT, 2008. https://ntrs.nasa.gov/api/citations/20080036590/downloads/20080036590.pdf?attachment=true.

Schrader, Christian M., Douglas L. Rickman, Carole A. Mclemore, John C. Fikes, Douglas B. Stoeser, Susan J. Wentworth, and David S. McKay. “Lunar Regolith Characterization for

Simulant Design and Evaluation Using Figure of Merit Algorithms." In *Aerospace Sciences (47th), Jan 5-8*, 7. Orlando, Florida: AIAA, 2009. https://doi.org/10.2514/6.2009-755.

Schrader, Christian M., Douglas L. Rickman, Carole A. Mclemore, and John C. Fikes. "Lunar Regolith Simulant User's Guide." *NASA TM*, TM, no. 2010–216446 (2010): 40p.

Sehlke, A., A.M. Hofmeister, and A.G. Whittington. "Thermal Properties of Glassy and Molten Planetary Candidate Lavas." *Planetary and Space Science* 193 (2020): 105089. https://doi.org/10.1016/j.pss.2020.105089.

Slabic, Ane, Douglas L Rickman, and John E Gruener. "Measurements of Silicosis Factors in Lunar and Martian Simulants." In *Space Resources Roundtable*. Colorado School of Mines, 2024.

Street, Kenneth W., Chandra Ray, Doug Rickman, and Daniel A. Scheiman. "Thermal Properties of Lunar Regolith Simulants," May 1, 2010. http://ntrs.nasa.gov/search.jsp?R=20100024178.

Stoeser, Douglas B., Douglas L. Rickman, and Stephen A. Wilson. "Design and Specifications for the Highland Regolith Prototype Simulants NU-LHT-1M and -2M." *NASA TM*, TM, no. 2010–216438 (2010): 24p.

Stoeser, Douglas B., and Steve A. Wilson. "NU-LHT-1M: Pilot Highlands Soil Simulant," 38. Huntsville, AL, 2007. https://www.nasa.gov/sites/default/files/atoms/files/day1_usgs.pdf.

Takeda, Hiroshi, Hiroshi Kanamori, Shigeru Aoki, Kai Matsui, and Akira Miyahara. "Development of New Lunar Soil Simulants in Japan." In *Space Resources Roundtable (8th), Oct 31 - Nov 2*. Golden, Colorado: LPI, 2006. http://www.isruinfo.com/docs/srr8/kanamori_et_al_nov_2.zip.

Vogel, Hans. "Das Temperaturabhaengigkeitsgesetz der Viskositaet von Fluessigkeiten [The temperature-dependent viscosity law for liquids]." *Physikalische Zeitschrift* (in German) 22 (1921): 645.

Weiblen, Paul W., and K. Gordon. "Characteristics of a Simulant for Lunar Surface Materials." In *Lunar Bases and Space Activites in the 21st Century (2nd), April 5-7*, 254. Houston, Texas: LPI, 1988. http://adsabs.harvard.edu/full/1988LPICo.652..254W.

Weiblen, Paul W., Marian J. Murawa, and Kenneth J. Reid. "Preparation of Simulants for Lunar Surface Materials." In *Space 90 (2nd), Apr 22-26*, 98–106. Albuquerque: ASCE, 1990. http://www.csa.com/partners/viewrecord.php?requester=gs&collection=TRD&recid=A9127583AH.

Weinstein, Michael, Stephen A. Wilson, Douglas L. Rickman, Douglas B. Stoeser. Synthesis for Lunar Simulants: Glass, Agglutinate, Plagioclase, Breccia. NASA Technical Reports Server, 2012. http://ntrs.nasa.gov/search.jsp?R=20120014184&hterms=synthesis+lunar+simulants&qs=Ntx=mode matchallpartial &Ntk=All&N=0&Ntt=synthesis for lunar simulants. https://www.youtube.com/watch?v=6kVUtsExLeU

Werkheiser, Niki, Gerald Sander, and Julie Kleinhenz. "In Situ Resource Utilization (ISRU) Strategy - Scope, Plans, and Priorities." Presented at the NASA Advisory Council (NAC) Technology Innovation, and Engineering Committee, NASA hQ, May 16, 2023. https://www.nasa.gov/wp-content/uploads/2023/10/werkheiser-and-sanders-isru-tagged.pdf.

Whittington, Alan G., and Anis Parsapoor. "Lower Cost Lunar Bricks: Energetics of Melting and Sintering Lunar Regolith Simulants." *New Space*, 2022, 12. https://doi.org/10.1089/space.2021.0055.

Whittington, Alan G., and Alexander Sehlke. “Spontaneous Reheating of Crystallizing Lava.” *Geology* 49, no. 12 (December 1, 2021): 1457–61. https://doi.org/10.1130/G49148.1.

Wilkerson, Ryan P., Mihail P. Petkov, Gerald E. Voecks, Catherine S. Lynch, Holly S. Shulman, Santhoshkumar Sundaramoorthy, Amitava Choudhury, Douglas L. Rickman, and Michael R. Effinger. “Outgassing Behavior and Heat Treatment Optimization of JSC-1A Lunar Regolith Simulant.” *Icarus* 400 (2023): 115577. https://doi.org/10.1016/j.icarus.2023.115577.

Wilkerson, Ryan P., Douglas L. Rickman, Justin R. McElderry, Sarah R. Walker, and Kevin M. Cannon. “On the Measurement of Shape: With Applications to Lunar Regolith.” *Icarus*, 2024, 115963. https://doi.org/10.1016/j.icarus.2024.115963.

Wilson, Stephen A., and Douglas B. Stoeser. “NASA/USGS Lunar Highland Regolith Simulant Development.” In *2009 Regolith Simulant Workshop*, 23. Marshall Space Flight Center, Huntsville, Alabama, 2009. https://www.nasa.gov/sites/default/files/atoms/files/04_wilson_stoeser_lh_regsimdev.pdf.

Zhang, Xiang, Shayan Gholami, Mahdieh Khedmati, Bai Cui, Yong-Rak Kim, Young-Jae Kim, Hyu-Soung Shin, and Jangguen Lee. “Spark Plasma Sintering of a Lunar Regolith Simulant: Effects of Parameters on Microstructure Evolution, Phase Transformation, and Mechanical Properties.” *Ceramics International* 47, no. 4 (2021): 5209–20. https://doi.org/10.1016/j.ceramint.2020.10.100.

Zhang, Xiang, Mahdieh Khedmati, Yong-Rak Kim, Hyu-Soung Shin, Jangguen Lee, Young-Jae Kim, and Bai Cui. “Microstructure Evolution during Spark Plasma Sintering of FJS-1 Lunar Soil Simulant.” *Journal of the American Ceramic Society* 103, no. 2 (2020): 899–911. https://doi.org/10.1111/jace.16808.

Zheng, Yongchun, Shijie Wang, Ziyuan Ouyang, Yongliao Zou, Jianzhong Liu, Chunlai Li, X. Li, and J. Feng. “CAS-1 Lunar Soil Simulant.” *Advances in Space Research* 43, no. 3 (February 2008): 448–54. https://doi.org/10.1016/j.asr.2008.07.006.

Appendix A Section 3 Supplemental Information

Manufacturing

Raw Materials
Lunar simulant NUW-LHT-5M was manufactured at Washington Mills Electro Minerals, Niagara Falls, NY. Three different mined minerals and a synthetic glass were used to produce the complete simulant. The mineral components were norite, anorthosite (both from Stillwater, Montana) and olivine (Turkey). The norite and anorthosite were provided by NASA MSFC.

Industrial grades (>98% purity) of SiO_2 (quartz sand), calcined Al_2O_3, dead burned MgO, CaO (quick lime), Fe_2O_3, and TiO_2 (rutile) were used to manufacture the synthetic glass. The fused glass was produced by blending these six oxide components according to the formulation in Table 1. Purity and moisture content were accounted for in the batched quantities of all raw materials. Batches of 60 kg each were prepared by dry blending the oxides using a 3 ft^3 twin shell V-blender dry blender (Patterson Kelly Co., Inc., East Stroudsburg, PA).

Table A1. Glass Target Composition.

Material	NUW-LHT-5M Formulation Target
SiO_2	45.29%
Al_2O_3	27.27%
Fe_2O_3	5.18%
MgO	5.87%
CaO	15.83%
TiO_2	0.56%

Glass Fusion
These batches were combined and fused in a graphite lined crucible and water quenched to prevent crystallization. The fused glass was a mixture of solid glass pieces and low-density, friable granules of glass approximately 1 to 2 cm in diameter, as shown in Figure A1.

Figure A1. Macro-structure of quenched glass prior to crushing/milling.

Particle Size Reduction

The three mineral components and glass were milled individually due to their different hardnesses. The first step in particle size reduction was roll crushing. A double-roll crusher with 12" diameter by 12" in wide rolls was used to reduce the size to <2 mm. Three passes were required. Ball milling to the final particle size distribution was done in a 12.4 L porcelain jar mill (U.S. Stoneware, Size 3). For all materials, 50 vol.% of the jar was filled with media and 25 vol.% powder. Norite and olivine were milled for 3 hr and 5 hr, respectively, at 45 revolutions per minute (rpm) using 0.5" cylindrical alumina media. Anorthosite was milled for 3.5 hr using a 50/50 blend of 1" alumina spheres and 0.5" alumina cylinders, rolling at 45 rpm.

The glass was crushed in the same way as the other components. Milling was broken into two steps. For the first step, the glass was ball milled under the same conditions as the norite and olivine for 2.5 hr. The milled material was then screened to create one fraction above 155 μm (coarse) and one below (fine). The coarse material was milled in a 5.6 L jar (U.S. Stoneware, Size 1) for 3 hr at 70 rpm. In this case the media consisted of a mixture of 1" alumina spheres and 0.5" in alumina cylinders in a 45/55 ratio. After milling the coarse and fine batches were combined in an 80/20 ratio of coarse to fine.

Particle Size Measurement

Particle size distributions were determined using a combination of results from RoTap Sieve Shaker, Model RX-29 (W.S. Tyler, Mentor, OH) screening and laser diffraction measurements (Microtrac S3500, Microtrac MRB, Montgomeryville, PA). Data from the RoTap were used for size information for the upper end of the distribution (>80 μm). Results from laser diffraction were used to find the sizing for the lower end of the distribution (<80 μm). The reason for combining measurements was that sieve data is most applicable to particle sizes >75 μm, while laser diffraction analysis is most applicable to small particle sizes (Al-Hashemi et al., 2021).

For sieve analysis, 18, 30, 70, 140, 200, and 270 mesh screens were used in the RoTap and 100.0 g of regolith was placed on the top screen. The stack was shaken for 5 minutes and the

mass of material on each sieve was recorded. Material collected during the sieve analysis from the 270 screen and below (i.e., passing the 200 mesh, 74 µm opening) was blended and used for laser diffraction analysis. The analysis was performed in distilled water using sodium hexametaphosphate as the dispersant.

In the >1 mm fraction, there can be rods of glass that get through the sieve. These rods may compose ~ 0.05 wt% of the total simulant.

Table A2. Average particle size distribution data of highlands lunar regolith collected by Apollo 16. (Carrier, 2003). Upper and lower error values represent a delta from the average of 10% based on an estimate from the Carrier data.

µm	% Passing	Upper Error	Lower Error
1300	94.9	104.9	84.9
1000	91.8	101.8	81.8
400	83.5	93.5	73.5
300	78.7	88.7	68.7
200	72.1	82.1	62.1
100	58.0	68.0	48.0
70	50.5	60.5	40.5
50	40.8	50.8	30.8
40	35.0	45.0	25.0
30	30.2	40.2	20.2
20	23.6	33.6	13.6
10	13.9	23.9	3.9
5	7.8	17.8	-2.2
3	4.8	14.8	-5.2

Regolith Assembly

When particle size distribution of each component was within the specified range, all four parts of the regolith were blended in a V-blender for 15 minutes to produce the finished regolith.

Table A3. Final mix weight and percentage values for each component.

Component	Percentage (%)
Anorthosite	37.7
Norite	17.6
Olivine	4.7
Glass	40

References

Al-Hashemi, Hamzah M. Beakawi, Omar S. Baghabra Al-Amoudi, Zain H. Yamani, Yassir M. Mustafa, and Habib-ur-Rehman Ahmed. “The Validity of Laser Diffraction System to Reproduce Hydrometer Results for Grain Size Analysis in Geotechnical Applications.” Edited by

Jianguo Wang. *PLOS ONE* 16, no. 1 (January 14, 2021): e0245452. https://doi.org/10.1371/journal.pone.0245452.

Appendix B Section 4 Supplemental Information

ALS Final Report

Note the labeling of appendices in this section is inherited from the source document.

ALS Canada Ltd.
Metallurgy Services
2957 Bowers Place
Kamloops, BC, Canada V1S 1W5
T +1 250 828 6157 F +1 250 828 6159

right solutions.
right partner.

April 14, 2023

Dr. Douglas Rickman
Staff Consultant
National Aeronautics and Space Administration
300 E. Street SW Suite 5R30
Washington, Post Code: 20546
United States

Dear Dr. Rickman;

Re: Mineralogical Assessment on Lunar Regolith Simulant Samples – KM6800

We have completed the mineralogical assessment on a new lunar highland simulant sample, labeled as NUW-LHT-5M-Test 2, which was received at ALS Metallurgy Kamloops on February 7, 2023. The sample was received in two jars with 100 and 110 grams of sample, respectively. The two jars of samples were homogenized into one sample for the analysis. The principal objective of this study was to determine the liberation and locking characteristics of dominant minerals in this sample, including feldspars, pyroxenes and olivine, using QEMSCAN Particle Mineral Analysis (PMA) protocols. The sizing and shape factors of these three minerals and the deportments of the elements of interest would be also estimated. To achieve the objective, the following test work was conducted:

Upon receipt, the NUW-LHT-5M-Test 2 sample was homogenized and dry screened into 3 size fractions for the mineralogical and chemical analyses. QEMSCAN Particle Mineral Analyses (PMA) were performed on each fraction to determine the mineral composition and fragmentation characteristics. Whole Rock Analyses by XRF (X-Ray

Fluorescence) were performed on both heads and size fractions while a 4-acid digestion multi-element ICP Scan (including Rare Earth Elements along with total sulphur and carbon assays by LECO were performed on the head, to quantify the chemical composition of this sample, and consequently to assist the QEMSCAN PMA calibrations. Details of the analysis are shown in three appendices at the end of this letter.

The data generated from this study are summarized in Table 1 and Figure 1 to Figure 3. The following notes may be of interest when reviewing the data:

- As shown in Table 1 and Figure 1, plagioclase feldspar was the dominant mineral in the NUW-LHT-5M-Test 2 sample and accounted for 81.3 percent of the sample mass. Approximately 83, 91 and 97 percent of the silicon, aluminum, and calcium, respectively, were carried by plagioclase feldspar. The remaining minerals in this sample were principally pyroxene/amphibole group minerals, olivine, chlorite, and quartz, in relatively smaller amounts.

- About 91 percent of the feldspars in this sample were liberated from other minerals. The unliberated feldspars were mainly located in the greater than 106μm fraction (see Figure 2B).

- Figure 3 data suggests that the dominant silicon minerals (plagioclase feldspar, pyroxene/amphibole and olivine) were relatively coarse grained in the NUW-LHT-5M-Test 2 sample. Half of these three minerals were distributed in the mineral grain sizes of above 60 microns in equivalent circle diameter and significant amounts of these mineral grains sized even coarser than 800 microns.

Thank you for the opportunity to participate in your mineralogical studies. If you have any questions regarding this report, or the results generated by this program, please do not hesitate to contact us.

Written by,

Wendy Ma, M.Sc. P. Geo.
Mineralogy Project Manager

Reviewed by,

Kimberly Roulston
Senior Metallurgist

April 14, 2023
KM6800
Permit to Practice Number: 1000952

Electronic Distribution:
Douglas Rickman, Staff Consultant, National Aeronautics and Space Administration

TABLE 1
CHEMICAL AND MINERAL COMPOSITION

Chemical Composition - percent			Mineral Composition - percent	
Element	Symbol	NUW-LHT-5M_Test 2	Mineral	NUW-LHT-5M_Test 2
Silicon	Si	21.8	Elemental Iron/Iron Oxides	0.16
Aluminum	Al	13.8	Quartz	0.58
Iron	Fe	2.39	Calcium Plagioclase Feldspar	81.3
Magnesium	Mg	4.62	Feldspar Albite (Na Feldspar)	0.49
Calcium	Ca	10.4	K-Feldspar	0.06
Sodium	Na	0.76	Orthopyroxenes	5.97
Titanium	Ti	0.17	Clinopyroxenes	3.15
Chromium	Cr	0.05	Amphibole	1.45
Potassium	K	0.03	Olivine	3.80
Manganese	Mn	0.03	Chlorite	1.61
Phosphorus	P	<0.01	Talc	0.20
Barium	Ba	<0.01	Micas	0.14
Strontium	Sr	0.01	Carbonates	0.08
Sulphur	S	0.02	Kaolinite (clay)	0.04
Carbon	C	0.05	Others	1.02
			Total	100.0

Notes: a) Elemental Iron\Iron Oxides includes Steel and may include Magnetite, Hematite and Goethite/Limonite.
b) Calcium Plagiocase Feldspar includes Epidote Clinozoisite?
c) Pyroxenes includes Clinopyroxenes and Orthopyroxenes.
d) Micas includes Biotite/Phlogopite and Muscovite.
e) Carbonates includes Calcite, Ankerite/Dolomite and Magnesite.
f) Others includes Sphene (Titanite), Rutile/Anatase, Epidote?, Serpentine, Sulphide Minerals, Apatite,Spinel and unresolved mineral species.

FIGURE 1
SILICON. ALUMINUM AND CALCIUM DEPORTMENT BY THEIR BEARING MINERALS
NUW-LHT-5M_Test 2 Jan 30, 2023

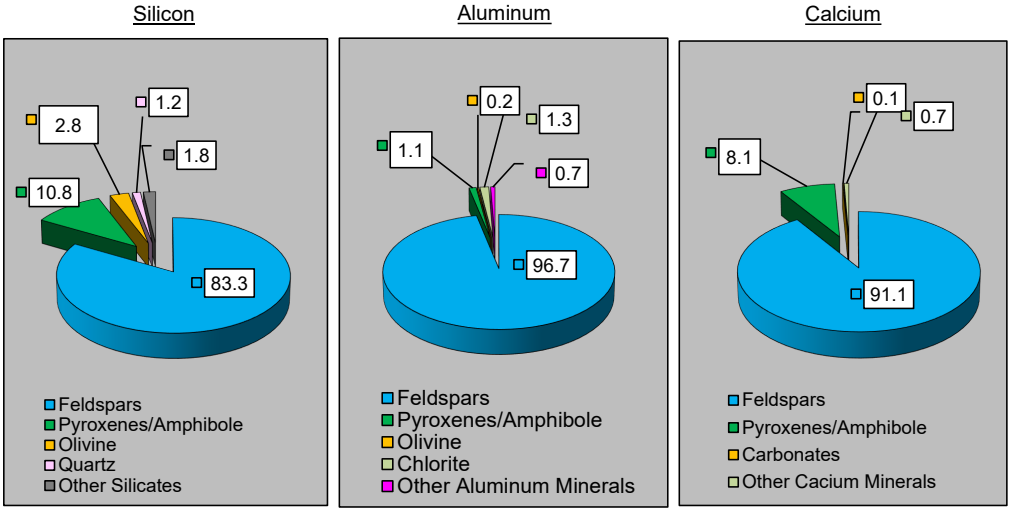

Notes: a) Other Silicates including Micas, Talc, Serpentine, Kaolinite and Sphene (Titanite)
b) Other Aluminum bearing minerals including Micas, Spinel, Kaolinite and Sphene (Titanite).
c) Other Calcium bearing minerals including Apatite and Sphene (Titanite).
d) Contents are displayed in percent.
e) Complete mineralogical analysis results can be located in Appendix III.

FIGURE 2A
MINERAL DISTRIBUTION BY CLASS OF ASSOCIATIONS
NUW-LHT-5M_Test 2 Jan 30, 2023, 222µm K_{80}

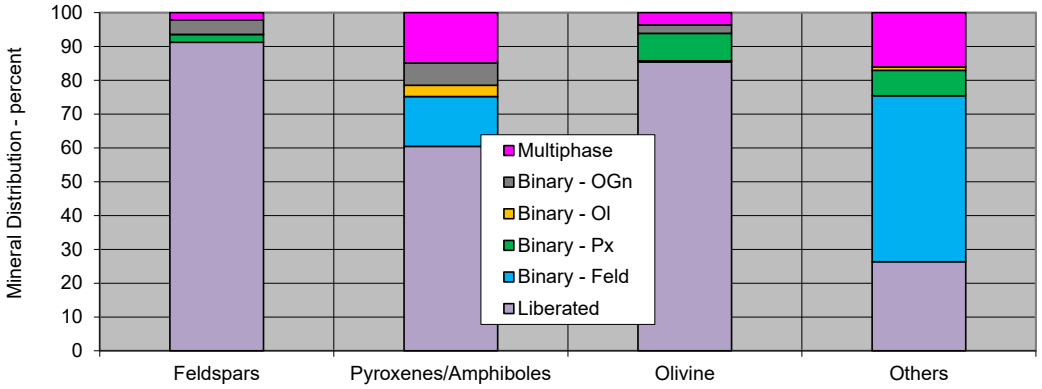

FIGURE 2B
MINERAL DISTRIBUTION BY ASSOCIATION CLASS AND BY SIZE
NUW-LHT-5M_Test 2 Jan 30, 2023, 222µm K_{80}

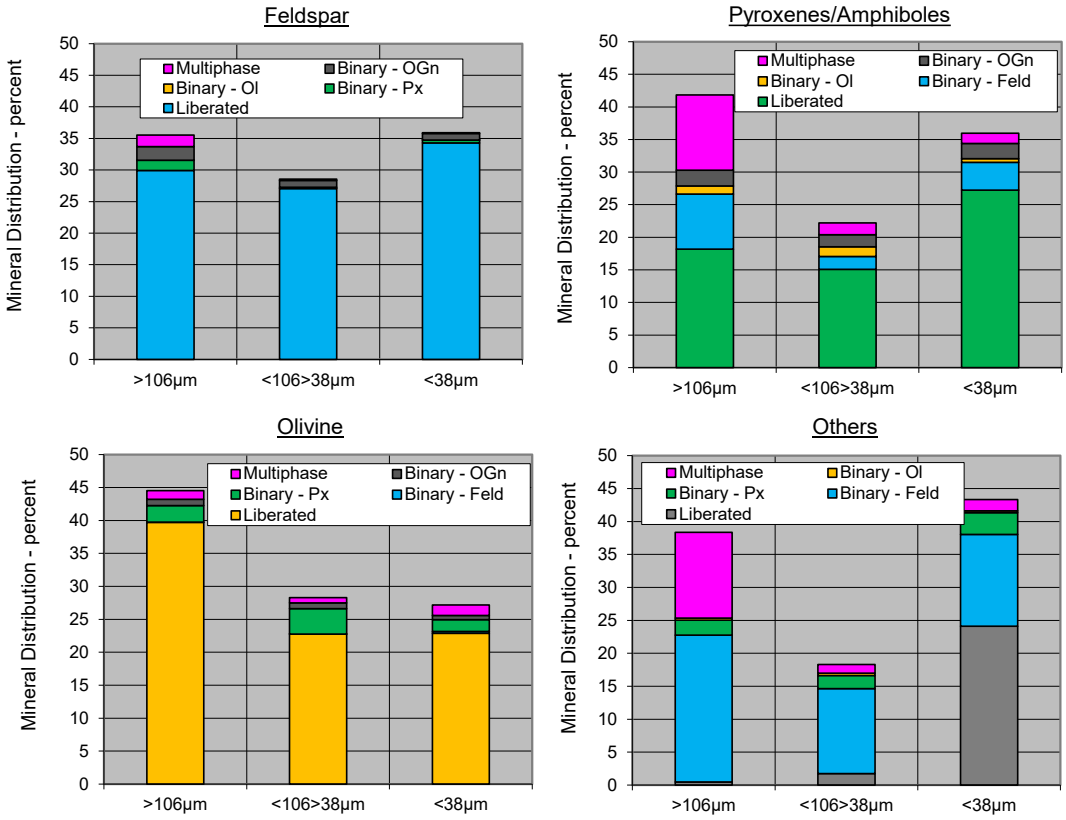

Notes: Feld-Feldspars including Calcium Plagioclase, Feldspar Albite, K Feldspar and Epidote Clinozoisite?, Px-Pyroxenes/Amphiboles, Ol-Olivine, OGn-Other Gangue Minerals.

FIGURE 3A
MINERAL DISTRIBUTION BY THE MINERAL GRAIN SIZES
NUW-LHT-5M_Test 2 Jan 30, 2023, 222µm K_{80}

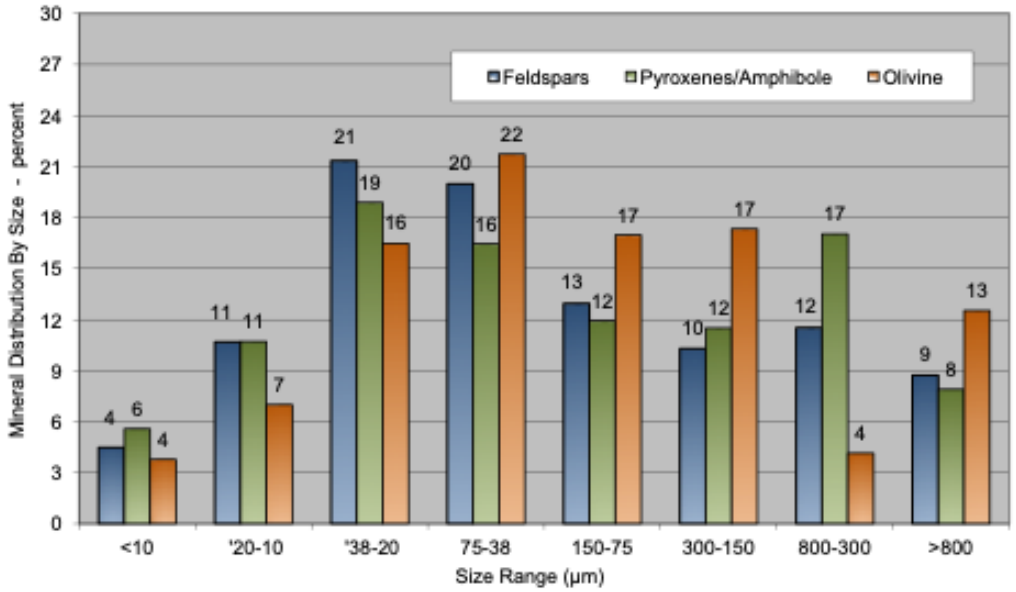

FIGURE 3B
CUMULATIVE DISTRIBUTION BY THE MINERAL GRAIN SIZES
NUW-LHT-5M_Test 2 Jan 30, 2023, 222µm K_{80}

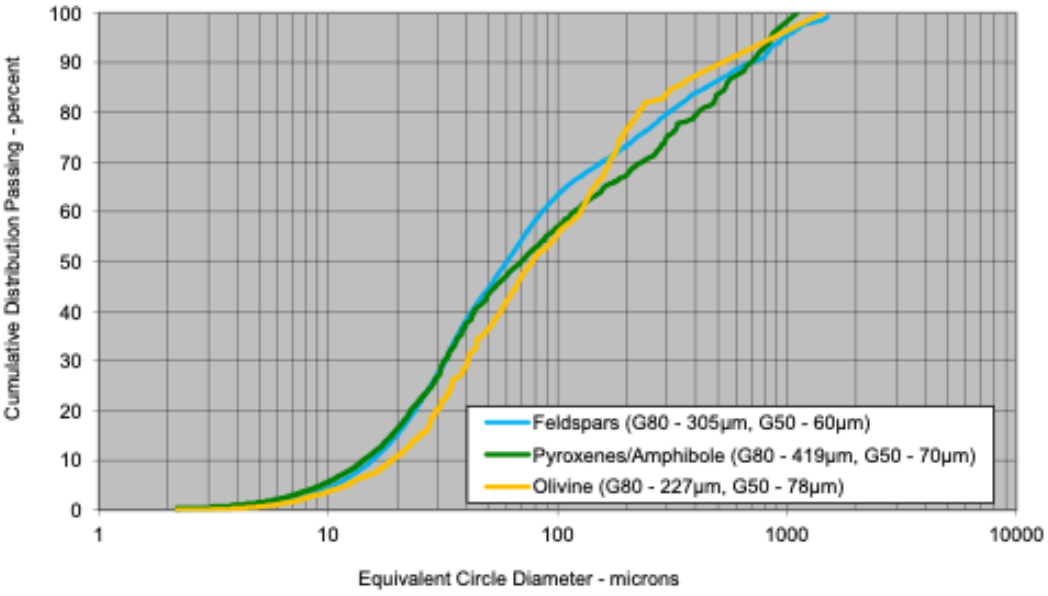

Note: The sizing maybe overestimated due to coarse particle effects.

APPENDIX I – KM6800

PARTICLE SIZING DATA

TABLE I-1
SCREEN ANALYSIS
KM6800 NUW-LHT-5M_Test 2 Jan 30, 2023

Product	Particle Size µm	Weight % Retained	Cumulative % Passing
28 Mesh	600	0.00	100.0
35 Mesh	425	9.28	90.7
48 Mesh	300	4.48	86.2
65 Mesh	212	7.12	79.1
100 Mesh	150	7.23	71.9
150 Mesh	106	8.54	63.3
200 Mesh	75	8.70	54.6
270 Mesh	53	9.55	45.1
400 Mesh	38	9.23	35.9
TOTAL	190g	100.00	**

K80= 222µm

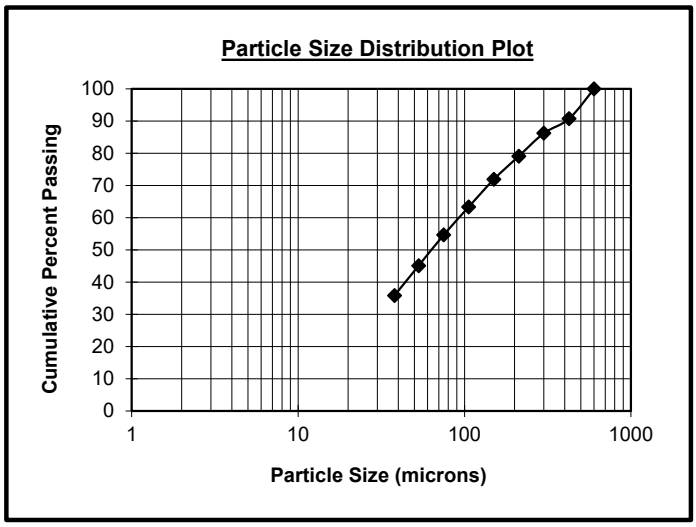

APPENDIX II – KM6800

SPECIAL DATA

TABLE II-1
CHEMICAL ANALYSIS DATA

No	Sample	Elements for Assay - percent	
		S	C
1	NUW-LHT-5M_Test 2 Jan 30, 2023	0.02	0.05

TABLE II-2
ICP SCAN (ME-MS61R) BY FOUR-ACID DIGESTIONS
KM6800 NUW-LHT-5M- Test 2 (Certificate No. VA23065337)

Chemical Compositions										
Elements Descriptions	Ag ppm	Al %	As ppm	Ba ppm	Be ppm	Bi ppm	Ca %	Cd ppm	Ce ppm	Co ppm
NUW-LHT-5M- Test 2	0.23	9.97	<0.2	20	0.07	0.1	10.35	0.03	1.18	15.9

Chemical Compositions										
Elements Descriptions	Cr ppm	Cs ppm	Cu ppm	Fe %	Ga ppm	Ge ppm	Hf ppm	In ppm	K %	La ppm
NUW-LHT-5M- Test 2	369	<0.05	25.4	2.22	10.6	0.15	1	0.012	<0.01	0.5

Chemical Compositions										
Elements Descriptions	Li ppm	Mg %	Mn ppm	Mo ppm	Na %	Nb ppm	Ni ppm	P ppm	Pb ppm	Rb ppm
NUW-LHT-5M- Test 2	1.7	4.25	357	2.63	0.67	3.5	247	20	2.2	<0.1

Chemical Compositions										
Elements Descriptions	Re ppm	S %	Sb ppm	Sc ppm	Se ppm	Sn ppm	Sr ppm	Ta ppm	Te ppm	Th ppm
NUW-LHT-5M- Test 2	<0.002	<0.01	0.98	4	3	0.7	88	0.15	<0.05	0.11

Chemical Compositions										
Elements Descriptions	Ti %	Tl ppm	U ppm	V ppm	W ppm	Y ppm	Zn ppm	Zr ppm	Dy ppm	Er ppm
NUW-LHT-5M- Test 2	0.163	<0.02	0.3	29	0.4	1.1	22	31.7	0.18	0.15

Chemical Compositions										
Elements Descriptions	Eu ppm	Gd ppm	Ho ppm	Lu ppm	Nd ppm	Pr ppm	Sm ppm	Tb ppm	Tm ppm	Yb ppm
NUW-LHT-5M- Test 2	0.07	0.13	0.03	0.02	0.5	0.12	0.12	0.02	0.02	0.13

TABLE II-3
WHOEL ROCK ANALYSIS BY XRF AND FERROUS IRON BY TITRATION
KM6800 NUW-LHT-5M- Test 2 (Certificate No. VA23039623)

Assay Methods	Fe-VOL05	Whole Rock Analysis by XRF (ME-XRF26)															
Elemental Composition	FeO %	Al2O3 %	BaO %	CaO %	Cr2O3 %	Fe2O3 %	K2O %	MgO %	MnO %	Na2O %	P2O5 %	SO3 %	SiO2 %	SrO %	TiO2 %	Total %	LOI 1000 %
Head	2.8	26.08	0.01	14.55	0.08	3.42	0.04	7.67	0.04	1.02	<0.01	0.02	46.8	0.01	0.29	100.4	0.26
>106um	3.33	25.06	<0.01	14.1	0.09	4.02	0.04	8.4	0.05	0.88	<0.01	0.06	46.07	0.01	0.32	99.43	0.23
<106>38um	2.79	25.73	<0.01	14.35	0.08	3.19	0.04	7.72	0.04	0.93	<0.01	0.06	46.63	0.01	0.29	99.4	0.2
<388um	2.16	26.79	0.01	14.55	0.09	2.77	0.06	6.95	0.04	1.1	<0.01	0.02	46.4	0.01	0.27	99.84	0.66

ALS Canada Ltd.
2103 Dollarton Hwy
North Vancouver BC V7H 0A7
Phone: +1 604 984 0221 Fax: +1 604 984 0218
www.alsglobal.com/geochemistry

To: ALS METALLURGY, DIV OF ALS CANADA LTD
2957 BOWERS PL
KAMLOOPS BC V1S 1W5

Page: 1
Total # Pages: 2 (A – D)
Plus Appendix Pages
Finalized Date: 23-MAR-2023
Account: KRL

CERTIFICATE VA23065337

Project: KM6800
P.O. No.: KM6800
This report is for 1 sample of Pulp submitted to our lab in Vancouver, BC, Canada on 13-MAR-2023.
The following have access to data associated with this certificate:

ALS METALLURGY	KRISTINA GRONDZIL	RYAN WILDS

SAMPLE PREPARATION

ALS CODE	DESCRIPTION
FND-02	Find Sample for Addn Analysis

ANALYTICAL PROCEDURES

ALS CODE	DESCRIPTION	INSTRUMENT
ME-MS61r	4A multi-element ICP-MS + REE	

This is the Final Report and supersedes any preliminary report with this certificate number.Results apply to samples as submitted.All pages of this report have been checked and approved for release.
***** See Appendix Page for comments regarding this certificate *****

Signature:
Saa Traxler, Director, North Vancouver Operations

ALS Canada Ltd.
2103 Dollarton Hwy
North Vancouver BC V7H 0A7
Phone: +1 604 984 0221 Fax: +1 604 984 0218
www.alsglobal.com/geochemistry

To: ALS METALLURGY, DIV OF ALS CANADA LTD
2957 BOWERS PL
KAMLOOPS BC V1S 1W5

Finalized Date: 23-MAR-2023
Account: KRL

Project: KM6800

CERTIFICATE OF ANALYSIS VA23065337

Sample Description	Method	ME-MS61r	ME-MS61r	ME-MS61r	ME-MS61r	ME-MS61r	ME-MS61r	ME-MS61r	ME-MS61r	ME-MS61r	ME-MS61r	ME-MS61r	ME-MS61r	ME-MS61r	ME-MS61r	ME-MS61r
	Analyte	Ag	Al	As	Ba	Be	Bi	Ca	Cd	Ce	Co	Cr	Cs	Cu	Fe	Ga
	Units	ppm	%	ppm	ppm	ppm	ppm	%	ppm	ppm	ppm	ppm	ppm	ppm	%	ppm
	LOD	0.01	0.01	0.2	10	0.05	0.01	0.01	0.02	0.01	0.1	1	0.05	0.2	0.01	0.05
KM6800 NUW-LHT-SM- Test 2 Head		0.23	9.97	<0.2	20	0.07	0.10	10.35	0.03	1.18	15.9	369	<0.05	25.4	2.22	10.60

***** See Appendix Page for comments regarding this certificate *****

ALS Canada Ltd.
2103 Dollarton Hwy
North Vancouver BC V7H 0A7
Phone: +1 604 984 0221 Fax: +1 604 984 0218
www.alsglobal.com/geochemistry

To: ALS METALLURGY, DIV OF ALS CANADA LTD
2957 BOWERS PL
KAMLOOPS BC V1S 1W5

Project: KM6800

CERTIFICATE OF ANALYSIS VA23065337

Sample Description	Method	ME-MS61r	ME-MS61r	ME-MS61r	ME-MS61r	ME-MS61r	ME-MS61r	ME-MS61r	ME-MS61r	ME-MS61r	ME-MS61r	ME-MS61r	ME-MS61r	ME-MS61r	ME-MS61r	ME-MS61r
	Analyte	Ge	Hf	In	K	La	Li	Mg	Mn	Mo	Na	Nb	Ni	P	Pb	Rb
	Units	ppm	ppm	ppm	%	ppm	ppm	%	ppm	ppm	%	ppm	ppm	ppm	ppm	ppm
	LOD	0.05	0.1	0.005	0.01	0.5	0.2	0.01	5	0.05	0.01	0.1	0.2	10	0.5	0.1
KM6800 NUW-LHT-SM- Test 2 Head		0.15	1.0	0.012	<0.01	0.5	1.7	4.25	357	2.63	0.67	3.5	247	20	2.2	<0.1

***** See Appendix Page for comments regarding this certificate *****

ALS Canada Ltd.
2103 Dollarton Hwy
North Vancouver BC V7H 0A7
Phone: +1 604 984 0221 Fax: +1 604 984 0218
www.alsglobal.com/geochemistry

To: ALS METALLURGY, DIV OF ALS CANADA LTD
2957 BOWERS PL
KAMLOOPS BC V1S 1W5

Finalized Date: 23-MAR-2023
Account: KRL

Project: KM6800

CERTIFICATE OF ANALYSIS VA23065337

Sample Description	Method	ME-MS61r	ME-MS61r	ME-MS61r	ME-MS61r	ME-MS61r	ME-MS61r	ME-MS61r	ME-MS61r	ME-MS61r	ME-MS61r	ME-MS61r	ME-MS61r	ME-MS61r	ME-MS61r	ME-MS61r
	Analyte	Re	S	Sb	Sc	Se	Sn	Sr	Ta	Te	Th	Ti	Tl	U	V	W
	Units	ppm	%	ppm	ppm	ppm	ppm	ppm	ppm	ppm	ppm	%	ppm	ppm	ppm	ppm
	LOD	0.002	0.01	0.05	0.1	1	0.2	0.2	0.05	0.05	0.01	0.005	0.02	0.1	1	0.1
KM6800 NJW-LHT-SM- Test 2 Head		<0.002	<0.01	0.98	4.0	3	0.7	88.0	0.15	<0.05	0.11	0.163	<0.02	0.3	29	0.4

***** See Appendix Page for comments regarding this certificate *****

ALS Canada Ltd.
2103 Dollarton Hwy
North Vancouver BC V7H 0A7
Phone: +1 604 984 0221 Fax: +1 604 984 0218
www.alsglobal.com/geochemistry

To: ALS METALLURGY, DIV OF ALS CANADA LTD
2957 BOWERS PL
KAMLOOPS BC V1S 1W5

Finalized Date: 23-MAR-2023
Account: KRL

Project: KM6800

CERTIFICATE OF ANALYSIS VA23065337

Sample Description	Method	ME-MS61r	ME-MS61r	ME-MS61r	ME-MS61r	ME-MS61r	ME-MS61r	ME-MS61r	ME-MS61r	ME-MS61r	ME-MS61r	ME-MS61r	ME-MS61r	ME-MS61r	ME-MS61r	ME-MS61r
	Analyte	Y	Zn	Zr	Dy	Er	Eu	Gd	Ho	Lu	Nd	Pr	Sm	Tb	Tm	Yb
	Units	ppm	ppm	ppm	ppm	ppm	ppm	ppm	ppm	ppm	ppm	ppm	ppm	ppm	ppm	ppm
	LOD	0.1	2	0.5	0.05	0.03	0.03	0.05	0.01	0.01	0.1	0.03	0.03	0.01	0.01	0.03
KM6800 NUW-LHT-SM- Test 2 Head		1.1	22	31.7	0.18	0.15	0.07	0.13	0.03	0.02	0.5	0.12	0.12	0.02	0.02	0.13

***** See Appendix Page for comments regarding this certificate *****

ALS Canada Ltd.
2103 Dollarton Hwy
North Vancouver BC V7H 0A7
Phone: +1 604 984 0221 Fax: +1 604 984 0218
www.alsglobal.com/geochemistry

To: ALS METALLURGY, DIV OF ALS CANADA LTD
2957 BOWERS PL
KAMLOOPS BC V1S 1W5

Project: KM6800

CERTIFICATE OF ANALYSIS VA23065337

CERTIFICATE COMMENTS

ANALYTICAL COMMENTS

Applies to Method: REEs may not be totally soluble in this method.
ME-MS61r

LABORATORY ADDRESSES

Applies to Method: Processed at ALS Vancouver located at 2103 Dollarton Hwy, North Vancouver, BC, Canada.
FND-02 ME-MS61r

ALS Canada Ltd.
2103 Dollarton Hwy
North Vancouver BC V7H 0A7
Phone: +1 604 984 0221 Fax: +1 604 984 0218
www.alsglobal.com/geochemistry

To: ALS METALLURGY, DIV OF ALS CANADA LTD
2957 BOWERS PL
KAMLOOPS BC V1S 1W5

CERTIFICATE VA23039623

Project: KM6800
P.O. No.: KM6800
This report is for 4 samples of Pulp submitted to our lab in Vancouver, BC, Canada on 13-FEB-2023.
The following have access to data associated with this certificate:

ALS METALLURGY	KRISTINA GRONDZIL	RYAN WILDS

SAMPLE PREPARATION

ALS CODE	DESCRIPTION
WEI-21	Received Sample Weight
DIS-PUL21	Disposal of M/+ Split after analysis.
LOG-24	Pulp Login - Rcd w/o Barcode

ANALYTICAL PROCEDURES

ALS CODE	DESCRIPTION	INSTRUMENT
ME-MS61	48 element four acid ICP-MS	
Fe-VOL05	FeO (Ferrous Iron)	
ME-XRF26	Whole Rock By Fusion/XRF	XRF
OA-GRA05x	LOI at 1000C for XRF	WST-SEQ

This is the Final Report and supersedes any preliminary report with this certificate number.Results apply to samples as submitted.All pages of this report have been checked and approved for release.
***** See Appendix Page for comments regarding this certificate *****

Signature:
Saa Traxler, Director, North Vancouver Operations

ALS Canada Ltd.
2103 Dollarton Hwy
North Vancouver BC V7H 0A7
Phone: +1 604 984 0221 Fax: +1 604 984 0218
www.alsglobal.com/geochemistry

To: ALS METALLURGY, DIV OF ALS CANADA LTD
2957 BOWERS PL
KAMLOOPS BC V1S 1W5

Project: KM6800

CERTIFICATE OF ANALYSIS VA23039623

Sample Description	Method	WEI-21	Fe-VOL05	ME-XRF26	ME-XRF26	ME-XRF26	ME-XRF26	ME-XRF26	ME-XRF26	ME-XRF26	ME-XRF26	ME-XRF26	ME-XRF26	ME-XRF26	ME-XRF26	ME-XRF26
	Analyte	Recvd Wt.	FeO	Al2O3	BaO	CaO	Cr2O3	Fe2O3	K2O	MgO	MnO	Na2O	P2O5	SO3	SiO2	SrO
	Units	kg	%	%	%	%	%	%	%	%	%	%	%	%	%	%
	LOD	0.02	0.01	0.01	0.01	0.01	0.01	0.01	0.01	0.01	0.01	0.01	0.01	0.01	0.01	0.01
KM6800 NUM-LHT-SM- Test 2 Head		<0.02	2.80	26.08	0.01	14.55	0.08	3.42	0.04	7.67	0.04	1.02	<0.01	0.02	46.80	0.01
KM6800 NUM-LHT-SM- Test +106um		<0.02	3.33	25.06	<0.01	14.10	0.09	4.02	0.04	8.40	0.05	0.88	<0.01	0.06	46.07	0.01
KM6800 NUM-LHT-SM- Test 2 +38um		<0.02	2.79	25.73	<0.01	14.35	0.08	3.19	0.04	7.72	0.04	0.93	<0.01	0.06	46.63	0.01
KM6800 NUM-LHT-SM- Test 2 -38um		<0.02	2.16	26.79	0.01	14.55	0.09	2.77	0.06	6.95	0.04	1.10	<0.01	0.02	46.40	0.01

***** See Appendix Page for comments regarding this certificate *****

ALS Canada Ltd.
2103 Dollarton Hwy
North Vancouver BC V7H 0A7
Phone: +1 604 984 0221 Fax: +1 604 984 0218
www.alsglobal.com/geochemistry

To: ALS METALLURGY, DIV OF ALS CANADA LTD
2957 BOWERS PL
KAMLOOPS BC V1S 1W5

Project: KM6800

CERTIFICATE OF ANALYSIS VA23039623

Sample Description	Method	ME-XRF26	ME-XRF26	OA-GRA05x	ME-MS61	ME-MS61	ME-MS61	ME-MS61	ME-MS61	ME-MS61	ME-MS61	ME-MS61	ME-MS61	ME-MS61	ME-MS61	ME-MS61
	Analyte	TiO2	Total	LOI 1000	Ag	Al	As	Ba	Be	Bi	Ca	Cd	Ce	Co	Cr	Cs
	Units	%	%	%	ppm	%	ppm	ppm	ppm	ppm	%	ppm	ppm	ppm	ppm	ppm
	LOD	0.01	0.01	0.01	0.01	0.01	0.2	10	0.05	0.01	0.01	0.02	0.01	0.1	1	0.05
KM6800 NUW-LHT-SM- Test 2 Head		0.29	100.40	0.26	0.21	10.65	0.7	20	0.07	0.07	10.25	0.02	1.43	16.6	357	<0.05
KM6800 NUW-LHT-SM- Test +106um		0.32	99.43	0.23												
KM6800 NUW-LHT-SM- Test 2 +38um		0.29	99.40	0.20												
KM6800 NUW-LHT-SM- Test 2 -38um		0.27	99.84	0.66												

***** See Appendix Page for comments regarding this certificate *****

ALS Canada Ltd.
2103 Dollarton Hwy
North Vancouver BC V7H 0A7
Phone: +1 604 984 0221 Fax: +1 604 984 0218
www.alsglobal.com/geochemistry

To: ALS METALLURGY, DIV OF ALS CANADA LTD
2957 BOWERS PL
KAMLOOPS BC V1S 1W5

Finalized Date: 27-MAR-2023
Account: KRL

Project: KM6800

CERTIFICATE OF ANALYSIS VA23039623

Sample Description	Method	ME-MS61	ME-MS61	ME-MS61	ME-MS61	ME-MS61	ME-MS61	ME-MS61	ME-MS61	ME-MS61	ME-MS61	ME-MS61	ME-MS61	ME-MS61	ME-MS61	ME-MS61
	Analyte	Cu	Fe	Ga	Ce	Hf	In	K	La	Li	Mg	Mn	Mo	Na	Nb	Ni
	Units	ppm	%	ppm	ppm	ppm	ppm	%	ppm	ppm	%	ppm	ppm	%	ppm	ppm
	LOD	0.2	0.01	0.05	0.05	0.1	0.005	0.01	0.5	0.2	0.01	5	0.05	0.01	0.1	0.2
KM6800 NUW-LHT-SM- Test 2 Head		28.4	2.26	10.20	0.14	0.8	0.016	<0.01	0.6	1.2	4.28	343	2.87	0.67	3.5	237
KM6800 NUW-LHT-SM- Test +106um																
KM6800 NUW-LHT-SM- Test 2 +38um																
KM6800 NUW-LHT-SM- Test 2 -38um																

***** See Appendix Page for comments regarding this certificate *****

ALS Canada Ltd.
2103 Dollarton Hwy
North Vancouver BC V7H 0A7
Phone: +1 604 984 0221 Fax: +1 604 984 0218
www.alsglobal.com/geochemistry

To: ALS METALLURGY, DIV OF ALS CANADA LTD
2957 BOWERS PL
KAMLOOPS BC V1S 1W5

Project: KM6800

CERTIFICATE OF ANALYSIS VA23039623

Sample Description	Method	ME-MS61	ME-MS61	ME-MS61	ME-MS61	ME-MS61	ME-MS61	ME-MS61	ME-MS61	ME-MS61	ME-MS61	ME-MS61	ME-MS61	ME-MS61	ME-MS61	ME-MS61
	Analyte	P	Pb	Rb	Re	S	Sb	Sc	Se	Sn	Sr	Ta	Te	Th	Ti	Tl
	Units	ppm	ppm	ppm	ppm	%	ppm	ppm	ppm	ppm	ppm	ppm	ppm	ppm	%	ppm
	LOD	10	0.5	0.1	0.002	0.01	0.05	0.1	1	0.2	0.2	0.05	0.05	0.01	0.005	0.02
KM6800 NUW-LHT-SM- Test 2 Head		20	2.3	0.1	<0.002	<0.01	0.96	4.2	2	0.7	89.1	0.14	0.05	0.12	0.162	<0.02
KM6800 NUW-LHT-SM- Test +106um																
KM6800 NUW-LHT-SM- Test 2 +38um																
KM6800 NUW-LHT-SM- Test 2 -38um																

***** See Appendix Page for comments regarding this certificate *****

ALS Canada Ltd.
2103 Dollarton Hwy
North Vancouver BC V7H 0A7
Phone: +1 604 984 0221 Fax: +1 604 984 0218
www.alsglobal.com/geochemistry

To: ALS METALLURGY, DIV OF ALS CANADA LTD
2957 BOWERS PL
KAMLOOPS BC V1S 1W5

Project: KM6800

CERTIFICATE OF ANALYSIS VA23039623

Sample Description	Method	ME-MS61	ME-MS61	ME-MS61	ME-MS61	ME-MS61	ME-MS61
	Analyte	U	V	W	Y	Zn	Zr
	Units	ppm	ppm	ppm	ppm	ppm	ppm
	LOD	0.1	1	0.1	0.1	2	0.5
KM6800 NUM-LHT-SM- Test 2 Head		0.3	29	0.3	1.2	22	32.9
KM6800 NUM-LHT-SM- Test +106um							
KM6800 NUM-LHT-SM- Test 2 +38um							
KM6800 NUM-LHT-SM- Test 2 -38um							

***** See Appendix Page for comments regarding this certificate *****

ALS Canada Ltd.
2103 Dollarton Hwy
North Vancouver BC V7H 0A7
Phone: +1 604 984 0221 Fax: +1 604 984 0218
www.alsglobal.com/geochemistry

To: ALS METALLURGY, DIV OF ALS CANADA LTD
2957 BOWERS PL
KAMLOOPS BC V1S 1W5

Page: Appendix 1
Total # Appendix Pages: 1
Finalized Date: 27-MAR-2023
Account: KRL

Project: KM6800

CERTIFICATE OF ANALYSIS VA23039623

CERTIFICATE COMMENTS

ANALYTICAL COMMENTS

Applies to Method: REEs may not be totally soluble in this method.
ME-MS61

LABORATORY ADDRESSES

Applies to Method: Processed at ALS Vancouver located at 2103 Dollarton Hwy, North Vancouver, BC, Canada.

DIS-PUL21	Fe-VOL05	LOG-24	ME-MS61
ME-XRF26	OA-GRA05x	WEI-21	

APPENDIX III – KM6800

MINERALOGICAL DATA

TABLE 1A
SUMMARY OF PERCENT LIBERATION BY SIZE AND CLASS
NUW-LHT-5M Test 2 Jan 30, 2023
KM6800

Size Range	>106µm				<106>38µm			
Mineral Status	Feld	Px	Ol	OGn	Feld	Px	Ol	OGn
Liberated	29.9	18.2	39.7	0.5	27.0	15.1	22.8	1.7
Binary - Feld		8.5	0.0	22.3		2.0	0.0	12.9
Binary - Px	1.6		2.5	2.3	0.2		3.8	2.0
Binary - Ol	0.0	1.3		0.3	0.0	1.5		0.4
Binary - OGn	2.1	2.4	0.9		1.1	1.9	0.9	
Multiphase	1.9	11.5	1.3	13.0	0.2	1.8	0.8	1.3
Total	35.5	41.8	44.5	38.4	28.6	22.2	28.3	18.3

Size Range	<38µm			
Mineral Status	Feld	Px	Ol	OGn
Liberated	34.3	27.2	22.9	24.1
Binary - Feld		4.2	0.3	13.9
Binary - Px	0.5		1.8	3.3
Binary - Ol	0.0	0.6		0.3
Binary - OGn	1.0	2.3	0.6	
Multiphase	0.1	1.6	1.6	1.7
Total	35.9	36.0	27.2	43.3

Size Range	Mineral Liberation-2 Dimensions			
Mineral Status	Feld	Px	Ol	OGn
Liberated	91.3	60.5	85.4	26.3
Binary - Feld		14.7	0.3	49.1
Binary - Px	2.3		8.1	7.5
Binary - Ol	0.0	3.3		1.0
Binary - OGn	4.2	6.6	2.5	
Multiphase	2.2	14.9	3.7	16.1
Total	100	100	100	100

Notes 1) Feld-Feldspars including Calcium Plagioclase, Feldspar Albite, K Feldspar and Epidote Clinozoisite?, Px-Pyroxenes/Amphiboles, Ol-Olivine, OGn-Other Gangue Minerals.
2) 0.0 Indicates these minerals were not observed during the counting procedure.
3) The 106 and 38µm sizing fractions correspond to the Tyler 150 and 400 mesh sieves.
4) The Total line is the distribution of mineral in the size fraction. Original data is from the size by assay and distribution tables.
5) Measurement was scanned on the QEMSCAN ®.
6) Liberations should be considered an estimate.

TABLE 1B
SIZE BY ASSAY AND DISTRIBUTION BASED ON METAL CONTENT
NUW-LHT-5M Test 2 Jan 30, 2023

Size	Mass	Assays-percent					Distribution				
Fraction	%	Al	Ca	Cr	Fe	K	Al	Ca	Cr	Fe	K
>106µm	36.7	13.3	10.1	0.06	2.81	0.03	35.5	36.1	37.8	44.1	31.1
<106>38µm	27.5	13.6	10.3	0.05	2.23	0.03	27.3	27.5	25.2	26.2	23.3
<38µm	35.9	14.2	10.4	0.06	1.94	0.05	37.1	36.4	37.0	29.7	45.6
Total	100	13.7	10.2	0.06	2.34	0.04	100	100	100	100	100

Size	Mass	Assays-percent					Distribution				
Fraction	%	Mg	Na	Si	Ti		Mg	Na	Si	Ti	
>106µm	36.7	5.07	0.65	21.5	0.19		40.0	33.2	36.4	39.9	
<106>38µm	27.5	4.65	0.69	21.8	0.17		27.6	26.3	27.6	27.1	
<38µm	35.9	4.19	0.82	21.7	0.16		32.4	40.6	35.9	33.0	
Total	100	4.64	0.72	21.6	0.18		100	100	100	100	

TABLE 1C
SIZE BY ASSAY AND DISTRIBUTION BASED ON MINERAL CONTENT
NUW-LHT-5M Test 2 Jan 30, 2023

Size	Mass	Assays-percent				Distribution			
Fraction	%	Feld	Px	Ol	OGn	Feld	Px	Ol	OGn
>106µm	36.7	79.3	12.1	4.61	4.00	35.5	41.8	44.5	38.4
<106>38µm	27.5	85.0	8.5	3.91	2.54	28.6	22.2	28.3	18.3
<38µm	35.9	81.9	10.6	2.88	4.61	35.9	36.0	27.2	43.3
Total	100	81.8	10.6	3.80	3.82	100	100	100	100

Notes 1) Feld-Feldspars including Calcium Plagioclase, Feldspar Albite, K Feldspar and Epidote Clinozoisite?, Px-Pyroxenes/Amphiboles, Ol-Olivine, OGn-Other Gangue Minerals.
2) Mineral Content was based on the QEMSCAN measurement.

TABLE 1D
COMPARATIVE ASSAY TABLE
NUW-LHT-5M Test 2 Jan 30, 2023

Method	Al	Ca	Fe	K	Mg	Na	Si
Chemical	13.7	10.2	2.3	<0.1	4.6	0.7	21.6
QEMSCAN	14.5	11.2	2.2	<0.1	3.8	0.8	20.8

Notes 1) This table compares the mineral composition of the samples determined by chemical analysis with the composition determined by QEMSCAN analysis.
2) The QEMSCAN data is based on the relative number of grains observed for each mineral and their estimated densities.

TABLE 1E
ESTIMATED RELATIVE PROPORTION AND COMPOSITION OF MINERAL GRAINS
NUW-LHT-5M Test 2 Jan 30, 2023

Binary	Proportion by Weight-2D				Composition of Grains			
Component	Feld	Px	Ol	OGn	Feld	Px	Ol	OGn
Liberated	74.7	6.4	3.2	1.0	100	100	100	100
Binary - Feld		1.6	0.0	1.9		45	60	35
Binary - Px	1.9		0.3	0.3	55		47	29
Binary - Ol	0.0	0.4		0.0	40	53		29
Binary - OGn	3.5	0.7	0.1		65	71	71	
Multiphase	1.8	1.6	0.1	0.6	44	38	3	15
Average Composition	81.8	10.6	3.8	3.8	93	68	46	33

Notes 1) The two-dimensional proportion of minerals is a weighted estimate which is based on the liberation and the mineral content of the sample.
2) Composition values of "0" represents values <2% and "100" represents values >95%.

TABLE 1F
DISTRIBUTION BY SIZE RANGE OF ALUMINUM, CALCIUM AND IRON BEARING MINERALS
NUW-LHT-5M Test 2 Jan 30, 2023

Size	Mass	% Al of Total Al					% Ca of Total Ca				% Fe of Total Fe				
Fraction	%	Feld	Px/Am	Ol	Chl	OAl	Feld	Px/Am	Car	OCa	FeOx	PxAm	Ol	Chl	OFe
>106µm	36.7	96.2	1.1	0.2	1.8	0.7	89.3	9.5	0.1	1.1	2.5	42.9	24.3	10.9	19.3
<106>38µm	27.5	97.8	0.8	0.2	0.7	0.5	93.7	5.7	0.1	0.5	4.0	37.0	25.3	6.2	27.6
<38µm	35.9	96.4	1.2	0.2	1.3	0.8	90.9	8.5	0.2	0.4	10.8	38.4	18.5	10.0	22.4
Total	100	96.7	1.1	0.2	1.3	0.7	91.1	8.1	0.1	0.7	5.4	40.0	22.8	9.4	22.4

Notes 1) Feld-Feldspars, Px/Am-Pyroxenes/Amphibole, Ol-Olivine, Chl-Chlorite, OAl-Other Aluminum bearing minerals including Micas, Spinel, Kaolinite and Sphene (Titanite).
2) Car-Carbonates including Calcite and Ankerite/Dolomite, OCa-Other Calcium bearing minerals including Apatite and Sphene (Titanite).
3) FeOx-Elemental Iron\Iron Oxides includes Steel and may include Magnetite, Hematite and Goethite/Limonite, OFe-Other Iron bearing minerals including Sulphide Minerals, Micas, Talc, Epidote? and Ankerite.

TABLE 1G
DISTRIBUTION BY SIZE RANGE OF MAGNESIUM AND SILICON BEARING MINERALS
NUW-LHT-5M_Test 2 Jan 30, 2023

Size	Mass	% Mg of Total Mg					% Si of Total Si				
Fraction	%	Feld	Px/Am	Ol	Chl	OMg	Feld	Px/Am	Ol	Qz	OSi
>106µm	36.7	18.8	41.8	31.3	7.1	1.1	81.3	12.2	3.4	0.8	2.2
<106>38µm	27.5	24.5	37.7	32.8	3.4	1.6	85.8	8.8	2.9	1.3	1.1
<38µm	35.9	24.4	43.5	22.7	6.3	3.2	83.5	10.9	2.1	1.6	1.9
Total	100	22.2	41.2	28.9	5.8	1.9	83.3	10.8	2.8	1.2	1.8

Notes 1) Feld-Feldspars, Px/Am-Pyroxenes/Amphibole, Ol-Olivine, Chl-Chlorite, OMg-Other Magnesium bearing minerals including Micas, Talc, Serpentine, Spinel, Ankerite/Dolomite and Magnesite.
2) Qz-Quartz, OSi-Other Silicates including Micas, Talc, Serpentine, Kaolinite and Sphene (Titanite).

TABLE 1H
THE WEIGHT OF THE OBSERVED MINERALS
NUW-LHT-5M Test 2 Jan 30, 2023

Mineral	Mineral Assays (percent)			
	>106µm	<106>38µm	<38µm	Total
Elemental Iron/Iron Oxides	0.07	0.09	0.29	0.16
Quartz	0.41	0.60	0.73	0.58
Calcium Plagioclase Feldspar	78.9	84.6	81.2	81.3
Feldspar Albite (Na Feldspar)	0.46	0.35	0.63	0.49
K-Feldspar	0.01	0.02	0.13	0.06
Orthopyroxenes	7.07	5.37	5.30	5.97
Clinopyroxenes	4.16	2.41	2.68	3.15
Amphibole	0.83	0.76	2.62	1.45
Olivine	4.61	3.91	2.88	3.80
Chlorite	2.13	0.91	1.62	1.61
Talc	0.14	0.13	0.30	0.20
Micas	0.12	0.09	0.20	0.14
Carbonates	0.06	0.07	0.11	0.08
Kaolinite (clay)	0.03	0.02	0.08	0.04
Others	1.03	0.63	1.29	1.02
Total	100	100	100	100

Notes: 1) Elemental Iron\Iron Oxides includes Steel and may include Magnetite, Hematite and Goethite/Limonite.
2) Calcium Plagiocase Feldspar includes Epidote Clinozoisite?.
3) Micas includes Biotite/Phlogopite and Muscovite.
4) Carbonates includes Calcite, Ankerite/Dolomite and Magnesite.
5) Others includes Sphene (Titanite), Rutile/Anatase, Epidote?, Serpentine, Sulphide Minerals, Apatite, Spinel and unresolved mineral species.

TABLE 1I
FELDSPAR GRAIN SEARCH SUMMARY
NUW-LHT-5M Test 2 Jan 30, 2023

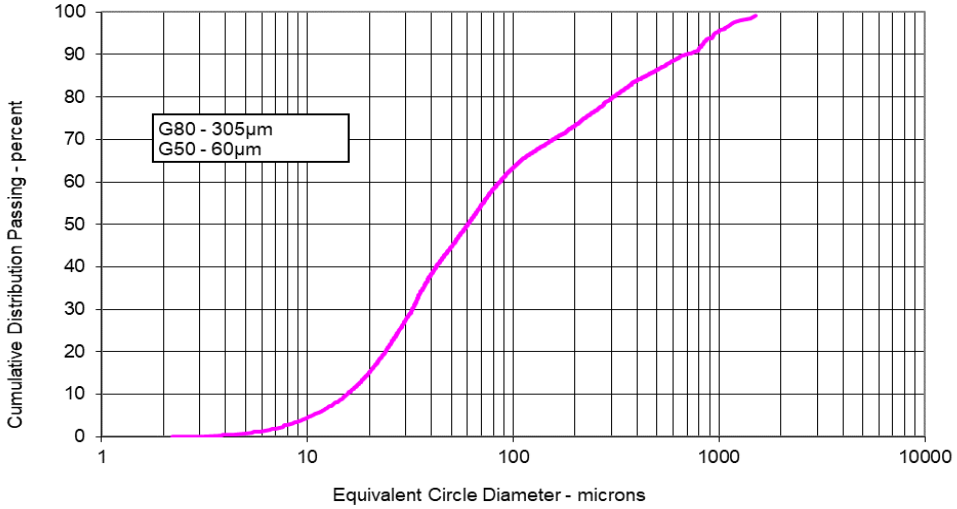

Particle Size Distribution					
Size Fraction µm	Distribution percent	Size Fraction µm	Distribution percent	Size Fraction µm	Distribution percent
>800	8.73	<60>55	2.50	<19>18	1.25
<800>700	1.09	<55>50	2.75	<18>17	1.15
<700>600	1.59	<50>48	1.11	<17>16	1.15
<600>500	2.15	<48>45	1.71	<16>15	1.08
<500>400	2.52	<45>42	2.08	<15>14	1.02
<400>300	4.18	<42>40	1.49	<14>13	1.06
<300>250	3.06	<40>38	1.79	<13>12	0.95
<250>200	3.38	<38>35	2.97	<12>11	1.00
<200>150	3.86	<35>32	3.97	<11>10	0.85
<150>100	6.11	<32>30	2.10	<10>9	0.91
<100>95	1.08	<30>28	2.29	<9>8	0.72
<95>90	1.15	<28>25	3.60	<8>7	0.73
<90>85	1.27	<25>24	1.50	<7>6	0.76
<85>80	1.49	<24>23	1.07	<6>5	0.49
<80>75	1.85	<23>22	1.38	<5>4	0.44
<75>70	2.01	<22>21	1.10	<4>3	0.34
<70>65	2.28	<21>20	1.35	<3	0.10
<65>60	2.26	<20>19	1.18		

Note 1) The sizing maybe overestimated due to coarse particle effects.
2) Feldspars includes Calcium Plagioclase, Feldspar Albite, K Feldspar and Epidote Clinozoisite?.

TABLE 1J
PYROXENE/AMPHIBOLE GRAIN SEARCH SUMMARY
NUW-LHT-5M_Test 2 Jan 30, 2023

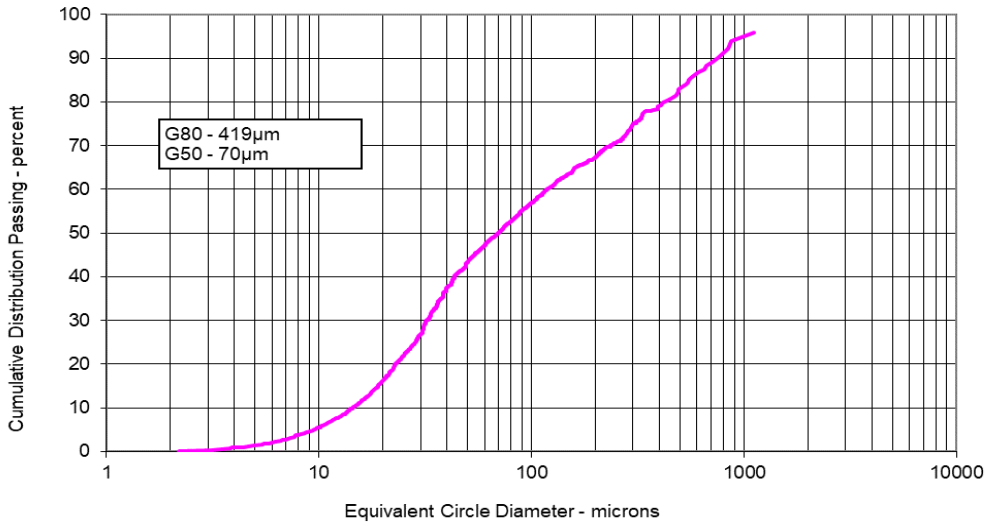

Particle Size Distribution					
Size Fraction µm	Distribution percent	Size Fraction µm	Distribution percent	Size Fraction µm	Distribution percent
>800	7.90	<60>55	1.57	<19>18	1.13
<800>700	2.87	<55>50	2.14	<18>17	1.30
<700>600	2.42	<50>48	1.43	<17>16	0.96
<600>500	3.37	<48>45	1.09	<16>15	0.96
<500>400	4.17	<45>42	2.57	<15>14	1.04
<400>300	4.21	<42>40	0.76	<14>13	1.31
<300>250	4.22	<40>38	2.39	<13>12	0.88
<250>200	3.43	<38>35	2.44	<12>11	0.97
<200>150	3.85	<35>32	2.66	<11>10	1.01
<150>100	6.60	<32>30	3.12	<10>9	0.98
<100>95	1.02	<30>28	2.39	<9>8	0.71
<95>90	0.77	<28>25	2.66	<8>7	0.83
<90>85	1.23	<25>24	0.93	<7>6	0.90
<85>80	1.23	<24>23	0.80	<6>5	0.55
<80>75	1.08	<23>22	1.69	<5>4	0.57
<75>70	1.51	<22>21	1.01	<4>3	0.63
<70>65	1.29	<21>20	1.19	<3	0.40
<65>60	1.72	<20>19	1.15		

Note 1) The sizing maybe overestimated due to coarse particle effects.

TABLE 1K
OLIVINE GRAIN SEARCH SUMMARY
NUW-LHT-5M_Test 2 Jan 30, 2023

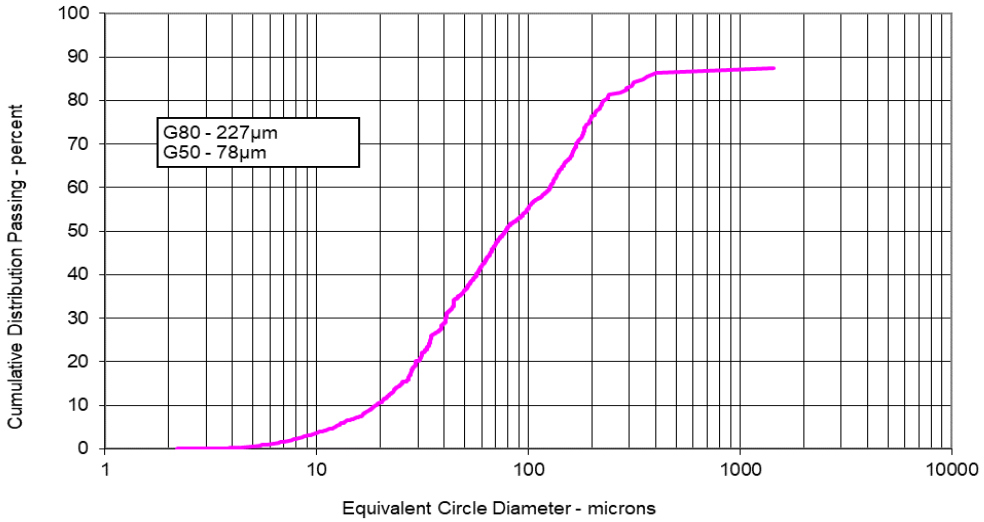

Particle Size Distribution					
Size Fraction µm	Distribution percent	Size Fraction µm	Distribution percent	Size Fraction µm	Distribution percent
>800	12.5	<60>55	2.90	<19>18	0.95
<800>700	0.00	<55>50	2.72	<18>17	0.85
<700>600	0.00	<50>48	0.90	<17>16	0.79
<600>500	0.00	<48>45	1.04	<16>15	0.36
<500>400	1.17	<45>42	2.85	<15>14	0.47
<400>300	2.98	<42>40	2.72	<14>13	0.79
<300>250	1.48	<40>38	1.65	<13>12	0.89
<250>200	5.13	<38>35	1.08	<12>11	0.63
<200>150	10.72	<35>32	3.97	<11>10	0.52
<150>100	10.58	<32>30	2.00	<10>9	0.75
<100>95	1.33	<30>28	2.28	<9>8	0.48
<95>90	1.07	<28>25	3.20	<8>7	0.81
<90>85	0.95	<25>24	0.68	<7>6	0.61
<85>80	0.95	<24>23	0.59	<6>5	0.40
<80>75	2.10	<23>22	1.06	<5>4	0.37
<75>70	1.70	<22>21	0.87	<4>3	0.31
<70>65	2.83	<21>20	0.77	<3	0.05
<65>60	2.43	<20>19	0.75		

Note 1) The sizing maybe overestimated due to coarse particle effects.

TABLE 2A
ELEMENTAL COMPOSITION OF CALCIUM PLAGIOCLASE FELDSPAR MINERALS
KM6800 NUW-LHT-5M_TEST 2 JANUARY 30, 2023

Particle	Weight Percent						Normal Weight Percent					
	Al	Ca	Na	O	Si	Total	Al	Ca	Na	O	Si	Total
1	18.8	16.4	1.4	30.2	18.3	85.1	22.1	19.3	1.6	35.5	21.5	100
2	15.1	12.8	0.9	25.0	14.7	68.5	22.0	18.7	1.4	36.4	21.5	100
3	15.3	13.1	0.9	25.0	14.6	68.9	22.2	19.0	1.3	36.3	21.2	100
4	15.8	13.9	0.7	25.2	14.6	70.2	22.6	19.8	1.0	35.9	20.8	100
5	15.7	13.3	1.0	25.7	15.2	70.8	22.2	18.8	1.4	36.2	21.4	100
6	14.9	12.6	1.0	24.4	14.8	67.6	22.0	18.6	1.5	36.1	21.9	100
7	15.9	13.8	0.8	25.5	14.9	70.9	22.4	19.4	1.1	36.0	21.0	100
8	15.1	12.7	1.1	25.0	15.0	68.8	21.9	18.5	1.5	36.3	21.8	100

Note: 1) Spectra was obtained using the Bruker X Flash 5030 detector.

TABLE 2B
ELEMENTAL COMPOSITION OF FELDSPAR ALBITE MINERALS
KM6800 NUW-LHT-5M_TEST 2 JANUARY 30, 2023

Particle	Weight Percent						Normal Weight Percent					
	Al	Ca	Na	O	Si	Total	Al	Ca	Na	O	Si	Total
1	8.9	0.7	5.0	22.7	21.0	58.3	15.3	1.2	8.6	38.9	35.9	100
2	11.0	1.5	6.3	27.9	23.8	70.6	15.6	2.1	9.0	39.5	33.8	100
3	9.9	0.6	5.9	25.3	23.1	64.8	15.3	0.9	9.1	39.0	35.7	100
4	10.3	-	6.2	26.7	23.0	66.2	15.5	-	9.4	40.3	34.8	100
5	10.5	-	5.2	24.2	22.6	62.5	16.7	-	8.4	38.8	36.1	100
6	10.6	-	4.5	22.4	20.1	57.7	18.4	-	7.9	38.9	34.8	100
7	7.1	0.2	4.5	19.4	17.7	48.8	14.5	0.5	9.2	39.7	36.2	100
8	7.4	-	4.8	20.2	18.0	50.5	14.7	-	9.5	40.1	35.7	100
9	7.3	0.7	4.0	18.0	16.5	46.5	15.6	1.6	8.6	38.7	35.5	100
10	6.8	0.3	4.3	17.9	16.5	45.7	14.9	0.6	9.5	39.1	36.0	100

Note: 1) Spectra was obtained using the Bruker X Flash 5030 detector.

TABLE 2C
ELEMENTAL COMPOSITION OF CHLORITE MINERALS
KM6800 NUW-LHT-5M_TEST 2 JANUARY 30, 2023

Particle	Weight Percent							Normal Weight Percent						
	Al	Cr	Fe	Mg	O	Si	Total	Al	Cr	Fe	Mg	O	Si	Total
1	10.1	-	7.9	14.9	28.2	10.0	71.1	14.1	-	11.1	21.0	39.7	14.1	100
2	8.8	0.7	2.0	15.2	24.9	9.4	61.0	14.4	1.2	3.3	24.9	40.8	15.4	100
3	12.3	-	12.5	11.3	31.2	12.3	79.7	15.5	-	15.7	14.2	39.2	15.5	100
4	10.0	-	11.7	11.5	23.6	9.6	66.3	15.0	-	17.6	17.3	35.6	14.5	100
5	10.0	-	10.3	12.7	25.1	9.5	67.6	14.7	-	15.2	18.8	37.2	14.1	100
6	9.6	-	10.4	12.6	27.9	10.0	70.5	13.6	-	14.7	17.8	39.6	14.2	100
7	8.4	-	9.9	10.6	24.5	8.2	61.8	13.7	-	16.1	17.2	39.7	13.3	100
8	12.2	-	13.9	12.6	32.2	12.7	83.6	14.6	-	16.6	15.0	38.5	15.2	100
9	10.2	-	8.3	12.2	22.3	9.8	62.6	16.2	-	13.3	19.4	35.5	15.6	100

Note: 1) Spectra was obtained using the Bruker X Flash 5030 detector.

TABLE 2D
ELEMENTAL COMPOSITION OF OLIVINE MINERALS
KM6800 NUW-LHT-5M_TEST 2 JANUARY 30, 2023

Particle	Weight Percent							Normal Weight Percent						
	Al	Fe	Mg	Ni	O	Si	Total	Al	Fe	Mg	Ni	O	Si	Total
1	-	12.9	26.5	0.4	25.3	14.5	79.7	-	16.2	33.3	0.5	31.8	18.2	100
2	-	13.5	25.8	0.4	24.6	14.0	78.3	-	17.3	32.9	0.5	31.4	17.9	100
3	-	12.8	25.5	0.4	24.4	13.8	76.8	-	16.6	33.1	0.5	31.8	18.0	100
4	-	13.0	26.1	0.4	25.0	14.1	78.5	-	16.6	33.2	0.5	31.8	17.9	100
5	-	13.4	25.1	0.4	23.9	13.7	76.4	-	17.5	32.8	0.5	31.3	17.9	100
6	-	13.0	25.3	0.4	23.6	14.1	76.3	-	17.0	33.1	0.5	30.9	18.5	100
7	0.8	7.4	28.6	0.5	25.9	14.6	77.7	1.0	9.5	36.8	0.6	33.4	18.7	100
8	0.7	7.4	27.8	0.5	25.1	14.2	75.7	1.0	9.8	36.7	0.6	33.2	18.7	100
9	0.6	6.5	28.6	0.4	25.5	14.4	76.1	0.8	8.6	37.6	0.5	33.5	19.0	100
10	0.6	7.5	27.6	0.5	24.7	14.3	75.2	0.8	10.0	36.7	0.6	32.9	19.0	100
11	1.0	6.8	28.0	0.4	24.8	14.5	75.6	1.4	9.0	37.1	0.6	32.8	19.2	100
12	0.6	7.1	27.9	0.4	25.1	14.2	75.4	0.8	9.4	37.1	0.6	33.3	18.9	100
13	0.6	6.7	27.2	0.4	23.8	14.3	73.1	0.8	9.2	37.3	0.6	32.6	19.6	100
14	0.6	6.8	28.5	0.4	25.4	14.4	76.2	0.8	8.9	37.4	0.6	33.4	19.0	100

Note: 1) Spectra was obtained using the Bruker X Flash 5030 detector.

TABLE 2E
ELEMENTAL COMPOSITION OF PYROXENE MINERALS
KM6800 NUW-LHT-5M_TEST 2 JANUARY 30, 2023

Particle	Weight Percent							Normal Weight Percent						
	Al	Ca	Fe	Mg	O	Si	Total	Al	Ca	Fe	Mg	O	Si	Total
1	1.2	0.5	10.1	14.9	22.9	17.7	67.2	1.7	0.7	15.0	22.2	34.0	26.4	100
2	0.9	0.6	10.3	14.6	22.7	17.5	66.7	1.3	0.9	15.5	21.9	34.1	26.3	100
3	0.8	1.4	9.9	14.6	23.2	17.6	67.6	1.2	2.1	14.6	21.6	34.4	26.1	100
4	0.9	1.1	10.6	15.5	24.1	18.6	70.7	1.2	1.6	15.0	21.8	34.1	26.2	100
5	0.8	1.4	10.1	14.4	23.3	17.4	67.4	1.2	2.1	15.0	21.4	34.6	25.9	100
6	0.9	0.4	8.0	15.7	22.9	17.9	65.9	1.4	0.6	12.1	23.9	34.8	27.2	100
7	1.1	1.4	7.6	15.4	23.1	17.8	66.5	1.7	2.2	11.4	23.2	34.8	26.8	100
8	1.0	1.2	7.2	15.0	22.7	17.3	64.3	1.5	1.8	11.2	23.3	35.2	26.9	100
9	1.2	18.5	5.2	7.8	24.5	17.1	74.3	1.6	24.9	7.0	10.4	33.0	23.0	100
10	1.0	17.8	6.1	8.2	24.5	17.4	75.0	1.3	23.7	8.1	10.9	32.7	23.2	100
11	0.9	16.8	5.0	7.8	23.6	16.4	70.5	1.3	23.8	7.0	11.1	33.5	23.2	100
12	1.2	17.2	7.9	7.2	24.2	16.7	74.5	1.6	23.1	10.7	9.7	32.5	22.4	100
13	1.1	17.8	5.9	7.7	24.1	16.9	73.5	1.4	24.2	8.0	10.5	32.8	23.0	100
14	1.0	17.7	5.2	7.7	24.0	16.9	72.4	1.4	24.4	7.2	10.6	33.1	23.3	100
15	1.2	17.4	5.4	7.9	24.0	16.7	72.5	1.7	24.0	7.4	10.9	33.1	23.0	100
16	1.0	10.6	7.1	8.8	23.5	17.1	68.1	1.5	15.6	10.5	12.9	34.4	25.1	100

Note: 1) Spectra was obtained using the Bruker X Flash 5030 detector.
2) Particles 1-8 Orthopyroxene and particles 9-16 Clinopyroxene.

TABLE 2F
ELEMENTAL COMPOSITION OF AMPHIBOLE MINERALS
KM6800 NUW-LHT-5M TEST 2 JANUARY 30, 2023

Particle	Weight Percent							Normal Weight Percent						
	Al	Ca	Fe	Mg	O	Si	Total	Al	Ca	Fe	Mg	O	Si	Total
1	0.6	7.1	1.8	7.7	18.6	12.9	48.6	1.2	14.6	3.7	15.7	38.2	26.6	100
2	0.4	6.8	1.1	8.3	18.6	13.1	48.2	0.8	14.1	2.2	17.2	38.6	27.1	100
3	1.9	6.8	1.2	7.6	18.2	12.2	47.8	4.0	14.1	2.4	15.9	38.0	25.6	100
4	0.8	6.2	1.1	7.5	17.1	11.8	44.5	1.7	13.9	2.5	16.8	38.5	26.6	100
5	6.9	10.7	2.3	4.4	17.9	10.1	52.3	13.2	20.5	4.3	8.5	34.3	19.2	100
6	0.6	6.0	2.0	7.3	17.3	11.9	45.2	1.4	13.3	4.4	16.2	38.2	26.4	100
7	2.1	6.4	2.7	7.2	18.7	12.0	49.1	4.3	13.0	5.6	14.7	38.0	24.3	100
8	1.8	6.1	0.9	7.4	18.2	11.3	45.6	3.9	13.4	1.9	16.2	39.9	24.7	100
9	1.8	6.2	1.0	7.4	18.1	11.6	46.1	3.9	13.5	2.1	16.1	39.3	25.2	100

Note: 1) Spectra was obtained using the Bruker X Flash 5030 detector.

BACKSCATTER IMAGE 1
NASA - NUW-LHT-5M_TEST 2 JANUARY 30, 2023
KM6800

<106>38µm

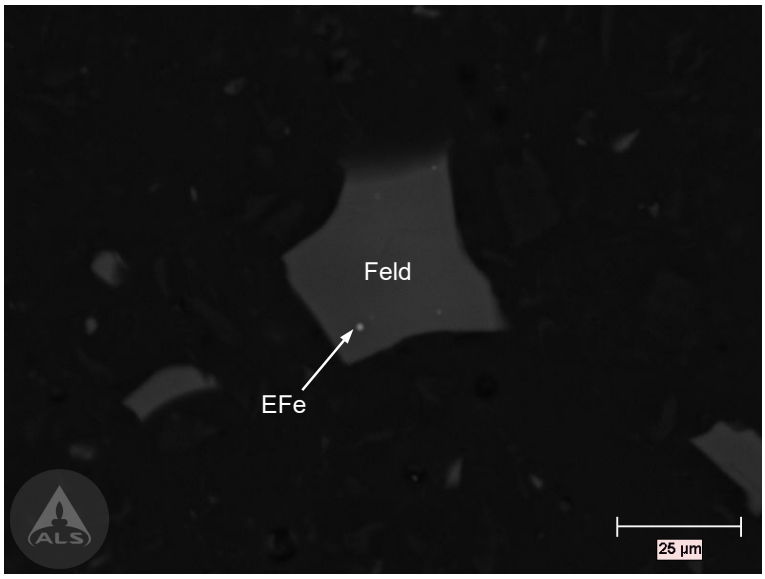

<106>38µm

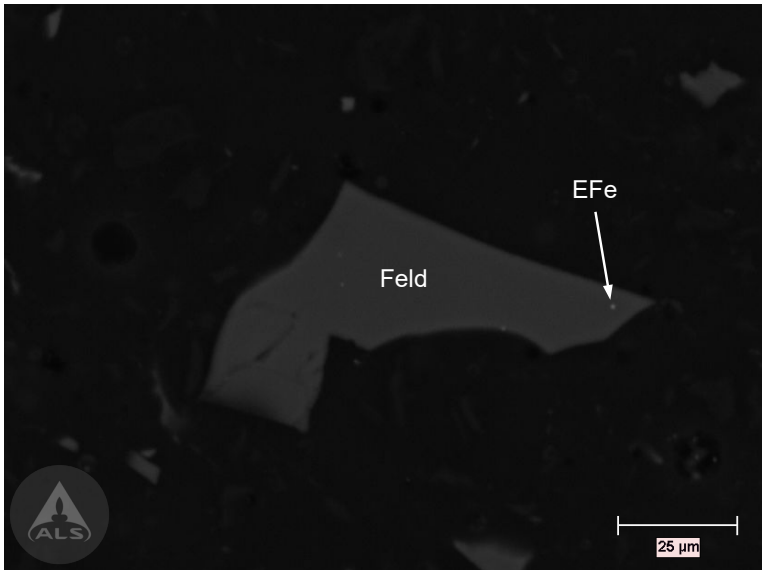

*Feld-Feldspar, EFe-Elemental Iron

BACKSCATTER IMAGE 2
NASA - NUW-LHT-5M_TEST 2 JANUARY 30, 2023
KM6800

>106µm

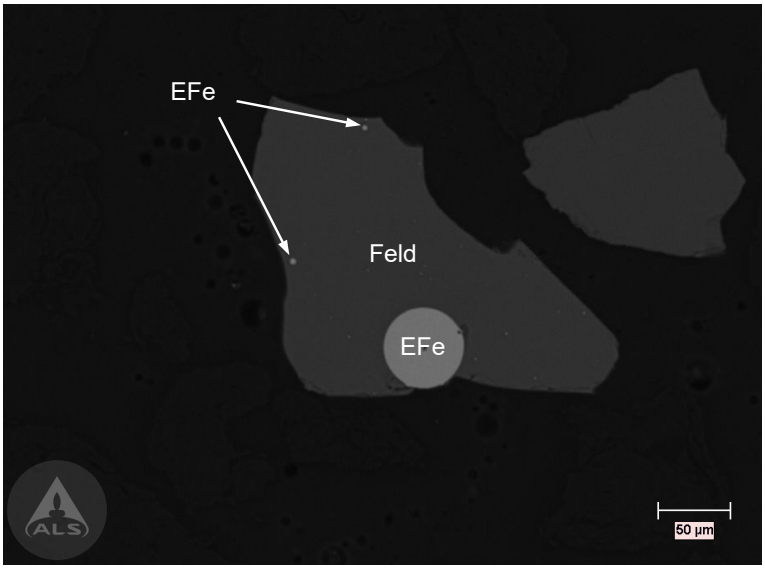

<106>38µm

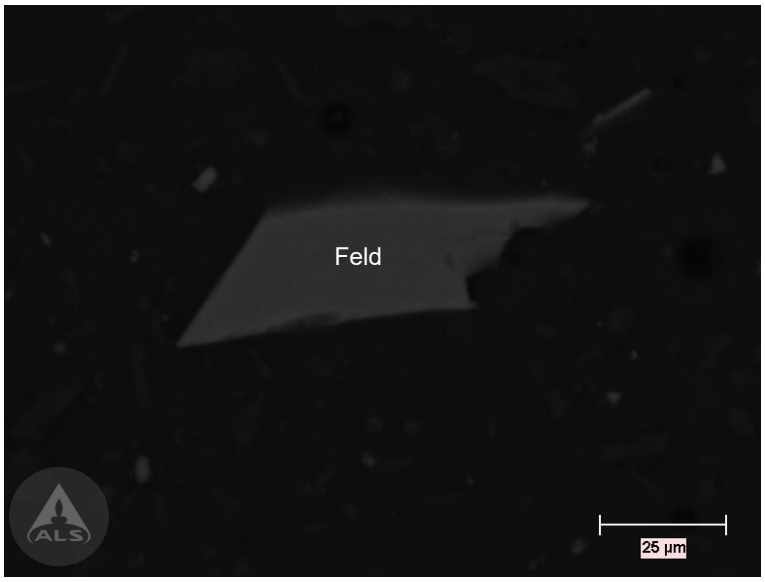

*Feld-Feldspar, EFe-Elemental Iron.

Appendix C Section 5 Supplemental Information

DCM Science

DCM SCIENCE LABORATORY, INC.
12421 W 49TH AVENUE, UNIT #6
WHEAT RIDGE, CO 80033 (303) 463-8270

CRYSTALLINE BULK SILICA TEST REPORT (TOTAL)
MODIFIED NIOSH 7500 METHOD
PAGE 1 of 1

Client:
George C Marshall Space Flight Center
Transportation Officer, Bldg 4631
Marshall Space Flight Center, AL 35812

Analysis Date:	3-30-23
Reporting Date:	3-31-23
Receipt Date:	3-27-23
Client Job No.:	NUW-LHT-5M
Client Project:	None Given
DCMSL Project:	NASA8

DCM NO.	SAMPLE NUMBER (C)	SAMPLE WEIGHT (mg)	MEASURED QUARTZ (mg)	PERCENT QUARTZ
-1	NUW-LHT-5M	13.2	0.106	0.80
-1QC	NUW-LHT-5M	13.1	0.117	0.89

(C) Information provided by client

The samples were washed in phosphoric acid to remove interferences.

The samples were analyzed using a modified version of the NIOSH 7500 method. A representative portion of each sample was micronized, weighed (sample wt.) and deposited on silver filters.

The samples were weighed with a Mettler XP56 microbalance with an estimated limit of detection of 0.030mg. The balance is certified within instrument specifications and traceable to National Institute of Standards and Technology.

The samples were analyzed in conjunction with prepared standards of crystalline silica. Calibration curves have been established for crystalline silica using NIST and NIOSH standard reference materials. Sample intensities were calculated relative to calibration curves. The quantitative detection limit of crystaline silica for this method is 0.005mg quartz and 0.010mg cristobalite and tridymite. The coefficent of variation as stated by NIOSH is 0.09 for concentrations between 0.025mg and 2.5mg. All calculations are based upon those in the NIOSH 7500, OSHA and MSHA methods. A computer spreadsheet program is used for all calculations. All results have been rounded by the program.

The bulk material was prepared for x-ray diffraction and scanned using a slow scan rate to determine the phases of crystalline silica present in the samples. Identified crystalline silica polymorphs were scanned over principal peaks using a slow scan rate to determine concentration. Per client request, the samples were only analyzed for quartz.

The samples were received in acceptable condition. This test report relates only to the items tested. The results of this report apply to the samples as received from the client and the validity of the results is dependent on any information supplied by the client. This report may not be reproduced except in full without the written approval of the laboratory.

Jason Barnes, Analyst

RON SCHOTT, LABORATORY DIRECTOR

DCM SCIENCE LABORATORY, INC.
12421 W. 49TH AVENUE, UNIT #6
WHEAT RIDGE, CO 80033 (303) 463-8270

CRYSTALLINE BULK SILICA TEST REPORT (RESPIRABLE)
MODIFIED NIOSH 7500 METHOD

Client:
George C Marshall Space Flight Center
Transportation Officer, Bldg 4631
Marshall Space Flight Center, AL 35812

Analysis Date:	3-30-23
Reporting Date:	3-31-23
Receipt Date:	3-27-23
Client Job No.:	NUW-LHT-5M
Client Project:	None Given
DCMSL Project:	NASA9

DCM NO.	SAMPLE NUMBER (C)	SAMPLE WEIGHT (mg)	MEASURED QUARTZ (mg)	PERCENT QUARTZ	PERCENT PASSING (<10um)	PERCENT RESP. SILICA TOTAL SAMPLE
-1	NUW-LHT-5M	12.0	0.110	0.92	13.9	0.13

(C) Information provided by client

The sample was analyzed using a modified version of the NIOSH 7500 method. The following modifications were made:

- The respirable fraction (<10µm) was removed by wet sieving through a 10µm sieve to determine percent passing.
- The sample was washed in phosphoric acid to remove interferences.

The sample was weighed with a Mettler XP56 microbalance with an estimated limit of detection of 0.030mg. The balance is certified within instrument specifications and traceable to National Institute of Standards and Technology.

The sample was analyzed using the NIOSH 7500 method and OSHA method ID-142. Calibration curves are established for crystalline silica using NIST and NIOSH standard reference materials. Sample intensities were calculated relative to calibration curves. The quantitative detection limit of crystalline silica for this method is 0.005mg quartz and 0.010mg cristobalite and tridymite. The coefficient of this method as stated by NIOSH 7500 is 0.09 for concentrations between 0.025mg and 2.5mg. All calculations are based upon those in NIOSH 7500, OSHA and MSHA methods.

The bulk material was prepared and scanned by x-ray diffraction to determine the phases of crystalline silica present in the samples. Identified crystalline silica polymorphs were scanned over principal peaks using a slow scan rate to determine concentration. Per client request, the sample was only analyzed for quartz.

The sample was received in acceptable condition. This test report relates only to the items tested. The results of this report apply to the samples as received from the client and the validity of the results is dependent on any information supplied by the client. This report may not be reproduced except in full without the written approval of the laboratory.

All information provided by clients, including sample results, is considered proprietary and confidential. Client results and other information will not be released to anyone but the client except by client request. When the laboratory is required by law or authorized by contractual arrangement to release confidential information, the client or individual concerned shall, unless prohibited by law, be notified of the informatin provided.

INDUSTRIAL HYGIENE Accredited Laboratory ISO/IEC 17025:2017 AIHA LAP, LLC AIHAACCREDITEDLABS.ORG Lab ID # 101526

Jason Barnes, Analyst

RON SCHOTT, LABORATORY DIRECTOR

Appendix D Section 7.1 Supplemental Information

2D Particle Shape

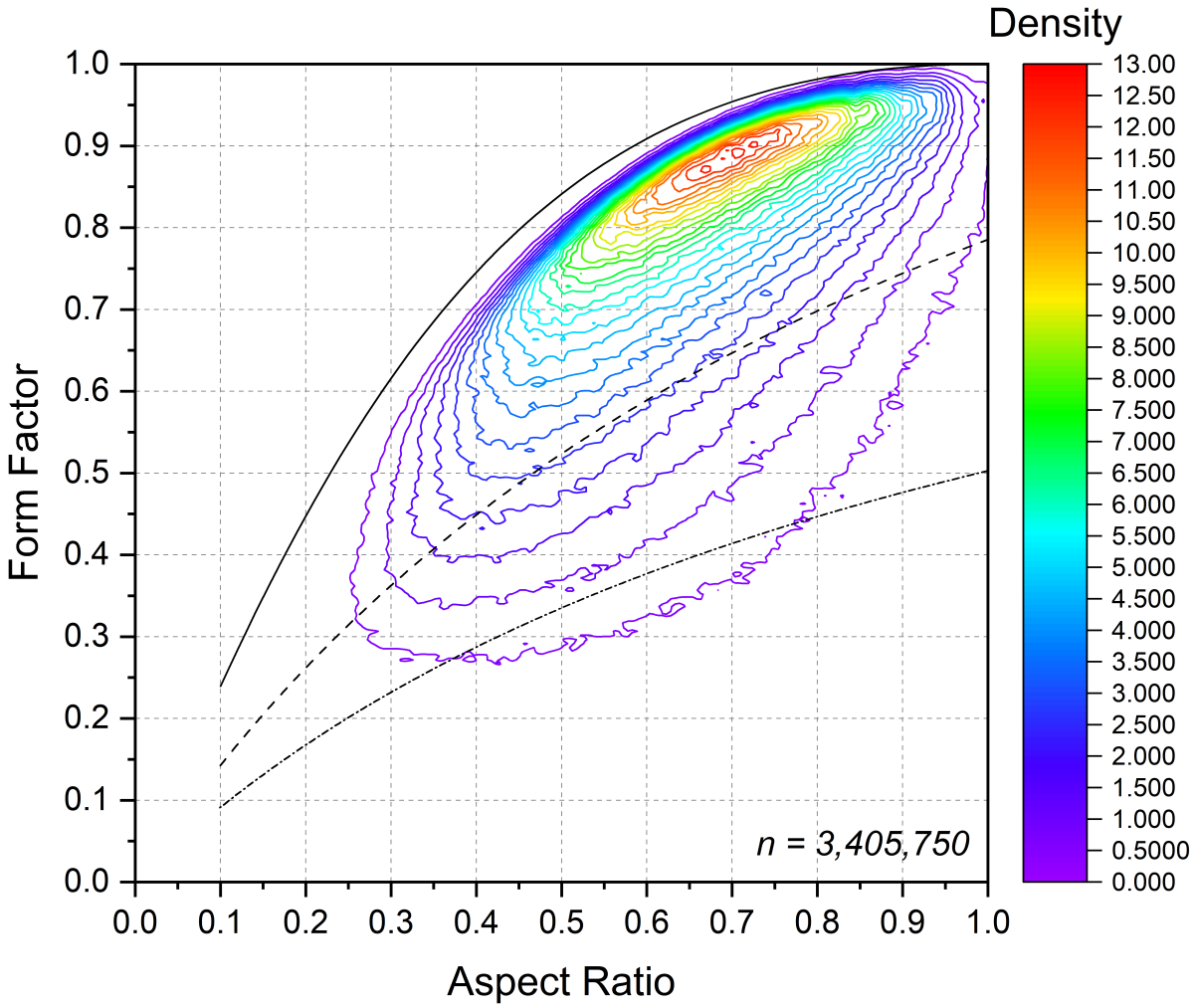

Figure D1. Particle shape distribution of NUW-LHT-5M following the methods of Wilkerson et al. (2024). The most common particle shape has an aspect ratio of ~0.7 and a form factor of ~8.9.

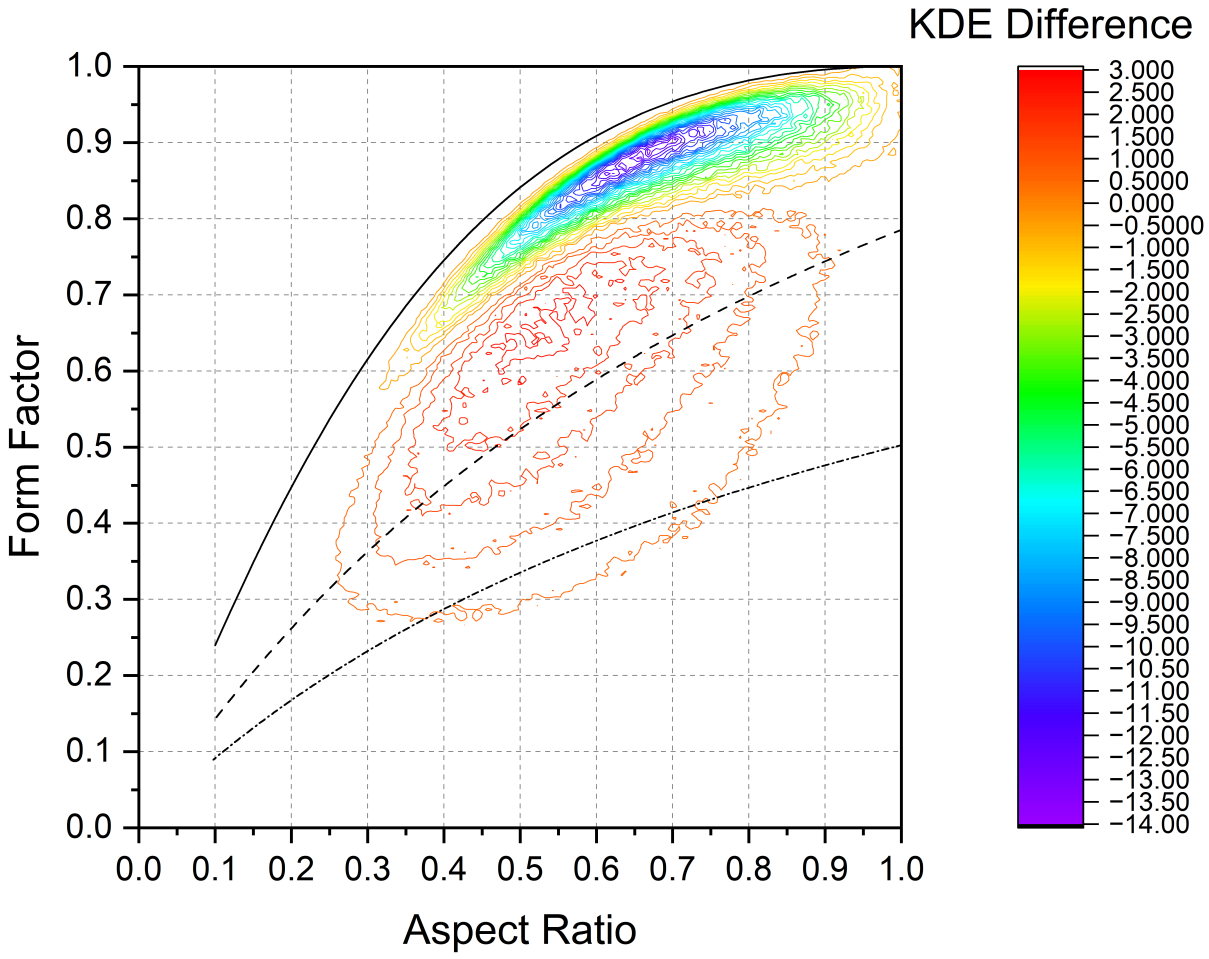

Figure D2. of particle shape distributions for NUW-LHT-5M – JSC-1A following the methods of Wilkerson et al. (2024). JSC-1A has comparatively simpler, lower aspect ratio, and higher form factor particles versus NUW-LHT-5M. The differences are small, but clearly measurable.

Appendix E Section 7.2 Supplemental Information

3D Particle Shape Methods

Comparison of NUW-LHT-5M to JSC-1A using 3D shape and size characterization
October 3, 2023
Edward Garboczi, Orion Kafka, Newell Moser
Applied Chemicals and Materials Division
National Institute of Standards and Technology
325 Broadway, MS647
Boulder CO 80305

Both simulants were sieved with an ASTM 75 μm sieve and an ASTM 300 μm sieve, with the sieves thoroughly cleaned between each simulant. This sieving process resulted in three sieve size ranges: (1) Passing the 75 μm sieve (75minus), (2) Retained on the 75 μm sieve and passing the 300 μm sieve (75–300), and (3) Retained on the 300 μm sieve (300plus). These three powders were stored separately in plastic bags for each simulant. Table 1 shows the measured mass percentage in each sieve range, as well as the actual numbers of particles for each sieve range that were analyzed by the 3D X-ray CT process. All three pairs (NUW-LHT-5M and JSC-1A) of mass fractions for the three sieve size ranges are similar. Mass measurements are very accurate. However, the limiting uncertainty would certainly be the sieving step. Only a few particles remained trapped in the sieve after each sieving step, suggesting that the sieving step was quite accurate. The material that passed through a sieve was gathered and weighed; a small amount of material stuck to the paper and thus was not measured. This amount was significantly less than 1% by mass. And even if the sieve openings were imperfect, so that the size of particles that did or did not pass through the sieve was slightly inaccurate, the same set of sieves were used for both materials. In this case, the best way to estimate the uncertainty of each mass fraction would be to complete the sieving step a second time. However, we did not have enough material left to do a second sieving. Based on this qualitative estimate, it is likely, considering Table E1, that the NUW-LHT-5M simulant has more material in the 75–300 range and less material in the 75minus range compared to JSC-1A. The differences in mass fraction were about ±4%, which is estimated to be well outside the sieving uncertainties.
A voxel size of about 0.9 μm was used for the 75minus material and a voxel size of about 3.5 μm was used for the 75–300 material for both simulants. A voxel size of about 16 μm was used for the 300plus materials, which were mostly scanned on a North Star Imaging X50 instrument (JSC-1A) while some were scanned on a Versa XRM500 instrument at a slightly smaller voxel size of about 12 μm (NUW-LHT-5M).

Minimum particle size was 512 voxels.

Table E1 shows the results for the number-based averages, in micrometers, of length (L), width (W), thickness (T), L/T, W/T, and L/W for the two simulants and the three sieve size ranges. The NUW-LHT-5M simulant seems a bit finer in the lower two size ranges. A clear result seems to be that the NUW-LHT-5M simulant is more angular than the JSC-1A simulant, since for every size range and for every aspect ratio, it has larger average ratios than the JSC-1A simulant. The relative differences between size ranges are also different, although both simulants show similar relative differences. This could be expected by the crushing process used to make smaller and

smaller particles [1]. The uncertainty in the aspect ratios L/T, W/T, and L/W is estimated at about ±0.1, based on experience with many different powders and knowledge of the algorithm used to calculate L, W, and T. It was found that the value of <L/W> was closely approximated by <L2D/W2D>, which is the average value of an aspect ratio formed by 2D quantities [2]. This result was for the case where the 2D data was measured by SEM, where it might be expected that the particles were laying on the sample surface with the smallest dimension, T, perpendicular to the surface. In that case, L2D and W2D would be approximately equal to L and W. However, this result was also found for metal powders using a dynamic light analysis instrument (Camsizer) [3].

Table E1: Dimension and shape results (number-based averages) per sieve range.

	JSC-1A			NUW-LHT-5M		
	75minus	75–300	300plus	75minus	75–300	300plus
< L > μm	28.3	159	661	26.5	134	717
< W > μm	19.6	115	495	17.3	85.9	524
< T > μm	11.8	78.8	369	10.0	51.2	336
< L/T >	2.58	2.08	1.80	2.90	2.84	2.27
< W/T >	1.77	1.52	1.37	1.86	1.80	1.66
< L/W >	1.48	1.38	1.34	1.59	1.61	1.38

How to put sieve range masses back together to get size and shape distributions for the entire powder

It was of interest to reconstruct, using the sieve results, the actual particle size distribution for the full powders. The relative mass of particles between sieve size ranges, which were analyzed using the X-ray CT, does not correspond to the measured relative masses from the sieve analysis. Table 1 gives the percentage mass fractions for each sieve range. Note that we are assuming that the density of the particles is the same across size ranges. To put the powder analysis back together to match the measured sieve measurements, we need to include enough copies of the 75minus and 75–300 particles analyzed so that the powder mass percentages of the total three sieve ranges equals the measured sieve mass percentages.

Example: JSC-1A

For the 75minus powder, 0.1744 mm^3 of powder was analyzed. For the 75–300 powder, 11.2 mm^3 of powder was analyzed, and for the 300plus powder, 191.9 mm^3 of powder was analyzed. These numbers equal the total volume of the particles analyzed, since the individual particle volume comes directly from the segmented X-ray CT images. These volumes directly correspond to masses, since we are assuming that density is constant across sieve size ranges. If there are average porosity differences across sieve size ranges, as is true for the JSC-1A powder, this analysis will be slightly in error. It could be corrected by considering these porosity differences, but these fairly small differences are neglected for now.

In the original sieve measurements, the 75minus powder had 3.20× as much mass as the 300plus powder and the 75–300 powder had 3.26× as much mass as the 300plus powder. Therefore, the number of times that the 75–300 particles should be repeated is $3.26 \times 191.9\ mm^3/11.2\ mm^3 = 55.86 \approx 56$. For 75minus, that number is $3.20 \times 191.9\ mm^3/0.1744\ mm^3 = 3521.1 \approx 3521$.

When combining the JSC-1A data, one can think of making a long list of particles, which includes the 300plus particles, 56 copies of the 75–300 particle list, and 3521 copies of the 75minus data. The mass fraction of each size range will be the same as the original sieve mass measurements. The total number of particles in this list is 117,759,880.
The equivalent calculation for the NUW-LHT-5M particle data gives a long list of particles containing the 300plus particles, 70 copies of the 75–300 particle list, and 4561 copies of the 75minus data. The total number of particles in this list is 245,171,569.

References

[1] E.J. Garboczi, X. Liu, and M.A. Taylor, The Shape of a Blasted and Crushed Rock Material Over More than Three Orders of Magnitude: 20 mm to 60 mm, Powder Technology 229, 84-89 (2012). DOI: 10.1016/j.powtec.2012.06.012.
[2] J. Goguen, A. Sharits, A. Chiaramonti, T. Lafarge, E.J. Garboczi, Three-dimensional characterization of particle size, shape, and internal porosity for Apollo 11 and Apollo 14 lunar regolith and JSC-1A lunar regolith soil simulant. To be submitted to Icarus (open access). Currently in internal NIST review.
[3] Rainer J. Hebert, Yu Sun, Mark Aindow, Edward J. Garboczi, Three-dimensional particle size, shape, and internal porosity characterization: Application to five similar titanium alloy (Ti–6Al–4V) powders and comparison to two-dimensional measurements, Additive Manufacturing 44, 102060 (2021). doi.org/10.1016/j.addma.2021.102060.

Appendix F Section 8 Supplemental Information

BET Data Notes

Notes for TABLE 8.1 BET

Work done at Alfred University was under the direction of Holly Shulman.
Work for JSC was done under contract by Micromeritics.
Work done at Stony Brook University was under the direction of Martin A. Schoonen. See Kaur et al., 2016. The samples used were provided by D. Rickman.
Apollo data taken from Cadenhead et al., 1977.

JSC-1A-MT4 and JSC-1A-MT8 are from quality control 2 kg splits taken from separate 1 ton lots of the JSC-1A material produced by James Carter for Orbitec and purchased by NASA.

The other JSC-1A samples are from unknown 1 ton lots.

JSC-1A-AGGL were processed by Orbitec to add an agglutinate-like component, Gustafson et al., 2007.

JSC-1A <10 μm was milled at Stony Brook from the material provided to them.

References

Cadenhead, D. A., M. G. Brown, D. K. Rice, and J. R. Stetter. “Some Surface Area and Porosity Characterizations of Lunar Soils.” In *Proc. 8th Lunar Sci. Conf.*, Volume 1. (A78-41551 18-91):1291–1303. Houston, TX: Pergamon Press, Inc., 1977. http://adsabs.harvard.edu/abs/1977LPSC....8.1291C.

Gustafson, Robert J., Brant C. White, Marty Gustafson, and J. Fournelle. “Development of High-Fidelity Lunar Regolith Simulants with Agglutinates.” Huntsville, AL: NASA/MSFC, 2007. https://www.nasa.gov/sites/default/files/atoms/files/day1_12_orbitec_agglutinate_bgustafson.pdf

Kaur, Jasmeet, Douglas Rickman, and Martin A. Schoonen. “Reactive Oxygen Species (ROS) Generation by Lunar Simulants.” *Acta Astronautica* 122 (May 1, 2016): 196–208. https://doi.org/10.1016/j.actaastro.2016.02.002.

Appendix G Section 9 Supplemental Information

Shear Methods

Direct Shear Characterization of NUW-LHT-5M Test 1

Jared Long-Fox[1], Brandon Dotson[1], and Catherine Millwater[1]
[1]University of Central Florida – Department of Physics, 4111 Libra Drive Room 430, Orlando, FL 32826

Introduction

The shear strength (σ_s) of the lunar regolith and its simulants is a key contributing factor to the net geomechanical properties of the material. The shear strength of the lunar regolith is driven by the particle size distribution, particle morphology, and mineralogy. It impacts the trafficability, bearing capacity, excavation mechanics, and flow characteristics of the lunar regolith. Thorough understanding of the shear strength of the lunar regolith is fundamentally important for exploration and infrastructure development. Therefore, it is key for lunar regolith simulants used in mechanical testing to mimic the shear strength of the lunar regolith itself. A common model used to quantify the shear strength of geologic materials is the Mohr-Coulomb Failure Criterion, a model that linearly relates normal stress (σ_n) to shear strength using the cohesion (c) and angle of internal friction (ϕ) as linear parameters. Cohesion and angle of internal friction are common inputs to computational models that simulate the mechanical behavior of rock and regolith. A proper characterization of the cohesion and angle of internal friction of lunar regolith and its simulants enables better predictive capabilities, which saves time and resources and decreases risk, both in the laboratory and on the lunar surface.

Methods

To estimate the cohesion and angle of internal friction of NUW-LHT-5M Test 1, a direct shear testing benchtop setup (Figure G1) and testing procedure established in Long-Fox et al. (2023) were used. This hardware and testing procedure follow ASTM D3080 to quantify the shear strength of NUW-LHT-5M.

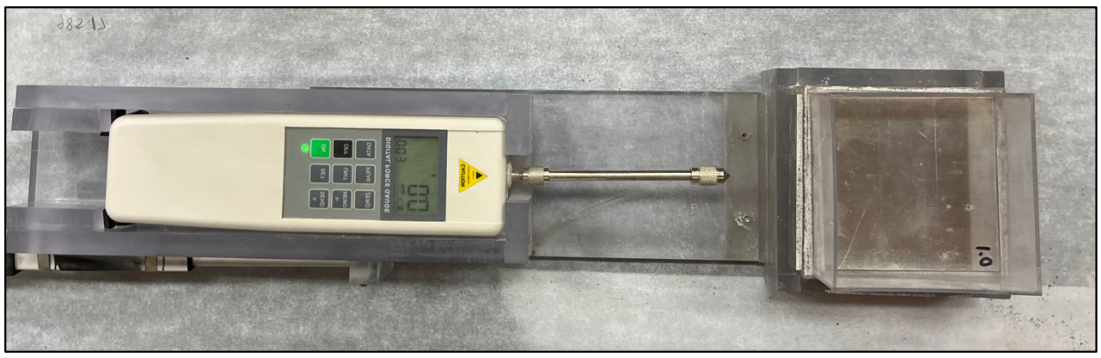

Figure G1. Direct shear hardware used to characterize the shear strength of NUW-LHT-5M Test 1. Shown are the force gauge and actuator system, the direct shear box, and the normal force box that applies normal load throughout the simulant during testing.

In this procedure, the simulant of known mass is sheared in the polycarbonate direct shear box (horizontal interior dimensions of 10.17 cm x 10.17 cm). The direct shear box consists of two halves stacked vertically. The bottom half is held stationary while an HP-500 force gauge (0.1 N or ~0.01 kPa resolution) mounted on an Actuonix L16-R linear servo is translated horizontally, driven by an Arduino UNO R3 microcontroller, to push the top half of the shear box along the guides in the bottom half (to ensure straight travel during shearing) and measuring the force applied in the horizontal (shearing) direction at failure. To ensure a low friction between the halves of the direct shear box, polycarbonate was used. First, the simulant was gently loaded into the shear box at a nominal uncompressed density and the simulant-filled normal force box (of known mass and volume) was weighed and the density of the simulant in the box was calculated. If the simulant is too dense when packed, the box was then emptied and refilled. If the simulant density in the box was too low, slight mechanical agitation was used to compact the simulant to the predetermined density. Once the simulant was properly loaded and level in the direct shear box, a polycarbonate normal force box filled with a predetermined mass of 6061 aluminum plates that is slightly smaller than the interior of the direct shear box is set on top of the simulant (with care taken to avoid it resting on the edge of the upper half of the direct shear box) to prescribe a constant normal load throughout the simulant during testing. Here, four different normal loads (0.098, 0.288, 0.478, and 0.67 kPa) were tested five times each with NUW-LHT-5M Test 1 at a target density of 1.265 g/cm^3. Data gathered from testing the shear strength of NUW-LHT-5M Test 1 at various amounts of normal load was used in a linear regression under the assumptions of the Mohr-Coulomb Failure Criterion (Equation 1) to estimate cohesion (intercept) and angle of internal friction (arctangent of the slope) and their respective 95% uncertainties along with the R^2 goodness-of-fit metric.

$$\sigma_s = \sigma_n \tan\phi + c \quad (1)$$

Results

The results linear regression analysis performed on the direct shear data from testing NUW-LHT-5M Test 1 according to the Mohr-Coulomb Failure Criterion (Equation 1) are shown graphically in Figure 2. This analysis of NUW-LHT-5M Test 1 to find the best-fit values of *c*

and ϕ, along with their 95% uncertainties, gives $c = 0.266 \pm 0.020$ kPa and $\phi = 30.69 \pm 2.68°$ with $R^2 = 0.975$. The average density of the simulant over the 20 total tests was 1.265 ± 0.0002 g/cm^3 (95% confidence). The results of the direct shear testing of NUW-LHT-5M Test 1 are shown graphically with the Mohr-Coulomb linear fit and 95% confidence intervals in Figure G2.

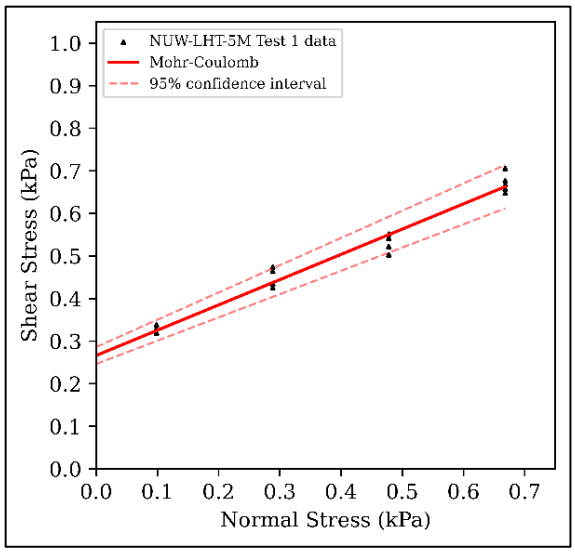

Figure G2. Results of direct shear testing and Mohr-Coulomb analysis of NUW-LHT-5M Test 1 at a nominal density of 1.265 g/cm^3.

Discussion

Estimates of the cohesion and angle of internal friction of lunar regolith given by the Surveyor and Apollo models in Carrier et al. (1991) are both very slightly higher than those of NUW-LHT-5M Test 1 measured here. However, the direct shear tests performed as part of this work were done at a low relative density and the shear strength of NUW-LHT-5M Test 1 will only increase at higher relative densities. It is expected that the cohesion and angle of internal friction ranges of NUW-LHT-5M Test 1 overlap well with lunar estimates and measurements as density during testing is increased. The range of cohesion and angle of internal friction of lunar samples given by Carrier et al. (1972) envelop the corresponding parameter estimates given here, further indicating that NUW-LHT-5M Test 1 aligns well with the strength of lunar regolith samples. Work is ongoing to characterize the shear strength as a function of density, so this assumption will be quantitatively evaluated when the relevant data are collected and analyzed (Dotson et al., 2023).

The cohesion and angle of internal friction of the standard lunar regolith simulant (JSC-1A) are well-characterized and have wide ranges of values for both parameters. Cohesion estimates for JSC-1A generally fall between 0.1 to 2.5 kPa depending on sample density and methods used (McKay et al., 1994; Schrader et al., 2010). The angle of internal friction reported with these estimates of cohesion vary from 41 to 48.8° (McKay et al., 1994; Schrader et al., 2010). It should be noted that the JSC-1 family of simulants are composed of basaltic cinders, meaning that they are better suited to serve as mare simulants; whereas NUW-LHT-5M Test 1 is a highlands simulant with different mineralogy than a basaltic mare simulant and therefore different physical properties.

LHS-1 is a mineralogically accurate lunar highlands simulant and has a cohesion of 0.311 kPa and an angle of internal friction of 31.49° measured at a density of 1.32 g/cm^3 (Long-Fox et al., 2023), higher than the density tested here for NUW-LHT-5M Test 1. The estimates for the cohesion and angle of internal friction of LHS-1 (Long-Fox et al., 2023) are in line with those of NUW-LHT-5M Test 1 presented here. Further, the data of Long-Fox et al. (2023) were collected using the same hardware as used here, so the consistency in results shows that NUW-LHT-5M provides a reasonable approximation of lunar highlands regolith in terms of shear strength.

Conclusions

The Mohr-Coulomb shear strength of NUW-LHT-5M Test 1 is consistent with estimates of the cohesion and angle of internal friction from both lunar regolith (Carrier et al.,1972; Carrier et al., 1991) and a comparable highlands simulant, LHS-1 (Long-Fox et al., 2023). The measurements of JSC-1A used different methods than both Carrier et al. (1972) and Long-Fox et al. (2023) and give higher estimates of both cohesion and angle of internal friction, but the ranges given for the JSC-1A lunar mare simulant do overlap with that of NUW-LHT-5M reported here. The consistency of results for NUW-LHT-5M presented here indicated that NUW-LHT-5M Test 1 is a suitable lunar highlands regolith analog in terms of shear strength.

References:

Carrier, W. D., Bromwell, L. G., and Martin, R. T. (1972) “Strength and compressibility of returned lunar soil”, *Proceedings of the 3rd Lunar Science Conference*.

Carrier, W. D., Olhoeft, L.G., and Mendell, W.. “Physical Properties of the Lunar Surface.” In *Lunar Sourcebook: A User’s Guide to the Moon*, edited by Grant Heiken, David Vaniman, and Bevan. M. French, 522:475–594. New York, NY: Cambridge University Press, 1991. http://www.lpi.usra.edu/publications/books/lunar_sourcebook/pdf/Chapter09.pdf.

Dotson, B., Sargeant, H., Millwater, C., Easter, P., Sanchez Valencia, D., Long-Fox, J., Britt, D., and Metzger, P. (2023), “New Insights into the Physical Properties of Regolith”, *54th Lunar and Planetary Science Conference*, Houston, TX, USA, March 13-17, 2023.

Long-Fox, J. M., Landsman, Z. A., Easter, P. B., Millwater, C. A., and Britt, D. T. (2023), “Geomechanical properties of lunar regolith simulants LHS-1 and LMS-1”, *Advances in Space Research* (In Press).

McKay, D. S., Carter, J. L., Boles, W. W., Allen, C. C., & Allton, J. H. (1994). “JSC-1: A new lunar soil simulant”, *Engineering, construction, and operations in space IV*, 2, 857-866

Schrader, C. M., Rickman, D. L., McLemore, C. A., & Fikes, J. C. (2010). “Lunar Regolith Simulant User's Guide”

Appendix H Section 12 Supplemental Information

High-Temperature Dielectric Methods

Methods: High-T Dielectric Measurements

The measurements are taken using the cavity perturbation method. The sample is made into a compressed pellet, which is placed into a furnace and then heated to a target temperature. At that temperature, the heated pellet is quickly transferred into a multimode microwave cavity for low power vector network analyzer measurements.

Measurements are taken of the sample's permittivity's real component, ε', and imaginary component, ε'', then the charge is returned to the furnace to be heated to the next target temperature. Once the target final temperature is reached, the furnace is allowed to cool, again with the sample taken out at set temperatures and measurements made in a multimode microwave cavity with a low power vector network analyzer. Measurements at a single temperature require only seconds out of the furnace, with total run times being between 6.4 and 21.5 hours. Heating and measurements are done while keeping the sample in ultra-high purity (UHP) flowing argon. Measurements on JSC-1AC were taken at two frequencies and measurements on NUW-LHT-5M were taken at six frequencies. In the data plotted, only the measurements at 2466 MHz (2.45 GHz) are used, as that is likely to be the frequency for any microwave equipment used for heating on the Moon. Data for other wavelengths and test conditions are included in the supplemental files, which includes out-of-furnace times, temperature drops during measurements, and time since the beginning of a run.

Note that the plotted results are sensitive to the density of the pellet; a change in packing density will change the values of ε' and ε''. As the pore space collapses at the highest temperatures used, the density shifts. The temporal relationship between compaction and temperature is not rigorously known, so there is a small error in the reported values at the highest temperature.

Both simulants were run in flowing UHP argon, with approximately 5–10 ppm O_2. This was definitely not enough to prevent minor oxidation of at least NUW-LHT-5M, which is seen as a distinct change of color in the post-heating images.

The heating measurements of JSC-1AC were done in 2.503 hours.

The NUW-LHT-5M sample was pre-baked to 750 °C in flowing argon with hydrogen (Wilkerson et al., 2023). Heating measurements took 3.95 hours.

Appendix H.1 MPN-285_NUW-LHT-5M_Rickman_3m
July 24, 2023

Lunar Simulant NUW-LHT-5M, Heat Treated in Ar/4%H_2
Measurements of Complex Dielectric Constant of Pellets
from Room Temperature to 1250 °C, in flowing (10 sccm) UHP Argon

Dr. Doug Rickman (NASA) requested that Microwave Properties North (MPN) measure the complex dielectric properties of heat-treated NUW-LHT-5M lunar regolith simulant up to a temperature of 1250 °C.

The first run, in vacuum, up to 1100 °C, had an unfamiliar feature at ~850 °C . We decided to try to repeat the run, but with conditions changed as much as reasonable. Thus the second run was done in flowing (10 sccm) ultra high purity (UHP) argon, with more temperature steps starting just above 800 °C. This required a different sample holder, different background subtractions and new calibrations. The results were essentially the same as the first run.

This third run (done again in flowing UHP argon) to 1250 °C used the same sample holder as the previous run and was done to see if the maximum temperature could be slightly higher without interaction with the sample holder. This was successful!

The powder sample material from Prof. H. Shulman arrived at MPN on June 6, 2023. Dr. Shulman had already heat-treated the powder at 750 °C in a 4% hydrogen/argon mixture.
For this measurement, MPN again pressed pellets of the powder material in a uniaxial press at ~33,000 psi. The pellets were not initially baked by MPN to ensure dryness. The sample holder was the same one used on the previous (2^{nd}) measurement . Thus the "empty holder" values were well established.

The initial sample parameters were:
a) Diameter: 3.64 ± 0.02 mm
b) Length of 3 Pellet Stack: 12.99 ± 0.05 mm
c) Mass: 0.283 ± 0.002 gm
d) Room Temperature (RT) Density: 2.09 ± 0.05 gm/cc
e) Appearance: Three light grey pellets
f) Magnetic Response: The pellets had a very weak attraction to a strong magnet.

The dielectric properties measurements were performed three times at RT, and then the temperature was ramped up to 800 °C in 50 °C steps, then to 1250 °C in 25 °C steps. After this, the temperature was brought back down to 100 °C in -50 °C steps, then RT. It was noted at the end of the run that the plug had come out of the top of the holder at some point, possibly allowing a slight backflow of air into the top of the holder.

The holder was removed from the apparatus, and it and the final sample were weighed together. The pellets had "fused" into a rod, which was easily removed, and its mass determined (no change). Then the empty holder was run up to 1250 °C to measure backgrounds and check for contamination. There was no significant contamination.

The final sample properties, at room temperature were:
a) Diameter: 3.59 ± 0.02 mm

b) Pellet Stack Length: 12.7 ± 0.1 mm
c) Mass: 0.283 ± 0.002 gm
d) RT Density: 2.20 ± 0.05 gm/cc
e) Appearance: Single brown rod with coloured flecks (see photos)
f) Magnetic Response: The rod had a very weak attraction to a strong magnet.

Note: The percent mass loss was zero within our errors.

The frequency coding is :

Legend for Data Plots :

#	Frequency (MHz)	Symbol
1	397	red diamond, solid line – sometimes the line is omitted!
2	912	blue square, solid line
3	1429	black cross, solid line
4	1948	blue circle, dotted line
5	2466	red cross, dotted line
6	2986	black diamond, dotted line

Comments on the data analysis:

A thermal expansion coefficient (CTE) of 0.0 * 10^{-6} °C was used.

The final sample looked as if the pellets had fused together, possibly with the assistance of the softening glass content. The colouring was somewhat darker than with the previous, lower temperature runs.

The data for the ramp up to 1250 °C is interrupted by a slight decrease of the ε′ values, which occurred between 850 °C and 950 °C. This resulted in a permanent change in ε′, suggesting a non-reversible phase change.

The slope of both ε′ and ε″ versus temperature increased dramatically at ~1180 ± 15 °C, suggesting softening of a glass component. The glass component may have diffused into the pores of the material, causing the slight decrease in sample volume.

The final sample (the three fused pellets) was sectioned (i.e., split in half) using a thin (20 thou) diamond saw. Unfortunately, the pellets were not completely in line in the stack, and when Joe put it in a clamp to saw it, one pellet snapped off the end. He did "section" both pieces.

Several photos are shown below, and demonstrate my lack of experience with lighting and microscopy.

The interior did not have the "light brown" tinge that the outer surface had. My lighting makes the outer surface look dark brown—it was not!

At higher magnification, what had looked like black "blobs" in the first low magnification photo turned out to be cavities!

Also, the “line” between the two pellets shows that the gap had not filled in completely—suggesting the glass had not completely flowed—even at 1250 °C!

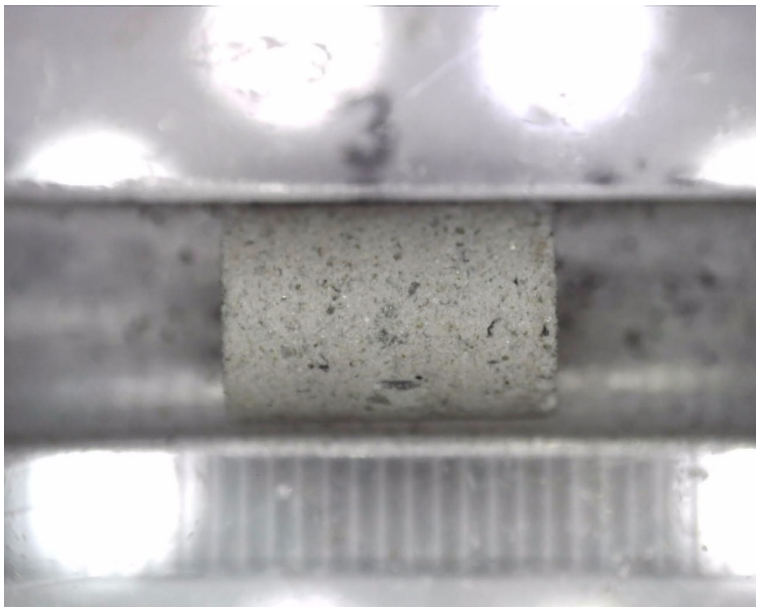

Figure 1. Typical initial pellet pressed at ~33,000 psi

Figure 2. Final sample, after cycle to 1250 °C in UHP argon.

Figure 3. Three final pellets (a "sintered" rod) from 3rd run—i.e., after the cycle to 1250 °C in UHP argon.

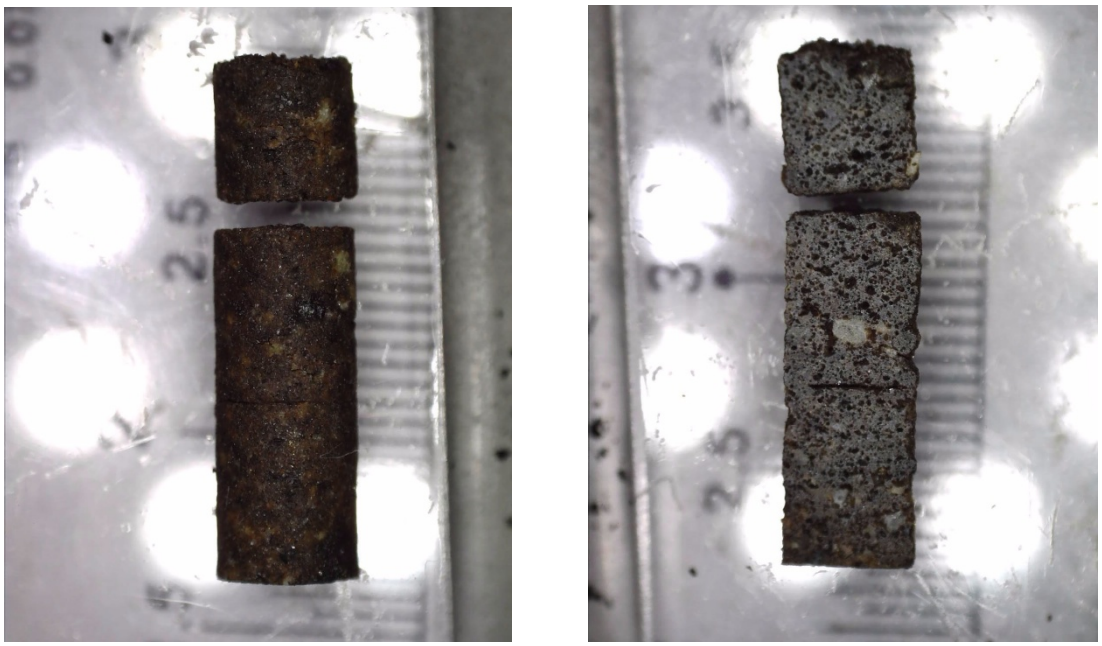

Figure 4. The diametrically sectioned final sample. The outer surface (left photo) was not as dark as this.
I thought I was looking at “dark” blobs of material in the interior (right hand photo), but when I increased the magnification, they were clearly voids.

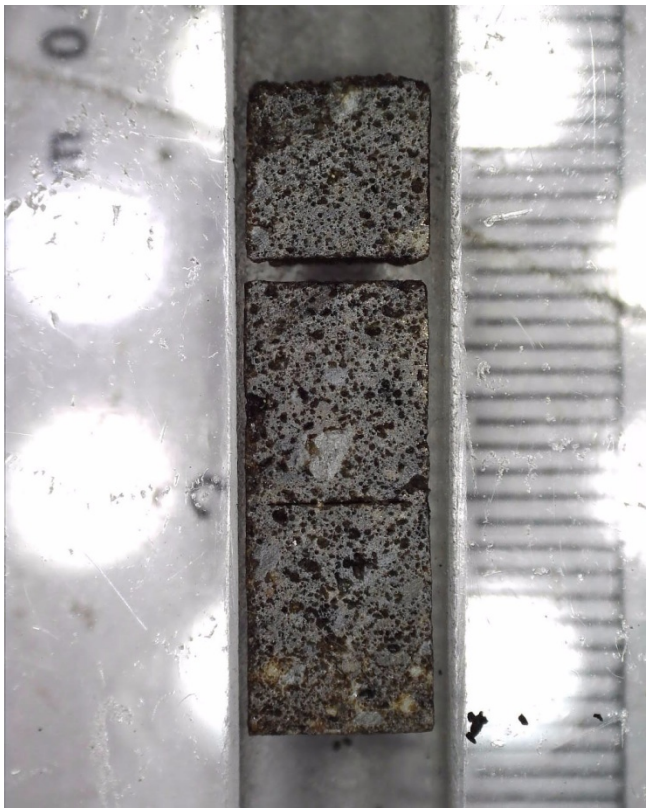

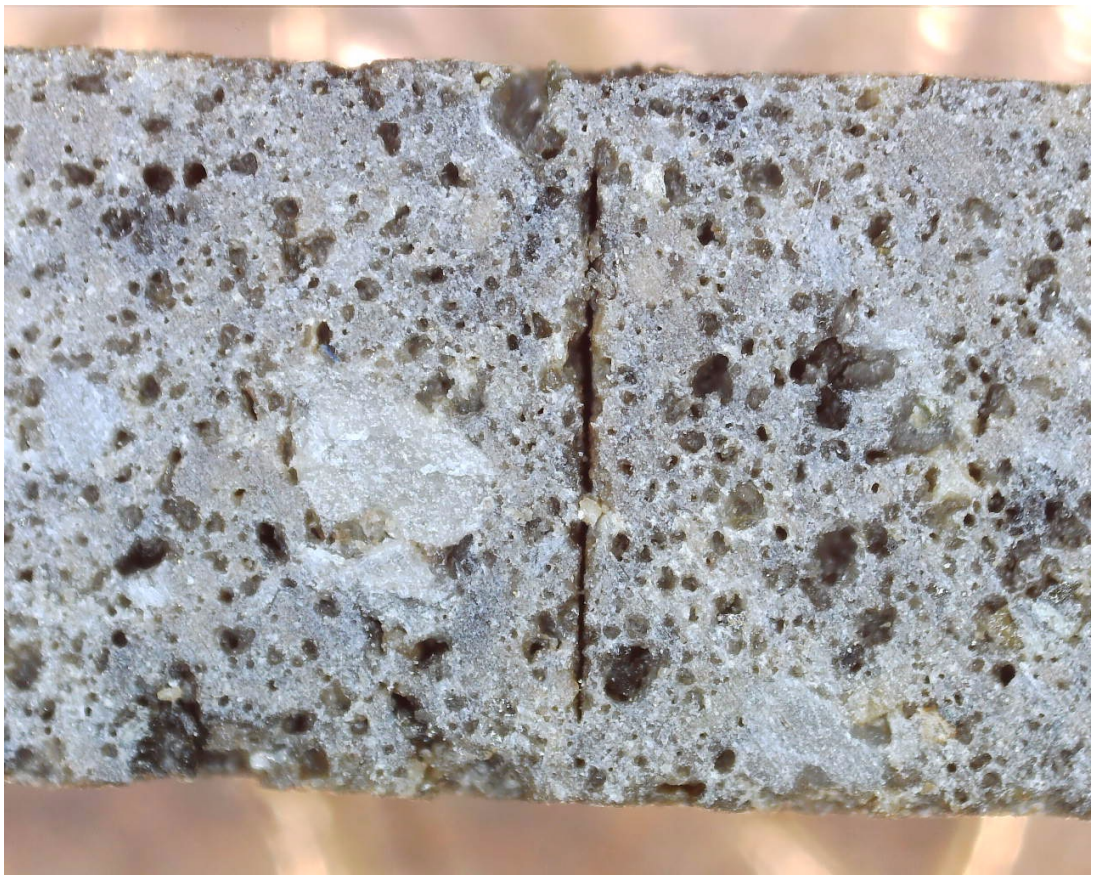

Figure 5. With increased magnification and better illumination, the voids are clearly seen. The fusing of the two pellets was not complete, as seen by the line between the partially joined pellets.

Code Calculates Estimated Sample Dimensions & Volume and Plots Density As a Function of Temperature

Test = 2023061101 NASA2361.mcd **AnDat = 20230612**

3rd Run, Lunar Simulant NUW-LHT-5M, pre-baked at 750C in Ar/H , to 1250C, in UHP argon, for D. Rickma

Assumed Effective Dimensions (mm) and Density (gm/cc) as a Function of Temperature for Solid

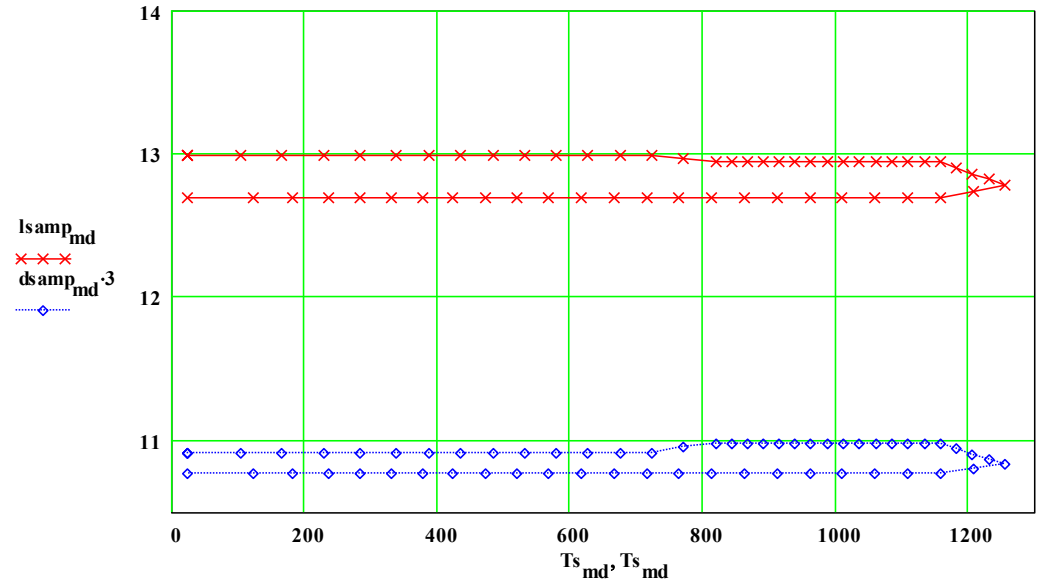

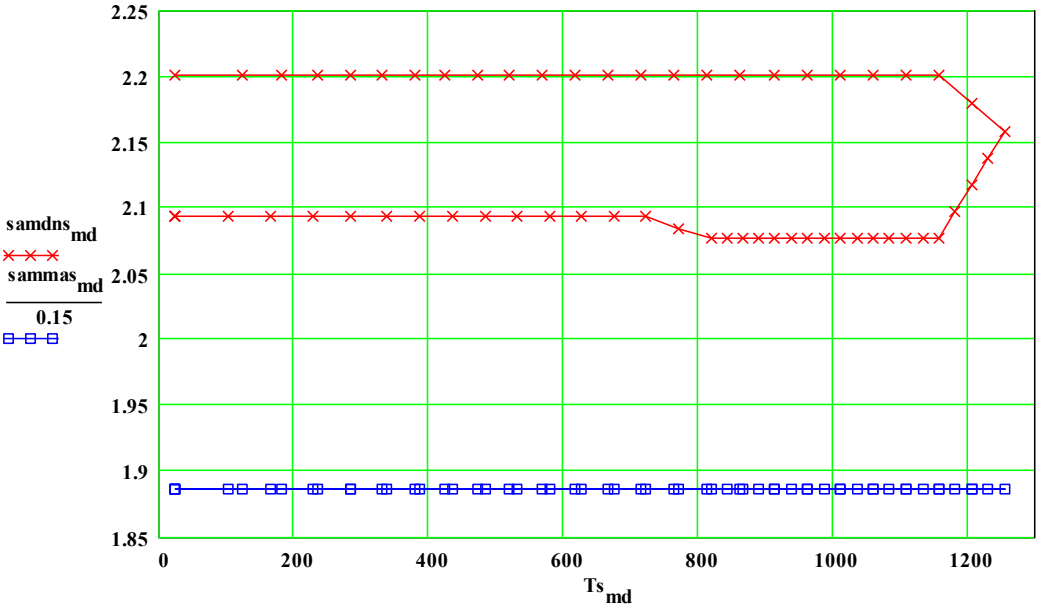

Test = 2023061101 NASA2361.mcd **AnDat = 20230612** **T**

3rd Run, Lunar Simulant NUW-LHT-5M, pre-baked at 750C in Ar/H, to 1250C, in flowing argon, for D.Rickman

Initial density = $\mathbf{samdns_{NCal+1}} = 2.09$ gm/cc, Final density(25C) = **dnsfinal = 2.2** gm/cc

FracMassChange = 1

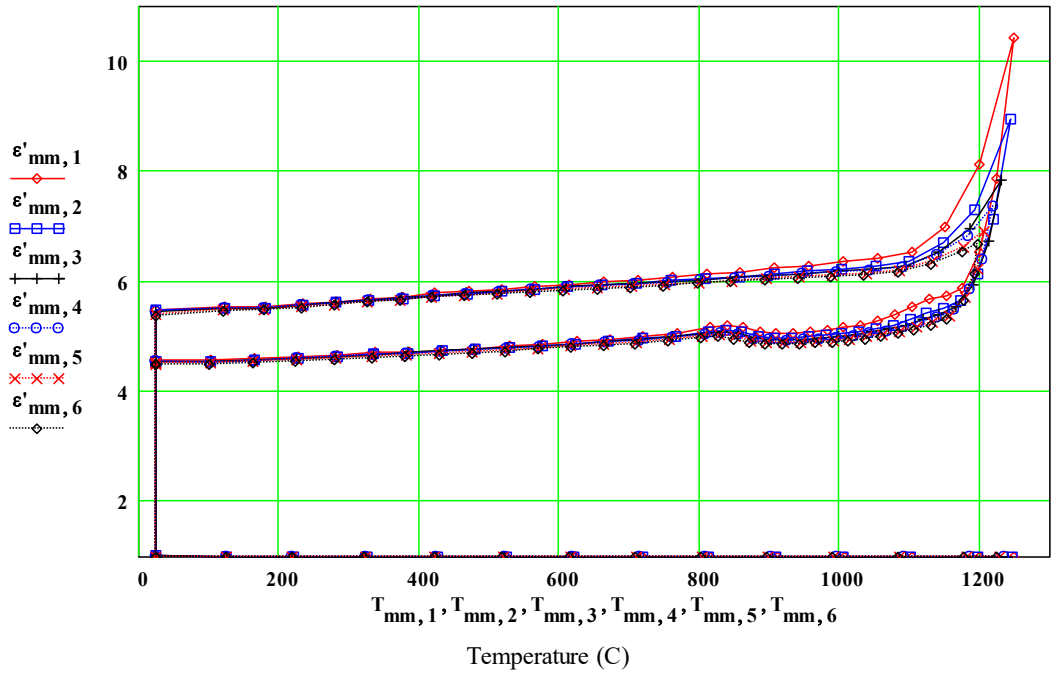

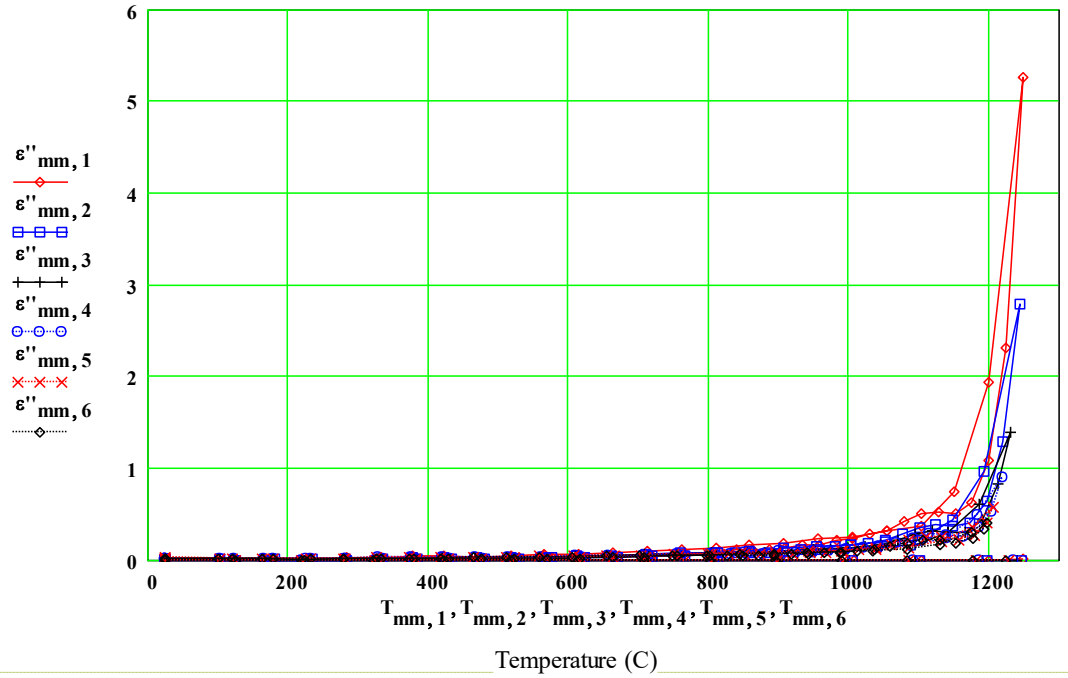

Note the rapid increase with temperature, starting at ~1180 °C .

Test = 2023061101 NASA2361.mcd **AnDat = 20230612**

3rd Run, Lunar Simulant NUW-LHT-5M, pre-baked at 750C in Ar/H, to 1250C, in flowing UHP argon, for Rickma

Initial density = $samdns_{NCal+1}$ **= 2.09** gm/cc, Final density(25C) = **dnsfinal = 2.2** gm/cc

Values for 2450 MHz - Increasing Temperature

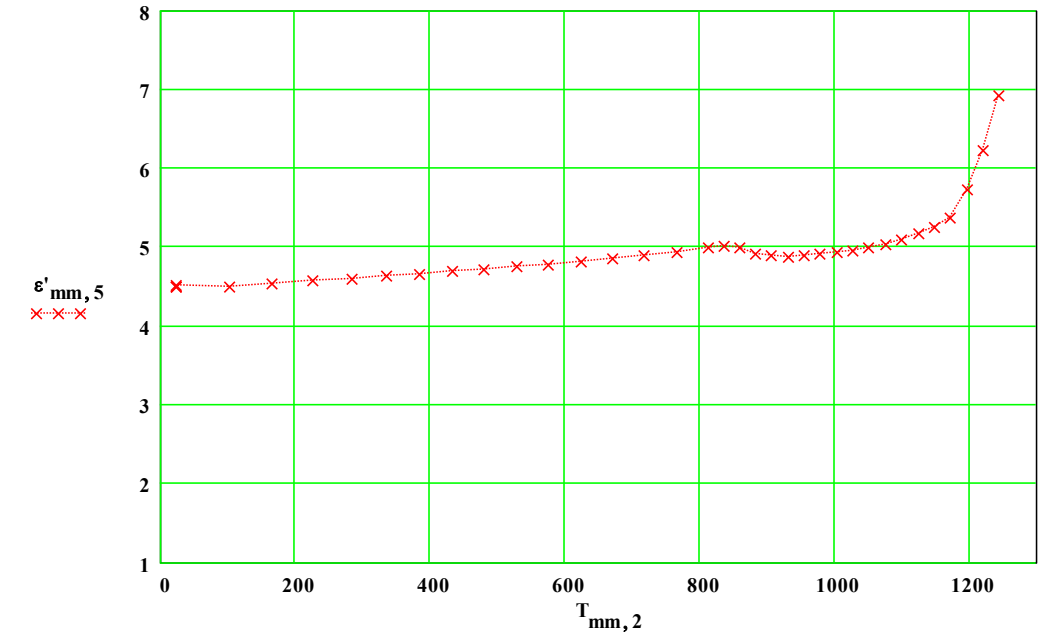

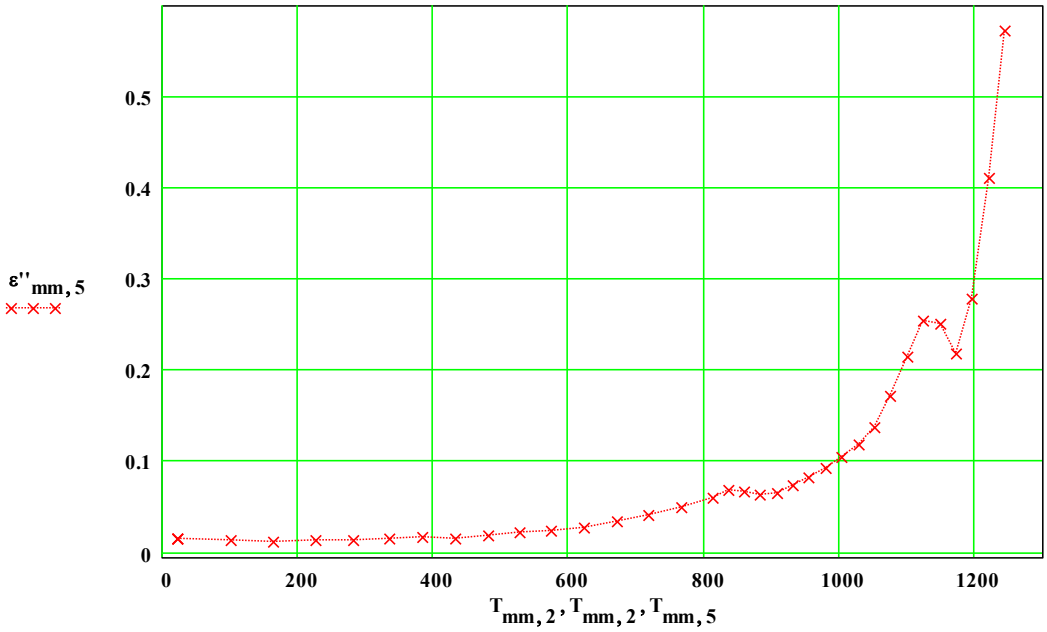

Test = 2023061101 NASA2361.mcd **AnDat = 20230612**

3rd Run, Lunar Simulant NUW-LHT-5M, pre-baked at 750C in Ar/H, to 1250C, in flowing UHP argon, for Rickma

Initial density = $\mathbf{samdns_{NCal+1}}$ **= 2.09** gm/cc, Final density(25C) = **dnsfinal = 2.2** gm/cc

Values for 2450 MHz - Decreasing Temperature

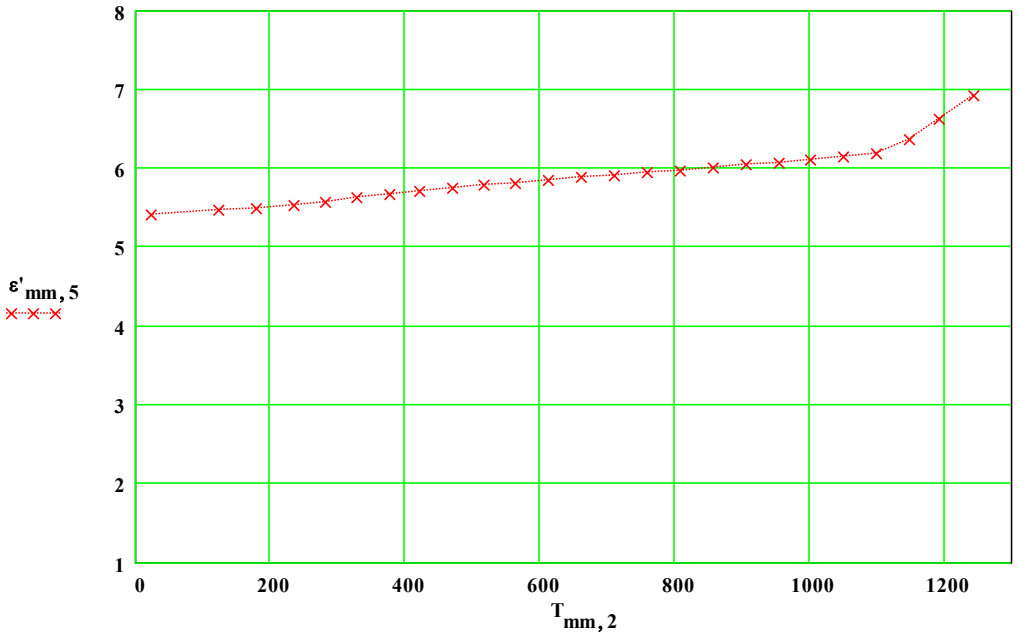

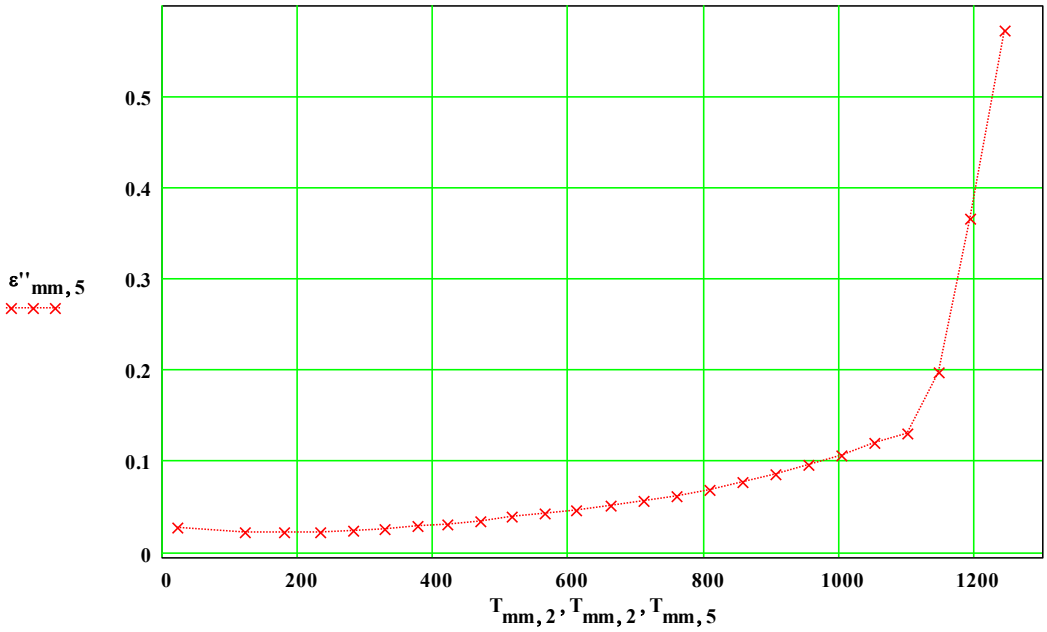

Test = 2023061101 NASA2361.mcd **AnDat = 20230612**

3rd Run, Lunar Simulant NUW-LHT-5M, pre-baked at 750C in Ar/H, to 1250C, in flowing UHP argon, for Rickma

Initial density = $\mathbf{samdns}_{\mathbf{NCal}+1}$ **= 2.09** gm/cc, Final density(25C) = **dnsfinal = 2.2** gm/cc

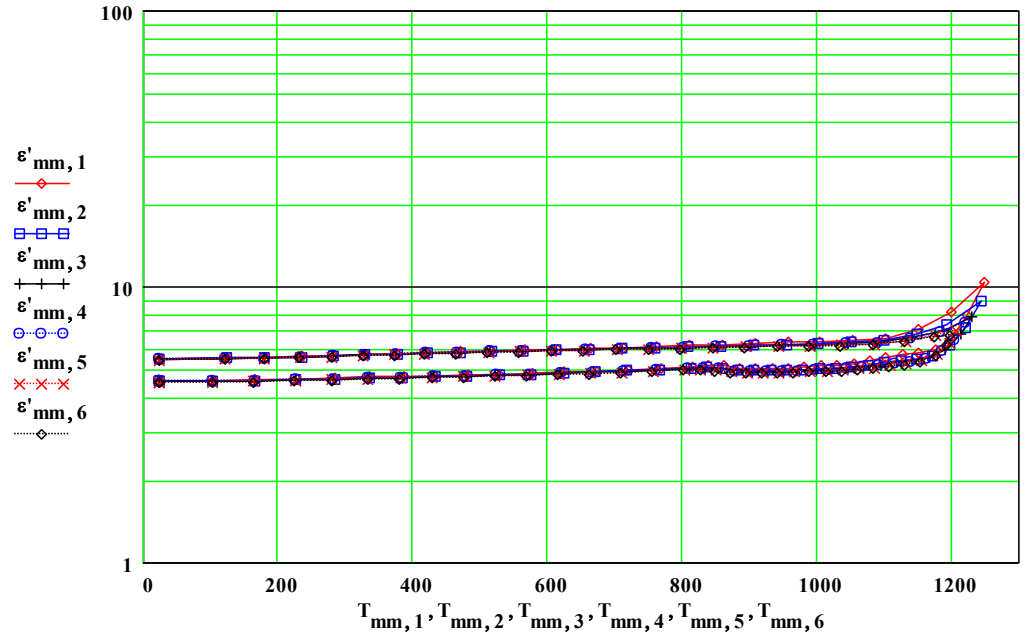

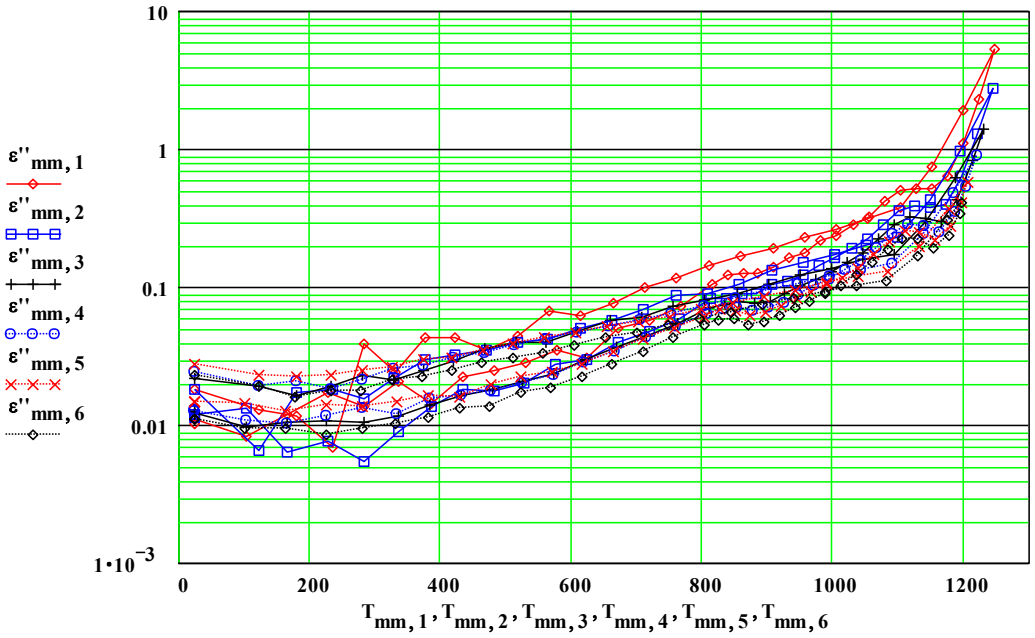

Test = 2023061101 NASA2361.mcd **AnDat = 20230612**

3rd Run, Lunar Simulant NUW-LHT-5M, pre-baked at 750C in Ar/H, to 1250C, in flowing UHP argon, for Rickm

Initial density = $samdns_{NCal+1}$ **= 2.09** gm/cc, Thermal exp. coeff. $\alpha_1 = 0$

Final density(25C) = **dnsfinal = 2.2** gm/cc **FracMassChange = 1**

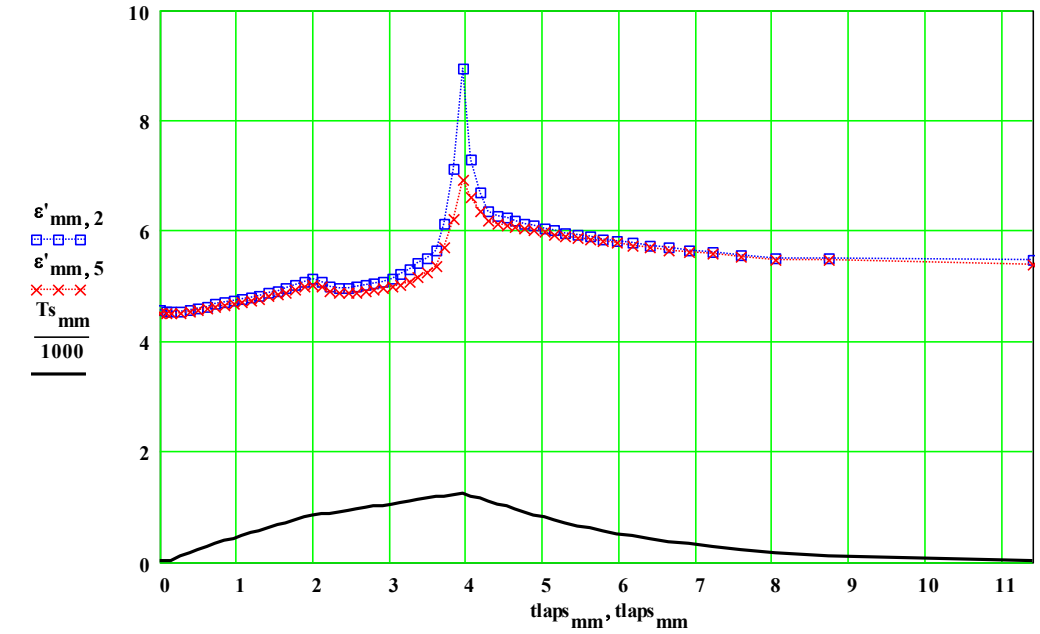

Lapsed Time (hours)

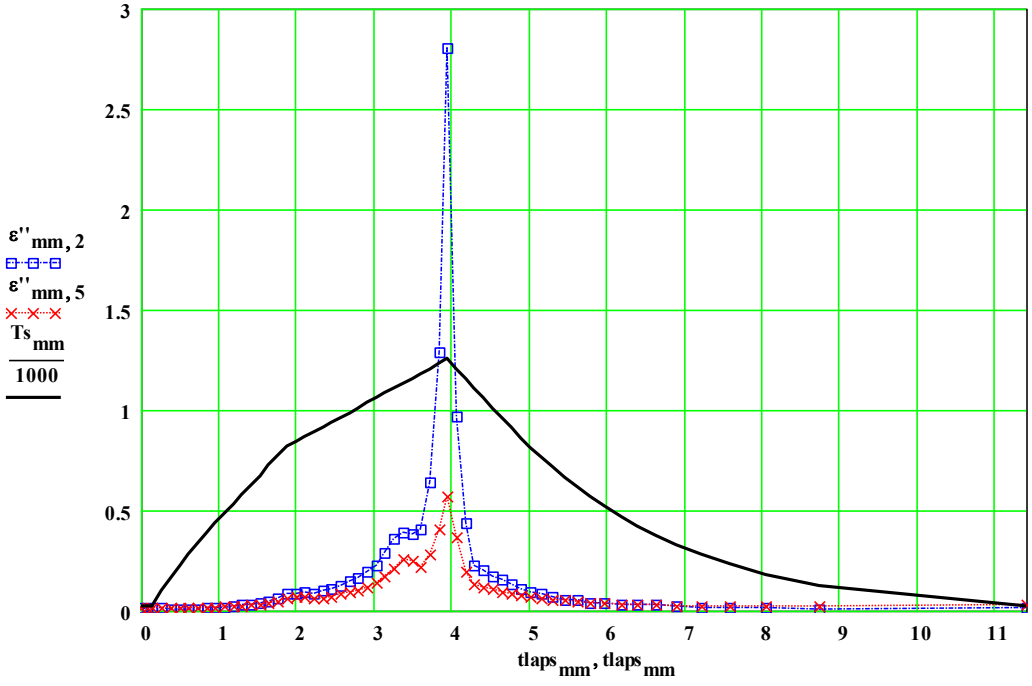

Test = 2023061101 NASA2361.mcd **AnDat = 20230612**

3rd Run, Lunar Simulant NUW-LHT-5M, pre-baked at 750C in Ar/H, to 1250C, in flowing argon, for D.Rickman

Equivalent Free Electron Conductivity (Siemens/metre)

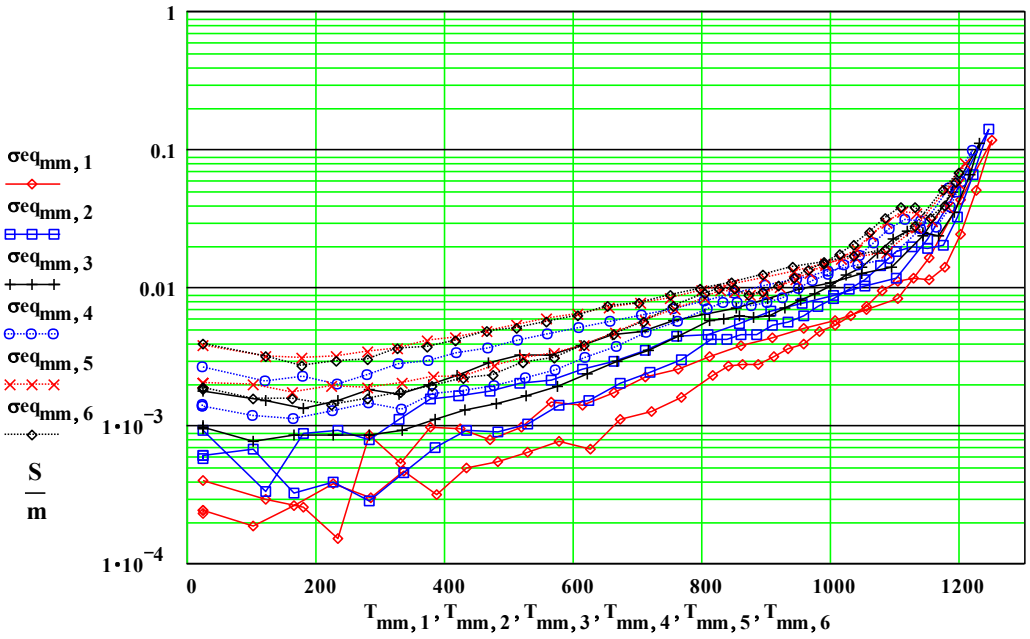

Temperature (C)

Test = 2023061101 NASA2361.mcd **AnDat = 20230612**

3rd Run, Lunar Simulant NUW-LHT-5M, pre-baked at 750C in Ar/H, to 1250C, in flowing UHP argon, for Rickma

Initial density = $samdns_{NCal+1}$ **= 2.09** gm/cc, Final density(25C) = **dnsfinal = 2.2** gm/cc

Thermal exp. coeff. $\alpha_1 = 0$

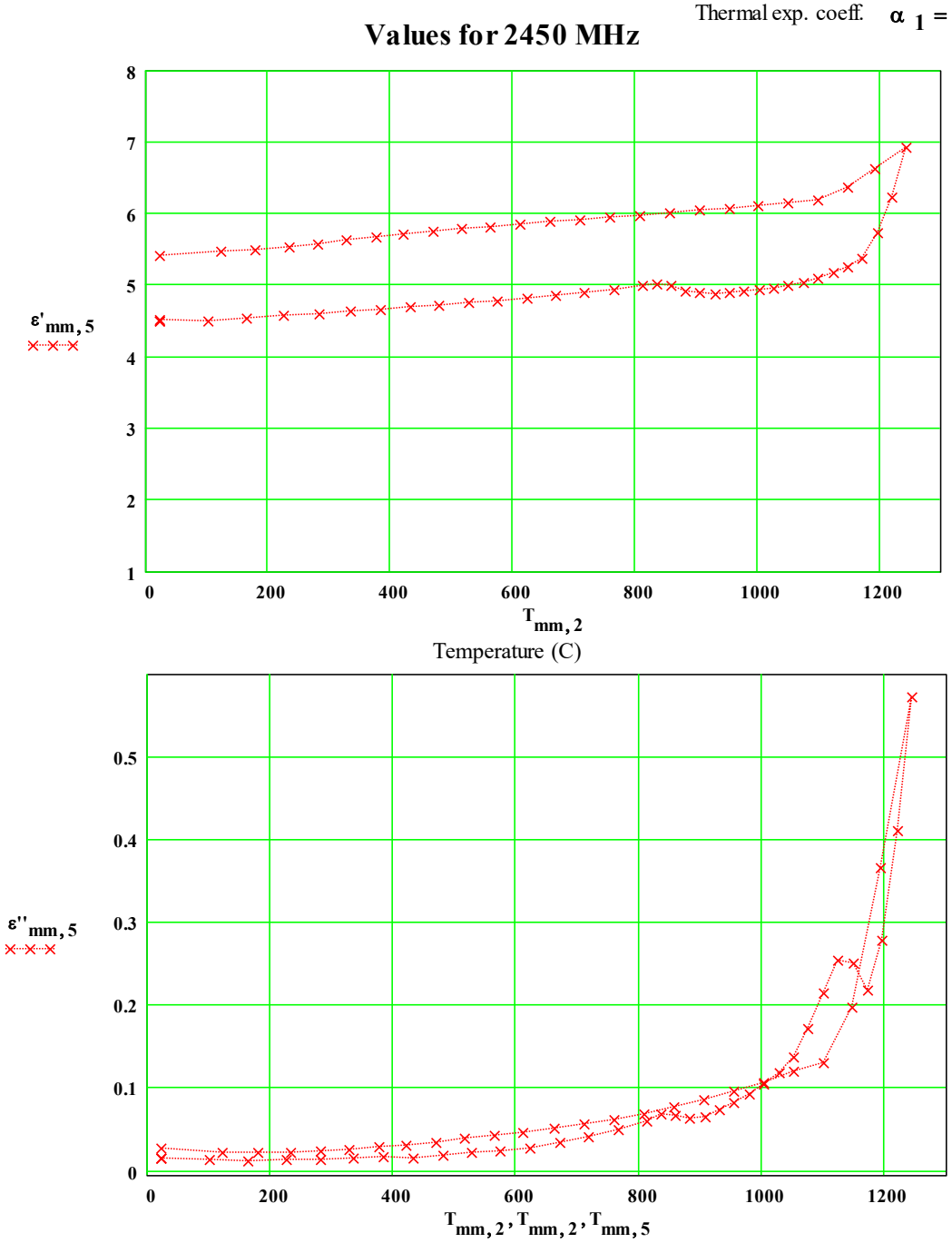

Test = 2023061101 NASA2361.mcd **AnDat = 20230612**

3rd Run, Lunar Simulant NUW-LHT-5M, pre-baked at 750C in Ar/H, to 1250C, in flowing UHP argon, for Rickman

Initial density = $\mathbf{samdns}_{NCal+1}$ **= 2.09** gm/cc, Final density(25C) = **dnsfinal = 2.2** gm/cc

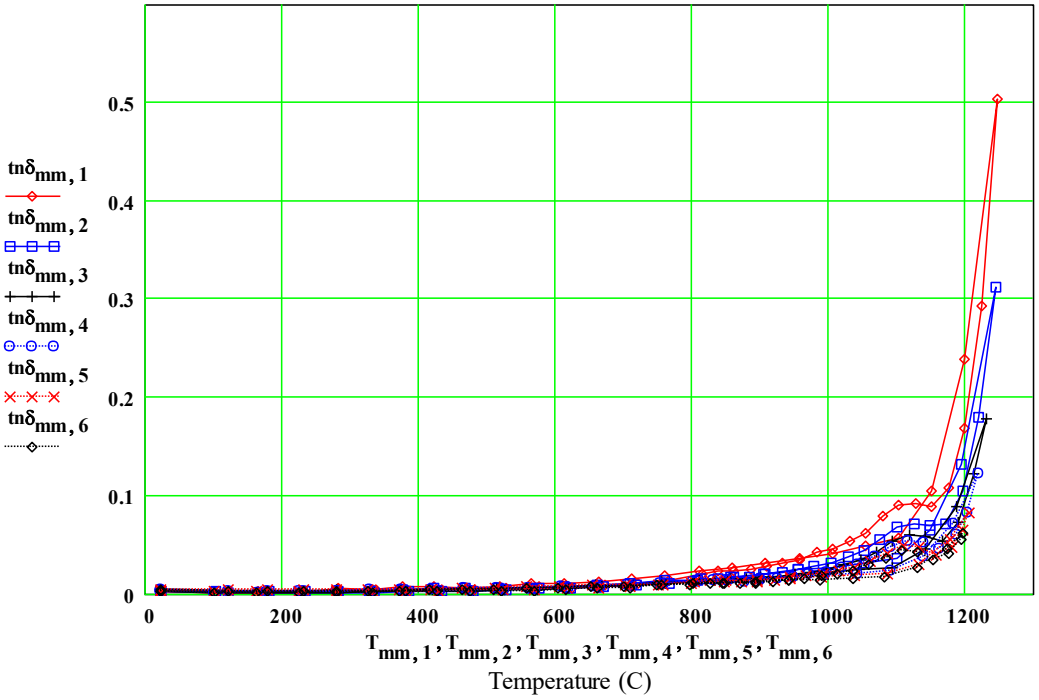

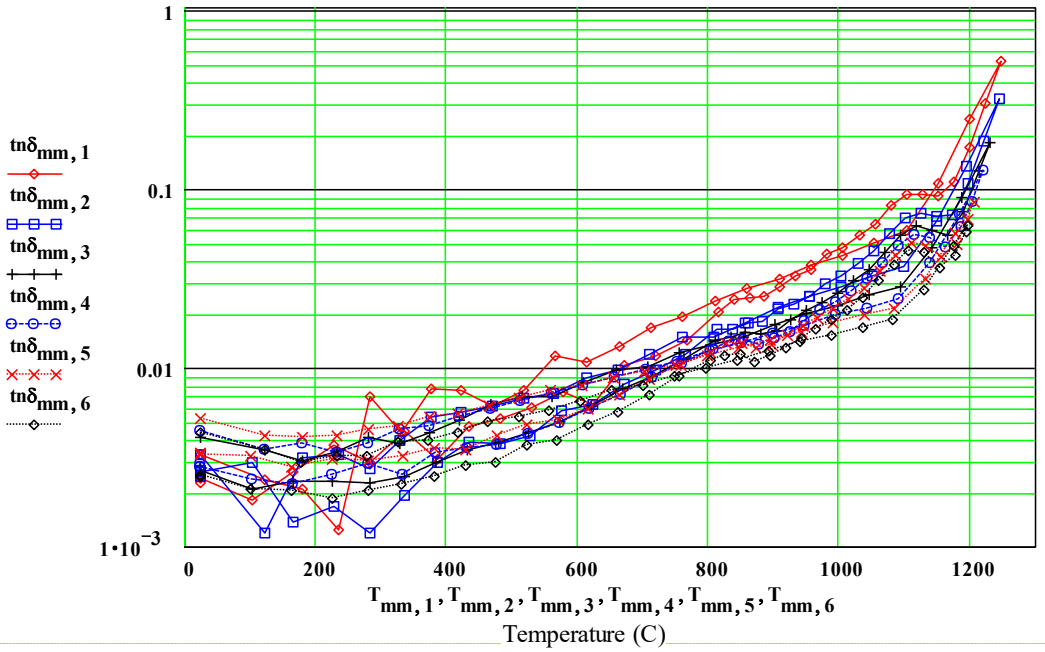

Half-power Depth (millimeters)

$$D\_halfP_{(mm,n)} := \left(\frac{\ln(2)}{2}\right)\cdot\left(inverse\alpha_{mm,n}\cdot 1\right)$$

Test = 2023061101 NASA2361.mcd **AnDat = 20230612**

3rd Run, Lunar Simulant NUW-LHT-5M, pre-baked at 750C in Ar/H, to 1250C, in flowing UHP argon, for Rickma

Initial density = $samdns_{NCal+1}$ **= 2.09** gm/cc, Final density(25C) = **dnsfinal = 2.2** gm/cc

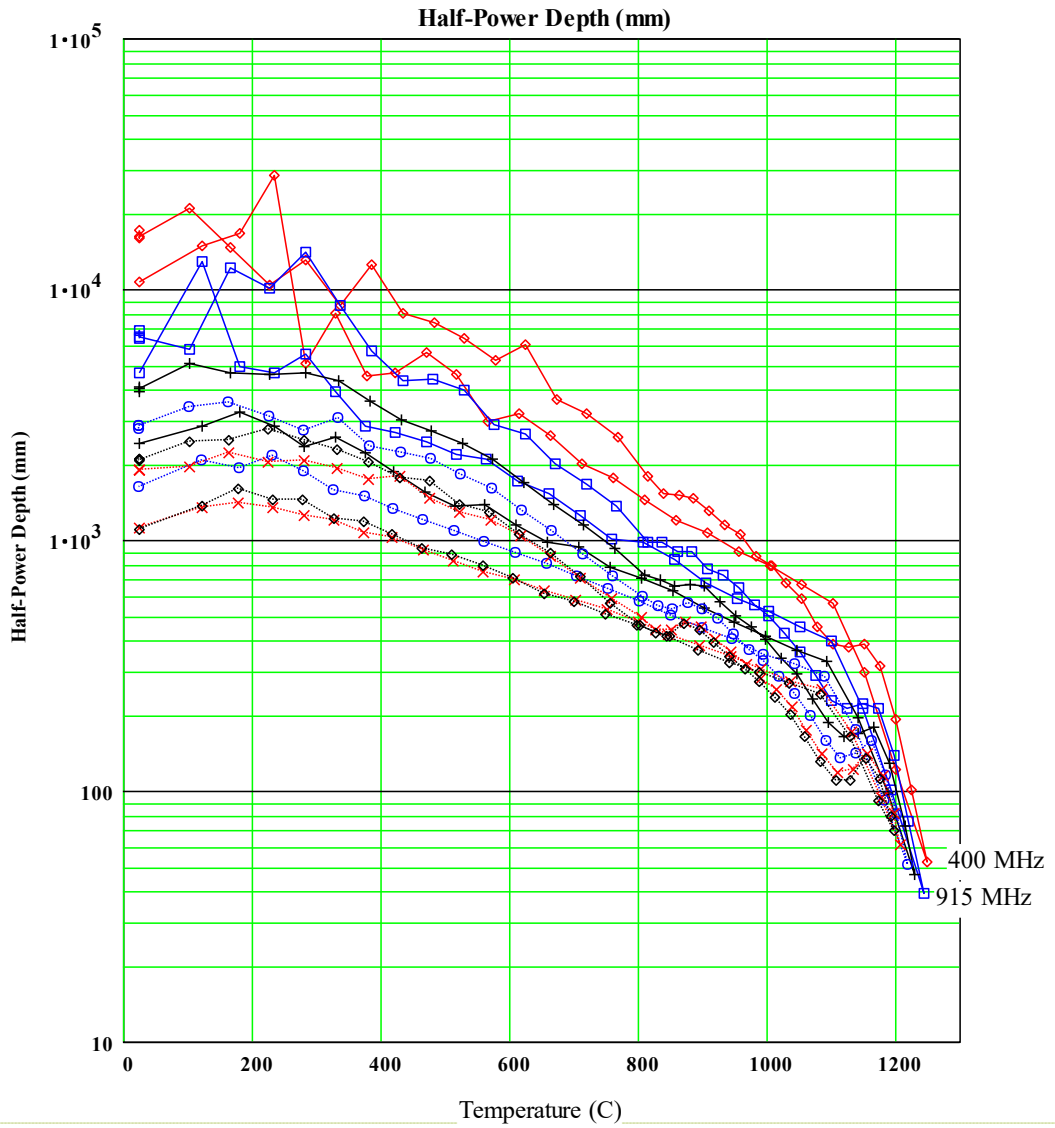

Test = 2023061101 NASA2361.mcd **AnDat = 20230612**

3rd Run, Lunar Simulant NUW-LHT-5M, pre-baked at 750C in Ar/H, to 1250C, in flowing argon, for D.Rickn

List of Measured Values of ε' and ε" :

Initial density = $samdns_{NCal+1} = 2.094$ gm/cc Final density(25C) = **dnsfinal = 2.201** gm/cc

density	index	T(C)	397MHz	912MHz	1429MH	1948MHz	2466MHz	2986MHz	Lapsed Time (hours)	
$samdns_{mm}$	mm	$T_{mm,1}$	$\varepsilon'_{mm,1}$	$\varepsilon'_{mm,2}$	$\varepsilon'_{mm,3}$	$\varepsilon'_{mm,4}$	$\varepsilon'_{mm,5}$	$\varepsilon'_{mm,6}$	$tlaps_{mm}$	$sammas_{mm}$
2.094	11	24	4.58	4.56	4.55	4.54	4.51	4.48	0	0.283
2.094	12	24	4.57	4.55	4.54	4.54	4.51	4.49	0.08	0.283
2.094	13	24	4.57	4.56	4.55	4.54	4.51	4.49	0.14	0.283
2.094	14	103	4.57	4.55	4.54	4.54	4.51	4.49	0.27	0.283
2.094	15	166	4.6	4.58	4.57	4.56	4.54	4.52	0.38	0.283
2.094	16	227	4.64	4.61	4.61	4.6	4.57	4.55	0.5	0.283
2.094	17	284	4.67	4.64	4.64	4.63	4.6	4.58	0.61	0.283
2.094	18	337	4.71	4.68	4.68	4.66	4.64	4.62	0.73	0.283
2.094	19	386	4.73	4.71	4.71	4.69	4.66	4.65	0.84	0.283
2.094	20	434	4.76	4.74	4.74	4.72	4.69	4.68	0.96	0.283
2.094	21	482	4.79	4.77	4.77	4.75	4.72	4.71	1.07	0.283
2.094	22	529	4.83	4.8	4.8	4.78	4.75	4.73	1.19	0.283
2.094	23	577	4.87	4.84	4.84	4.82	4.79	4.77	1.3	0.283
2.094	24	625	4.92	4.87	4.87	4.85	4.82	4.8	1.42	0.283
2.094	25	672	4.96	4.91	4.91	4.89	4.86	4.84	1.53	0.283
2.094	26	720	5.02	4.97	4.95	4.93	4.9	4.87	1.65	0.283
2.084	27	768	5.07	5.02	5	4.98	4.94	4.91	1.76	0.283
2.077	28	815	5.16	5.09	5.07	5.04	5	4.97	1.88	0.283
2.077	29	839	5.2	5.13	5.1	5.07	5.03	5	1.99	0.283
2.077	30	862	5.17	5.09	5.06	5.04	4.99	4.96	2.11	0.283
2.077	31	886	5.08	5.01	4.98	4.96	4.92	4.89	2.22	0.283
2.077	32	910	5.06	4.98	4.96	4.94	4.9	4.87	2.34	0.283
2.077	33	934	5.06	4.98	4.95	4.93	4.88	4.86	2.45	0.283
2.077	34	958	5.09	4.99	4.96	4.94	4.89	4.86	2.57	0.283
2.077	35	982	5.12	5.02	4.98	4.96	4.91	4.88	2.68	0.283
2.077	36	1006	5.18	5.06	5.01	4.99	4.93	4.9	2.8	0.283
2.077	37	1030	5.22	5.09	5.05	5.01	4.96	4.93	2.91	0.283
2.077	38	1054	5.29	5.14	5.08	5.05	5	4.96	3.03	0.283
2.077	39	1079	5.39	5.21	5.14	5.1	5.04	5	3.14	0.283
2.077	40	1103	5.54	5.31	5.22	5.17	5.1	5.05	3.26	0.283
2.077	41	1127	5.68	5.43	5.32	5.25	5.17	5.12	3.37	0.283
2.077	42	1152	5.75	5.51	5.4	5.34	5.25	5.2	3.49	0.283
2.097	43	1176	5.89	5.66	5.53	5.48	5.38	5.33	3.61	0.283
2.118	44	1200	6.53	6.15	5.94	5.86	5.72	5.65	3.72	0.283
2.138	45	1224	7.88	7.13	6.73	6.4	6.23	6.13	3.84	0.283
2.159	46	1248	10.44	8.94	7.84	7.36	6.92	6.68	3.95	0.283
2.18	47	1200	8.14	7.31	6.97	6.83	6.63	6.54	4.07	0.283
2.201	48	1151	7.01	6.71	6.55	6.48	6.37	6.31	4.18	0.283
2.201	49	1102	6.53	6.37	6.3	6.26	6.2	6.16	4.3	0.283
2.201	50	1054	6.42	6.29	6.23	6.21	6.15	6.12	4.41	0.283
2.201	51	1005	6.36	6.24	6.19	6.16	6.11	6.08	4.53	0.283
2.201	52	957	6.29	6.19	6.15	6.13	6.08	6.05	4.65	0.283
2.201	53	908	6.24	6.14	6.12	6.09	6.05	6.02	4.77	0.283
2.201	54	859	6.18	6.09	6.07	6.05	6.01	5.99	4.89	0.283
2.201	55	810	6.13	6.06	6.04	6.02	5.98	5.96	5.02	0.283
2.201	56	761	6.08	6.02	6.01	5.98	5.95	5.93	5.16	0.283
2.201	57	712	6.04	5.98	5.97	5.95	5.92	5.9	5.3	0.283
2.201	58	663	5.99	5.94	5.94	5.92	5.88	5.87	5.45	0.283
2.201	59	614	5.95	5.9	5.9	5.88	5.85	5.84	5.62	0.283
2.201	60	565	5.91	5.86	5.87	5.85	5.82	5.81	5.79	0.283

mq := 61 , 62 .. nd - Nempties

$samdns_{mq}$	mq	$T_{mq,1}$	$\varepsilon'_{mq,1}$	$\varepsilon'_{mq,2}$	$\varepsilon'_{mq,3}$	$\varepsilon'_{mq,4}$	$\varepsilon'_{mq,5}$	$\varepsilon'_{mq,6}$	$tlaps_{mq}$	$sammas_{mq}$
2.201	61	518	5.87	5.83	5.83	5.81	5.78	5.77	5.98	0.283
2.201	62	471	5.83	5.78	5.79	5.77	5.75	5.73	6.18	0.283
2.201	63	422	5.79	5.75	5.75	5.74	5.72	5.7	6.4	0.283
2.201	64	377	5.73	5.7	5.7	5.69	5.67	5.66	6.64	0.283
2.201	65	330	5.68	5.67	5.67	5.66	5.63	5.62	6.91	0.283
2.201	66	283	5.64	5.62	5.62	5.61	5.58	5.57	7.21	0.283
2.201	67	235	5.59	5.57	5.57	5.56	5.54	5.53	7.59	0.283
2.201	68	181	5.54	5.52	5.52	5.51	5.49	5.48	8.05	0.283
2.201	69	123	5.53	5.52	5.51	5.51	5.48	5.47	8.74	0.283
2.201	70	24	5.5	5.49	5.47	5.45	5.41	5.38	11.41	0.283

Test = 2023061101 NASA2361.mcd **AnDat = 20230612**

3rd Run, Lunar Simulant NUW-LHT-5M, pre-baked at 750C in Ar/H, to 1250C, in flowing argon, for D.Rickm

List of Measured Values of ε' and ε" :

Initial density = $samdns_{NCal+1}$ = 2.094 gm/cc Final density(25C) = dnsfinal = 2.201 gm/cc

$samdns_{mm}$	mm	$T_{mm,1}$	density index T(C) 397MHz $\varepsilon''_{mm,1}$	912MHz $\varepsilon''_{mm,2}$	1429MH $\varepsilon''_{mm,3}$	1948MHz $\varepsilon''_{mm,4}$	2466MHz $\varepsilon''_{mm,5}$	2986MHz $\varepsilon''_{mm,6}$	Lapsed Time (hours) $tlaps_{mm}$	$sammas_{mm}$
2.094	11	24	0.01	0.012	0.013	0.013	0.015	0.011	0	0.283
2.094	12	24	0.011	0.011	0.012	0.013	0.015	0.011	0.08	0.283
2.094	13	24	0.011	0.012	0.012	0.013	0.015	0.011	0.14	0.283
2.094	14	103	0.008	0.013	0.01	0.011	0.014	0.01	0.27	0.283
2.094	15	166	0.012	0.006	0.011	0.01	0.013	0.009	0.38	0.283
2.094	16	227	0.017	0.008	0.011	0.012	0.014	0.009	0.5	0.283
2.094	17	284	0.014	0.006	0.011	0.013	0.014	0.009	0.61	0.283
2.094	18	337	0.021	0.009	0.012	0.012	0.015	0.01	0.73	0.283
2.094	19	386	0.014	0.014	0.014	0.016	0.017	0.012	0.84	0.283
2.094	20	434	0.022	0.018	0.017	0.017	0.016	0.013	0.96	0.283
2.094	21	482	0.025	0.018	0.018	0.018	0.02	0.014	1.07	0.283
2.094	22	529	0.029	0.02	0.021	0.02	0.023	0.017	1.19	0.283
2.094	23	577	0.035	0.028	0.024	0.023	0.024	0.019	1.3	0.283
2.094	24	625	0.031	0.03	0.03	0.029	0.028	0.023	1.42	0.283
2.094	25	672	0.051	0.04	0.037	0.034	0.034	0.027	1.53	0.283
2.094	26	720	0.058	0.048	0.045	0.043	0.042	0.034	1.65	0.283
2.084	27	768	0.072	0.059	0.055	0.052	0.051	0.043	1.76	0.283
2.077	28	815	0.104	0.084	0.072	0.064	0.061	0.054	1.88	0.283
2.077	29	839	0.124	0.084	0.075	0.07	0.069	0.058	1.99	0.283
2.077	30	862	0.125	0.09	0.079	0.071	0.068	0.059	2.11	0.283
2.077	31	886	0.127	0.09	0.077	0.067	0.063	0.053	2.22	0.283
2.077	32	910	0.142	0.105	0.079	0.071	0.066	0.056	2.34	0.283
2.077	33	934	0.163	0.111	0.09	0.078	0.073	0.062	2.45	0.283
2.077	34	958	0.178	0.125	0.103	0.089	0.083	0.071	2.57	0.283
2.077	35	982	0.218	0.146	0.114	0.103	0.092	0.08	2.68	0.283
2.077	36	1006	0.24	0.164	0.129	0.115	0.105	0.09	2.8	0.283
2.077	37	1030	0.282	0.192	0.153	0.133	0.118	0.103	2.91	0.283
2.077	38	1054	0.329	0.228	0.178	0.156	0.138	0.122	3.03	0.283
2.077	39	1079	0.426	0.288	0.225	0.194	0.172	0.151	3.14	0.283
2.077	40	1103	0.509	0.362	0.282	0.244	0.215	0.189	3.26	0.283
2.077	41	1127	0.526	0.394	0.325	0.286	0.255	0.226	3.37	0.283
2.077	42	1152	0.518	0.383	0.315	0.279	0.251	0.227	3.49	0.283
2.097	43	1176	0.636	0.404	0.301	0.252	0.219	0.19	3.61	0.283
2.118	44	1200	1.099	0.643	0.438	0.354	0.278	0.236	3.72	0.283
2.138	45	1224	2.315	1.287	0.829	0.534	0.41	0.344	3.84	0.283
2.159	46	1248	5.27	2.803	1.403	0.906	0.572	0.411	3.95	0.283
2.18	47	1200	1.946	0.97	0.618	0.486	0.366	0.307	4.07	0.283
2.201	48	1151	0.742	0.438	0.302	0.245	0.197	0.169	4.18	0.283
2.201	49	1102	0.38	0.23	0.175	0.148	0.13	0.112	4.3	0.283
2.201	50	1054	0.318	0.201	0.158	0.133	0.121	0.102	4.41	0.283
2.201	51	1005	0.264	0.174	0.138	0.121	0.108	0.092	4.53	0.283
2.201	52	957	0.232	0.153	0.122	0.104	0.096	0.084	4.65	0.283
2.201	53	908	0.195	0.132	0.106	0.094	0.086	0.074	4.77	0.283
2.201	54	859	0.171	0.107	0.09	0.083	0.078	0.065	4.89	0.283
2.201	55	810	0.143	0.09	0.081	0.074	0.069	0.059	5.02	0.283
2.201	56	761	0.116	0.088	0.072	0.065	0.061	0.053	5.16	0.283
2.201	57	712	0.101	0.07	0.06	0.057	0.056	0.047	5.3	0.283
2.201	58	663	0.078	0.057	0.057	0.051	0.052	0.044	5.45	0.283
2.201	59	614	0.063	0.051	0.048	0.046	0.047	0.038	5.62	0.283
2.201	60	565	0.068	0.042	0.04	0.042	0.043	0.034	5.79	0.283

mq := 61 , 62 .. nd - Nempties

$samdns_{mq}$	mq	$T_{mq,1}$	$\varepsilon''_{mq,1}$	$\varepsilon''_{mq,2}$	$\varepsilon''_{mq,3}$	$\varepsilon''_{mq,4}$	$\varepsilon''_{mq,5}$	$\varepsilon''_{mq,6}$	$tlaps_{mq}$	$sammas_{mq}$
2.201	61	518	0.044	0.04	0.04	0.038	0.039	0.03	5.98	0.283
2.201	62	471	0.036	0.035	0.036	0.034	0.035	0.029	6.18	0.283
2.201	63	422	0.043	0.032	0.029	0.031	0.031	0.025	6.4	0.283
2.201	64	377	0.044	0.03	0.025	0.027	0.03	0.022	6.64	0.283
2.201	65	330	0.024	0.022	0.021	0.026	0.027	0.021	6.91	0.283
2.201	66	283	0.039	0.015	0.023	0.021	0.025	0.018	7.21	0.283
2.201	67	235	0.007	0.018	0.019	0.018	0.023	0.018	7.59	0.283
2.201	68	181	0.012	0.017	0.017	0.021	0.022	0.016	8.05	0.283
2.201	69	123	0.013	0.007	0.019	0.019	0.023	0.019	8.74	0.283
2.201	70	24	0.018	0.018	0.022	0.024	0.028	0.023	11.41	0.283

Appendix H.2 Dr. Holly Shulman
Apr. 29, 2009

The sample was prepared by pressing two pellets, each ~6 mm long, and stacking them in the holder.

The initial sample parameters were:

a) Length: 12.37± 0.05 mm
b) Diameter: 3.63 ± 0.05 mm
c) Mass: 0.267 ± 0.002 gm
d) Appearance: Dark grey cylinders
e) Room Temperature Density: 2.09 ± 0.15 gm/cc.

Two cycles of dielectric measurements were performed on the same sample without removing it from the holder. Each cycle consisted of measurements at room temperature, 100 °C, and then in 50 °C steps to 1100 °C, and then in –100 °C steps back down to 200 °C, then again at room temperature. The empty holder could not be measured at the end of the run because the sample had expanded and adhered to the walls of the holder (see photo of sample, which broke when we broke the holder to get it out).

Final sample parameters were:

a) Length: 10.15 ± 0.20 mm
b) Diameter: 3.90 ± 0.15 mm
c) Mass: 0.265 ± 0.002 gm
d) Appearance: Pellets adhered to each other, and darker!
e) Room Temperature Density: 2.19 ±0.20 gm/cc.

For the data analysis, a value of the thermal expansion coefficient of $\alpha = 0.0 * 10^{-6}/K$ was used since sintering or melting occurred.

The frequency coding is:
Legend for Data Plots :

#	Frequency(MHz)	Symbol
1	912	blue square, solid line
2	2466	red cross, dotted line

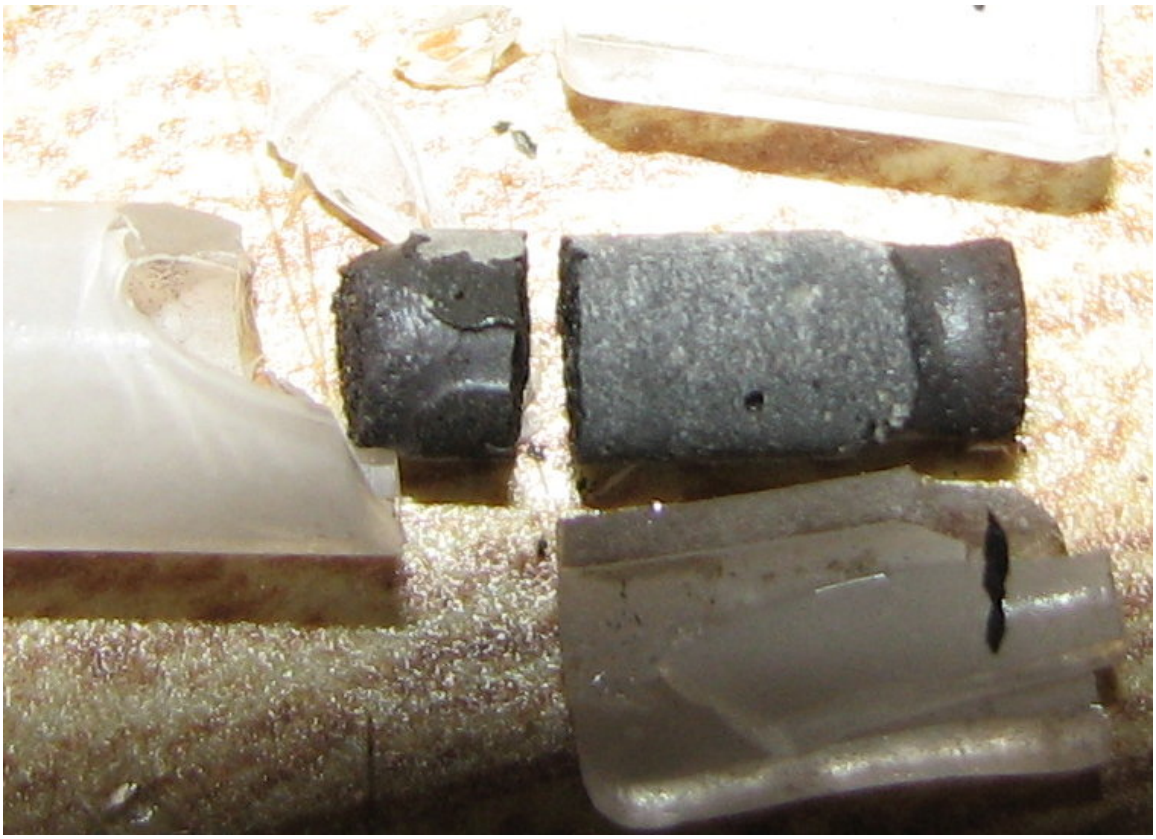

Code Calculates Sample Volume and Plots Sample Density As a Function of Temperature or Lapsed Time

Test = 2009042601 CERL0960.mcd **AnDat = 20090428**

JSC-1 Linar Simulant, RT to 1100C, in flowing UHP argon , Shawn Allen, CERALINK

Assumed Dimensions (mm), Mass(gm) and Density (gm/cc) as a Function of Temperature for Pellet Stac

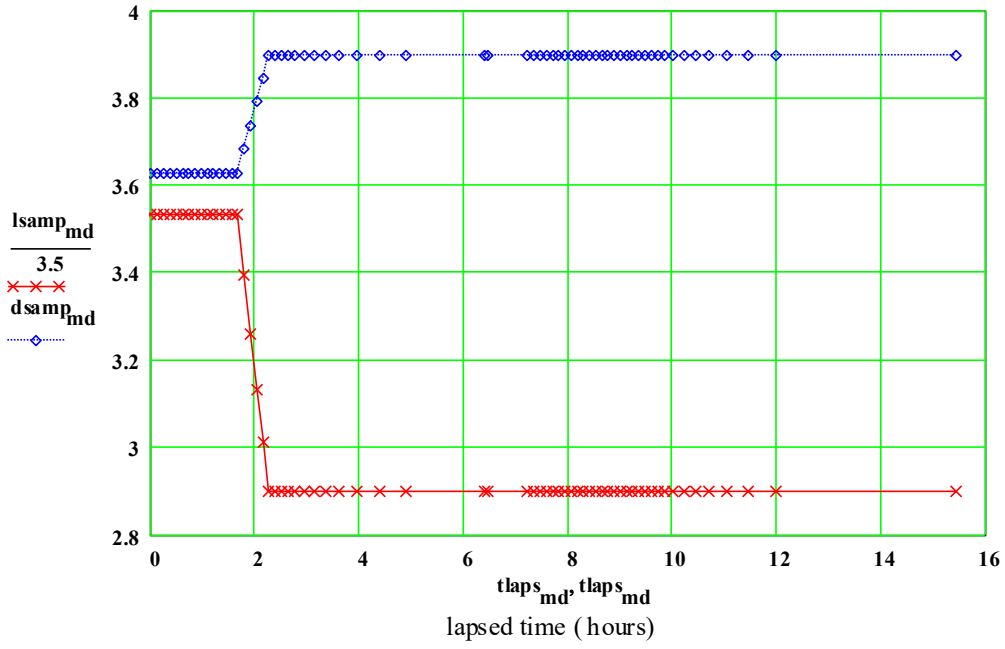

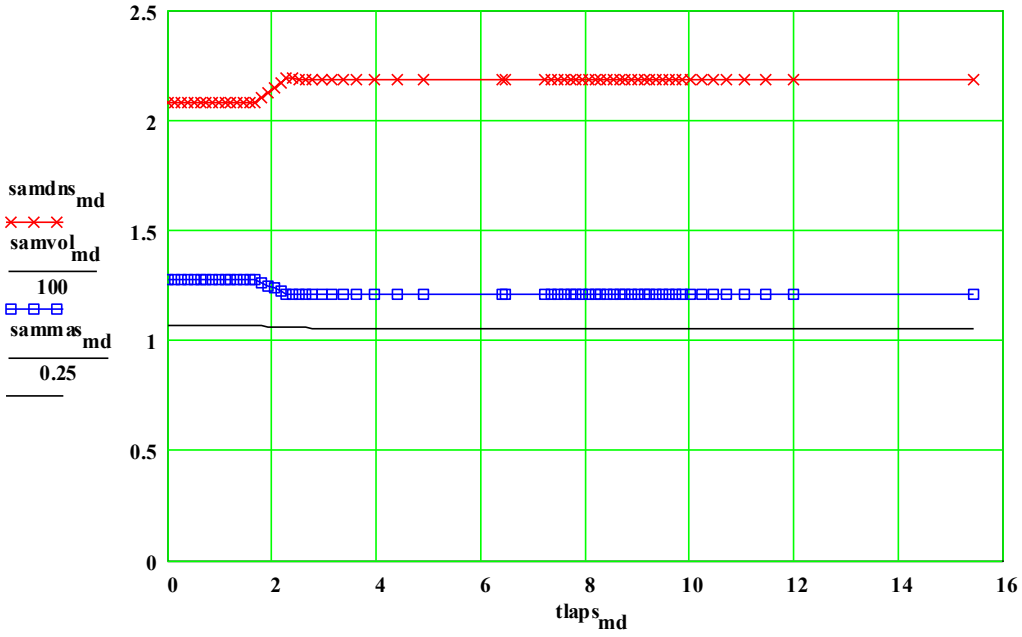

Test = 2009042601 CERL0960A.mcd **AnDat = 20090428**

JSC-1 Linar Simulant, First Cycle, RT to 1100C, in flowing UHP argon , Shawn Allen, CERALINK

Initial density = **samdns$_{NCal+1}$ = 2.09** gm/cc, Thermal exp. coeff.

Final density(25C) = **dnsfinal = 2.19** gm/cc **FracMassChange = $-7.49\cdot10^{-3}$** **$\alpha_1 = 0$**

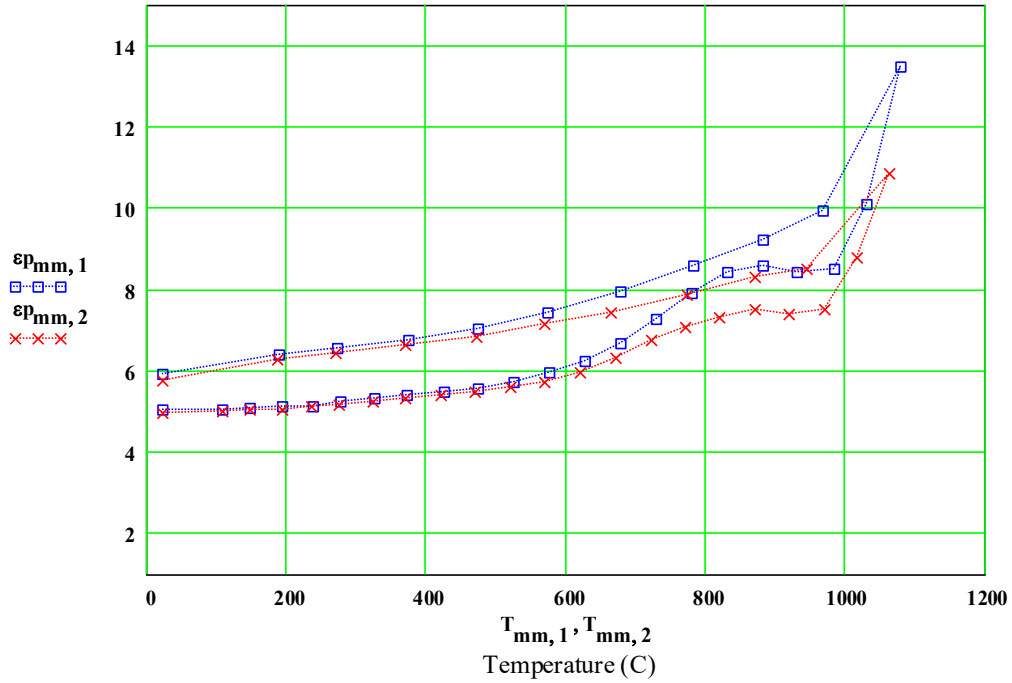

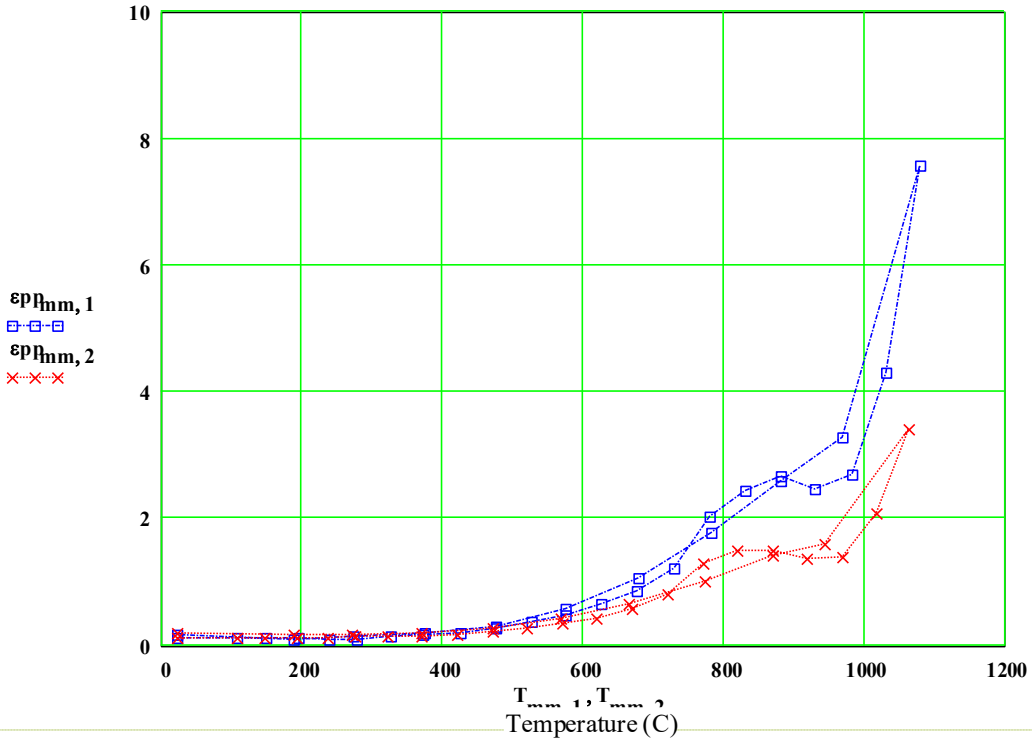

Test = 2009042601 CERL0960A.mcd **AnDat = 20090428**

JSC-1 Linar Simulant, First Cycle, RT to 1100C, in flowing UHP argon , Shawn Allen, CERALINK

Initial density = $samdns_{NCal+1}$ **= 2.09** gm/cc. Final density(25C) = **dnsfinal = 2.19** gm/cc

FracMassChange = $-7.49 \cdot 10^{-3}$ α_1 **= 0** /C

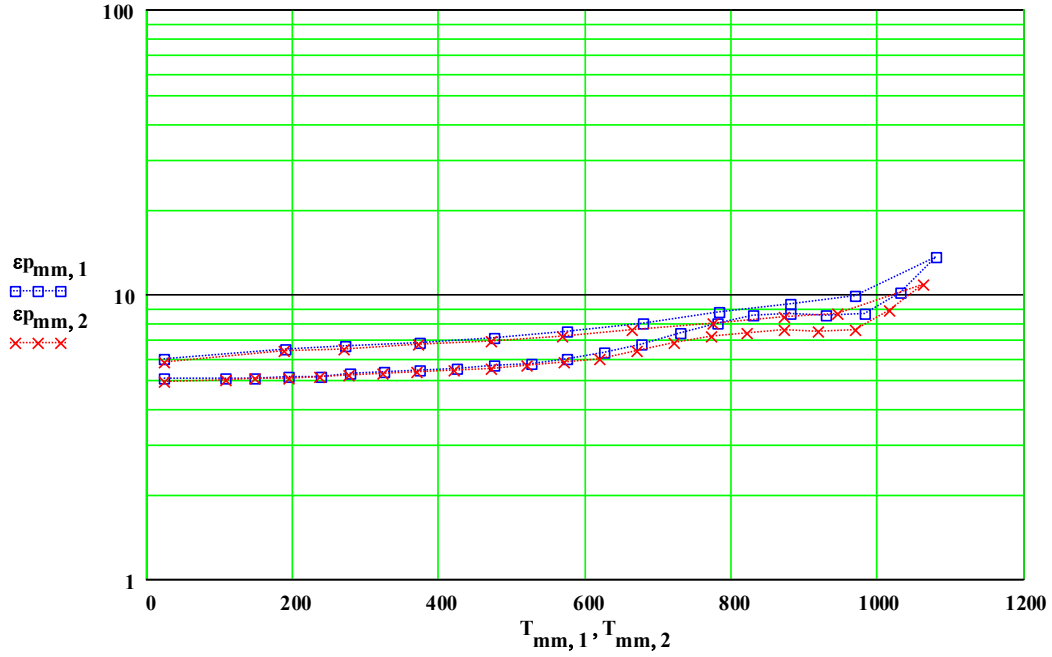

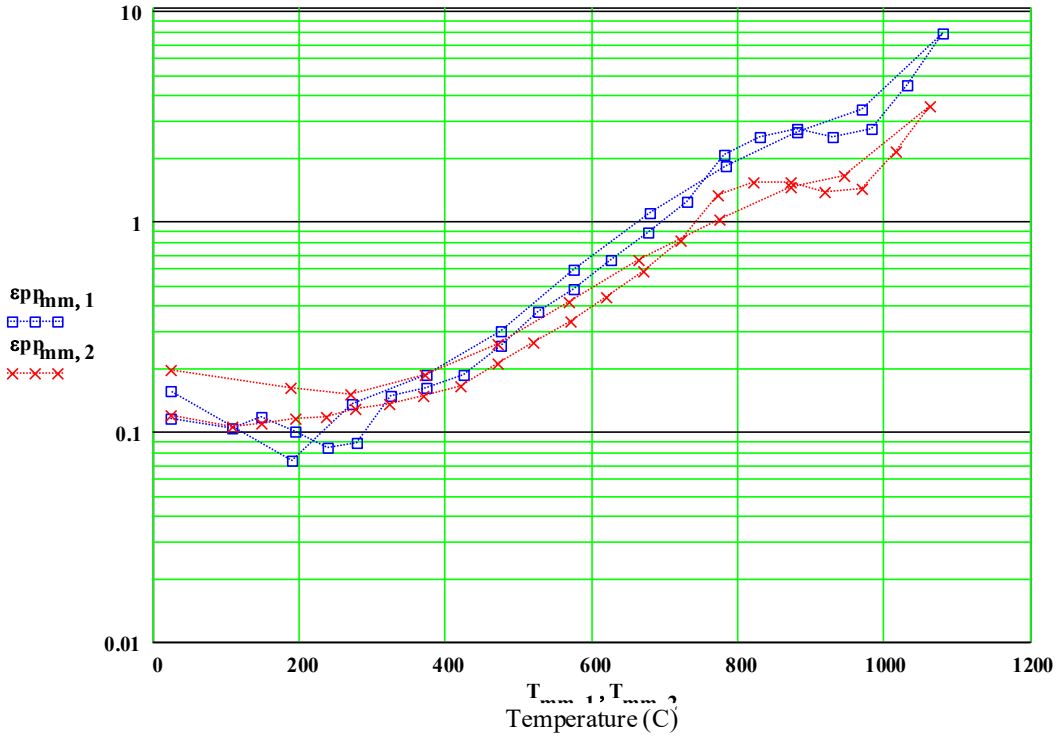

Test = 2009042601 CERL0960A.mcd **AnDat = 20090428**

JSC-1 Linar Simulant, First Cycle, RT to 1100C, in flowing UHP argon , Shawn Allen, CERALINK

Initial density = $\mathbf{samdns}_{NCal+1}$ **= 2.09** gm/cc, Final density(25C) = **dnsfinal = 2.19** gm/cc

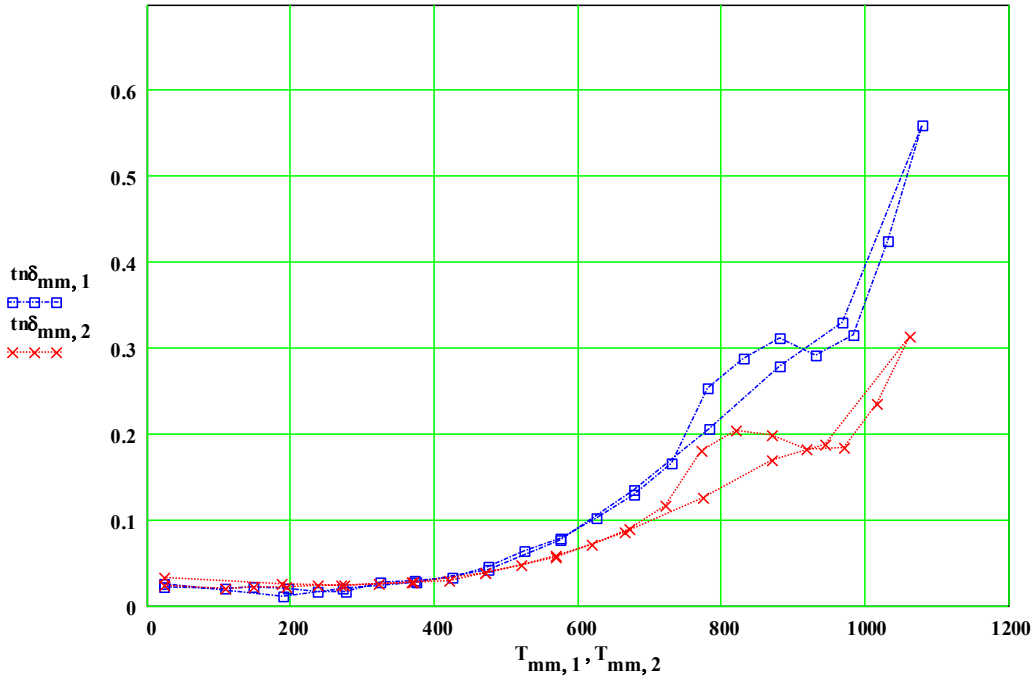

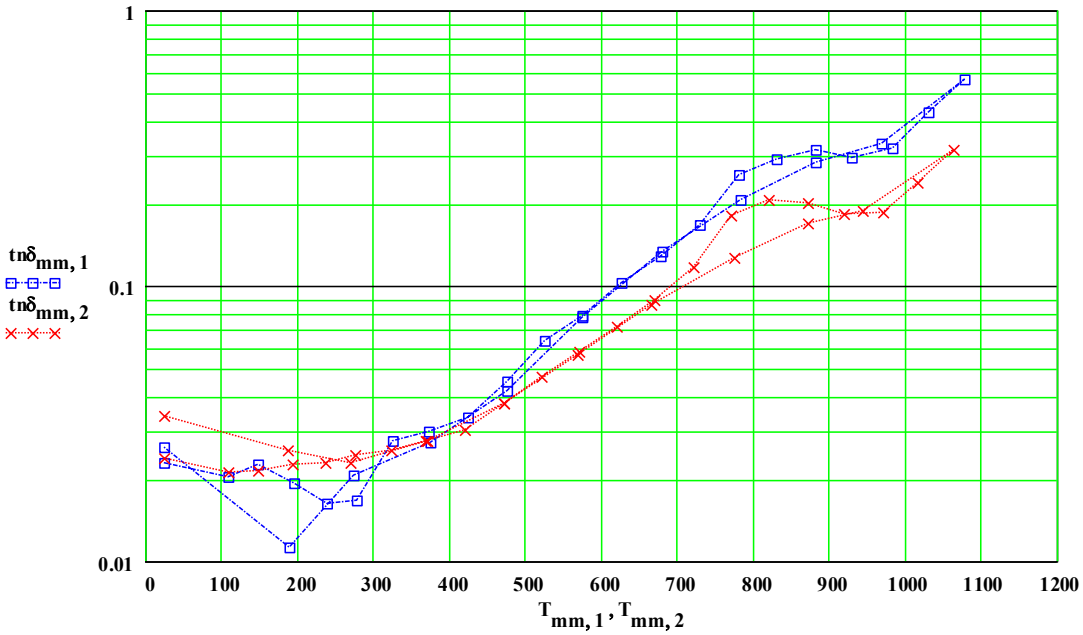

Test = 2009042601 CERL0960A.mcd **AnDat = 20090428**

JSC-1 Linar Simulant, First Cycle, RT to 1100C, in flowing UHP argon , Shawn Allen, CERALINK

Initial density = $\mathbf{samdns_{NCal+1}}$ **= 2.09** gm/cc, Final density(25C) = **dnsfinal = 2.19** gm/cc

α_1 **= 0** /C

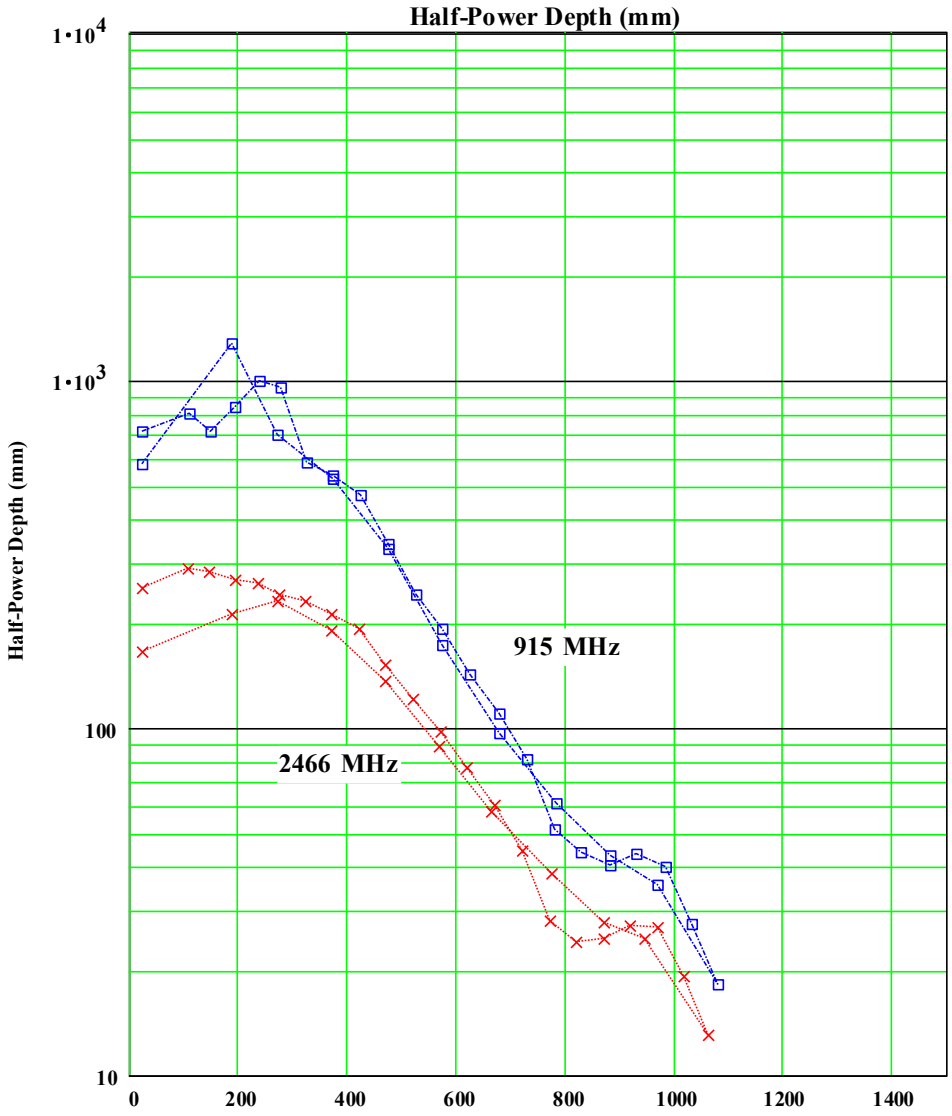

Test = 2009042601 CERL0960A.mcd **AnDat = 20090428**

JSC-1 Linar Simulant, RT to 1100C, in flowing UHP argon , Shawn Allen, CERALINK

Initial density = $samdns_{NCal+1}$ **= 2.09** gm/cc, Final density(25C) = **dnsfinal = 2.19** gm/cc

Eg = 4 eV **σint = 1.2·10^7** Siemens/metre **α_1 = 0** /C

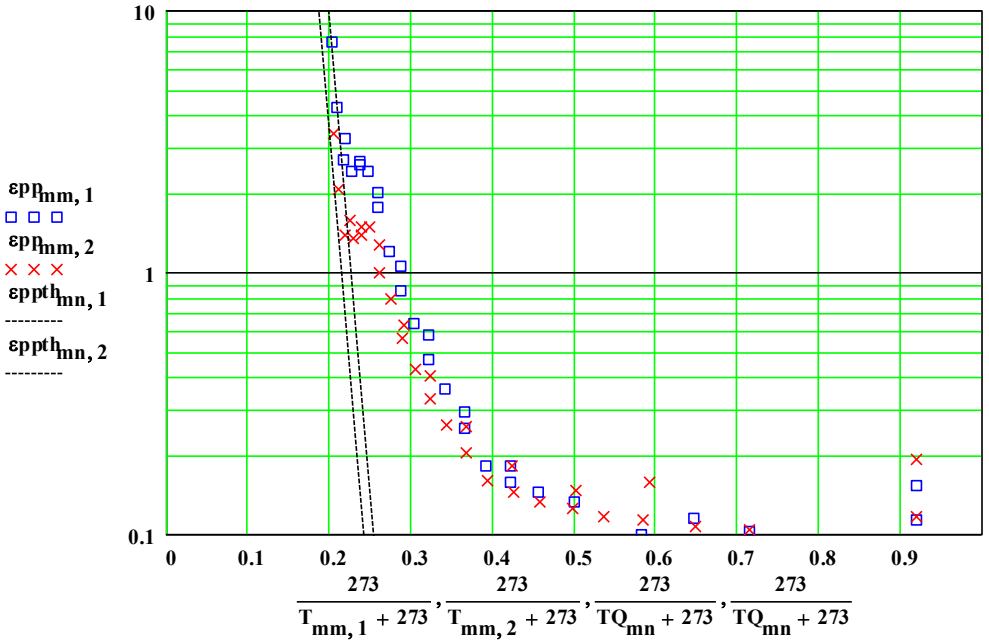

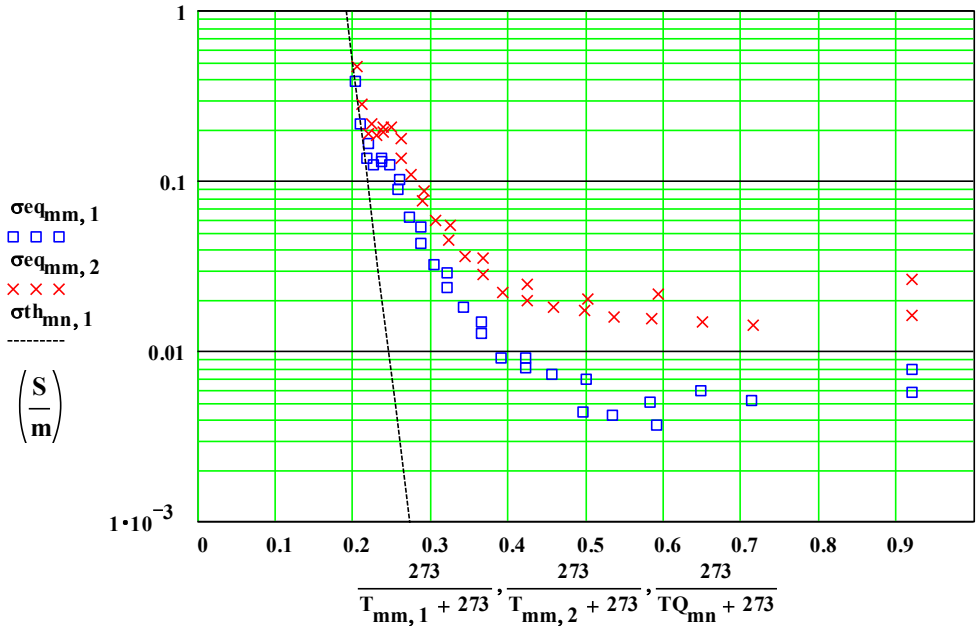

Operator: Chose the Functional Dependence, Input the Chosen Values for Eg and the Intrinsic Conducσint

$Eg := 4.0$ eV

$\sigma int := 1.2 \cdot 10^{7}$ Siemens/metre

$Hactiv := \frac{Eg}{2} \cdot 96.5$ Kjoule/mol

$Hactiv = 193$

$mn := 1 .. 16$

$kB := 8.617 \cdot 10^{-5}$ eV/K

$$\varepsilon ppth_{mn,n} := \left[\frac{\sigma int}{2 \cdot \pi \cdot fh_n \cdot 8.85 \cdot 10^{-6}} \cdot \exp\left[\frac{-Eg}{2 \cdot kB \cdot \left(TQ_{mn} + 273. \right)} \right] \right]$$

$$\sigma th_{mn,n} := \overrightarrow{\varepsilon ppth_{mn,n} \cdot 2 \cdot \pi \cdot fh_n \cdot 8.85 \cdot 10^{-6}}$$

$\varepsilon ppth_{(16,2)} = 180.57$

Test = 2009042601 CERL0960B.mcd **AnDat = 20090428**

JSC-1 Linar Simulant, 2nd Cycle, RT to 1100C, flowing UHP argon, Shawn Allen, CERALINK

Final density(25C) = **dnsfinal = 2.19** gm/cc **FracMassChange = $-7.49 \cdot 10^{-3}$**

Thermal exp. coeff.

$\alpha_1 = 0$

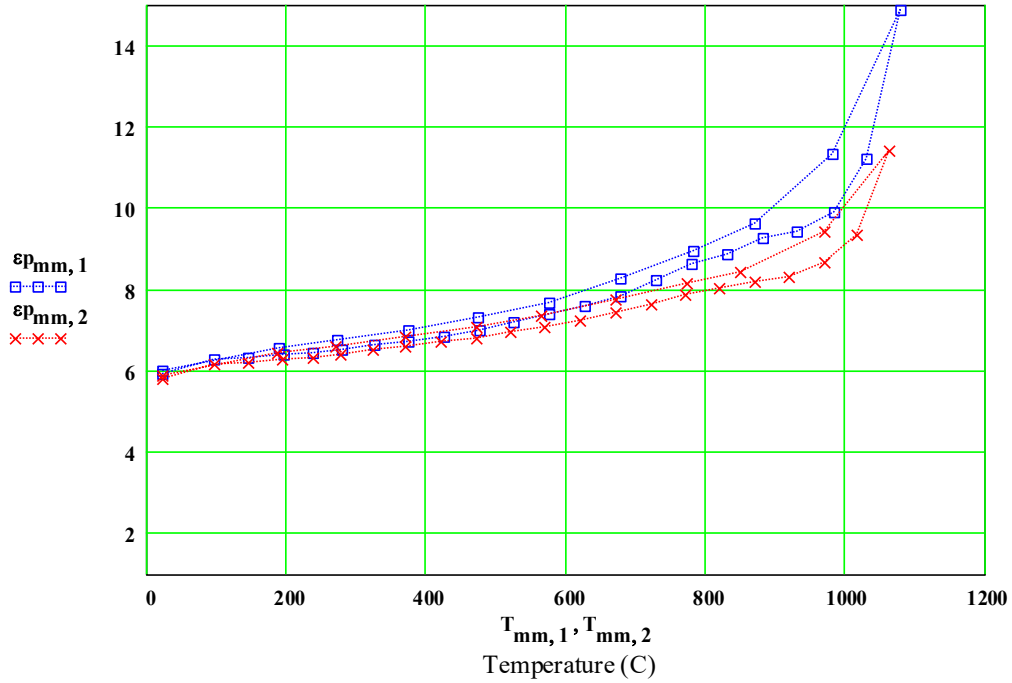

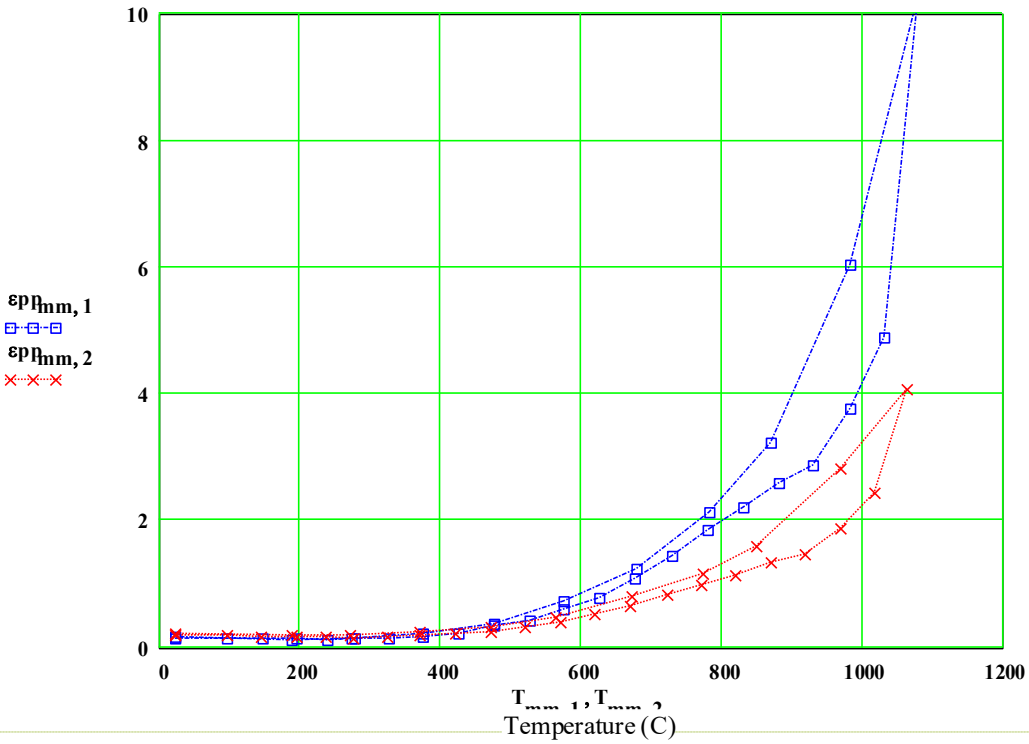

Test = 2009042601 CERL0960B.mcd **AnDat = 20090428**

JSC-1 Linar Simulant, 2nd Cycle, RT to 1100C, flowing UHP argon, Shawn Allen, CERALINK

Initial density = $samdns_{NCal+1}$ **= 2.09** gm/cc, Final density(25C) = **dnsfinal = 2.19** gm/cc

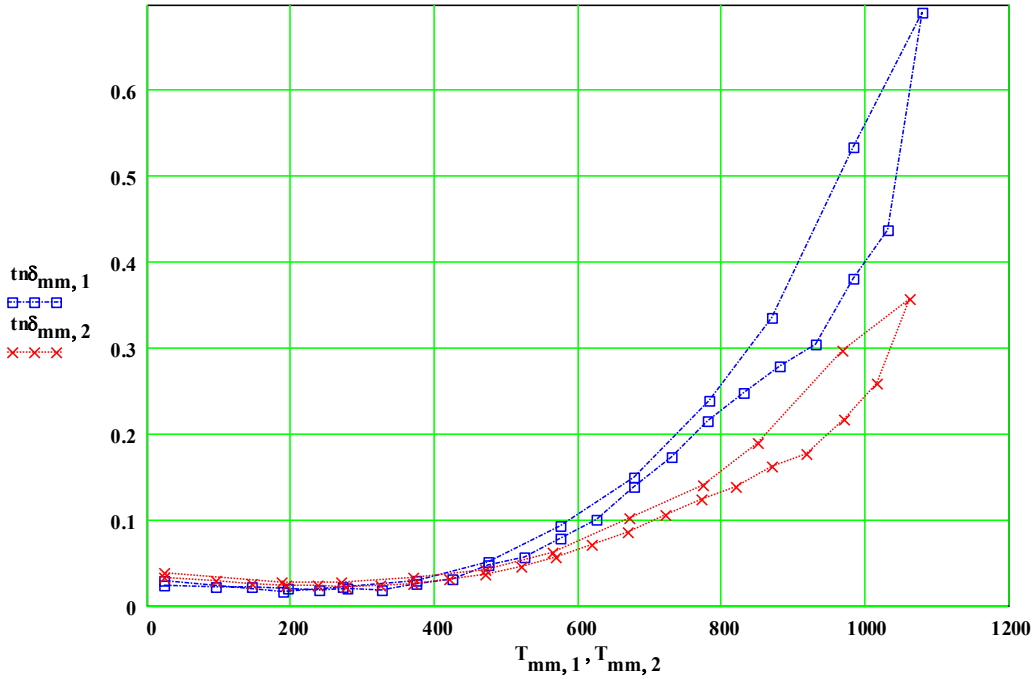

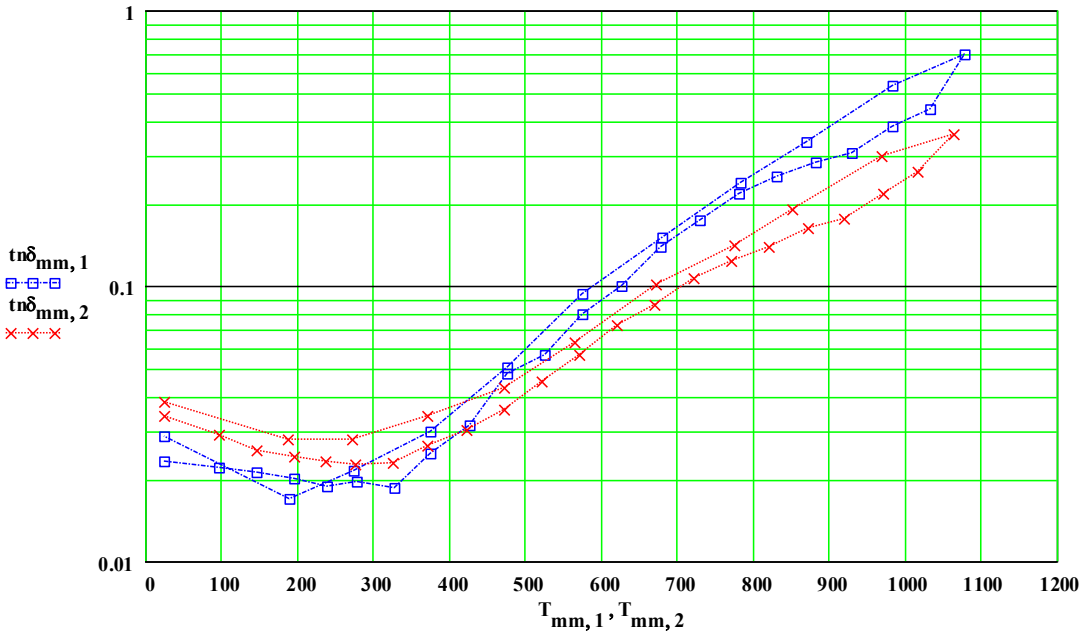

Test = 2009042601 CERL0960B.mcd **AnDat = 20090428**

JSC-1 Linar Simulant, 2nd Cycle, RT to 1100C, flowing UHP argon, Shawn Allen, CERALINK

Initial density = $samdns_{NCal+1}$ **= 2.09** gm/cc, Final density(25C) = **dnsfinal = 2.19** gm/cc

α_1 **= 0** /C

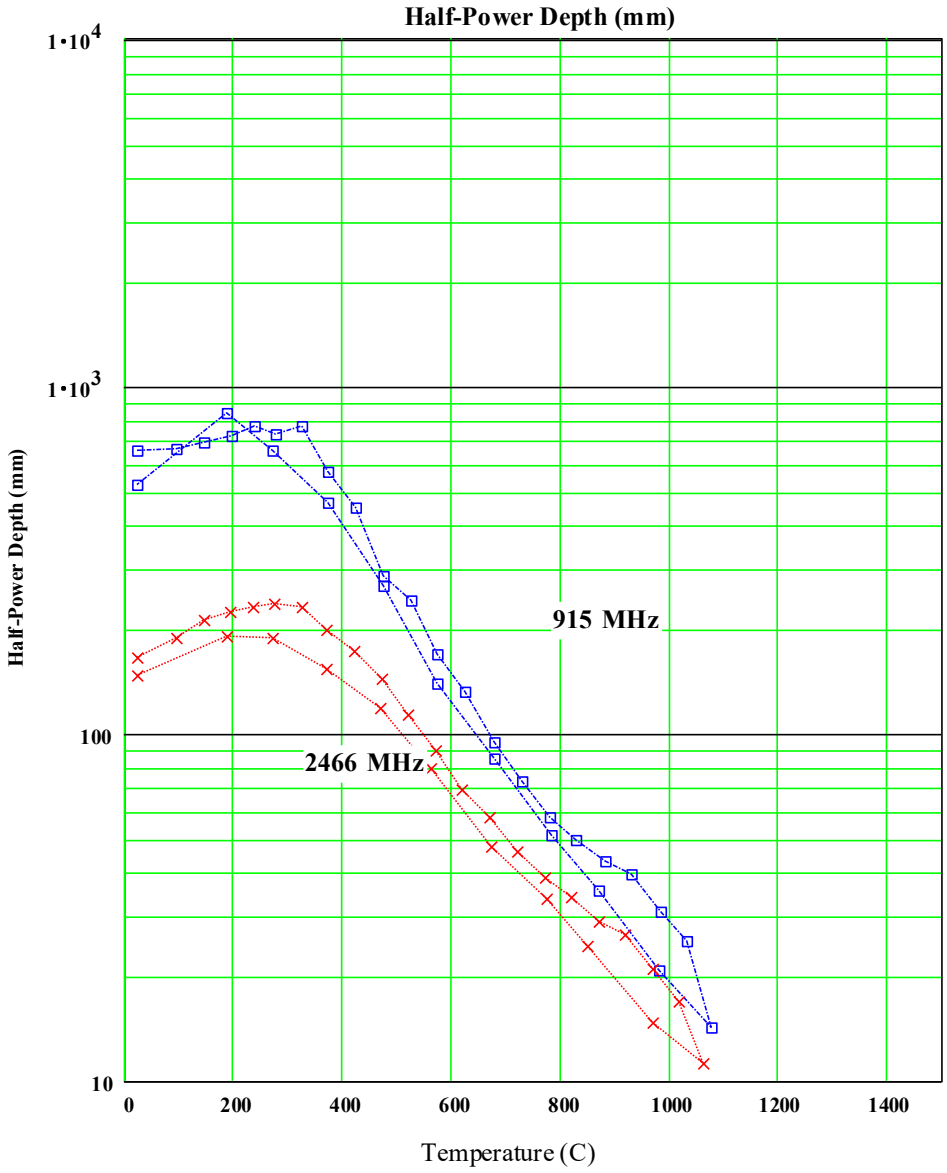

Test = 2009042601 CERL0960B.mcd **AnDat = 20090428**

JSC-1 Linar Simulant, 2nd Cycle, RT to 1100C, flowing UHP argon, Shawn Allen, CERALINK

Initial density = $samdns_{NCal+1}$ **= 2.09** gm/cc, Final density(25C) = **dnsfinal = 2.19** gm/cc

Eg = 4 eV **σint = 1.5·10^7** Siemens/metre **α_1 = 0** /C

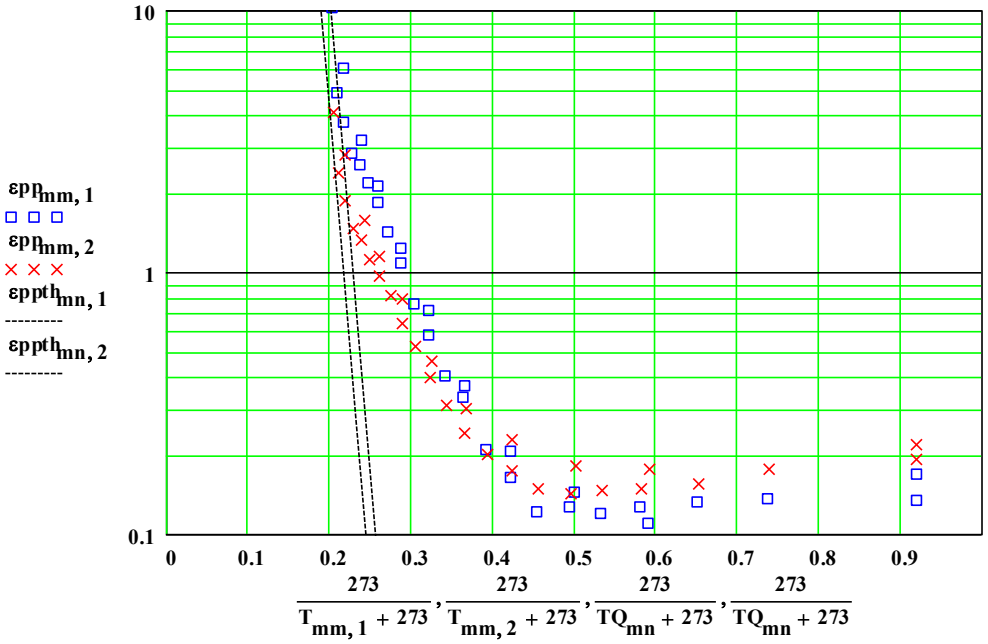

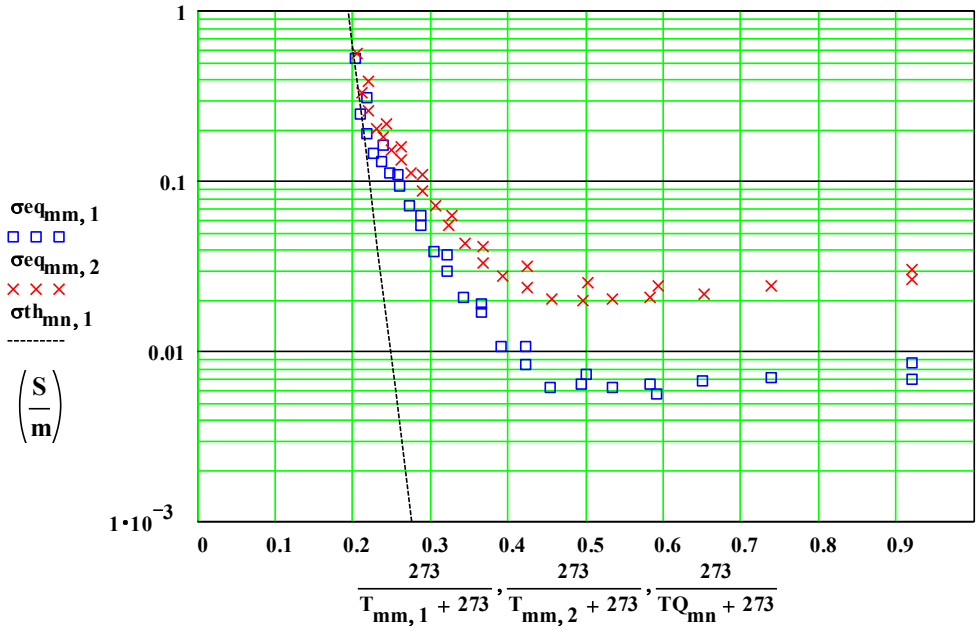

Test = 2009042601 CERL0960.mcd **AnDat = 20090428**

JSC-1 Linar Simulant, RT to 1100C, in flowing UHP argon , Shawn Allen, CERALINK

Initial density = $samdns_{NCal+1}$ **= 2.09** gm/cc, Final density(25C) = **dnsfinal = 2.19** gm/cc

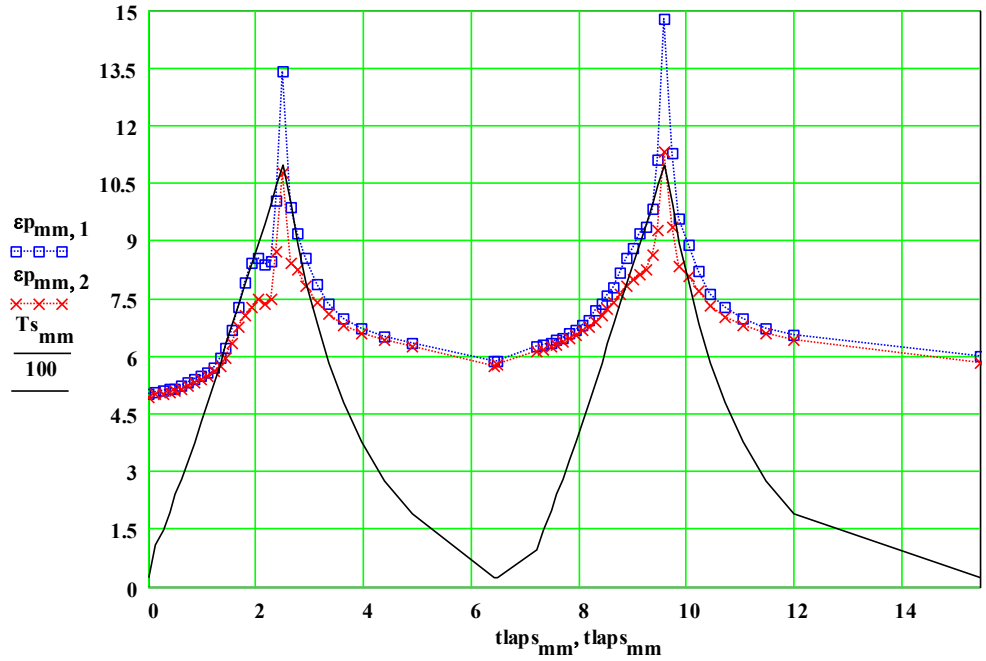

lapsed time (hours)

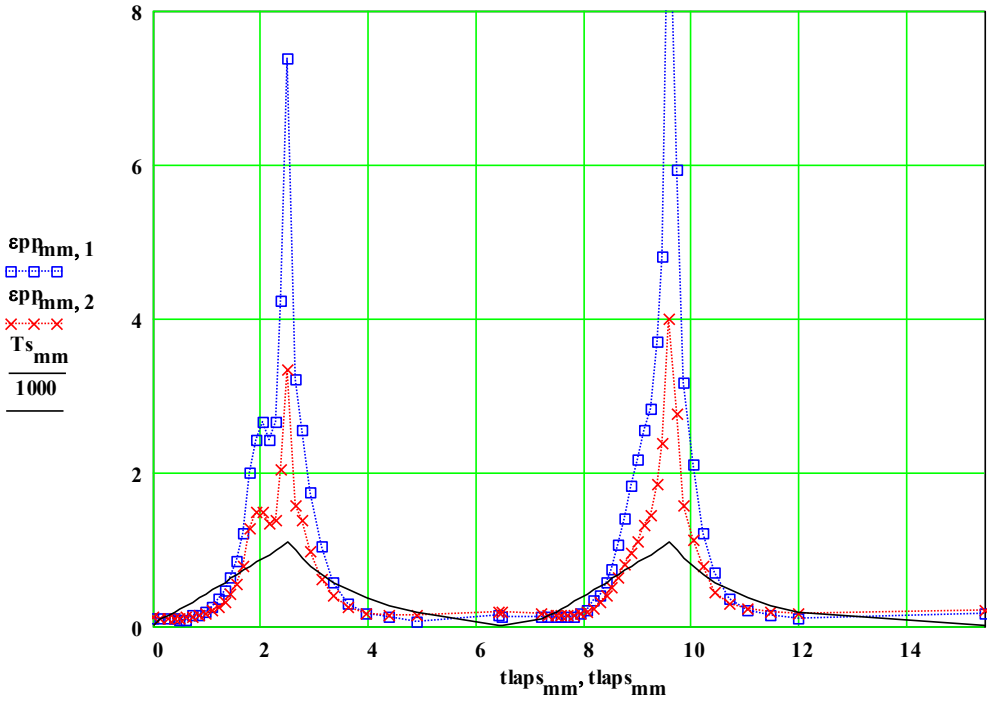

List of Measured Values of ε' and ε'' and tan δ :

Test = 2009042601 CERL0960A.mcd **AnDat = 20090428**

JSC-1 Linar Simulant, First Cycle, RT to 1100C, in flowing UHP argon , Shawn Allen, CERALINK

Initial density = **samdns** $_{NCal+1}$ **= 2.086** gm/cc Final density(25C) = **dnsfinal = 2.186** gm/cc

		T(degC)	912 MHz			Lapsed Time(minutes)	T(degC)	2460 MHz		
samdns $_{mm}$	**mm**	$T_{mm,1}$	$\varepsilon p_{mm,1}$	$\varepsilon pp_{mm,1}$	$tn\delta_{mm,1}$	$60 \cdot tlaps_{mm}$	$T_{mm,2}$	$\varepsilon p_{mm,2}$	$\varepsilon pp_{mm,2}$	$tn\delta_{mm,2}$
2.086	1	24	5.04	0.1146	0.0227	0	24	4.96	0.1178	0.0238
2.086	2	109	5.07	0.1026	0.0202	8	109	5.01	0.1049	0.0209
2.086	3	149	5.1	0.1152	0.0226	15.5	148	5.04	0.1076	0.0213
2.086	4	195	5.14	0.0987	0.0192	22.8	194	5.07	0.1138	0.0224
2.086	5	239	5.15	0.0831	0.0161	30	237	5.12	0.1168	0.0228
2.086	6	278	5.25	0.087	0.0166	37.1	276	5.17	0.1256	0.0243
2.086	7	326	5.34	0.1453	0.0272	44.2	323	5.25	0.133	0.0253
2.086	8	373	5.4	0.1596	0.0296	51.2	370	5.32	0.1451	0.0273
2.086	9	425	5.49	0.1825	0.0333	58.3	421	5.41	0.1617	0.0299
2.086	10	476	5.59	0.253	0.0453	65.4	471	5.49	0.2068	0.0377
2.086	11	526	5.73	0.3612	0.0631	72.4	521	5.6	0.262	0.0468
2.086	12	576	5.96	0.4631	0.0776	79.5	570	5.74	0.3298	0.0575
2.086	13	627	6.24	0.6374	0.1022	86.6	620	5.95	0.4262	0.0716
2.086	14	678	6.67	0.8581	0.1286	93.6	671	6.33	0.5636	0.089
2.086	15	730	7.3	1.2119	0.1661	100.7	722	6.78	0.7889	0.1164
2.108	16	781	7.92	2.0128	0.254	107.8	772	7.09	1.2847	0.1812
2.129	17	831	8.43	2.4358	0.2888	114.8	821	7.31	1.4993	0.205
2.15	18	882	8.6	2.6766	0.3112	121.9	871	7.51	1.4985	0.1995
2.172	19	931	8.42	2.4538	0.2913	129	919	7.42	1.3521	0.1823
2.194	20	984	8.51	2.6882	0.3158	136.1	970	7.54	1.3906	0.1845
2.192	21	1032	10.13	4.2996	0.4246	143.1	1017	8.78	2.0702	0.2358
2.19	22	1079	13.5	7.5632	0.5604	150.2	1063	10.88	3.4016	0.3127
2.188	23	969	9.93	3.2683	0.329	157.8	945	8.5	1.5878	0.1869
2.186	24	882	9.25	2.5877	0.2798	166.4	871	8.3	1.4019	0.1689
2.186	25	783	8.61	1.7707	0.2057	176.1	774	7.87	0.9935	0.1263
2.186	26	680	7.95	1.0658	0.1341	187.5	665	7.46	0.6351	0.0851
2.186	27	576	7.43	0.575	0.0774	201.1	570	7.15	0.4044	0.0565
2.186	28	476	7.03	0.2942	0.0418	217.2	471	6.87	0.2579	0.0376
2.186	29	375	6.78	0.1825	0.0269	237.1	371	6.64	0.182	0.0274
2.186	30	273	6.56	0.1343	0.0205	262.7	271	6.45	0.1476	0.0229
2.186	31	190	6.4	0.0724	0.0113	294.5	188	6.3	0.1587	0.0252
2.186	32	24	5.91	0.1543	0.0261	384.9	24	5.79	0.1943	0.0336

List of Measured Values of ε' and ε'' and tan δ :

Test = 2009042601 CERL0960B.mcd **AnDat = 20090428**

JSC-1 Linar Simulant, 2nd Cycle, RT to 1100C, in flowing UHP argon , Shawn Allen, CERALINK

Initial density = **samdns** $_{NCal+1}$ **= 2.086** gm/cc Final density(25C) = **dnsfinal = 2.186** gm/cc

		Lapsed Time(minutes)	T(degC) 912 MHz				T(degC) 2460 MHz			
samdns $_{mi}$	**mm**	$60 \cdot tlaps_{mm}$	$T_{mm,1}$	$\varepsilon p_{mm,1}$	$\varepsilon pp_{mm,1}$	$tn\delta_{mm,1}$	$T_{mm,2}$	$\varepsilon p_{mm,2}$	$\varepsilon pp_{mm,2}$	$tn\delta_{mm,2}$
2.186	33	387.9	24	5.92	0.136	0.023	24	5.8	0.1949	0.0336
2.186	34	432.5	97	6.27	0.138	0.022	96	6.16	0.1766	0.0287
2.186	35	440.7	147	6.33	0.1333	0.0211	146	6.22	0.157	0.0253
2.186	36	448.1	197	6.39	0.1274	0.0199	195	6.27	0.1505	0.024
2.186	37	455.2	239	6.45	0.1204	0.0187	237	6.34	0.1465	0.0231
2.186	38	462.4	279	6.51	0.127	0.0195	277	6.4	0.1436	0.0224
2.186	39	469.4	328	6.64	0.1222	0.0184	325	6.52	0.1486	0.0228
2.186	40	476.5	375	6.72	0.1655	0.0246	371	6.61	0.1742	0.0264
2.186	41	483.6	426	6.84	0.2128	0.0311	422	6.71	0.2021	0.0301
2.186	42	490.6	476	6.99	0.3365	0.0481	472	6.82	0.2432	0.0356
2.186	43	497.7	527	7.22	0.4052	0.0561	522	6.96	0.3121	0.0449
2.186	44	504.8	576	7.39	0.5826	0.0788	570	7.09	0.4002	0.0564
2.186	45	511.8	627	7.61	0.7634	0.1003	620	7.26	0.5211	0.0718
2.186	46	518.9	678	7.83	1.0835	0.1383	671	7.44	0.6378	0.0857
2.186	47	526	730	8.24	1.429	0.1735	722	7.65	0.8134	0.1063
2.186	48	533	781	8.62	1.8572	0.2153	772	7.89	0.9749	0.1236
2.186	49	540.1	831	8.87	2.2046	0.2487	821	8.04	1.1206	0.1394
2.186	50	547.2	882	9.27	2.5894	0.2794	871	8.19	1.3344	0.163
2.186	51	554.2	931	9.43	2.8675	0.3041	919	8.33	1.4697	0.1765
2.186	52	561.3	984	9.91	3.771	0.3806	971	8.7	1.8813	0.2163
2.186	53	568.4	1032	11.21	4.9002	0.4371	1017	9.33	2.4224	0.2596
2.186	54	575.4	1079	14.88	10.2868	0.6915	1063	11.4	4.0729	0.3572
2.186	55	583.1	983	11.34	6.0473	0.5332	970	9.44	2.8083	0.2975
2.186	56	591.6	871	9.63	3.2232	0.3347	851	8.42	1.5909	0.1889
2.186	57	601.3	784	8.94	2.1338	0.2387	775	8.16	1.1521	0.1412
2.186	58	612.7	679	8.27	1.2369	0.1496	672	7.77	0.7908	0.1017
2.186	59	626.3	576	7.69	0.7212	0.0938	564	7.36	0.4583	0.0623
2.186	60	642.5	476	7.32	0.3709	0.0507	471	7.08	0.3015	0.0426
2.186	61	662.3	375	7.02	0.2086	0.0297	372	6.84	0.2295	0.0336
2.186	62	687.8	274	6.77	0.1453	0.0215	271	6.62	0.1837	0.0278
2.186	63	719.6	190	6.57	0.1109	0.0169	188	6.44	0.1784	0.0277
2.186	64	926.9	24	6.01	0.1706	0.0284	24	5.88	0.2222	0.0378

Appendix H.3 MPN-292_MPN_Glass for 5M Simulant_Creedon_Washington Mills Sept. 11, 2023

Glass Used in NUW-LHT-5M Lunar Simulant, from Washington Mills, Measurements of Complex Dielectric Constant of Pressed Pellets Room Temperature to 1150 °C to RT, in flowing (10 sccm) UHP Argon

Dr. Doug Rickman (NASA) was interested in knowing the dielectric properties of the special glass that was manufactured by Washington Mills and used in the making of the NUW-LHT-5M simulant. Dr. Matt Creedon of Washington Mills sent a sample of the 5M simulant glass powder to Microwave Properties North (MPN), who had offered to measure its microwave dielectric properties.

MPN had already done three complex dielectric properties measurement runs on heat-treated NUW-LHT-5M lunar regolith simulant up to temperatures of 1100 °C, 1150 °C and 1250 °C under a NASA contract. The first dielectric measurement run on the full NUW-LHT-5M simulant, in vacuum, up to 1100 °C, had an unfamiliar feature at ~850 °C. The second full simulant run was done up to 1150 °C in flowing (10 sccm) ultra-high purity (UHP) argon. This required a different sample holder, different background subtractions, and new calibrations. However, the same feature was noted in the dielectric constant, as shown in the plots in Figure 1.

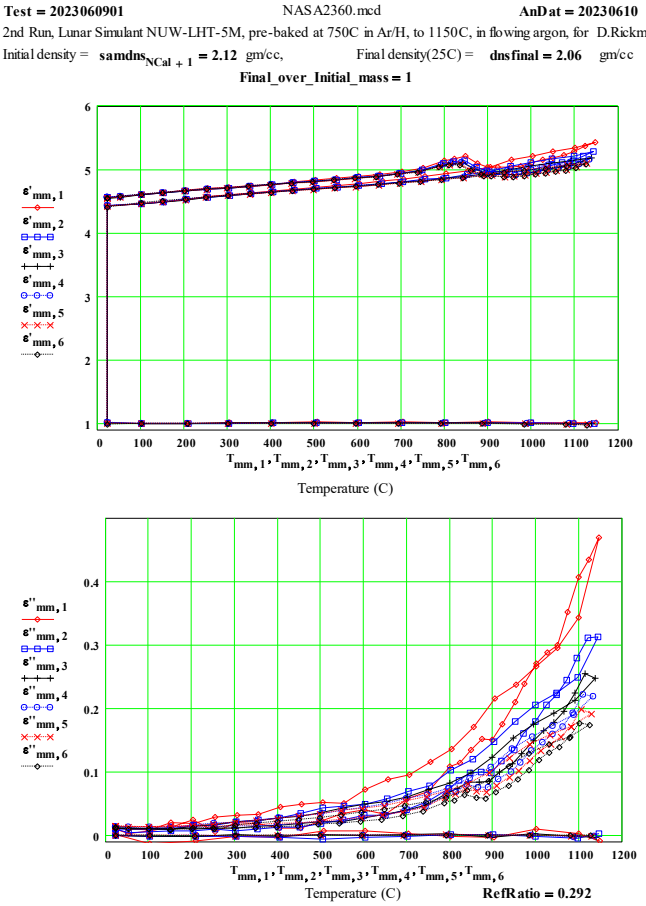

Figure 1. The top line of the ε′ plots (initial value of ε′ is ~4.7) are the values measured during the ramp up to 1150 °C. The bottom line in the plots are the empty holder measurements done immediately after the sample measurements. Only the initial and final sample dimensions were actually measured.

The NUW-LHT-5M lunar simulant has ~40 wt% of a relatively unique (on Earth at least) glass, largely composed of the same elements as the crystalline content of the simulant. It seemed useful to measure the properties of the glass alone, but under similar conditions.

For this 5M glass measurement, MPN again pressed pellets of the powder material in a uniaxial press at ~33,000 psi. The pellets were not initially baked by MPN to ensure dryness. This run was a simple cycle to 1150 °C and back to room temperature (RT). The sample holder for this run was initially cycled (and measured while empty) to 1150 °C before the run to "clean" the holder and measure the "empty holder" values, which were later used during the off-line data analysis.
For this measurement, a holder with a small hole in the base was used, so UHP argon gas could flow up, past the sample pellets, at ~10 sccm regulated flow rate.

The initial sample parameters were:
a) Diameter: 3.63 ± 0.02 mm
b) Length of 3 Pellet Stack: 13.54 ± 0.05 mm
c) Mass: 0.280 ± 0.002 gm
d) RT Density 1.90 ± 0.05 gm/cc
e) Appearance: Three light grey pellets (Figures 2 and 3)
f) Magnetic Response: The pellets had a very weak attraction to a strong magnet.

The dielectric properties measurements were performed three times at RT, and then the temperature was ramped up to 800C in 50C steps, then to 1150C in 25 C steps. After this, the temperature was brought back down to 100C in -50C steps, then RT.
The holder was removed from the apparatus and it and the final sample were weighed together. The pellets were easily removed, and their combined mass determined. Then the empty holder was run up to 1100C to measure backgrounds and check for contamination. There was no significant contamination.

The final sample properties at RT were:
a) Diameter: 3.60 ± 0.03 mm
b) Length of 3 Pellet Stack: 13.52 ± 0.05 mm
c) Mass: 0.280 ± 0.002 gm
d) RT Density: 1.81 ± 0.05 gm/cc
e) Appearance: three very light beige pellets (Figures 4 and 5)
f) Magnetic Response: The pellets had a very weak attraction to a strong magnet

Note: The percent mass loss was zero within our errors.

The frequency coding is :

Legend for Data Plots :

#	Frequency(MHz)	Symbol
1	397	red diamond, solid line – sometimes the line is omitted!
2	912	blue square, solid line
3	1429	black cross, solid line

4	1948	blue circle, dotted line
5	2466	red cross, dotted line
6	2986	black diamond, dotted line

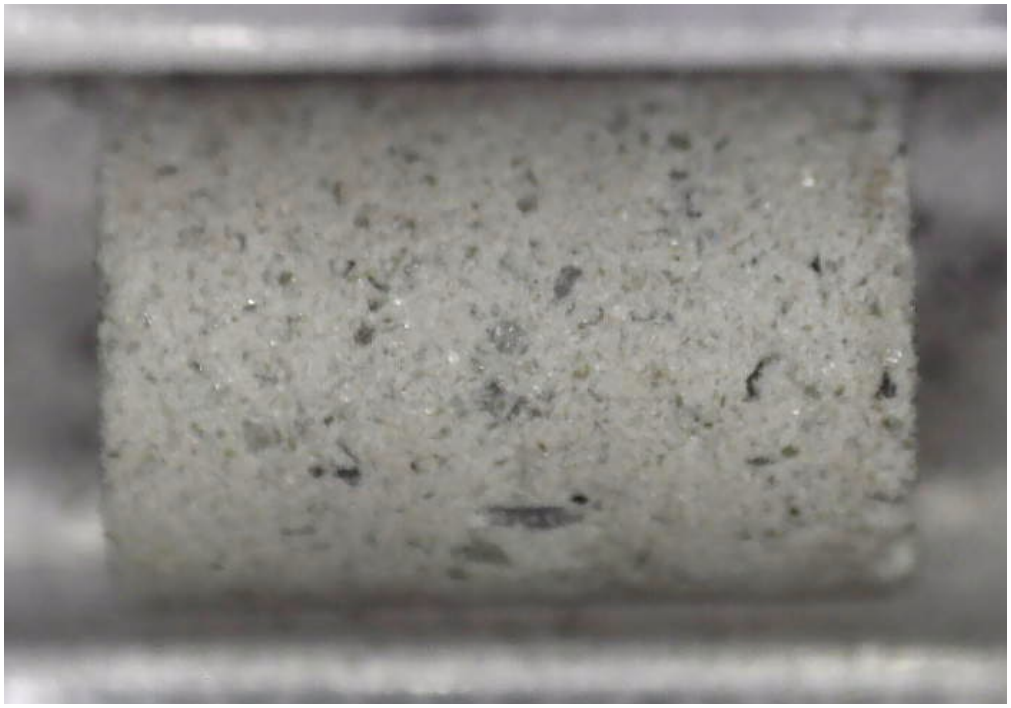

Figure 2. Typical initial NUW-LHT-5M pellet pressed at ~33,000 psi.

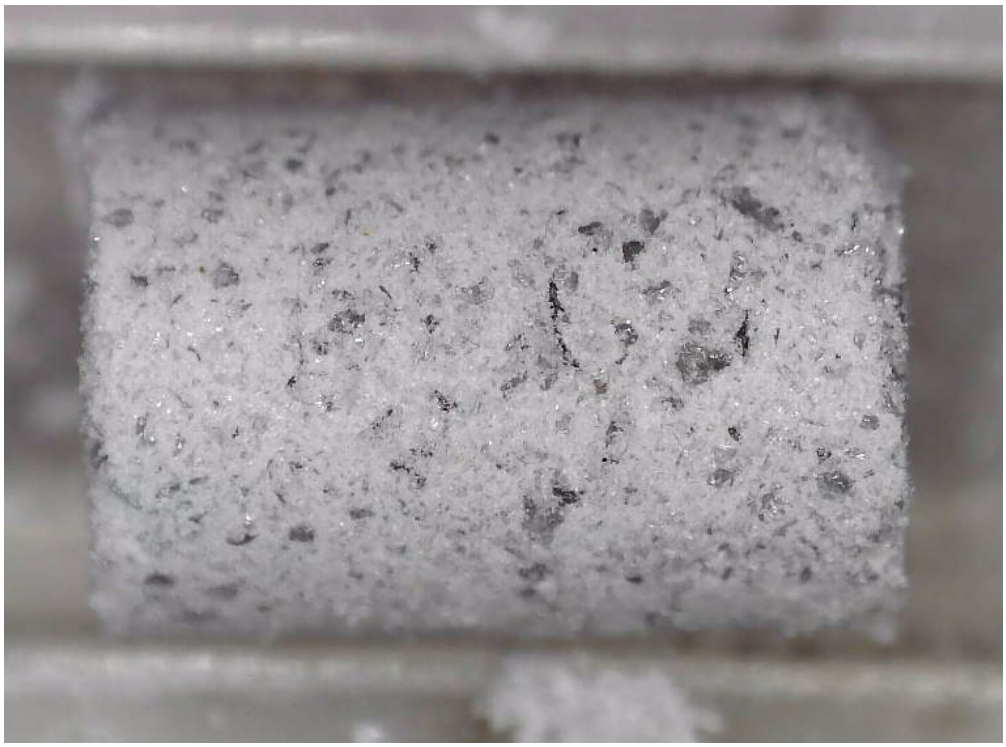

Figure 3. Initial 5M Glass (Washington Mills) pellet pressed at ~33,000 psi.

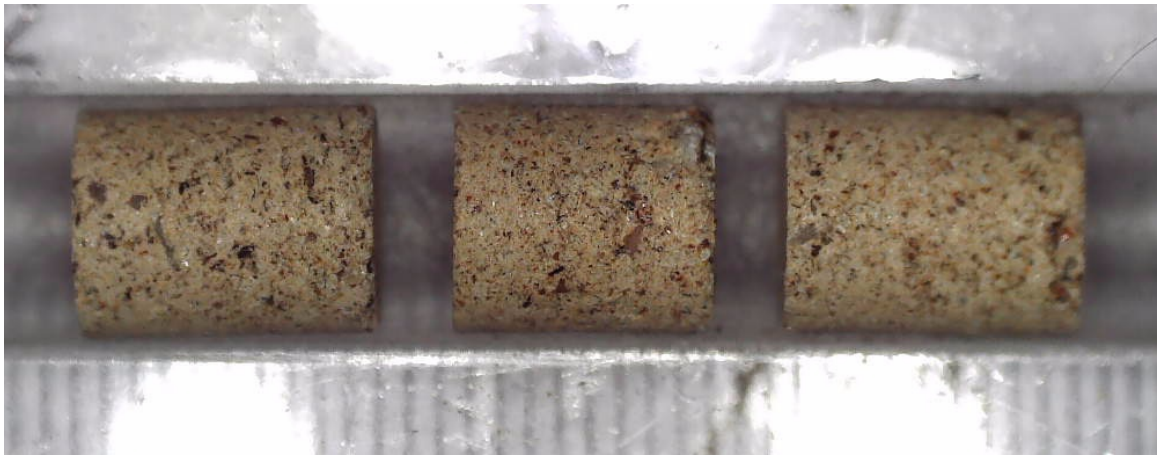

Figure 4. Three final NUW-LHT-5M pellets after a cycle to 1150 °C in UHP argon.

Figure 5. Three final 5M glass pellets after the cycle to 1150 °C in UHP argon.

Test = 2023090501 MPN023100.mcd **AnDat = 20230907**

5M Glass for Simulant, from Matt Creedon, Washington Mills, RT to 1150C to RT, in flowing UHP argon

Initial density = $samdns_{NCal+1}$ = **2** gm/cc, Final density(25C) = **dnsfinal = 1.98** gm/cc

Final_over_Initial_mass = 1

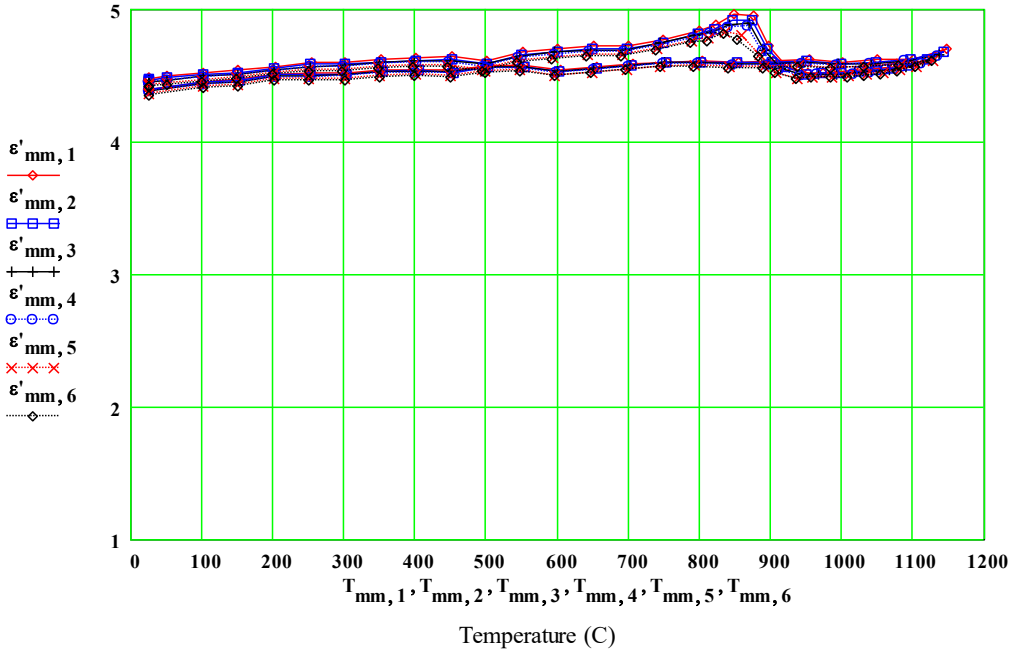

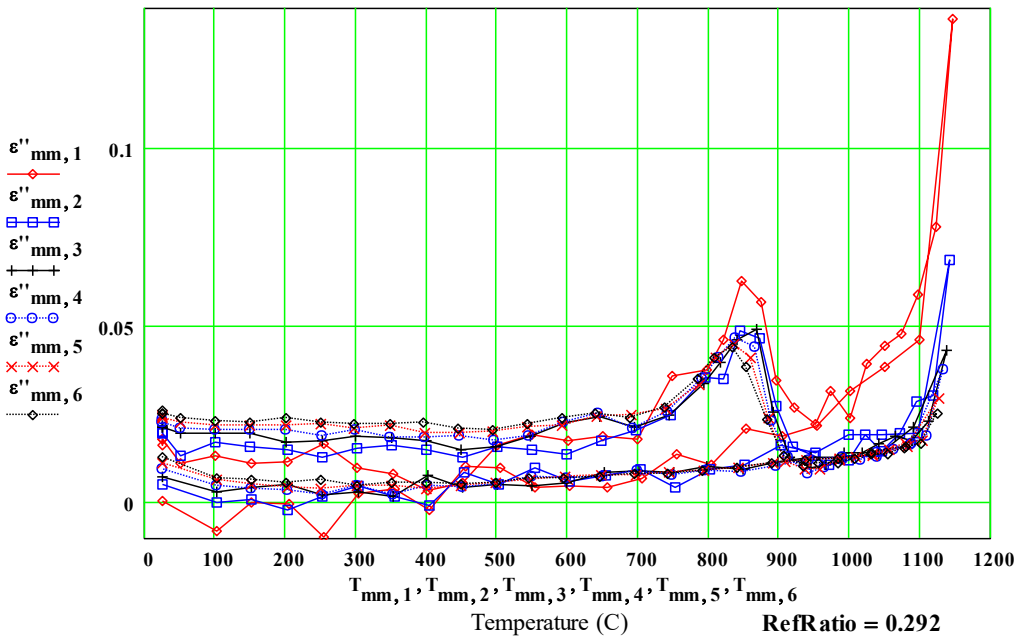

RefRatio = 0.292

Figure 6. Note the very rapid increase in ε″ values above 1100 °C. This is indicative of approaching the melting point. The thermal activation energy is large – very approximately 400 Kjoule/mole (~4.2 eV) by fitting the points between 1100 °C and 1150 °C. The feature at 850 °C seen in the stimulant runs is evident in this glass 5M run.

The two data points at 850 °C and 875 °C in the "ramp-up" have been changed throughout this report to match the values measured in a second run and shown in Appendix 1. This was done to improve the usefulness and accuracy of the plots for the reader.

Comments on the data run :

A thermal expansion coefficient (CTE) of 0.0 * 10^{-6}/°C was used.

The final pellets appeared unchanged except for a very slight beige colouring of some components.

The smooth ramp up of the values to 1150 °C was interrupted only by a slight drop of the ε′ values at 850 °C and 875 °C (MPN023100, plot below). This was very difficult to understand, so another run was done to 1000 °C (MPN023101) on a new set of pellets in a solid-bottom holder, with the argon gas flowing down onto the top of the test sample. In this configuration, expansion of the pellet diametrically cannot result in vertical movement of the test sample caused by the cover gas flow. This second run demonstrated that, in fact, a transformation (re-crystallization?) was occurring between 700 °C and 925 °C, which resulted in small increases in both ε′ and ε″, with a maxima at ~860 °C. The details of this run are presented in Appendix 1 at the end of this report.

The explanation for the dip in the first run to 1150 °C (MPN023100, plot below) would seem to be that the pellets expanded in diameter during this transformation (which actually started at ~600 °C), and at 850 °C the expansion blocked the vertical flow of argon and increased the pressure sufficiently to lift the pellet(s?) into a region of the cavity that had a slightly lower electric field (the equivalent of shortening the sample). By changing the "effective" pellet length (and thus the volume) slightly for only the two temperatures (850 °C and 875 °C) during the data analysis, the peak shape was made to match that seen in the second run to 1000 °C (shown in Appendix 1).

This feature, although interesting, is small and probably not very significant in the high temperature properties of the 5M simulant.

Test = 2023090501 MPN023100.mcd **AnDat = 20230907**

5M Glass for Simulant, from Matt Creedon, Washington Mills, RT to 1150C to RT, in flowing UHP argon

Initial density = $samdns_{NCal+1}$ **= 2** gm/cc, Final density(25C) = **dnsfinal = 1.98** gm/cc

Final_over_Initial_mass = 1

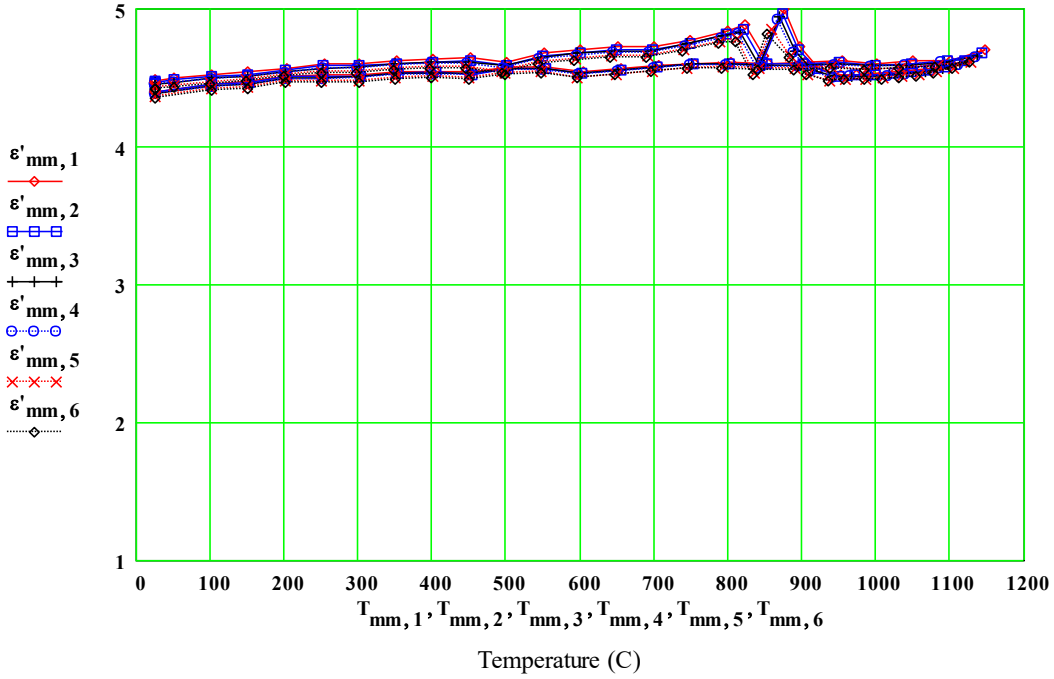

Test = 2023090501 MPN023100.mcd **AnDat = 20230907**

5M Glass for Simulant, from Matt Creedon, Washington Mills, RT to 1150C, in flowing UHP argon

Initial density = $\mathbf{samdns}_{NCal+1} = 2$ gm/cc, Final density(25C) = **dnsfinal = 1.98** gm/cc

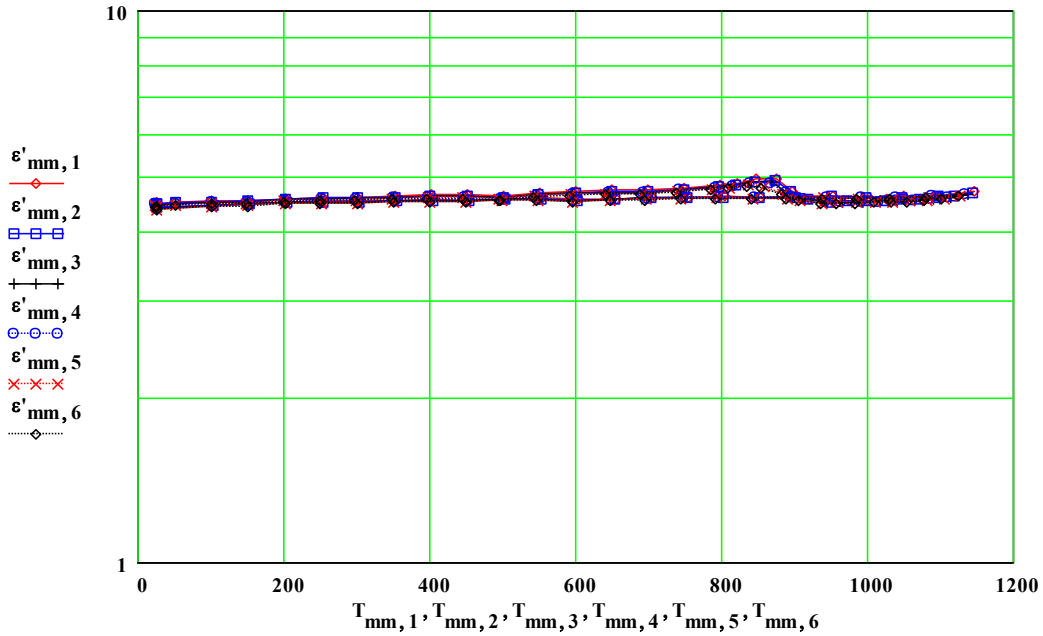

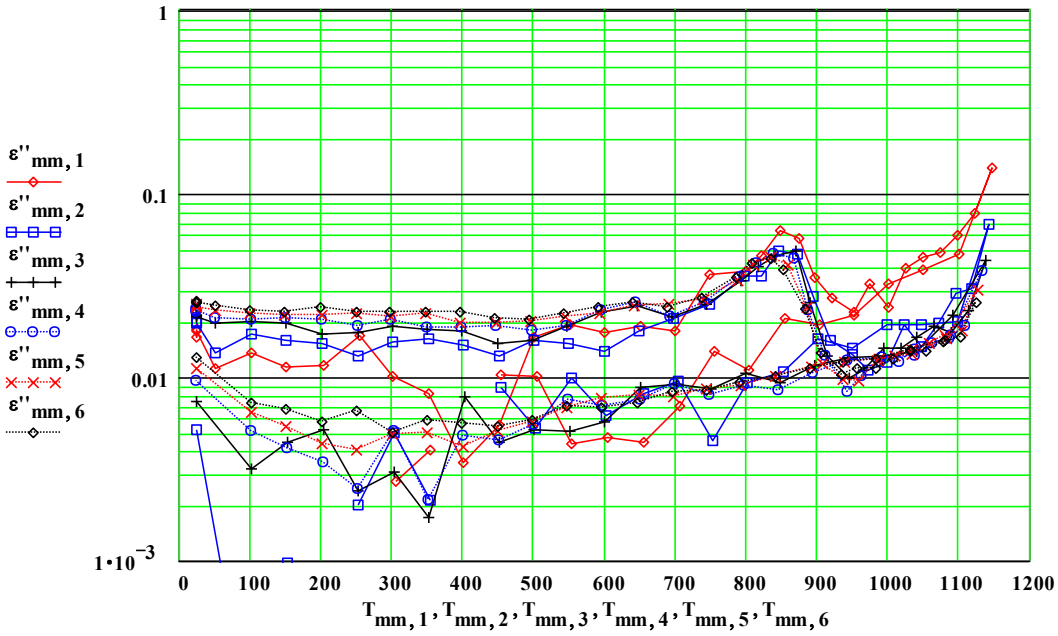

Test = 2023090501 MPN023100.mcd **AnDat = 20230907**

5M Glass for Simulant, from Matt Creedon, Washington Mills, RT to 1150C, in flowing UHP argon

Initial density = $\mathbf{samdns_{14} = 2}$ gm/cc, Final density(25C) = **dnsfinal = 1.98** gm/cc

Equivalent Free Electron Conductivity (Siemens/metre)

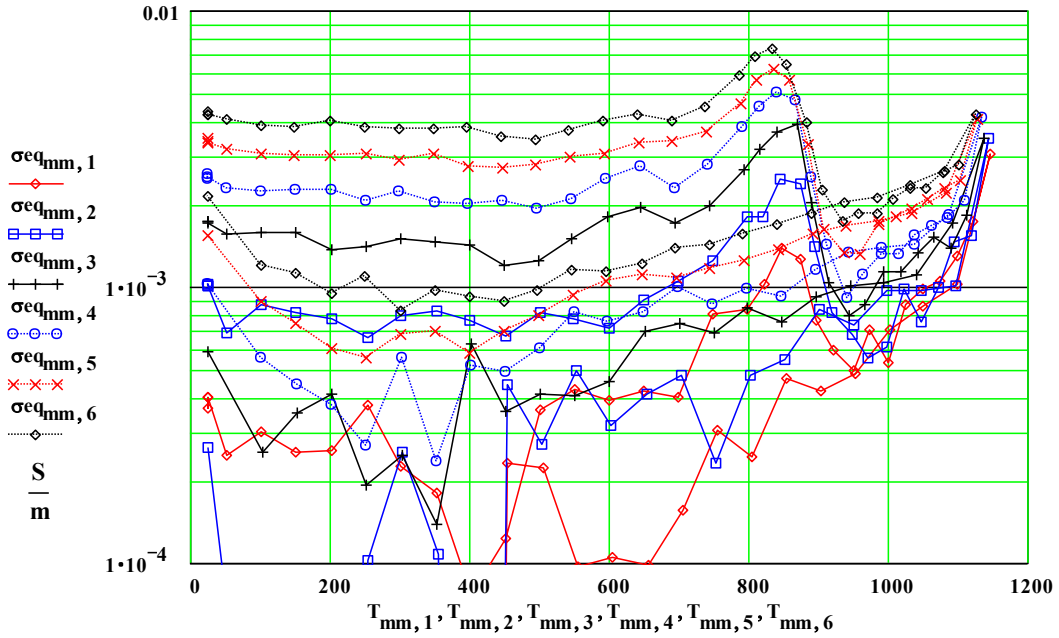

Temperature (C)

Test = 2023090501 MPN023100.mcd **AnDat = 20230907**

5M Glass for Simulant, from Matt Creedon, Washington Mills, RT to 1150C, in flowing UHP argon

Initial density = $samdns_{NCal+1} = 2$ gm/cc, Final density(25C) = **dnsfinal = 1.98** gm/cc

Thermal exp. coeff. $\alpha_1 = 0$

Values for 2450 MHz

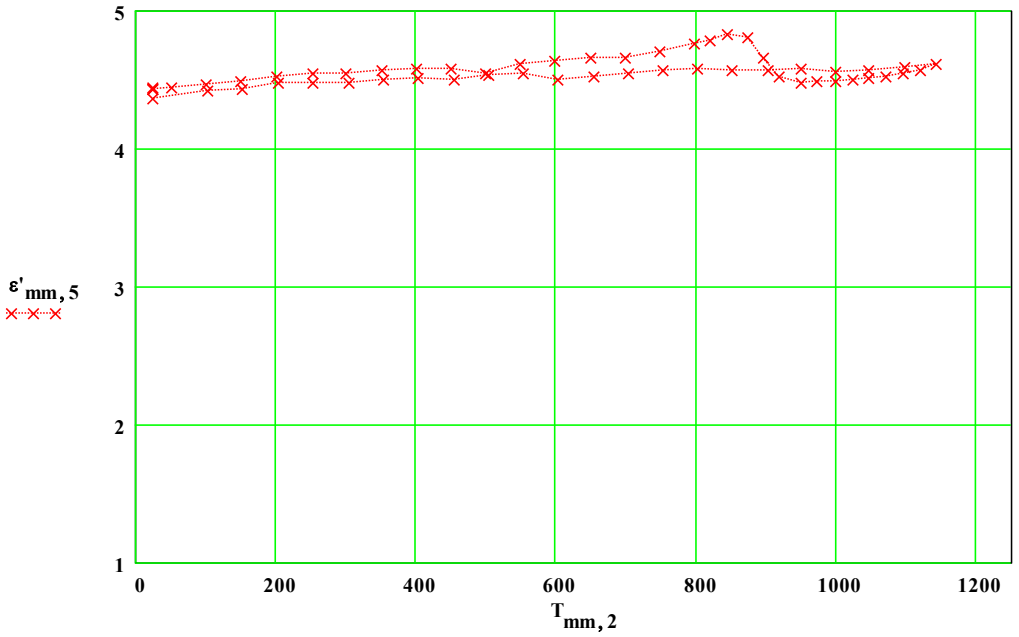

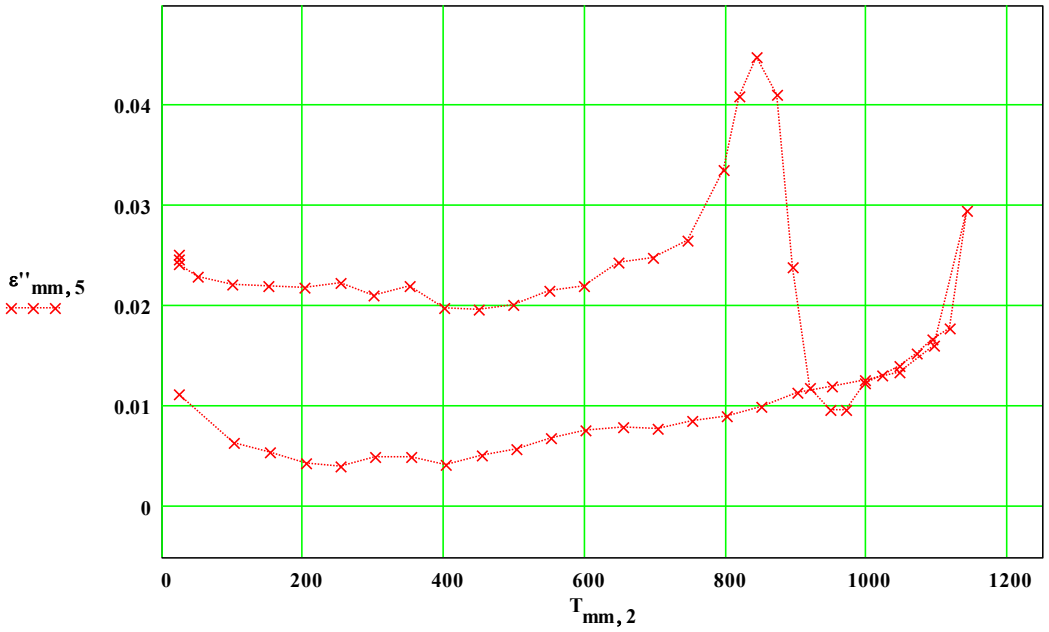

Test = 2023090501 MPN023100.mcd **AnDat = 20230907**

5M Glass for Simulant, from Matt Creedon, Washington Mills, RT to 1150C, in flowing UHP argon

Initial density = $\mathbf{samdns_{NCal+1}} = 2$ gm/cc, Final density(25C) = **dnsfinal = 1.98** gm/cc

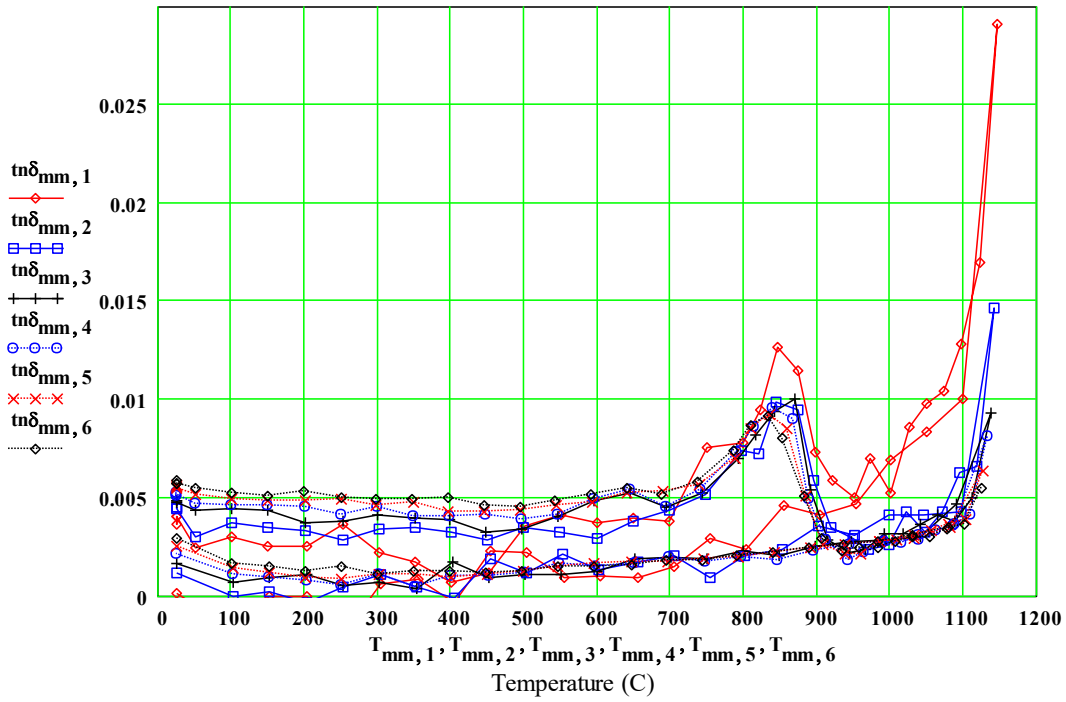

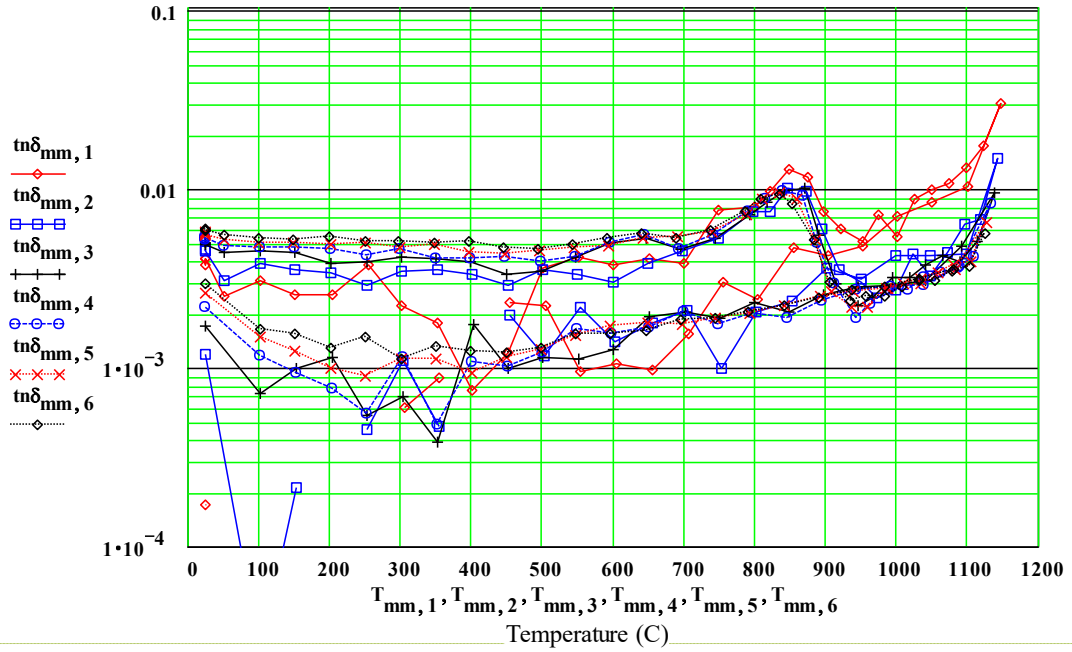

Half-power Depth (millimeters)

$$D\_halfP_{(mm,n)} := \left(\frac{\ln(2)}{2}\right)\cdot\left(inverse\alpha_{mm,n}\cdot 1\right)$$

Test = 2023090501 MPN023100.mcd **AnDat = 20230907**

5M Glass for Simulant, from Matt Creedon, Washington Mills, RT to 1150C, in flowing UHP argon

Initial density = $samdns_{NCal+1} = 2$ gm/cc, Final density(25C) = **dnsfinal = 1.98** gm/cc

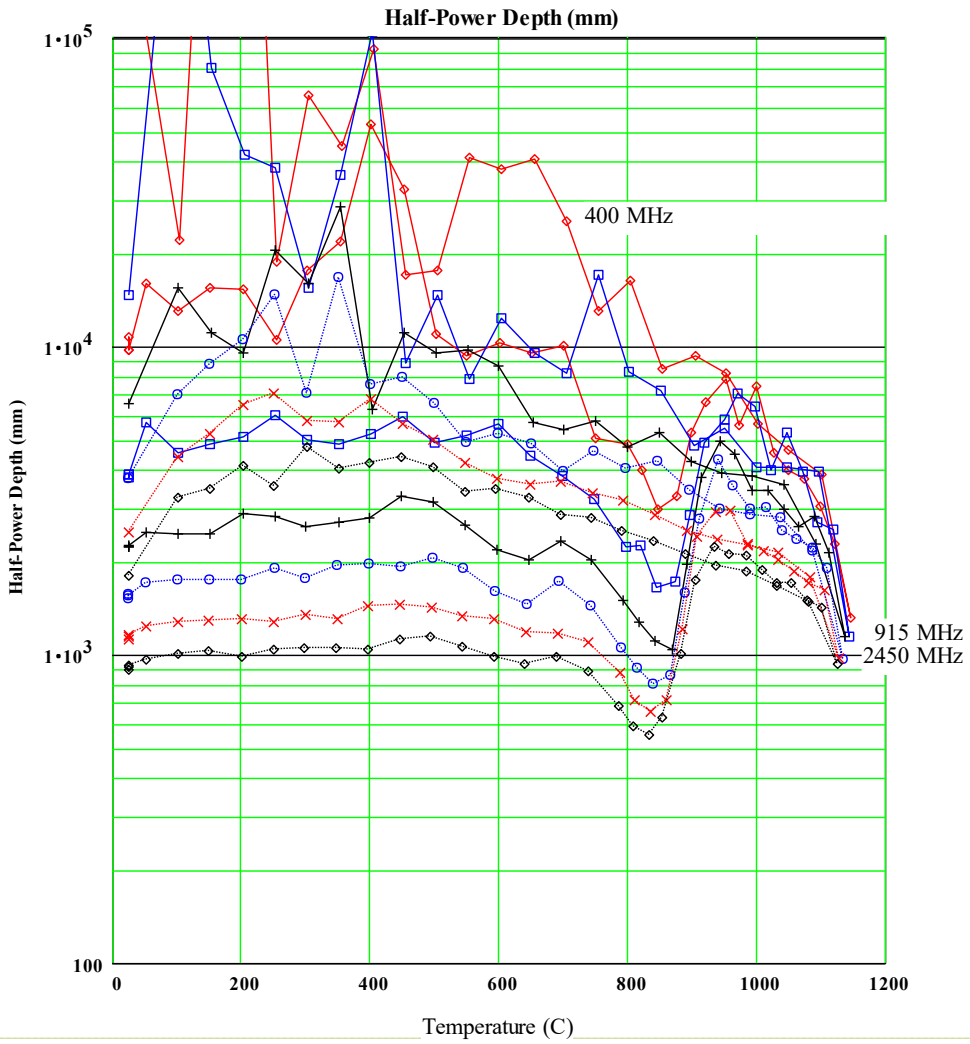

Test = 2023090501 MPN023100.mcd **AnDat = 20230907**

5M Glass for Simulant, from Matt Creedon, Washington Mills, RT to 1150C, in flowing UHP argon

List of Measured Values of ε' and ε" :

Initial density = $samdns_{NCal+1}$ **= 1.998** gm/cc Final density(25C) = **dnsfinal = 1.979** gm/cc

density	index	T(C)	397MHz	912MHz	1429MH	1948MHz	2466MHz	2986MHz	Lapsed Time (hours)	
$samdns_{mm}$	r_{mm}	$T_{mm,1}$	$\varepsilon'_{mm,1}$	$\varepsilon'_{mm,2}$	$\varepsilon'_{mm,3}$	$\varepsilon'_{mm,4}$	$\varepsilon'_{mm,5}$	$\varepsilon'_{mm,6}$	$tlaps_{mm}$	$sammas_{mm}$
1.998	11	25	4.49	4.48	4.47	4.46	4.44	4.43	0	0.28
1.998	12	25	4.48	4.47	4.45	4.45	4.43	4.41	0.15	0.28
1.998	13	25	4.48	4.47	4.45	4.45	4.43	4.42	0.22	0.28
1.998	14	52	4.5	4.49	4.47	4.46	4.44	4.43	0.4	0.28
1.998	15	101	4.52	4.51	4.5	4.49	4.47	4.46	0.7	0.28
1.998	16	151	4.55	4.53	4.51	4.51	4.49	4.47	1.01	0.28
1.998	17	203	4.57	4.56	4.55	4.54	4.52	4.51	1.36	0.28
1.998	18	254	4.6	4.59	4.57	4.56	4.54	4.53	1.7	0.28
1.998	19	302	4.6	4.59	4.58	4.57	4.55	4.54	2.03	0.28
1.998	20	352	4.63	4.61	4.6	4.59	4.57	4.56	2.32	0.28
1.998	21	402	4.64	4.62	4.61	4.6	4.58	4.57	2.6	0.28
1.998	22	452	4.65	4.63	4.62	4.6	4.58	4.57	2.89	0.28
1.998	23	501	4.61	4.59	4.59	4.57	4.55	4.54	3.18	0.28
1.998	24	550	4.68	4.66	4.65	4.64	4.61	4.6	3.43	0.28
1.998	25	600	4.7	4.68	4.68	4.66	4.64	4.63	3.68	0.28
1.998	26	650	4.73	4.7	4.7	4.68	4.66	4.64	3.94	0.28
1.998	27	699	4.73	4.7	4.7	4.68	4.66	4.65	4.19	0.28
1.998	28	749	4.78	4.75	4.75	4.73	4.71	4.7	4.44	0.28
1.98	29	799	4.84	4.82	4.8	4.79	4.76	4.74	4.7	0.28
1.961	30	822	4.88	4.85	4.83	4.81	4.78	4.77	4.86	0.28
2.063	31	847	4.96	4.91	4.89	4.86	4.83	4.81	5.04	0.28
1.909	32	875	4.96	4.93	4.9	4.87	4.81	4.77	5.21	0.28
1.907	33	897	4.73	4.7	4.69	4.68	4.66	4.65	5.38	0.28
1.89	34	921	4.57	4.56	4.56	4.55	4.53	4.52	5.54	0.28
1.872	35	951	4.52	4.51	4.51	4.5	4.48	4.47	5.73	0.28
1.872	36	974	4.53	4.52	4.51	4.51	4.49	4.49	5.89	0.28
1.872	37	1000	4.54	4.53	4.52	4.51	4.49	4.49	6.07	0.28
1.872	38	1026	4.55	4.53	4.52	4.51	4.49	4.49	6.24	0.28
1.872	39	1050	4.56	4.55	4.53	4.53	4.51	4.5	6.41	0.28
1.872	40	1074	4.57	4.56	4.55	4.54	4.52	4.51	6.58	0.28
1.877	41	1098	4.59	4.58	4.57	4.56	4.54	4.54	6.74	0.28
1.881	42	1122	4.62	4.62	4.6	4.6	4.57	4.56	6.91	0.28
1.886	43	1146	4.7	4.68	4.66	4.65	4.62	4.61	7.08	0.28
1.89	44	1100	4.63	4.63	4.61	4.61	4.59	4.58	7.31	0.28
1.895	45	1049	4.62	4.61	4.6	4.59	4.57	4.56	7.57	0.28
1.899	46	1001	4.6	4.59	4.59	4.58	4.56	4.55	7.82	0.28
1.904	47	953	4.62	4.61	4.6	4.6	4.58	4.57	8.06	0.28
1.909	48	904	4.61	4.6	4.59	4.58	4.57	4.56	8.31	0.28
1.913	49	854	4.61	4.6	4.59	4.58	4.57	4.56	8.57	0.28
1.918	50	804	4.62	4.6	4.61	4.6	4.58	4.57	8.82	0.28
1.922	51	755	4.6	4.6	4.6	4.59	4.57	4.56	9.07	0.28
1.927	52	706	4.59	4.58	4.58	4.57	4.55	4.54	9.32	0.28
1.932	53	656	4.57	4.56	4.56	4.55	4.53	4.52	9.57	0.28
1.936	54	604	4.55	4.54	4.54	4.53	4.51	4.5	9.84	0.28
1.941	55	554	4.58	4.57	4.57	4.56	4.54	4.53	10.09	0.28
1.946	56	504	4.58	4.56	4.56	4.55	4.54	4.53	10.36	0.28
1.951	57	455	4.54	4.53	4.53	4.52	4.5	4.49	10.66	0.28
1.955	58	405	4.55	4.54	4.54	4.53	4.51	4.5	11	0.28
1.96	59	355	4.55	4.53	4.53	4.52	4.5	4.49	11.39	0.28
1.965	60	305	4.52	4.51	4.51	4.5	4.48	4.47	11.83	0.28

mq := 61 , 62 .. nd – Nempties

$samdns_{mq}$	m_{mq}	$T_{mq,1}$	$\varepsilon'_{mq,1}$	$\varepsilon'_{mq,2}$	$\varepsilon'_{mq,3}$	$\varepsilon'_{mq,4}$	$\varepsilon'_{mq,5}$	$\varepsilon'_{mq,6}$	$tlaps_{mq}$	$sammas_{mq}$
1.97	61	254	4.52	4.51	4.5	4.49	4.47	4.46	12.35	0.28
1.974	62	204	4.51	4.51	4.5	4.49	4.47	4.46	12.96	0.28
1.979	63	153	4.48	4.47	4.46	4.45	4.43	4.43	13.8	0.28
1.979	64	103	4.46	4.45	4.44	4.44	4.42	4.41	15.06	0.28
1.979	65	25	4.4	4.4	4.39	4.39	4.37	4.35	21.46	0.28

Test = 2023090501 MPN023100.mcd **AnDat = 20230907**

5M Glass for Simulant, from Matt Creedon, Washington Mills, RT to 1150C, in flowing UHP argon

List of Measured Values of ε' and ε" :

Initial density = $samdns_{NCal+1}$ = **1.998** gm/cc Final density(25C) = **dnsfinal = 1.979** gm/cc

density	index	T(C)	397MHz	912MHz	1429MH	1948MHz	2466MHz	2986MHz	Lapsed Time (hours)	
$samdns_{mm}$	mm	$T_{mm,1}$	$\varepsilon''_{mm,1}$	$\varepsilon''_{mm,2}$	$\varepsilon''_{mm,3}$	$\varepsilon''_{mm,4}$	$\varepsilon''_{mm,5}$	$\varepsilon''_{mm,6}$	$tlaps_{mm}$	$sammas_{mm}$
1.998	11	25	0.018	0.02	0.022	0.024	0.025	0.026	0	0.28
1.998	12	25	0.016	0.02	0.022	0.023	0.025	0.026	0.15	0.28
1.998	13	25	0.018	0.02	0.021	0.023	0.024	0.025	0.22	0.28
1.998	14	52	0.011	0.014	0.02	0.021	0.023	0.024	0.4	0.28
1.998	15	101	0.014	0.017	0.02	0.021	0.022	0.023	0.7	0.28
1.998	16	151	0.011	0.016	0.02	0.021	0.022	0.023	1.01	0.28
1.998	17	203	0.012	0.015	0.017	0.021	0.022	0.024	1.36	0.28
1.998	18	254	0.017	0.013	0.018	0.019	0.022	0.023	1.7	0.28
1.998	19	302	0.01	0.016	0.019	0.021	0.021	0.023	2.03	0.28
1.998	20	352	0.008	0.016	0.018	0.019	0.022	0.023	2.32	0.28
1.998	21	402	0.003	0.015	0.018	0.019	0.02	0.023	2.6	0.28
1.998	22	452	0.006	0.013	0.015	0.019	0.02	0.021	2.89	0.28
1.998	23	501	0.016	0.016	0.016	0.018	0.02	0.021	3.18	0.28
1.998	24	550	0.019	0.015	0.019	0.019	0.021	0.022	3.43	0.28
1.998	25	600	0.018	0.014	0.023	0.023	0.022	0.024	3.68	0.28
1.998	26	650	0.019	0.018	0.025	0.025	0.024	0.026	3.94	0.28
1.998	27	699	0.018	0.021	0.021	0.021	0.025	0.024	4.19	0.28
1.998	28	749	0.036	0.025	0.025	0.026	0.027	0.027	4.44	0.28
1.98	29	799	0.038	0.036	0.034	0.035	0.034	0.035	4.7	0.28
1.961	30	822	0.046	0.035	0.04	0.041	0.041	0.041	4.86	0.28
2.063	31	847	0.063	0.049	0.046	0.047	0.045	0.044	5.04	0.28
1.909	32	875	0.057	0.047	0.049	0.044	0.041	0.039	5.21	0.28
1.907	33	897	0.035	0.028	0.026	0.023	0.024	0.024	5.38	0.28
1.89	34	921	0.027	0.016	0.013	0.013	0.012	0.013	5.54	0.28
1.872	35	951	0.023	0.013	0.01	0.008	0.01	0.01	5.73	0.28
1.872	36	974	0.032	0.011	0.011	0.01	0.01	0.011	5.89	0.28
1.872	37	1000	0.024	0.012	0.014	0.012	0.012	0.011	6.07	0.28
1.872	38	1026	0.039	0.019	0.014	0.012	0.013	0.012	6.24	0.28
1.872	39	1050	0.045	0.015	0.017	0.014	0.014	0.014	6.41	0.28
1.872	40	1074	0.048	0.02	0.019	0.015	0.015	0.014	6.58	0.28
1.877	41	1098	0.059	0.029	0.018	0.016	0.017	0.016	6.74	0.28
1.881	42	1122	0.078	0.03	0.023	0.019	0.018	0.017	6.91	0.28
1.886	43	1146	0.137	0.069	0.043	0.038	0.03	0.025	7.08	0.28
1.89	44	1100	0.046	0.02	0.022	0.017	0.016	0.016	7.31	0.28
1.895	45	1049	0.039	0.019	0.014	0.013	0.013	0.014	7.57	0.28
1.899	46	1001	0.032	0.019	0.013	0.013	0.013	0.013	7.82	0.28
1.904	47	953	0.022	0.014	0.013	0.012	0.012	0.012	8.06	0.28
1.909	48	904	0.019	0.016	0.012	0.011	0.011	0.011	8.31	0.28
1.913	49	854	0.021	0.011	0.009	0.009	0.01	0.01	8.57	0.28
1.918	50	804	0.011	0.009	0.011	0.009	0.009	0.009	8.82	0.28
1.922	51	755	0.014	0.005	0.009	0.008	0.009	0.009	9.07	0.28
1.927	52	706	0.007	0.009	0.009	0.009	0.008	0.008	9.32	0.28
1.932	53	656	0.004	0.008	0.009	0.008	0.008	0.007	9.57	0.28
1.936	54	604	0.005	0.006	0.006	0.007	0.008	0.007	9.84	0.28
1.941	55	554	0.004	0.01	0.005	0.007	0.007	0.007	10.09	0.28
1.946	56	504	0.01	0.005	0.005	0.006	0.006	0.006	10.36	0.28
1.951	57	455	0.01	0.009	0.004	0.005	0.005	0.005	10.66	0.28
1.955	58	405	-0.002	-0.001	0.008	0.005	0.004	0.006	11	0.28
1.96	59	355	0.004	0.002	0.002	0.002	0.005	0.006	11.39	0.28
1.965	60	305	0.003	0.005	0.003	0.005	0.005	0.005	11.83	0.28

mq := 61 , 62 .. nd - Nempties

$samdns_{mq}$	mq	$T_{mq,1}$	$\varepsilon''_{mq,1}$	$\varepsilon''_{mq,2}$	$\varepsilon''_{mq,3}$	$\varepsilon''_{mq,4}$	$\varepsilon''_{mq,5}$	$\varepsilon''_{mq,6}$	$tlaps_{mq}$	$sammas_{mq}$
1.97	61	254	-0.009	0.002	0.002	0.002	0.004	0.007	12.35	0.28
1.974	62	204	-0	-0.002	0.005	0.003	0.004	0.006	12.96	0.28
1.979	63	153	0	0.001	0.004	0.004	0.005	0.007	13.8	0.28
1.979	64	103	-0.008	0	0.003	0.005	0.006	0.007	15.06	0.28
1.979	65	25	0.001	0.005	0.007	0.01	0.011	0.013	21.46	0.28

Appendix H.4 Second Run to 1000 °C on 5M Simulant Glass

Glass Used in NUW-LHT-5M Lunar Simulant , from Washington Mills, Measurements of Complex Dielectric Constant of Pressed Pellets RT to 1000°C to RT, in downward-flowing (30 sccm) UHP Argon

For this 5M glass measurement, MPN again pressed pellets of the powder material in a uniaxial press at ~33,000 psi. The pellets were not initially baked by MPN to ensure dryness. This run was a simple cycle to 1000 °C and back to RT. A steel tube was inserted into the top of the holder and its bottom end positioned 5 cm above the top of the pellet stack, bathing the pellets in UHP argon.

The initial sample parameters were:

a) Effective Diameter: 3.65 ± 0.02 mm
b) Length of 3 Pellet Stack: 14.89 ± 0.05 mm
c) Mass: 0.295 ± 0.002 gm
d) RT Density: 1.90 ± 0.05 gm/cc
e) Appearance: Three light grey pellets
f) Magnetic Response: The pellets had a very weak attraction to a strong magnet.

The dielectric properties measurements were performed three times at RT, and then the temperature was ramped up to 500 °C in 50 °C steps, then to 1000 °C in 25 °C steps. After this, the temperature was brought back down to 100 °C in -50 °C steps, then RT.
The holder was removed from the apparatus and it and the final sample were weighed together. The pellets were easily removed, and their combined mass determined. Then the empty holder was run up to 1000 °C to measure backgrounds and check for contamination. There was no significant contamination.

The final sample properties, at room temperature were:

a) Effective Diameter: 3.74 ± 0.03 mm
b) Length of 3 Pellet Stack: 14.89 ± 0.05 mm
c) Mass: 0.296 ± 0.002 gm
d) RT Density: 1.81 ± 0.05 gm/cc
e) Appearance: Three light grey pellets
f) Magnetic Response: The pellets had a very weak attraction to a strong magnet.

Note: The percent mass loss was zero within our errors.

Test = 2023090801 MPN023101.mcd **AnDat = 20230910**

Repeat: 5M Glass for Simulant, from Matt Creedon, Washington Mills, RT to 1000C to RT, in flowing UHP argon

Initial density = $\mathbf{samdns_{NCal+1}}$ **= 1.9** gm/cc, Final density(25C) = **dnsfinal = 1.81** gm/cc

Final_over_Initial_mass = 1.003

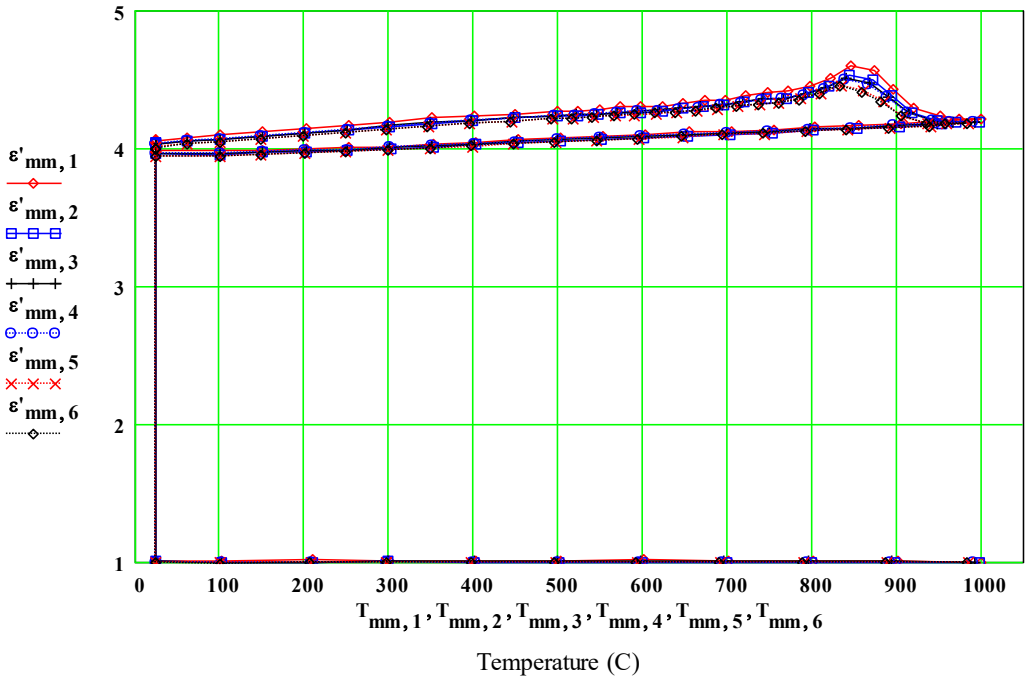

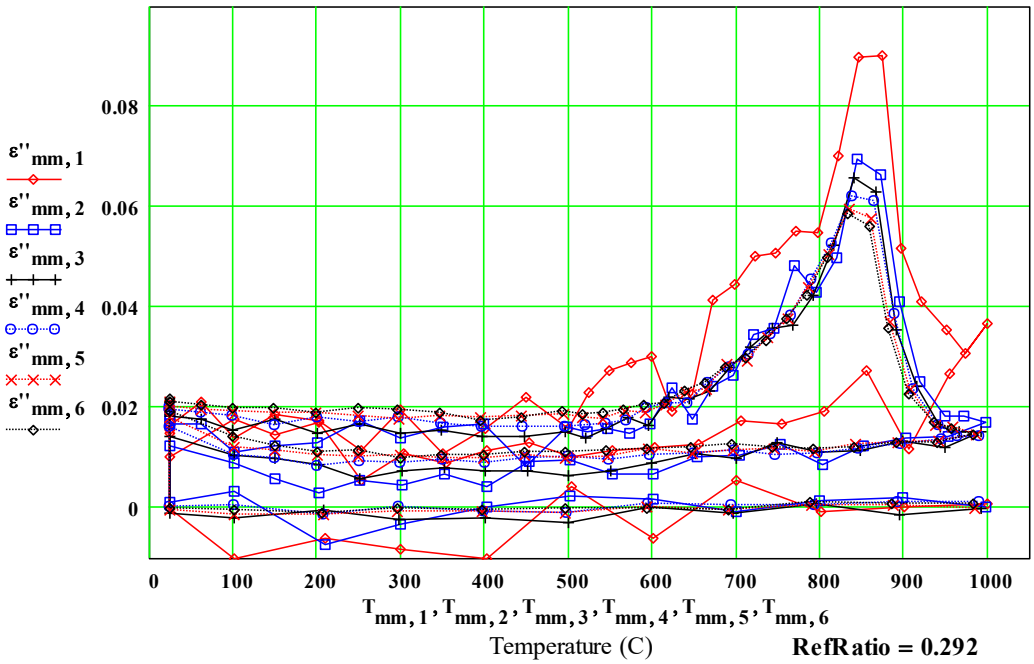

RefRatio = 0.292

Test = 2023090801 MPN023101.mcd **AnDat = 20230910**

5M Glass for Simulant, from Matt Creedon, Washington Mills, RT to 1000C to RT, in flowing UHP argon

Equivalent Free Electron Conductivity (Siemens/metre)

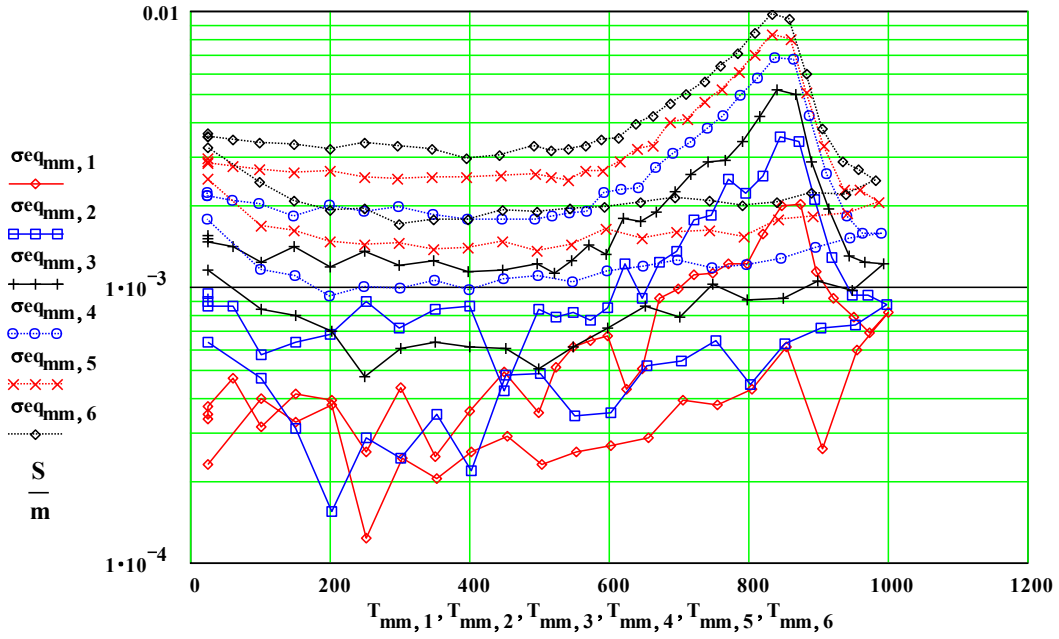

Temperature (C)

RefRatio = 0.292

Test = 2023090801 MPN023101.mcd **AnDat = 20230910**

5M Glass for Simulant, from Matt Creedon, Washington Mills, RT to 1000C to RT, in flowing UHP argon

Initial density = $samdns_{NCal+1}$ **= 1.9** gm/cc, Final density(25C) = **dnsfinal = 1.81** gm/cc

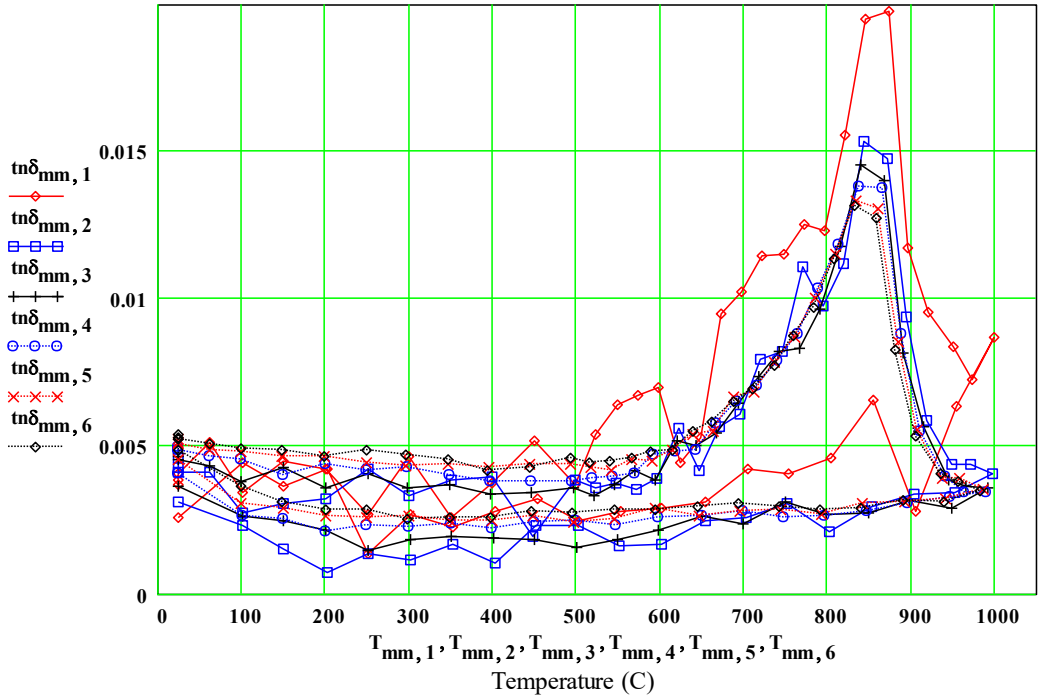

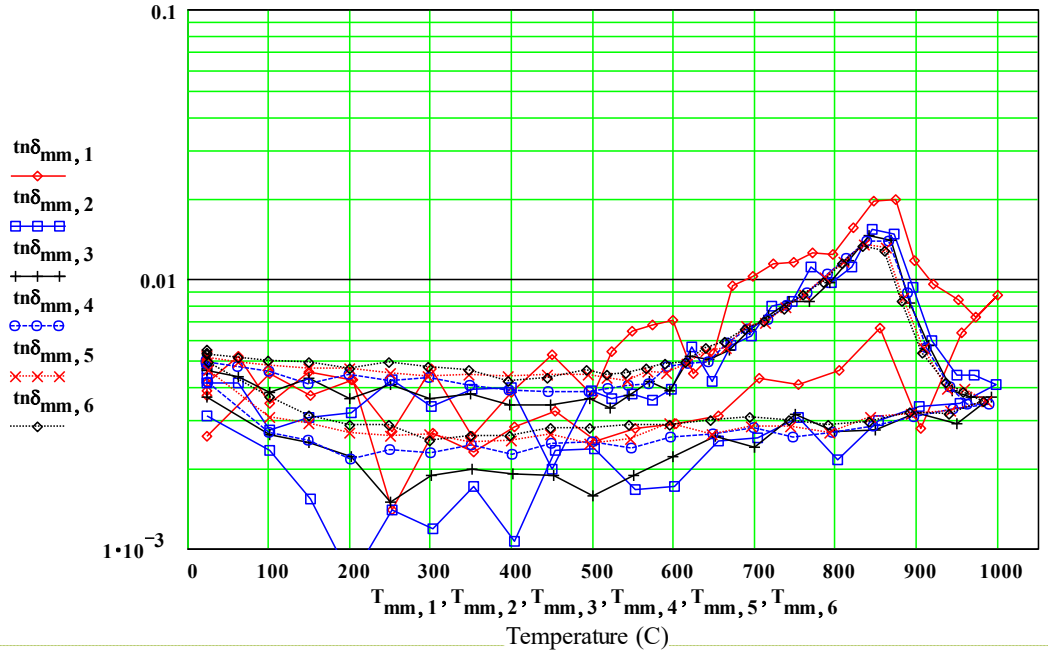

Half-power Depth (millimeters)

$$D\_halfP_{(mm,n)} := \left(\frac{\ln(2)}{2}\right)\cdot\left(inverse\alpha_{mm,n}\cdot 1\right)$$

Test = 2023090801 MPN023101.mcd **AnDat = 20230910**

Repeat: 5M Glass for Simulant, from Matt Creedon, Washington Mills, RT to 1000C to RT, in flowing UHP argo

Initial density = $samdns_{NCal+1}$ **= 1.9** gm/cc, Final density(25C) = **dnsfinal = 1.81** gm/cc

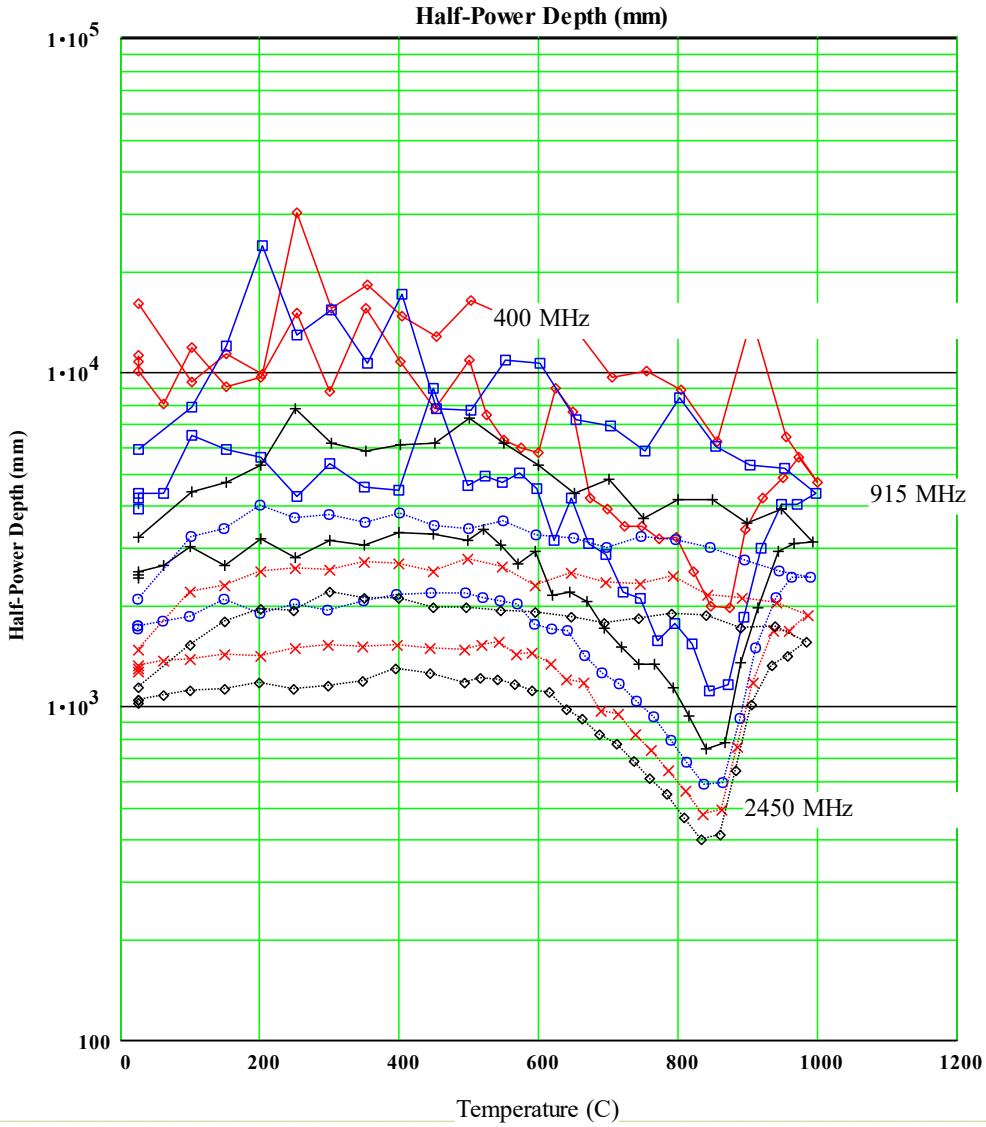

f

Test = 2023090801 MPN023101.mcd **AnDat = 20230910**

Repeat: 5M Glass for Simulant, from Matt Creedon, Washington Mills, RT to 1000C to RT, in flowing UHP arg

List of Measured Values of ε' and ε" :

Initial density = $samdns_{NCal+1}$ = 1.898 gm/cc Final density(25C) = **dnsfinal = 1.81** gm/cc

density	index	T(C)	397MHz	912MHz	1429MH	1948MHz	2466MHz	2986MHz	Lapsed Time (hours)	
$samdns_{mm}$	mm	$T_{mm,1}$	$\varepsilon'_{mm,1}$	$\varepsilon'_{mm,2}$	$\varepsilon'_{mm,3}$	$\varepsilon'_{mm,4}$	$\varepsilon'_{mm,5}$	$\varepsilon'_{mm,6}$	$tlaps_{mm}$	$sammas_{mm}$
1.898	3	24	4.07	4.05	4.04	4.04	4.01	4	0	0.295
1.898	4	24	4.06	4.04	4.04	4.04	4.01	4	0.19	0.295
1.898	5	24	4.06	4.04	4.03	4.04	4.01	4.01	0.25	0.295
1.898	6	62	4.08	4.06	4.05	4.06	4.03	4.03	0.51	0.295
1.898	7	101	4.1	4.07	4.07	4.07	4.05	4.04	0.76	0.295
1.898	8	150	4.12	4.09	4.09	4.09	4.06	4.06	1.08	0.295
1.898	9	201	4.15	4.12	4.11	4.11	4.09	4.09	1.43	0.295
1.898	10	252	4.17	4.14	4.14	4.14	4.11	4.11	1.77	0.295
1.898	11	300	4.19	4.16	4.17	4.16	4.14	4.14	2.1	0.295
1.898	12	351	4.23	4.19	4.19	4.19	4.16	4.16	2.39	0.295
1.898	13	400	4.24	4.2	4.21	4.2	4.18	4.18	2.68	0.295
1.898	14	450	4.25	4.22	4.23	4.22	4.2	4.2	2.97	0.295
1.898	15	499	4.27	4.24	4.24	4.24	4.21	4.21	3.26	0.295
1.898	16	524	4.28	4.24	4.25	4.24	4.22	4.22	3.45	0.295
1.898	17	549	4.29	4.25	4.25	4.25	4.23	4.23	3.62	0.295
1.898	18	574	4.3	4.26	4.26	4.26	4.23	4.24	3.8	0.295
1.898	19	598	4.3	4.27	4.27	4.27	4.24	4.25	3.97	0.295
1.898	20	624	4.31	4.28	4.28	4.28	4.25	4.26	4.15	0.295
1.898	21	648	4.32	4.29	4.29	4.29	4.26	4.26	4.32	0.295
1.898	22	673	4.35	4.3	4.3	4.3	4.27	4.28	4.49	0.295
1.899	23	698	4.36	4.32	4.32	4.31	4.29	4.29	4.67	0.295
1.9	24	722	4.38	4.34	4.34	4.33	4.3	4.3	4.85	0.295
1.901	25	747	4.41	4.36	4.36	4.35	4.32	4.32	5.02	0.295
1.889	26	772	4.42	4.36	4.37	4.36	4.33	4.33	5.2	0.296
1.878	27	797	4.46	4.41	4.4	4.39	4.36	4.36	5.38	0.296
1.867	28	821	4.51	4.46	4.45	4.43	4.4	4.39	5.56	0.296
1.856	29	846	4.61	4.53	4.51	4.5	4.46	4.45	5.74	0.296
1.844	30	874	4.56	4.5	4.48	4.46	4.42	4.41	5.92	0.296
1.833	31	897	4.43	4.39	4.38	4.37	4.34	4.34	6.1	0.296
1.821	32	921	4.3	4.26	4.26	4.26	4.23	4.23	6.28	0.296
1.81	33	951	4.23	4.2	4.2	4.2	4.18	4.18	6.48	0.296
1.81	34	973	4.22	4.19	4.2	4.2	4.18	4.18	6.65	0.296
1.81	35	1000	4.22	4.2	4.2	4.2	4.18	4.18	6.84	0.296
1.81	36	955	4.21	4.18	4.18	4.18	4.16	4.16	7.06	0.296
1.81	37	905	4.18	4.16	4.17	4.17	4.15	4.15	7.3	0.296
1.81	38	854	4.17	4.15	4.15	4.15	4.13	4.14	7.54	0.296
1.81	39	804	4.16	4.13	4.14	4.14	4.12	4.13	7.78	0.296
1.81	40	754	4.14	4.12	4.13	4.13	4.11	4.11	8.02	0.296
1.81	41	705	4.13	4.11	4.12	4.12	4.1	4.1	8.27	0.296
1.81	42	655	4.12	4.1	4.1	4.1	4.08	4.09	8.51	0.296
1.81	43	603	4.11	4.08	4.09	4.09	4.07	4.07	8.76	0.296
1.81	44	553	4.1	4.07	4.08	4.07	4.06	4.06	9.01	0.296
1.81	45	503	4.08	4.06	4.07	4.07	4.05	4.05	9.27	0.296
1.81	46	453	4.07	4.04	4.05	4.05	4.03	4.04	9.57	0.296
1.81	47	403	4.05	4.03	4.04	4.03	4.02	4.02	9.89	0.296
1.81	48	353	4.04	4.01	4.02	4.02	4	4.01	10.26	0.296
1.81	49	303	4.02	4	4.01	4.01	3.99	3.99	10.67	0.296
1.81	50	252	4.01	3.99	3.99	3.99	3.97	3.98	11.16	0.296
1.81	51	203	4	3.98	3.98	3.98	3.97	3.97	11.73	0.296
1.81	52	151	3.99	3.97	3.97	3.97	3.95	3.96	12.5	0.296

$mq := 53, 54 .. nd - Nempties$

$samdns_{mq}$	mq	$T_{mq,1}$	$\varepsilon'_{mq,1}$	$\varepsilon'_{mq,2}$	$\varepsilon'_{mq,3}$	$\varepsilon'_{mq,4}$	$\varepsilon'_{mq,5}$	$\varepsilon'_{mq,6}$	$tlaps_{mq}$	$sammas_{mq}$
1.81	53	101	3.98	3.96	3.96	3.96	3.95	3.95	13.64	0.296
1.81	54	24	3.99	3.97	3.97	3.97	3.94	3.94	17.15	0.296

Test = 2023090801 MPN023101.mcd **AnDat = 20230910**

Repeat: 5M Glass for Simulant, from Matt Creedon, Washington Mills, RT to 1000C to RT, in flowing UHP argon

List of Measured Values of ε' and ε" :

Initial density = $samdns_{NCal+1}$ **= 1.898** gm/cc Final density(25C) = **dnsfinal = 1.81** gm/cc

density $samdns_{mm}$	index mm	T(C) $T_{mm,1}$	397MHz $\varepsilon''_{mm,1}$	912MHz $\varepsilon''_{mm,2}$	1429MH $\varepsilon''_{mm,3}$	1948MHz $\varepsilon''_{mm,4}$	2466MHz $\varepsilon''_{mm,5}$	2986MHz $\varepsilon''_{mm,6}$	Lapsed Time (hours) $tlaps_{mm}$	$sammas_{mm}$
1.898	3	24	0.015	0.019	0.019	0.02	0.021	0.022	0	0.295
1.898	4	24	0.016	0.017	0.019	0.02	0.021	0.021	0.19	0.295
1.898	5	24	0.017	0.017	0.018	0.02	0.02	0.021	0.25	0.295
1.898	6	62	0.021	0.017	0.018	0.019	0.02	0.021	0.51	0.295
1.898	7	101	0.014	0.011	0.016	0.019	0.019	0.02	0.76	0.295
1.898	8	150	0.019	0.013	0.018	0.017	0.019	0.02	1.08	0.295
1.898	9	201	0.018	0.013	0.015	0.018	0.019	0.019	1.43	0.295
1.898	10	252	0.011	0.018	0.017	0.017	0.018	0.02	1.77	0.295
1.898	11	300	0.02	0.014	0.015	0.018	0.018	0.02	2.1	0.295
1.898	12	351	0.011	0.016	0.016	0.017	0.018	0.019	2.39	0.295
1.898	13	400	0.016	0.017	0.014	0.016	0.018	0.018	2.68	0.295
1.898	14	450	0.022	0.008	0.015	0.016	0.018	0.018	2.97	0.295
1.898	15	499	0.016	0.016	0.015	0.016	0.019	0.02	3.26	0.295
1.898	16	524	0.023	0.015	0.014	0.017	0.018	0.019	3.45	0.295
1.898	17	549	0.028	0.016	0.016	0.017	0.018	0.019	3.62	0.295
1.898	18	574	0.029	0.015	0.018	0.017	0.019	0.02	3.8	0.295
1.898	19	598	0.03	0.017	0.017	0.02	0.019	0.021	3.97	0.295
1.898	20	624	0.019	0.024	0.022	0.021	0.021	0.021	4.15	0.295
1.898	21	648	0.023	0.018	0.022	0.021	0.023	0.024	4.32	0.295
1.898	22	673	0.042	0.024	0.023	0.025	0.024	0.025	4.49	0.295
1.899	23	698	0.045	0.027	0.028	0.028	0.029	0.028	4.67	0.295
1.9	24	722	0.05	0.035	0.032	0.031	0.029	0.03	4.85	0.295
1.901	25	747	0.051	0.036	0.036	0.035	0.034	0.034	5.02	0.295
1.889	26	772	0.055	0.049	0.036	0.038	0.038	0.038	5.2	0.296
1.878	27	797	0.055	0.043	0.043	0.045	0.044	0.042	5.38	0.296
1.867	28	821	0.07	0.05	0.053	0.053	0.051	0.05	5.56	0.296
1.856	29	846	0.09	0.07	0.066	0.062	0.06	0.059	5.74	0.296
1.844	30	874	0.09	0.067	0.063	0.061	0.058	0.056	5.92	0.296
1.833	31	897	0.052	0.041	0.036	0.039	0.037	0.036	6.1	0.296
1.821	32	921	0.041	0.025	0.024	0.024	0.024	0.023	6.28	0.296
1.81	33	951	0.036	0.019	0.016	0.017	0.016	0.017	6.48	0.296
1.81	34	973	0.031	0.018	0.015	0.014	0.016	0.016	6.65	0.296
1.81	35	1000	0.037	0.017	0.015	0.014	0.015	0.015	6.84	0.296
1.81	36	955	0.027	0.014	0.012	0.014	0.013	0.013	7.06	0.296
1.81	37	905	0.012	0.014	0.013	0.013	0.013	0.013	7.3	0.296
1.81	38	854	0.027	0.012	0.011	0.012	0.013	0.012	7.54	0.296
1.81	39	804	0.019	0.009	0.011	0.011	0.011	0.012	7.78	0.296
1.81	40	754	0.017	0.013	0.013	0.011	0.012	0.012	8.02	0.296
1.81	41	705	0.018	0.011	0.01	0.012	0.012	0.013	8.27	0.296
1.81	42	655	0.013	0.01	0.011	0.011	0.011	0.012	8.51	0.296
1.81	43	603	0.012	0.007	0.009	0.011	0.012	0.012	8.76	0.296
1.81	44	553	0.012	0.007	0.008	0.01	0.01	0.012	9.01	0.296
1.81	45	503	0.01	0.01	0.006	0.01	0.01	0.011	9.27	0.296
1.81	46	453	0.013	0.009	0.008	0.01	0.011	0.011	9.57	0.296
1.81	47	403	0.011	0.004	0.008	0.009	0.01	0.011	9.89	0.296
1.81	48	353	0.009	0.007	0.008	0.01	0.01	0.011	10.26	0.296
1.81	49	303	0.011	0.005	0.008	0.009	0.011	0.01	10.67	0.296
1.81	50	252	0.006	0.006	0.006	0.009	0.01	0.012	11.16	0.296
1.81	51	203	0.017	0.003	0.009	0.009	0.011	0.011	11.73	0.296
1.81	52	151	0.015	0.006	0.01	0.01	0.012	0.012	12.5	0.296

mq := 53 , 54 .. nd - Nempties

$samdns_{mq}$	mq	$T_{mq,1}$	$\varepsilon''_{mq,1}$	$\varepsilon''_{mq,2}$	$\varepsilon''_{mq,3}$	$\varepsilon''_{mq,4}$	$\varepsilon''_{mq,5}$	$\varepsilon''_{mq,6}$	$tlaps_{mq}$	$sammas_{mq}$
1.81	53	101	0.018	0.009	0.011	0.011	0.012	0.014	13.64	0.296
1.81	54	24	0.01	0.012	0.014	0.016	0.018	0.019	17.15	0.296

Appendix H.5 MPN-292_MPN_Glass for 5M Simulant_Creedon_Washington Mills Sept. 11, 2023

Glass Used in NUW-LHT-5M Lunar Simulant, from Washington Mills, Measurements of Complex Dielectric Constant of Pressed Pellets Room Temperature to 1150 °C to RT, in flowing (10 sccm) UHP Argon

Dr. Doug Rickman (NASA) was interested in knowing the dielectric properties of the special glass that was manufactured by Washington Mills and used in the making of the NUW-LHT-5M simulant. Dr. Matt Creedon of Washington Mills sent a sample of the 5M simulant glass powder to Microwave Properties North (MPN), who had offered to measure its microwave dielectric properties.

MPN had already done three complex dielectric properties measurement runs on heat-treated NUW-LHT-5M lunar regolith simulant up to temperatures of 1100 °C, 1150 °C and 1250 °C under a NASA contract. The first dielectric measurement run on the full NUW-LHT-5M simulant, in vacuum, up to 1100 °C, had an unfamiliar feature at ~850 °C. The second full simulant run was done up to 1150 °C in flowing (10 sccm) ultra-high purity (UHP) argon. This required a different sample holder, different background subtractions, and new calibrations. However, the same feature was noted in the dielectric constant, as shown in the plots in Figure 1.

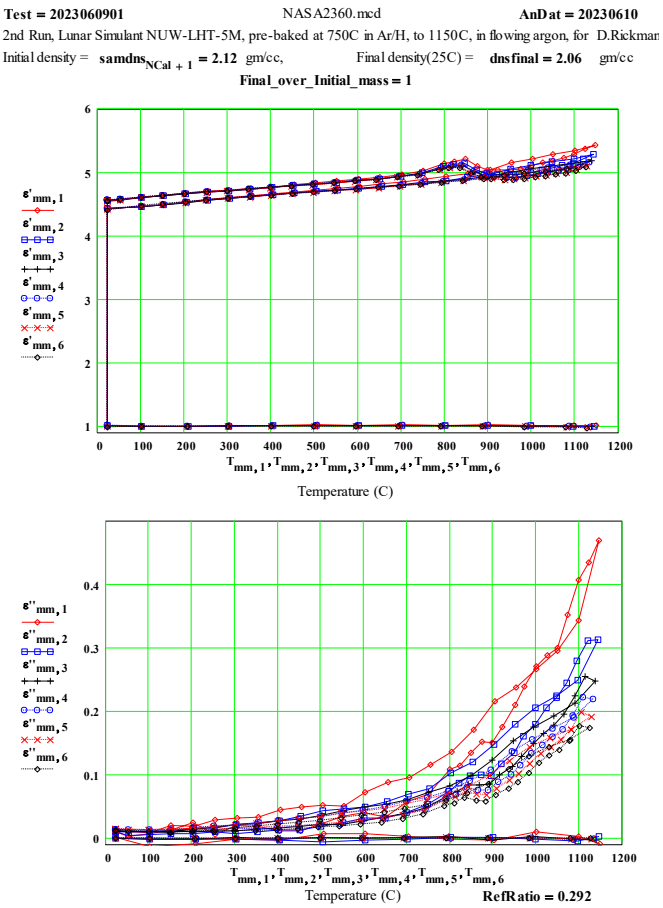

Figure 1. The top line of the ε′ plots (initial value of ε′ is ~4.7) are the values measured during the ramp up to 1150 °C. The bottom line in the plots are the empty holder measurements done immediately after the sample measurements. Only the initial and final sample dimensions were actually measured.

The NUW-LHT-5M lunar simulant has ~40 wt% of a relatively unique (on Earth at least) glass, largely composed of the same elements as the crystalline content of the simulant. It seemed useful to measure the properties of the glass alone, but under similar conditions.

For this 5M glass measurement, MPN again pressed pellets of the powder material in a uniaxial press at ~33,000 psi. The pellets were not initially baked by MPN to ensure dryness. This run was a simple cycle to 1150 °C and back to room temperature (RT). The sample holder for this run was initially cycled (and measured while empty) to 1150 °C before the run to "clean" the holder and measure the "empty holder" values, which were later used during the off-line data analysis.
For this measurement, a holder with a small hole in the base was used, so UHP argon gas could flow up, past the sample pellets, at ~10 sccm regulated flow rate.

The initial sample parameters were:
g) Diameter: 3.63 ± 0.02 mm
h) Length of 3 Pellet Stack: 13.54 ± 0.05 mm
i) Mass: 0.280 ± 0.002 gm
j) RT Density 1.90 ± 0.05 gm/cc
k) Appearance: Three light grey pellets (Figures 2 and 3)
l) Magnetic Response: The pellets had a very weak attraction to a strong magnet.

The dielectric properties measurements were performed three times at RT, and then the temperature was ramped up to 800C in 50C steps, then to 1150C in 25 C steps. After this, the temperature was brought back down to 100C in -50C steps, then RT.
The holder was removed from the apparatus and it and the final sample were weighed together. The pellets were easily removed, and their combined mass determined. Then the empty holder was run up to 1100C to measure backgrounds and check for contamination. There was no significant contamination.

The final sample properties at RT were:
g) Diameter: 3.60 ± 0.03 mm
h) Length of 3 Pellet Stack: 13.52 ± 0.05 mm
i) Mass: 0.280 ± 0.002 gm
j) RT Density: 1.81 ± 0.05 gm/cc
k) Appearance: three very light beige pellets (Figures 4 and 5)
l) Magnetic Response: The pellets had a very weak attraction to a strong magnet

Note: The percent mass loss was zero within our errors.

The frequency coding is :

Legend for Data Plots :

#	Frequency(MHz)	Symbol
1	397	red diamond, solid line – sometimes the line is omitted!
2	912	blue square, solid line

3	1429	black cross, solid line
4	1948	blue circle, dotted line
5	2466	red cross, dotted line
6	2986	black diamond, dotted line

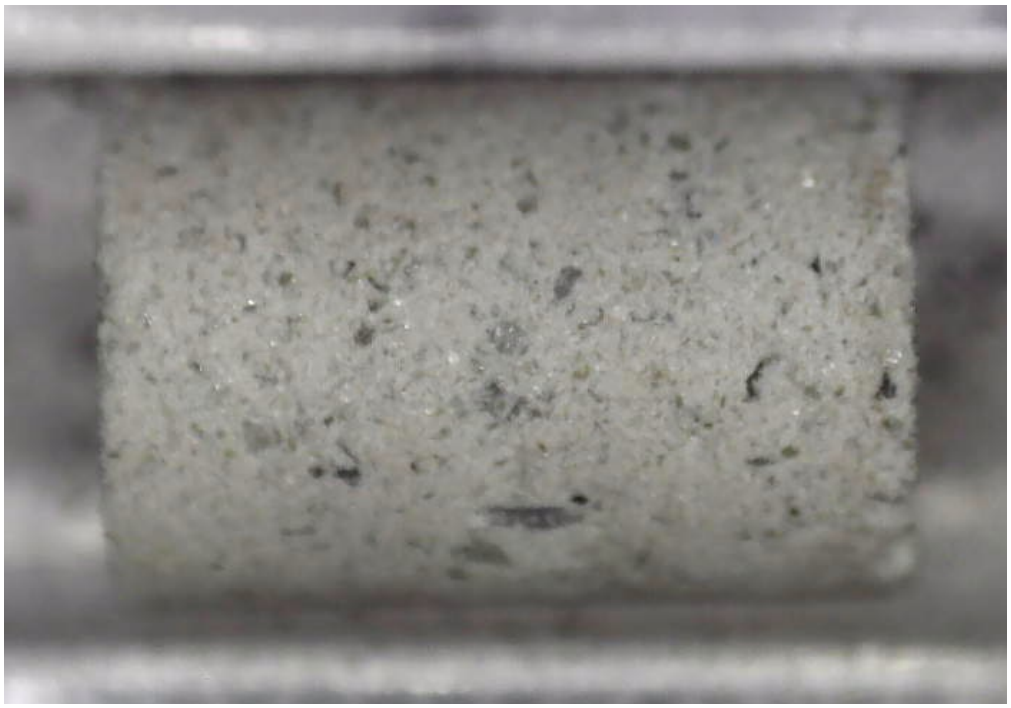

Figure 2. Typical initial NUW-LHT-5M pellet pressed at ~33,000 psi.

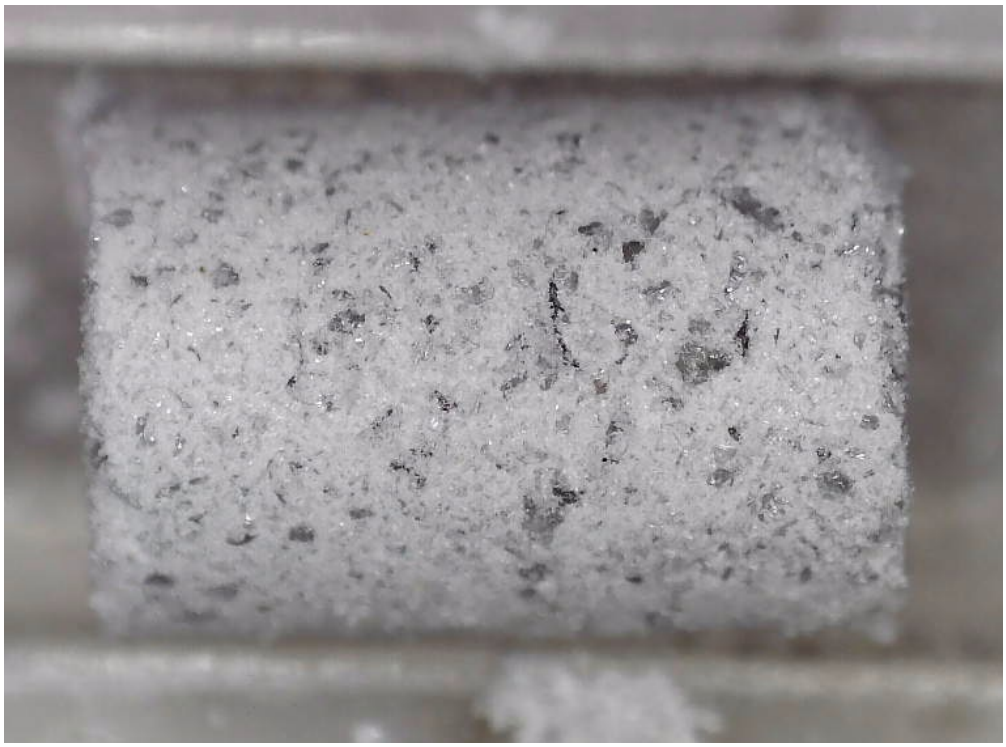

Figure 3. Initial 5M Glass (Washington Mills) pellet pressed at ~33,000 psi.

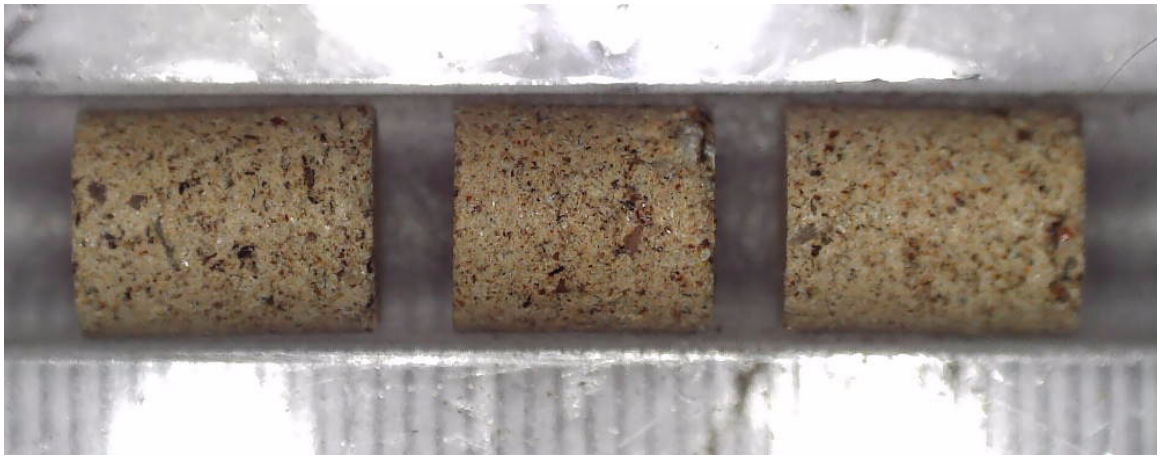

Figure 4. Three final NUW-LHT-5M pellets after a cycle to 1150 °C in UHP argon.

Figure 5. Three final 5M glass pellets after the cycle to 1150 °C in UHP argon.

Test = 2023090501 MPN023100.mcd **AnDat = 20230907**

5M Glass for Simulant, from Matt Creedon, Washington Mills, RT to 1150C to RT, in flowing UHP argon

Initial density = $samdns_{NCal+1}$ **= 2** gm/cc, Final density(25C) = **dnsfinal = 1.98** gm/cc

Final_over_Initial_mass = 1

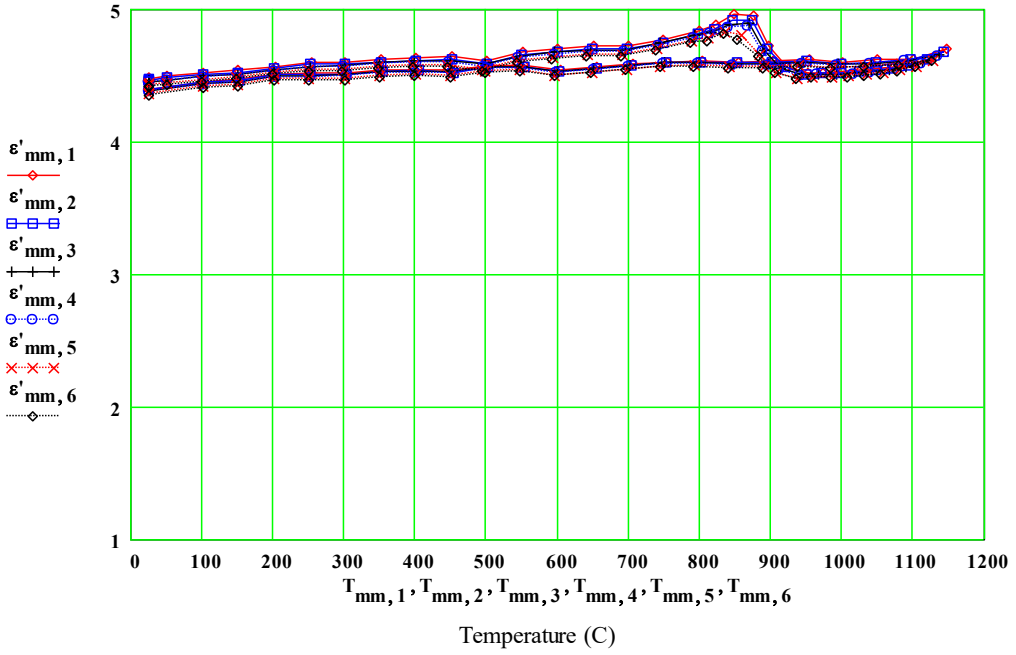

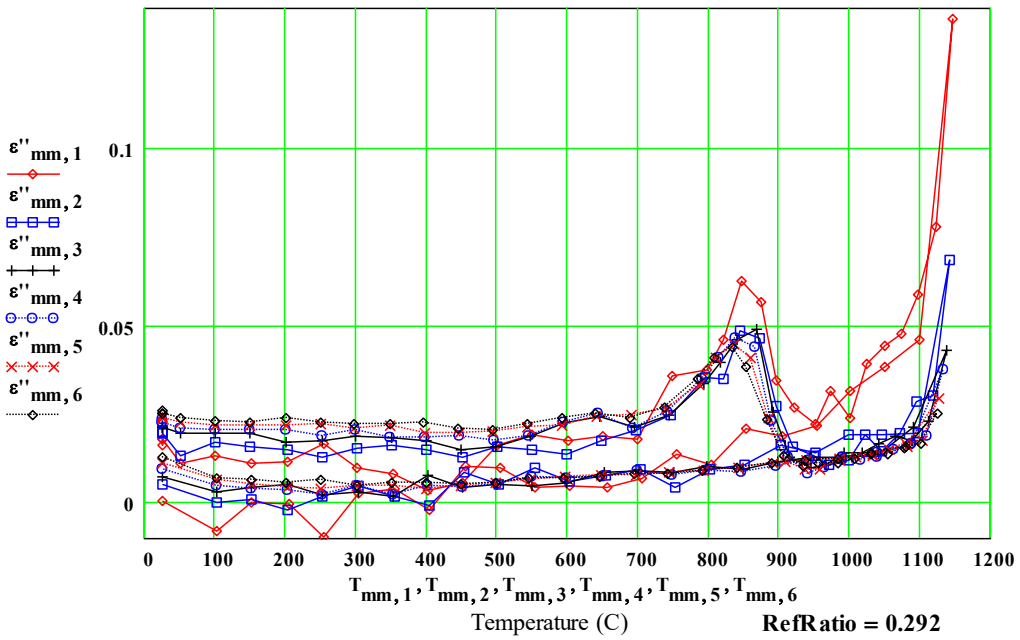

RefRatio = 0.292

Figure 6. Note the very rapid increase in ε″ values above 1100 °C. This is indicative of approaching the melting point. The thermal activation energy is large – very approximately 400 Kjoule/mole (~4.2 eV) by fitting the points between 1100 °C and 1150 °C. The feature at 850 °C seen in the stimulant runs is evident in this glass 5M run.

The two data points at 850 °C and 875 °C in the "ramp-up" have been changed throughout this report to match the values measured in a second run and shown in Appendix 1. This was done to improve the usefulness and accuracy of the plots for the reader.

Comments on the data run :

A thermal expansion coefficient (CTE) of 0.0 * 10^{-6}/°C was used.

The final pellets appeared unchanged except for a very slight beige colouring of some components.

The smooth ramp up of the values to 1150 °C was interrupted only by a slight drop of the ε′ values at 850 °C and 875 °C (MPN023100, plot below). This was very difficult to understand, so another run was done to 1000 °C (MPN023101) on a new set of pellets in a solid-bottom holder, with the argon gas flowing down onto the top of the test sample. In this configuration, expansion of the pellet diametrically cannot result in vertical movement of the test sample caused by the cover gas flow. This second run demonstrated that, in fact, a transformation (re-crystallization?) was occurring between 700 °C and 925 °C, which resulted in small increases in both ε′ and ε″, with a maxima at ~860 °C. The details of this run are presented in Appendix 1 at the end of this report.

The explanation for the dip in the first run to 1150 °C (MPN023100, plot below) would seem to be that the pellets expanded in diameter during this transformation (which actually started at ~600 °C), and at 850 °C the expansion blocked the vertical flow of argon and increased the pressure sufficiently to lift the pellet(s?) into a region of the cavity that had a slightly lower electric field (the equivalent of shortening the sample). By changing the "effective" pellet length (and thus the volume) slightly for only the two temperatures (850 °C and 875 °C) during the data analysis, the peak shape was made to match that seen in the second run to 1000 °C (shown in Appendix 1).

This feature, although interesting, is small and probably not very significant in the high temperature properties of the 5M simulant.

Test = 2023090501 MPN023100.mcd **AnDat = 20230907**

5M Glass for Simulant, from Matt Creedon, Washington Mills, RT to 1150C to RT, in flowing UHP argon

Initial density = $samdns_{NCal+1}$ = **2** gm/cc, Final density(25C) = **dnsfinal = 1.98** gm/cc

Final_over_Initial_mass = 1

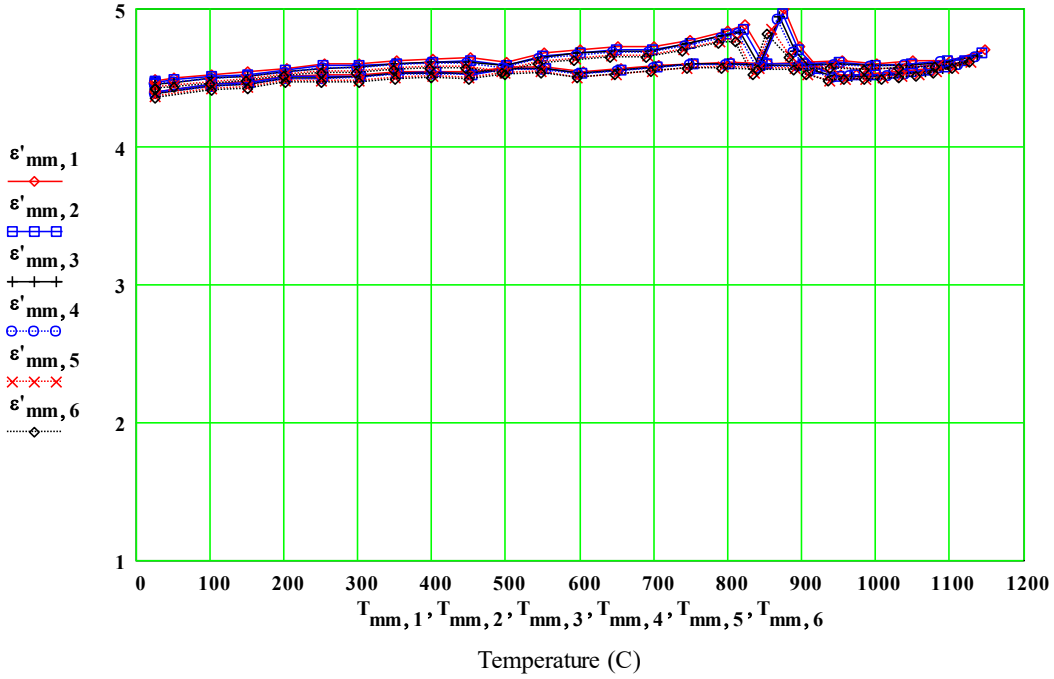

Test = 2023090501 MPN023100.mcd **AnDat = 20230907**

5M Glass for Simulant, from Matt Creedon, Washington Mills, RT to 1150C, in flowing UHP argon

Initial density = $\mathbf{samdns}_{NCal+1} = 2$ gm/cc, Final density(25C) = **dnsfinal = 1.98** gm/cc

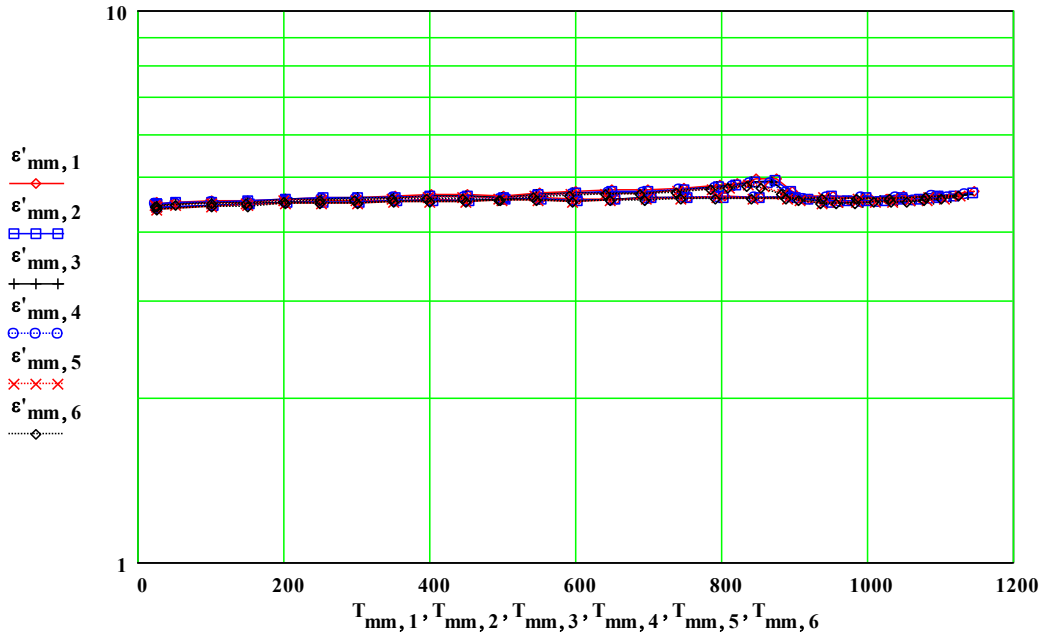

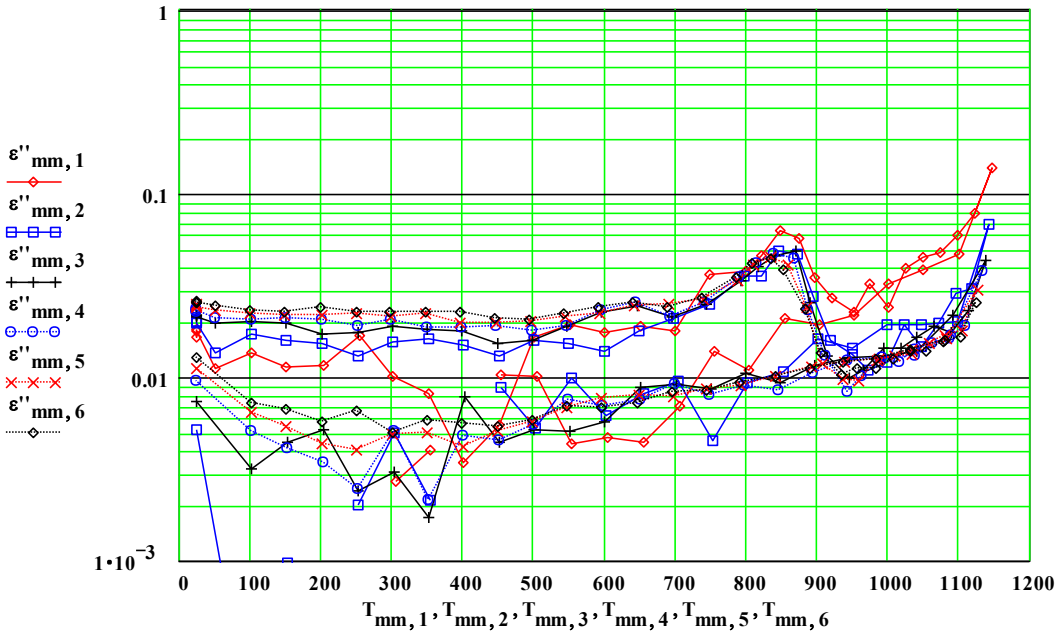

Test = 2023090501 MPN023100.mcd **AnDat = 20230907**

5M Glass for Simulant, from Matt Creedon, Washington Mills, RT to 1150C, in flowing UHP argon

Initial density = **$samdns_{14}$ = 2** gm/cc, Final density(25C) = **dnsfinal = 1.98** gm/cc

Equivalent Free Electron Conductivity (Siemens/metre)

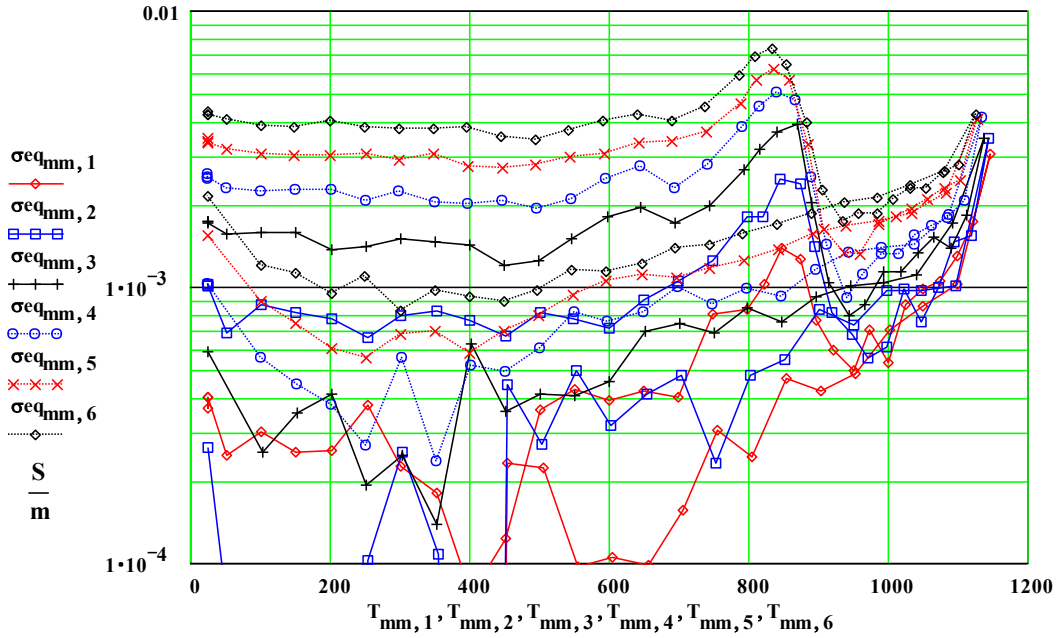

Temperature (C)

Test = 2023090501 MPN023100.mcd **AnDat = 20230907**

5M Glass for Simulant, from Matt Creedon, Washington Mills, RT to 1150C, in flowing UHP argon

Initial density = $samdns_{NCal+1} = 2$ gm/cc, Final density(25C) = **dnsfinal = 1.98** gm/cc

Thermal exp. coeff. $\alpha_1 = 0$

Values for 2450 MHz

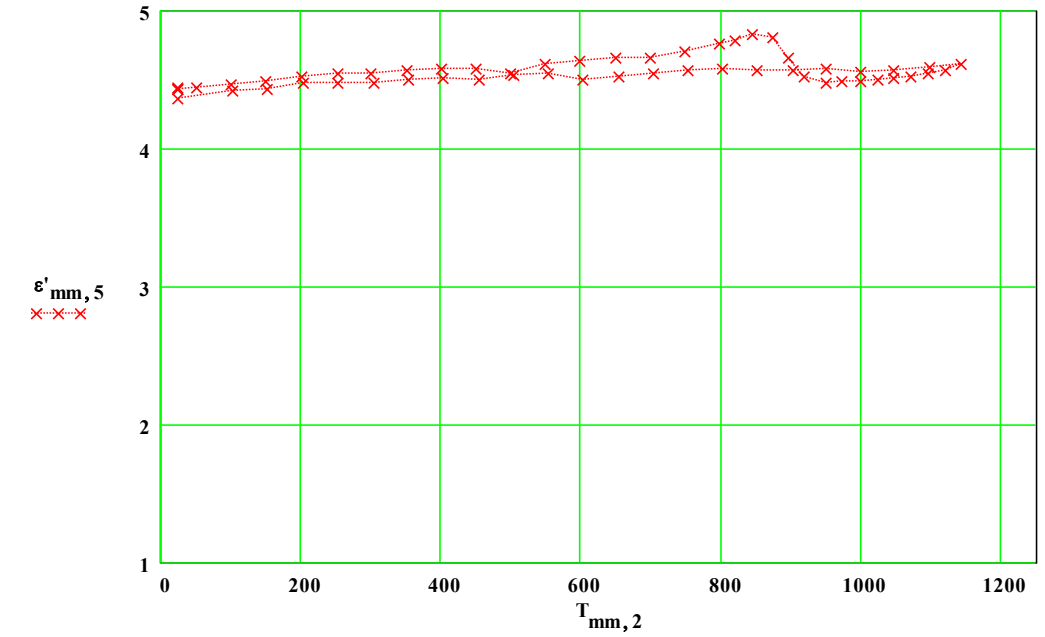

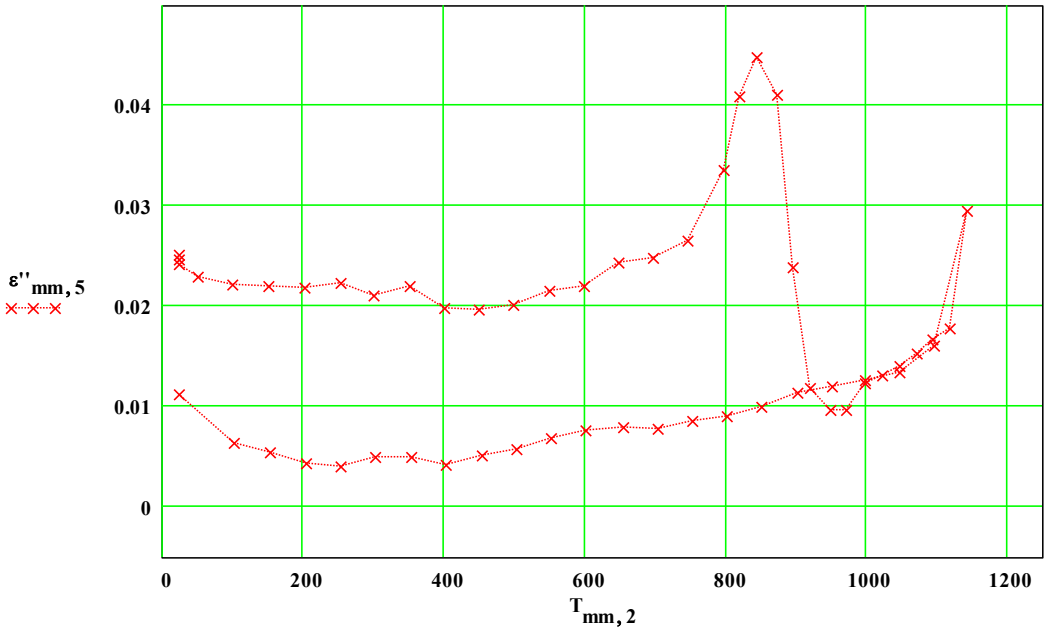

Test = 2023090501 MPN023100.mcd **AnDat = 20230907**

5M Glass for Simulant, from Matt Creedon, Washington Mills, RT to 1150C, in flowing UHP argon

Initial density = $\mathbf{samdns_{NCal+1}} = 2$ gm/cc, Final density(25C) = **dnsfinal = 1.98** gm/cc

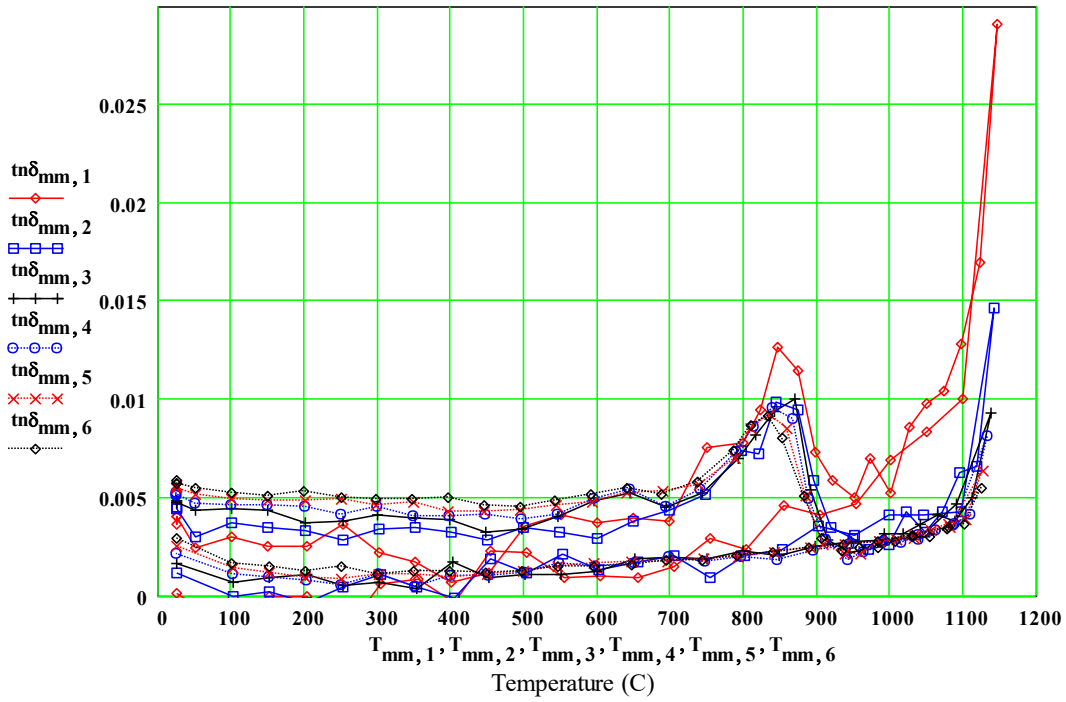

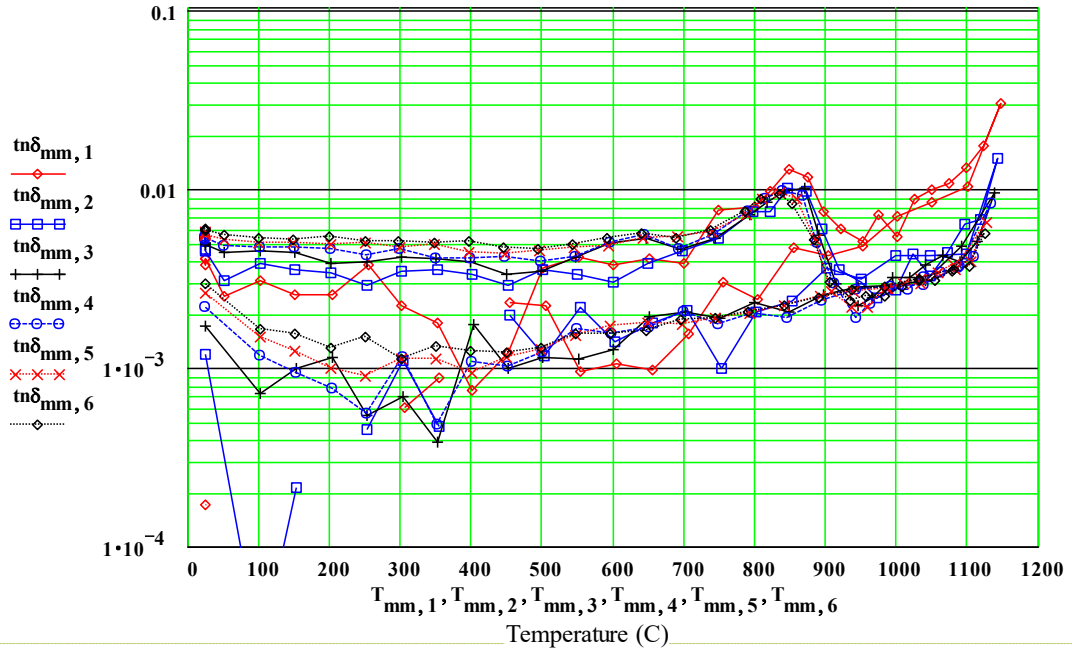

Half-power Depth (millimeters)

$$D\_halfP_{(mm,n)} := \left(\frac{\ln(2)}{2}\right)\cdot\left(inverse\alpha_{mm,n}\cdot 1\right)$$

Test = 2023090501 MPN023100.mcd **AnDat = 20230907**

5M Glass for Simulant, from Matt Creedon, Washington Mills, RT to 1150C, in flowing UHP argon

Initial density = $samdns_{NCal+1} = 2$ gm/cc, Final density(25C) = **dnsfinal = 1.98** gm/cc

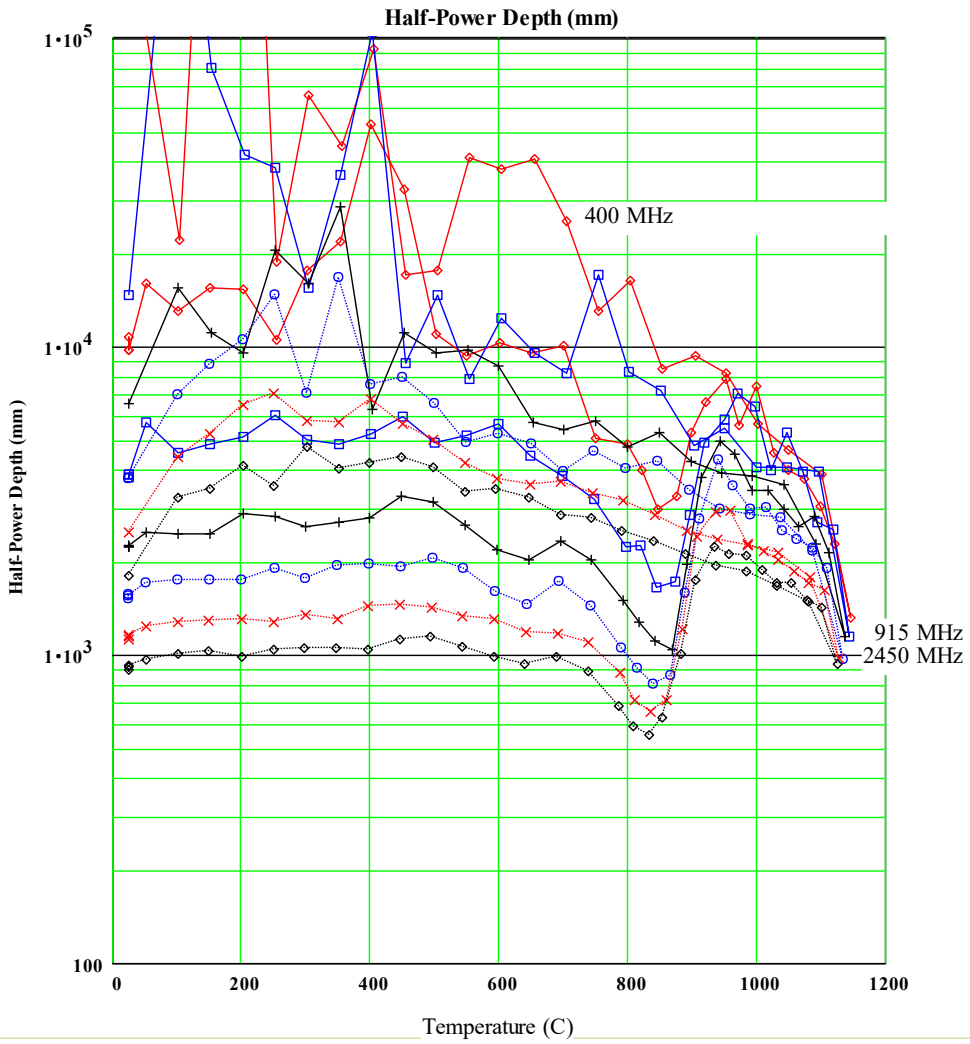

Test = 2023090501 MPN023100.mcd **AnDat = 20230907**

5M Glass for Simulant, from Matt Creedon, Washington Mills, RT to 1150C, in flowing UHP argon

List of Measured Values of ε' and ε" :

Initial density = $samdns_{NCal+1}$ **= 1.998** gm/cc Final density(25C) = **dnsfinal = 1.979** gm/cc

density	index	T(C)	397MHz	912MHz	1429MH	1948MHz	2466MHz	2986MHz	Lapsed Time (hours)	
$samdns_{mm}$	r_{mm}	$T_{mm,1}$	$\varepsilon'_{mm,1}$	$\varepsilon'_{mm,2}$	$\varepsilon'_{mm,3}$	$\varepsilon'_{mm,4}$	$\varepsilon'_{mm,5}$	$\varepsilon'_{mm,6}$	$tlaps_{mm}$	$sammas_{mm}$
1.998	11	25	4.49	4.48	4.47	4.46	4.44	4.43	0	0.28
1.998	12	25	4.48	4.47	4.45	4.45	4.43	4.41	0.15	0.28
1.998	13	25	4.48	4.47	4.45	4.45	4.43	4.42	0.22	0.28
1.998	14	52	4.5	4.49	4.47	4.46	4.44	4.43	0.4	0.28
1.998	15	101	4.52	4.51	4.5	4.49	4.47	4.46	0.7	0.28
1.998	16	151	4.55	4.53	4.51	4.51	4.49	4.47	1.01	0.28
1.998	17	203	4.57	4.56	4.55	4.54	4.52	4.51	1.36	0.28
1.998	18	254	4.6	4.59	4.57	4.56	4.54	4.53	1.7	0.28
1.998	19	302	4.6	4.59	4.58	4.57	4.55	4.54	2.03	0.28
1.998	20	352	4.63	4.61	4.6	4.59	4.57	4.56	2.32	0.28
1.998	21	402	4.64	4.62	4.61	4.6	4.58	4.57	2.6	0.28
1.998	22	452	4.65	4.63	4.62	4.6	4.58	4.57	2.89	0.28
1.998	23	501	4.61	4.59	4.59	4.57	4.55	4.54	3.18	0.28
1.998	24	550	4.68	4.66	4.65	4.64	4.61	4.6	3.43	0.28
1.998	25	600	4.7	4.68	4.68	4.66	4.64	4.63	3.68	0.28
1.998	26	650	4.73	4.7	4.7	4.68	4.66	4.64	3.94	0.28
1.998	27	699	4.73	4.7	4.7	4.68	4.66	4.65	4.19	0.28
1.998	28	749	4.78	4.75	4.75	4.73	4.71	4.7	4.44	0.28
1.98	29	799	4.84	4.82	4.8	4.79	4.76	4.74	4.7	0.28
1.961	30	822	4.88	4.85	4.83	4.81	4.78	4.77	4.86	0.28
2.063	31	847	4.96	4.91	4.89	4.86	4.83	4.81	5.04	0.28
1.909	32	875	4.96	4.93	4.9	4.87	4.81	4.77	5.21	0.28
1.907	33	897	4.73	4.7	4.69	4.68	4.66	4.65	5.38	0.28
1.89	34	921	4.57	4.56	4.56	4.55	4.53	4.52	5.54	0.28
1.872	35	951	4.52	4.51	4.51	4.5	4.48	4.47	5.73	0.28
1.872	36	974	4.53	4.52	4.51	4.51	4.49	4.49	5.89	0.28
1.872	37	1000	4.54	4.53	4.52	4.51	4.49	4.49	6.07	0.28
1.872	38	1026	4.55	4.53	4.52	4.51	4.49	4.49	6.24	0.28
1.872	39	1050	4.56	4.55	4.53	4.53	4.51	4.5	6.41	0.28
1.872	40	1074	4.57	4.56	4.55	4.54	4.52	4.51	6.58	0.28
1.877	41	1098	4.59	4.58	4.57	4.56	4.54	4.54	6.74	0.28
1.881	42	1122	4.62	4.62	4.6	4.6	4.57	4.56	6.91	0.28
1.886	43	1146	4.7	4.68	4.66	4.65	4.62	4.61	7.08	0.28
1.89	44	1100	4.63	4.63	4.61	4.61	4.59	4.58	7.31	0.28
1.895	45	1049	4.62	4.61	4.6	4.59	4.57	4.56	7.57	0.28
1.899	46	1001	4.6	4.59	4.59	4.58	4.56	4.55	7.82	0.28
1.904	47	953	4.62	4.61	4.6	4.6	4.58	4.57	8.06	0.28
1.909	48	904	4.61	4.6	4.59	4.58	4.57	4.56	8.31	0.28
1.913	49	854	4.61	4.6	4.59	4.58	4.57	4.56	8.57	0.28
1.918	50	804	4.62	4.6	4.61	4.6	4.58	4.57	8.82	0.28
1.922	51	755	4.6	4.6	4.6	4.59	4.57	4.56	9.07	0.28
1.927	52	706	4.59	4.58	4.58	4.57	4.55	4.54	9.32	0.28
1.932	53	656	4.57	4.56	4.56	4.55	4.53	4.52	9.57	0.28
1.936	54	604	4.55	4.54	4.54	4.53	4.51	4.5	9.84	0.28
1.941	55	554	4.58	4.57	4.57	4.56	4.54	4.53	10.09	0.28
1.946	56	504	4.58	4.56	4.56	4.55	4.54	4.53	10.36	0.28
1.951	57	455	4.54	4.53	4.53	4.52	4.5	4.49	10.66	0.28
1.955	58	405	4.55	4.54	4.54	4.53	4.51	4.5	11	0.28
1.96	59	355	4.55	4.53	4.53	4.52	4.5	4.49	11.39	0.28
1.965	60	305	4.52	4.51	4.51	4.5	4.48	4.47	11.83	0.28

mq := 61 , 62 .. nd – Nempties

$samdns_{mq}$	mq	$T_{mq,1}$	$\varepsilon'_{mq,1}$	$\varepsilon'_{mq,2}$	$\varepsilon'_{mq,3}$	$\varepsilon'_{mq,4}$	$\varepsilon'_{mq,5}$	$\varepsilon'_{mq,6}$	$tlaps_{mq}$	$sammas_{mq}$
1.97	61	254	4.52	4.51	4.5	4.49	4.47	4.46	12.35	0.28
1.974	62	204	4.51	4.51	4.5	4.49	4.47	4.46	12.96	0.28
1.979	63	153	4.48	4.47	4.46	4.45	4.43	4.43	13.8	0.28
1.979	64	103	4.46	4.45	4.44	4.44	4.42	4.41	15.06	0.28
1.979	65	25	4.4	4.4	4.39	4.39	4.37	4.35	21.46	0.28

Test = 2023090501 MPN023100.mcd **AnDat = 20230907**

5M Glass for Simulant, from Matt Creedon, Washington Mills, RT to 1150C, in flowing UHP argon

List of Measured Values of ε' and ε" :

Initial density = $samdns_{NCal+1}$ = **1.998** gm/cc Final density(25C) = **dnsfinal = 1.979** gm/cc

density	index	T(C)	397MHz	912MHz	1429MH	1948MHz	2466MHz	2986MHz	Lapsed Time (hours)	
$samdns_{mm}$	mm	$T_{mm,1}$	$\varepsilon''_{mm,1}$	$\varepsilon''_{mm,2}$	$\varepsilon''_{mm,3}$	$\varepsilon''_{mm,4}$	$\varepsilon''_{mm,5}$	$\varepsilon''_{mm,6}$	$tlaps_{mm}$	$sammas_{mm}$
1.998	11	25	0.018	0.02	0.022	0.024	0.025	0.026	0	0.28
1.998	12	25	0.016	0.02	0.022	0.023	0.025	0.026	0.15	0.28
1.998	13	25	0.018	0.02	0.021	0.023	0.024	0.025	0.22	0.28
1.998	14	52	0.011	0.014	0.02	0.021	0.023	0.024	0.4	0.28
1.998	15	101	0.014	0.017	0.02	0.021	0.022	0.023	0.7	0.28
1.998	16	151	0.011	0.016	0.02	0.021	0.022	0.023	1.01	0.28
1.998	17	203	0.012	0.015	0.017	0.021	0.022	0.024	1.36	0.28
1.998	18	254	0.017	0.013	0.018	0.019	0.022	0.023	1.7	0.28
1.998	19	302	0.01	0.016	0.019	0.021	0.021	0.023	2.03	0.28
1.998	20	352	0.008	0.016	0.018	0.019	0.022	0.023	2.32	0.28
1.998	21	402	0.003	0.015	0.018	0.019	0.02	0.023	2.6	0.28
1.998	22	452	0.006	0.013	0.015	0.019	0.02	0.021	2.89	0.28
1.998	23	501	0.016	0.016	0.016	0.018	0.02	0.021	3.18	0.28
1.998	24	550	0.019	0.015	0.019	0.019	0.021	0.022	3.43	0.28
1.998	25	600	0.018	0.014	0.023	0.023	0.022	0.024	3.68	0.28
1.998	26	650	0.019	0.018	0.025	0.025	0.024	0.026	3.94	0.28
1.998	27	699	0.018	0.021	0.021	0.021	0.025	0.024	4.19	0.28
1.998	28	749	0.036	0.025	0.025	0.026	0.027	0.027	4.44	0.28
1.98	29	799	0.038	0.036	0.034	0.035	0.034	0.035	4.7	0.28
1.961	30	822	0.046	0.035	0.04	0.041	0.041	0.041	4.86	0.28
2.063	31	847	0.063	0.049	0.046	0.047	0.045	0.044	5.04	0.28
1.909	32	875	0.057	0.047	0.049	0.044	0.041	0.039	5.21	0.28
1.907	33	897	0.035	0.028	0.026	0.023	0.024	0.024	5.38	0.28
1.89	34	921	0.027	0.016	0.013	0.013	0.012	0.013	5.54	0.28
1.872	35	951	0.023	0.013	0.01	0.008	0.01	0.01	5.73	0.28
1.872	36	974	0.032	0.011	0.011	0.01	0.01	0.011	5.89	0.28
1.872	37	1000	0.024	0.012	0.014	0.012	0.012	0.011	6.07	0.28
1.872	38	1026	0.039	0.019	0.014	0.012	0.013	0.012	6.24	0.28
1.872	39	1050	0.045	0.015	0.017	0.014	0.014	0.014	6.41	0.28
1.872	40	1074	0.048	0.02	0.019	0.015	0.015	0.014	6.58	0.28
1.877	41	1098	0.059	0.029	0.018	0.016	0.017	0.016	6.74	0.28
1.881	42	1122	0.078	0.03	0.023	0.019	0.018	0.017	6.91	0.28
1.886	43	1146	0.137	0.069	0.043	0.038	0.03	0.025	7.08	0.28
1.89	44	1100	0.046	0.02	0.022	0.017	0.016	0.016	7.31	0.28
1.895	45	1049	0.039	0.019	0.014	0.013	0.013	0.014	7.57	0.28
1.899	46	1001	0.032	0.019	0.013	0.013	0.013	0.013	7.82	0.28
1.904	47	953	0.022	0.014	0.013	0.012	0.012	0.012	8.06	0.28
1.909	48	904	0.019	0.016	0.012	0.011	0.011	0.011	8.31	0.28
1.913	49	854	0.021	0.011	0.009	0.009	0.01	0.01	8.57	0.28
1.918	50	804	0.011	0.009	0.011	0.009	0.009	0.009	8.82	0.28
1.922	51	755	0.014	0.005	0.009	0.008	0.009	0.009	9.07	0.28
1.927	52	706	0.007	0.009	0.009	0.009	0.008	0.008	9.32	0.28
1.932	53	656	0.004	0.008	0.009	0.008	0.008	0.007	9.57	0.28
1.936	54	604	0.005	0.006	0.006	0.007	0.008	0.007	9.84	0.28
1.941	55	554	0.004	0.01	0.005	0.007	0.007	0.007	10.09	0.28
1.946	56	504	0.01	0.005	0.005	0.006	0.006	0.006	10.36	0.28
1.951	57	455	0.01	0.009	0.004	0.005	0.005	0.005	10.66	0.28
1.955	58	405	-0.002	-0.001	0.008	0.005	0.004	0.006	11	0.28
1.96	59	355	0.004	0.002	0.002	0.002	0.005	0.006	11.39	0.28
1.965	60	305	0.003	0.005	0.003	0.005	0.005	0.005	11.83	0.28

mq := 61 , 62 .. nd - Nempties

$samdns_{mq}$	mq	$T_{mq,1}$	$\varepsilon''_{mq,1}$	$\varepsilon''_{mq,2}$	$\varepsilon''_{mq,3}$	$\varepsilon''_{mq,4}$	$\varepsilon''_{mq,5}$	$\varepsilon''_{mq,6}$	$tlaps_{mq}$	$sammas_{mq}$
1.97	61	254	-0.009	0.002	0.002	0.002	0.004	0.007	12.35	0.28
1.974	62	204	-0	-0.002	0.005	0.003	0.004	0.006	12.96	0.28
1.979	63	153	0	0.001	0.004	0.004	0.005	0.007	13.8	0.28
1.979	64	103	-0.008	0	0.003	0.005	0.006	0.007	15.06	0.28
1.979	65	25	0.001	0.005	0.007	0.01	0.011	0.013	21.46	0.28

Appendix H.6 Second Run to 1000 °C on 5M Simulant Glass

Glass Used in NUW-LHT-5M Lunar Simulant , from Washington Mills, Measurements of Complex Dielectric Constant of Pressed Pellets RT to 1000°C to RT, in downward-flowing (30 sccm) UHP Argon

For this 5M glass measurement, MPN again pressed pellets of the powder material in a uniaxial press at ~33,000 psi. The pellets were not initially baked by MPN to ensure dryness. This run was a simple cycle to 1000 °C and back to RT. A steel tube was inserted into the top of the holder and its bottom end positioned 5 cm above the top of the pellet stack, bathing the pellets in UHP argon.

The initial sample parameters were:

g) Effective Diameter: 3.65 ± 0.02 mm
h) Length of 3 Pellet Stack: 14.89 ± 0.05 mm
i) Mass: 0.295 ± 0.002 gm
j) RT Density: 1.90 ± 0.05 gm/cc
k) Appearance: Three light grey pellets
l) Magnetic Response: The pellets had a very weak attraction to a strong magnet.

The dielectric properties measurements were performed three times at RT, and then the temperature was ramped up to 500 °C in 50 °C steps, then to 1000 °C in 25 °C steps. After this, the temperature was brought back down to 100 °C in -50 °C steps, then RT.
The holder was removed from the apparatus and it and the final sample were weighed together. The pellets were easily removed, and their combined mass determined. Then the empty holder was run up to 1000 °C to measure backgrounds and check for contamination. There was no significant contamination.

The final sample properties, at room temperature were:

g) Effective Diameter: 3.74 ± 0.03 mm
h) Length of 3 Pellet Stack: 14.89 ± 0.05 mm
i) Mass: 0.296 ± 0.002 gm
j) RT Density: 1.81 ± 0.05 gm/cc
k) Appearance: Three light grey pellets
l) Magnetic Response: The pellets had a very weak attraction to a strong magnet.

Note: The percent mass loss was zero within our errors.

Test = 2023090801 MPN023101.mcd **AnDat = 20230910**

Repeat: 5M Glass for Simulant, from Matt Creedon, Washington Mills, RT to 1000C to RT, in flowing UHP argon

Initial density = $\mathbf{samdns_{NCal+1}}$ **= 1.9** gm/cc, Final density(25C) = **dnsfinal = 1.81** gm/cc

Final_over_Initial_mass = 1.003

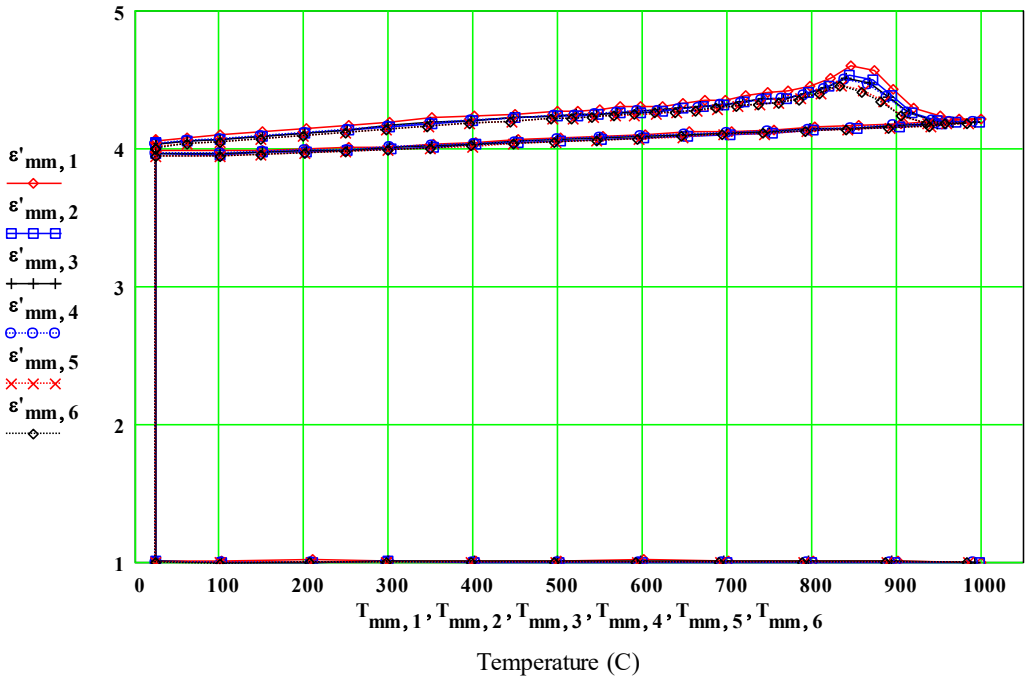

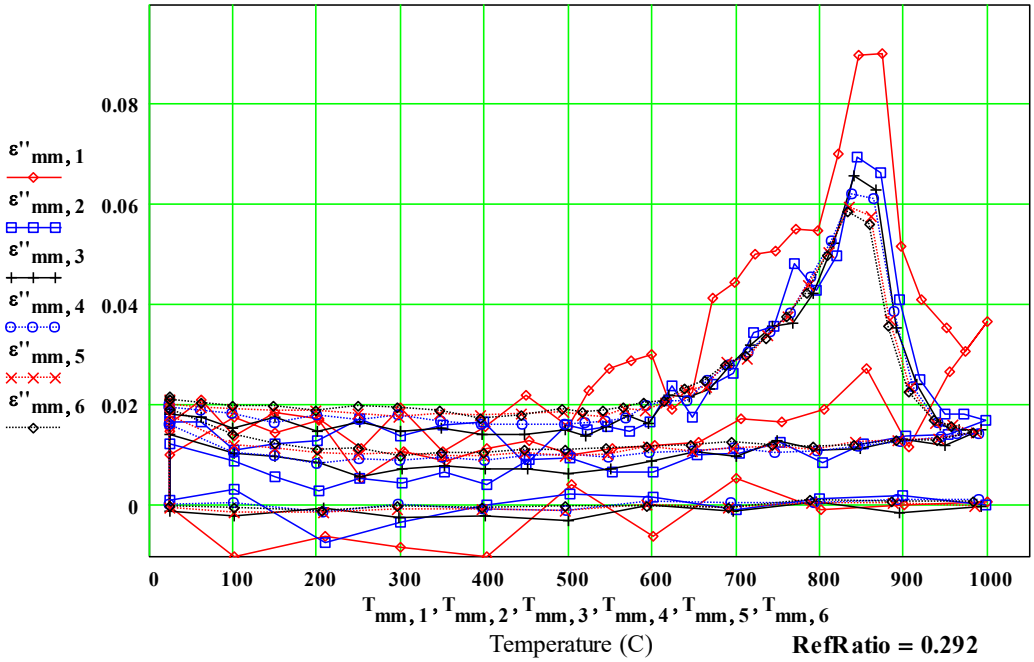

RefRatio = 0.292

Test = 2023090801 MPN023101.mcd **AnDat = 20230910**

5M Glass for Simulant, from Matt Creedon, Washington Mills, RT to 1000C to RT, in flowing UHP argon

Equivalent Free Electron Conductivity (Siemens/metre)

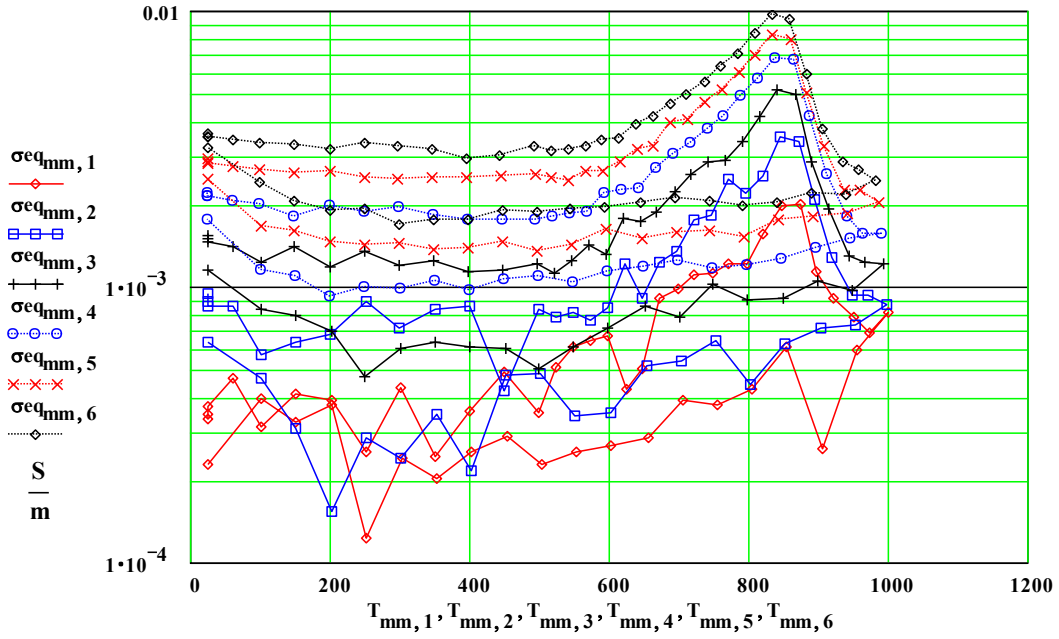

Temperature (C)

RefRatio = 0.292

Test = 2023090801 MPN023101.mcd **AnDat = 20230910**

5M Glass for Simulant, from Matt Creedon, Washington Mills, RT to 1000C to RT, in flowing UHP argon

Initial density = $samdns_{NCal+1}$ **= 1.9** gm/cc, Final density(25C) = **dnsfinal = 1.81** gm/cc

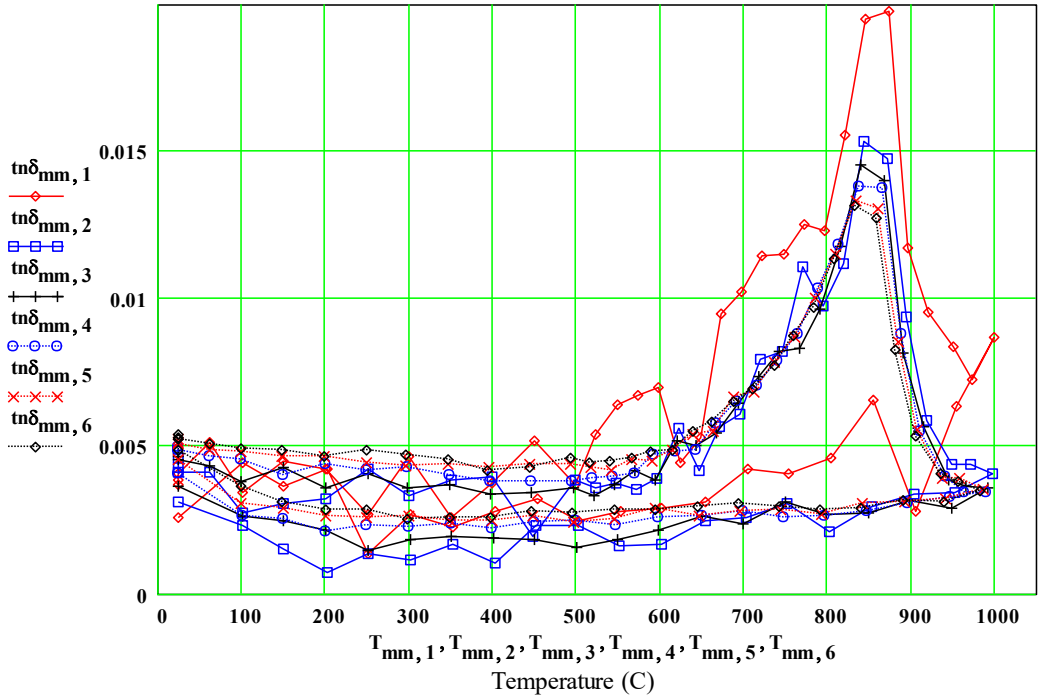

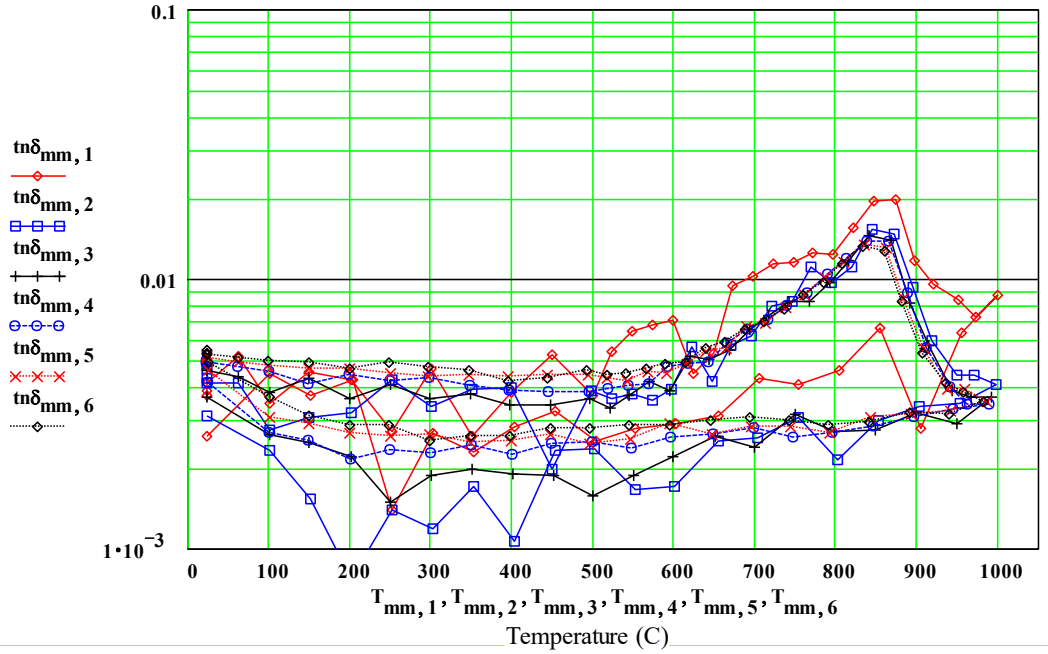

Half-power Depth (millimeters)

$$D\_halfP_{(mm,n)} := \left(\frac{\ln(2)}{2}\right)\cdot\left(inversealpha_{mm,n}\cdot 1\right)$$

Test = 2023090801 MPN023101.mcd **AnDat = 20230910**

Repeat: 5M Glass for Simulant, from Matt Creedon, Washington Mills, RT to 1000C to RT, in flowing UHP argo

Initial density = $samdns_{NCal+1}$ **= 1.9** gm/cc, Final density(25C) = **dnsfinal = 1.81** gm/cc

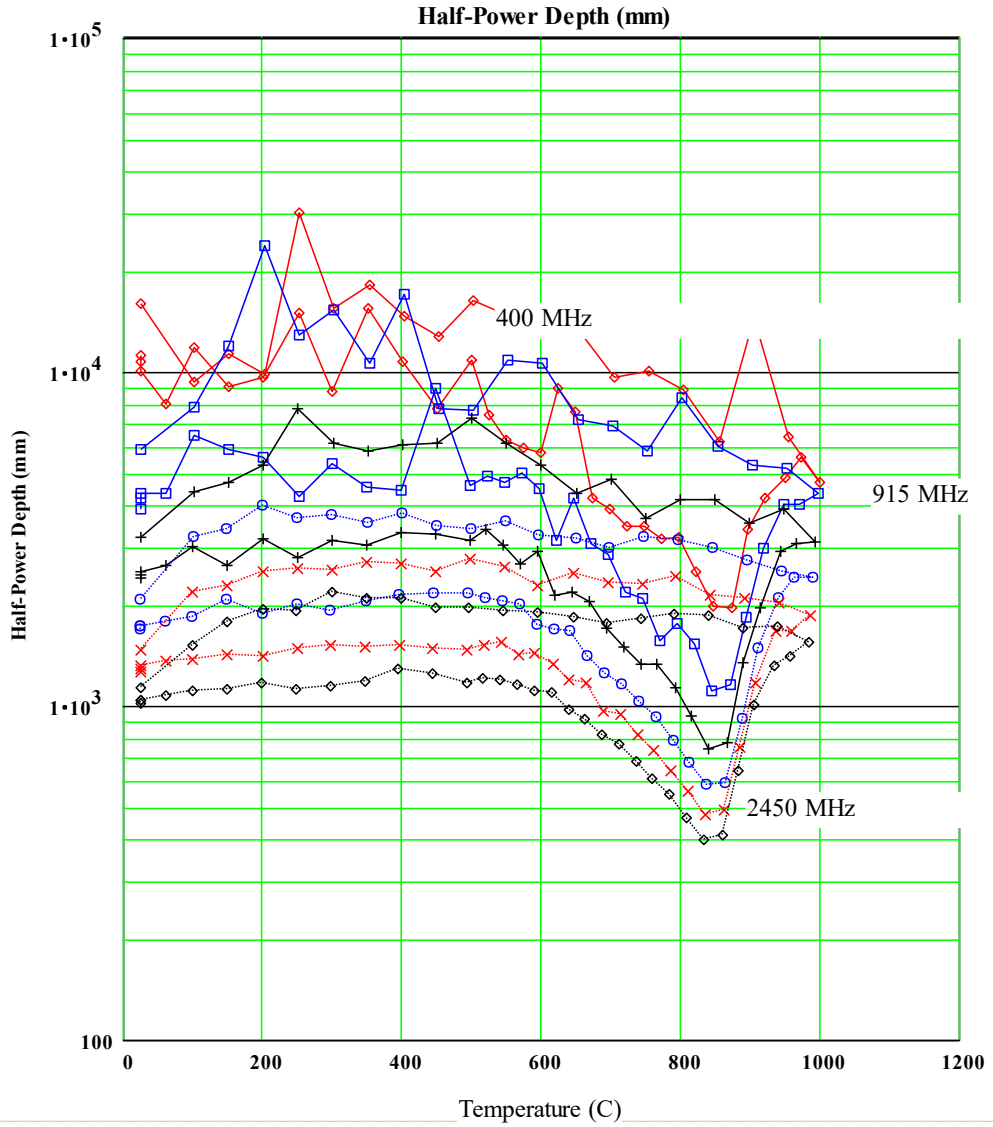

Test = 2023090801 MPN023101.mcd **AnDat = 20230910**

Repeat: 5M Glass for Simulant, from Matt Creedon, Washington Mills, RT to 1000C to RT, in flowing UHP arg

List of Measured Values of ε' and ε" :

Initial density = $samdns_{NCal+1}$ = 1.898 gm/cc Final density(25C) = **dnsfinal = 1.81** gm/cc

density	index	T(C)	397MHz	912MHz	1429MH	1948MHz	2466MHz	2986MHz	Lapsed Time (hours)	
$samdns_{mm}$		$T_{mm,1}$	$\varepsilon'_{mm,1}$	$\varepsilon'_{mm,2}$	$\varepsilon'_{mm,3}$	$\varepsilon'_{mm,4}$	$\varepsilon'_{mm,5}$	$\varepsilon'_{mm,6}$	$tlaps_{mm}$	$sammas_{mm}$
1.898	3	24	4.07	4.05	4.04	4.04	4.01	4	0	0.295
1.898	4	24	4.06	4.04	4.04	4.04	4.01	4	0.19	0.295
1.898	5	24	4.06	4.04	4.03	4.04	4.01	4.01	0.25	0.295
1.898	6	62	4.08	4.06	4.05	4.06	4.03	4.03	0.51	0.295
1.898	7	101	4.1	4.07	4.07	4.07	4.05	4.04	0.76	0.295
1.898	8	150	4.12	4.09	4.09	4.09	4.06	4.06	1.08	0.295
1.898	9	201	4.15	4.12	4.11	4.11	4.09	4.09	1.43	0.295
1.898	10	252	4.17	4.14	4.14	4.14	4.11	4.11	1.77	0.295
1.898	11	300	4.19	4.16	4.17	4.16	4.14	4.14	2.1	0.295
1.898	12	351	4.23	4.19	4.19	4.19	4.16	4.16	2.39	0.295
1.898	13	400	4.24	4.2	4.21	4.2	4.18	4.18	2.68	0.295
1.898	14	450	4.25	4.22	4.23	4.22	4.2	4.2	2.97	0.295
1.898	15	499	4.27	4.24	4.24	4.24	4.21	4.21	3.26	0.295
1.898	16	524	4.28	4.24	4.25	4.24	4.22	4.22	3.45	0.295
1.898	17	549	4.29	4.25	4.25	4.25	4.23	4.23	3.62	0.295
1.898	18	574	4.3	4.26	4.26	4.26	4.23	4.24	3.8	0.295
1.898	19	598	4.3	4.27	4.27	4.27	4.24	4.25	3.97	0.295
1.898	20	624	4.31	4.28	4.28	4.28	4.25	4.26	4.15	0.295
1.898	21	648	4.32	4.29	4.29	4.29	4.26	4.26	4.32	0.295
1.898	22	673	4.35	4.3	4.3	4.3	4.27	4.28	4.49	0.295
1.899	23	698	4.36	4.32	4.32	4.31	4.29	4.29	4.67	0.295
1.9	24	722	4.38	4.34	4.34	4.33	4.3	4.3	4.85	0.295
1.901	25	747	4.41	4.36	4.36	4.35	4.32	4.32	5.02	0.295
1.889	26	772	4.42	4.36	4.37	4.36	4.33	4.33	5.2	0.296
1.878	27	797	4.46	4.41	4.4	4.39	4.36	4.36	5.38	0.296
1.867	28	821	4.51	4.46	4.45	4.43	4.4	4.39	5.56	0.296
1.856	29	846	4.61	4.53	4.51	4.5	4.46	4.45	5.74	0.296
1.844	30	874	4.56	4.5	4.48	4.46	4.42	4.41	5.92	0.296
1.833	31	897	4.43	4.39	4.38	4.37	4.34	4.34	6.1	0.296
1.821	32	921	4.3	4.26	4.26	4.26	4.23	4.23	6.28	0.296
1.81	33	951	4.23	4.2	4.2	4.2	4.18	4.18	6.48	0.296
1.81	34	973	4.22	4.19	4.2	4.2	4.18	4.18	6.65	0.296
1.81	35	1000	4.22	4.2	4.2	4.2	4.18	4.18	6.84	0.296
1.81	36	955	4.21	4.18	4.18	4.18	4.16	4.16	7.06	0.296
1.81	37	905	4.18	4.16	4.17	4.17	4.15	4.15	7.3	0.296
1.81	38	854	4.17	4.15	4.15	4.15	4.13	4.14	7.54	0.296
1.81	39	804	4.16	4.13	4.14	4.14	4.12	4.13	7.78	0.296
1.81	40	754	4.14	4.12	4.13	4.13	4.11	4.11	8.02	0.296
1.81	41	705	4.13	4.11	4.12	4.12	4.1	4.1	8.27	0.296
1.81	42	655	4.12	4.1	4.1	4.1	4.08	4.09	8.51	0.296
1.81	43	603	4.11	4.08	4.09	4.09	4.07	4.07	8.76	0.296
1.81	44	553	4.1	4.07	4.08	4.07	4.06	4.06	9.01	0.296
1.81	45	503	4.08	4.06	4.07	4.07	4.05	4.05	9.27	0.296
1.81	46	453	4.07	4.04	4.05	4.05	4.03	4.04	9.57	0.296
1.81	47	403	4.05	4.03	4.04	4.03	4.02	4.02	9.89	0.296
1.81	48	353	4.04	4.01	4.02	4.02	4	4.01	10.26	0.296
1.81	49	303	4.02	4	4.01	4.01	3.99	3.99	10.67	0.296
1.81	50	252	4.01	3.99	3.99	3.99	3.97	3.98	11.16	0.296
1.81	51	203	4	3.98	3.98	3.98	3.97	3.97	11.73	0.296
1.81	52	151	3.99	3.97	3.97	3.97	3.95	3.96	12.5	0.296

mq := 53 , 54 .. nd - Nempties

$samdns_{mq}$	mq	$T_{mq,1}$	$\varepsilon'_{mq,1}$	$\varepsilon'_{mq,2}$	$\varepsilon'_{mq,3}$	$\varepsilon'_{mq,4}$	$\varepsilon'_{mq,5}$	$\varepsilon'_{mq,6}$	$tlaps_{mq}$	$sammas_{mq}$
1.81	53	101	3.98	3.96	3.96	3.96	3.95	3.95	13.64	0.296
1.81	54	24	3.99	3.97	3.97	3.97	3.94	3.94	17.15	0.296

Test = 2023090801 MPN023101.mcd **AnDat = 20230910**

Repeat: 5M Glass for Simulant, from Matt Creedon, Washington Mills, RT to 1000C to RT, in flowing UHP argon

List of Measured Values of ε' and ε" :

Initial density = $samdns_{NCal+1}$ **= 1.898** gm/cc Final density(25C) = **dnsfinal = 1.81** gm/cc

density $samdns_{mm}$	index mm	T(C) $T_{mm,1}$	397MHz $\varepsilon''_{mm,1}$	912MHz $\varepsilon''_{mm,2}$	1429MH $\varepsilon''_{mm,3}$	1948MHz $\varepsilon''_{mm,4}$	2466MHz $\varepsilon''_{mm,5}$	2986MHz $\varepsilon''_{mm,6}$	Lapsed Time (hours) $tlaps_{mm}$	$sammas_{mm}$
1.898	3	24	0.015	0.019	0.019	0.02	0.021	0.022	0	0.295
1.898	4	24	0.016	0.017	0.019	0.02	0.021	0.021	0.19	0.295
1.898	5	24	0.017	0.017	0.018	0.02	0.02	0.021	0.25	0.295
1.898	6	62	0.021	0.017	0.018	0.019	0.02	0.021	0.51	0.295
1.898	7	101	0.014	0.011	0.016	0.019	0.019	0.02	0.76	0.295
1.898	8	150	0.019	0.013	0.018	0.017	0.019	0.02	1.08	0.295
1.898	9	201	0.018	0.013	0.015	0.018	0.019	0.019	1.43	0.295
1.898	10	252	0.011	0.018	0.017	0.017	0.018	0.02	1.77	0.295
1.898	11	300	0.02	0.014	0.015	0.018	0.018	0.02	2.1	0.295
1.898	12	351	0.011	0.016	0.016	0.017	0.018	0.019	2.39	0.295
1.898	13	400	0.016	0.017	0.014	0.016	0.018	0.018	2.68	0.295
1.898	14	450	0.022	0.008	0.015	0.016	0.018	0.018	2.97	0.295
1.898	15	499	0.016	0.016	0.015	0.016	0.019	0.02	3.26	0.295
1.898	16	524	0.023	0.015	0.014	0.017	0.018	0.019	3.45	0.295
1.898	17	549	0.028	0.016	0.016	0.017	0.018	0.019	3.62	0.295
1.898	18	574	0.029	0.015	0.018	0.017	0.019	0.02	3.8	0.295
1.898	19	598	0.03	0.017	0.017	0.02	0.019	0.021	3.97	0.295
1.898	20	624	0.019	0.024	0.022	0.021	0.021	0.021	4.15	0.295
1.898	21	648	0.023	0.018	0.022	0.021	0.023	0.024	4.32	0.295
1.898	22	673	0.042	0.024	0.023	0.025	0.024	0.025	4.49	0.295
1.899	23	698	0.045	0.027	0.028	0.028	0.029	0.028	4.67	0.295
1.9	24	722	0.05	0.035	0.032	0.031	0.029	0.03	4.85	0.295
1.901	25	747	0.051	0.036	0.036	0.035	0.034	0.034	5.02	0.295
1.889	26	772	0.055	0.049	0.036	0.038	0.038	0.038	5.2	0.296
1.878	27	797	0.055	0.043	0.043	0.045	0.044	0.042	5.38	0.296
1.867	28	821	0.07	0.05	0.053	0.053	0.051	0.05	5.56	0.296
1.856	29	846	0.09	0.07	0.066	0.062	0.06	0.059	5.74	0.296
1.844	30	874	0.09	0.067	0.063	0.061	0.058	0.056	5.92	0.296
1.833	31	897	0.052	0.041	0.036	0.039	0.037	0.036	6.1	0.296
1.821	32	921	0.041	0.025	0.024	0.024	0.024	0.023	6.28	0.296
1.81	33	951	0.036	0.019	0.016	0.017	0.016	0.017	6.48	0.296
1.81	34	973	0.031	0.018	0.015	0.014	0.016	0.016	6.65	0.296
1.81	35	1000	0.037	0.017	0.015	0.014	0.015	0.015	6.84	0.296
1.81	36	955	0.027	0.014	0.012	0.014	0.013	0.013	7.06	0.296
1.81	37	905	0.012	0.014	0.013	0.013	0.013	0.013	7.3	0.296
1.81	38	854	0.027	0.012	0.011	0.012	0.013	0.012	7.54	0.296
1.81	39	804	0.019	0.009	0.011	0.011	0.011	0.012	7.78	0.296
1.81	40	754	0.017	0.013	0.013	0.011	0.012	0.012	8.02	0.296
1.81	41	705	0.018	0.011	0.01	0.012	0.012	0.013	8.27	0.296
1.81	42	655	0.013	0.01	0.011	0.011	0.011	0.012	8.51	0.296
1.81	43	603	0.012	0.007	0.009	0.011	0.012	0.012	8.76	0.296
1.81	44	553	0.012	0.007	0.008	0.01	0.01	0.012	9.01	0.296
1.81	45	503	0.01	0.01	0.006	0.01	0.01	0.011	9.27	0.296
1.81	46	453	0.013	0.009	0.008	0.01	0.011	0.011	9.57	0.296
1.81	47	403	0.011	0.004	0.008	0.009	0.01	0.011	9.89	0.296
1.81	48	353	0.009	0.007	0.008	0.01	0.01	0.011	10.26	0.296
1.81	49	303	0.011	0.005	0.008	0.009	0.011	0.01	10.67	0.296
1.81	50	252	0.006	0.006	0.006	0.009	0.01	0.012	11.16	0.296
1.81	51	203	0.017	0.003	0.009	0.009	0.011	0.011	11.73	0.296
1.81	52	151	0.015	0.006	0.01	0.01	0.012	0.012	12.5	0.296

mq := 53 , 54 .. nd - Nempties

$samdns_{mq}$	mq	$T_{mq,1}$	$\varepsilon''_{mq,1}$	$\varepsilon''_{mq,2}$	$\varepsilon''_{mq,3}$	$\varepsilon''_{mq,4}$	$\varepsilon''_{mq,5}$	$\varepsilon''_{mq,6}$	$tlaps_{mq}$	$sammas_{mq}$
1.81	53	101	0.018	0.009	0.011	0.011	0.012	0.014	13.64	0.296
1.81	54	24	0.01	0.012	0.014	0.016	0.018	0.019	17.15	0.296

Appendix I Section 13 Supplemental Information

Methods: Reflectance Measurements

Notes on characterization of NUW-LHT-5M at UTSA

Visible to near infrared (VNIR) and mid infrared (MIR) spectral reflectance measurements were made at Brown University's Reflectance Experiment Laboratory (RELAB) using its bidirectional (BDR) and Thermo Nexus 870 Fourier Transform Infrared (FTIR) spectrometers, respectively. VNIR reflectance measurements were made across the 0.3 – 2.6 μm wavelength range at a 5 nm sampling interval and were calibrated using a SRS-99 Spectralon standard from Labsphere. The BDR measurements were made with a geometry of incidence (i) = 30°, emission (e) = 0°, and phase (g) = 30°. MIR biconical reflectance measurements were measured across the 1.0 – 50.0 μm wavelength range with a spectral resolution of 4 cm^{-1} and were calibrated using a brushed diffuse gold standard. **Figure I1** shows the NU-LHT-5M simulant in one of RELAB's black sample cups prior to measurement.

Figure I1. NU-LHT-5M in a RELAB black sample cup.

Appendix J Section 14 Supplemental Information

Melt

Notes on characterization of NUW-LHT-5M at UTSA

Austin Patridge and Alan Whittington

Department of Earth and Planetary Sciences, The University of Texas at San Antonio, 1 UTSA Circle, San Antonio TX 78249
Alan.Whittington@utsa.edu
Austin.Patridge@utsa.edu

Heating and cooling rates were held at 30 °C/min.

1. Powder Density

Method: Specific gravity of ~50–80 g of powder was measured using an Anton Paar Ultrapyc 3000 helium pycnometer. All space between grains is filled with helium, so this measures the volume and density of only the solid grains. The number of measurements and 2-sigma uncertainties are given. Powders were dried overnight at 110 °C prior to measurement.

Samples:
HQ glass powder, as received
NUW-LHT-5M Test 1, as received
NUW-LHT-5M Test 2, as received
JSC-1A, from a bucket of powder we received from MSFC a few years ago

2. Remelted Glass Density

Method: Chips of glass typically ~0.5–3 g were weighed, first in air and then while submerged in anhydrous ethanol. Sample density was calculated using Archimedes' principle.

Samples:
HQ glass powder, remelted at 1600°C in air and quenched
NUW-LHT-5M Test 1, remelted at 1600°C in air and quenched
NUW-LHT-5M Test 2, remelted at 1600°C in air and quenched
JSC-1A, remelted at 1600˚C in air and quenched (from Morrison et al., 2019).

References:
Morrison, A.A., Zanetti, M., Hamilton, C.W., Lev, E., Neish, C.D., and Whittington, A.G., 2019. Rheological investigation of lunar highland and mare impact melt simulants. *Icarus*, 317: 307-323, https://doi.org/10.1016/j.icarus.2018.08.001

3. Loss on Ignition (LOI)

Method: A few grams of powder were weighed into a porcelain crucible and heated to 1050 °C in a muffle furnace for ~1 hour, then weighed again after cooling. Powders were dried overnight at 110 °C prior to measurement.

Notes: Mass loss occurs when volatiles are lost, e.g. from hydrous or carbonate minerals breaking down. Both test batches of NUW-LHT-5M lost about 0.5 wt.%, which is much greater than measurement uncertainty. Since the HQ glass component does not gain or lose significant mass, this change reflects volatile loss from the rock/mineral constituents.

Mass gain occurs when Fe^0 or Fe^{2+} are oxidized. The slight mass gain for HQ glass is within uncertainty of no change. If it is real, it could be oxidation of small flakes of metallic iron. The strong gain of ~0.5 wt.% for JSC is due to oxidation; it is dark green when it goes in and orange-red when it comes out.

4. Major Element Chemistry

Method: Fused disks for major element analysis were prepared from 1.8 g of sample mixed with 9 g of lithium tetraborate. Analyses were performed on a Rigaku Primus II WD-XRF, with USGS standard BIR-1 prepared and run along with every batch of samples. Each disk is analyzed three times and we report the average.

Notes: Sample analyses were consistent in every case with previously published values, including HQ glass from Rickman et al. (2022) LPSC and NUW-LHT-5M Test 2, personal communication from Doug Rickman. Our results for NUW-LHT-5M Test 1 and Test 2 are identical within analytical uncertainty.

5. Fe2+/Fe3+ measurement on "raw" simulants

Method: The oxidation state of iron in 10–20 mg of each simulant powder was determined using colorimetry, based on the method of Wilson (1960) as modified by Schuessler et al. (2008) and summarized in Sehlke et al. (2014). Fe^{2+} in the dissolved sample formed a red complex with 2:2 bypyridine solution, which was measured using with Ultraviolet/Visible (UV/Vis) spectrometry at 523nm and 700nm wavelengths. Hydroxylamine hydrochloride was added to reduce all Fe^{3+} to Fe^{2+}, and the sample was measured again to determine the total iron content. From these two measurements, the individual FeO and Fe_2O_3 contents of the starting material were calculated. USGS Standard BIR-1a was run as an unknown along with the simulants.

Samples: HQ glass powder, NUW-LHT-5M test 1 and test 2, JSC-1A, all as received.

Notes: All three of HQ glass powder, NUW-LHT-5M test 1, and test 2 contain only Fe2+. Total iron content by wet chemistry and colorimetry are similar to those obtained by XRF. JSC-1A contains about 75% Fe2+ on an atomic basis. Results for BIR-1a have slightly higher total Fe and slightly more reduced iron than the certified values from USGS.

References:

Rickman, D. L., H. Shulman, M. Creedon, and M. R. Effinger. “Design of NU-LHT-5M and -6M, Lunar Highland Simulants.” In *53rd Lunar and Planetary Science Conference*, Abstract #1146. Houston: Lunar and Planetary Institute, 2022. https://www.hou.usra.edu/meetings/lpsc2022/pdf/1146.pdf.

Schuessler JA, Botcharnikov RE, Behrens H, Misiti V, Freda C (2008) Amorphous materials: properties, structure, and durability: oxidation state of iron in hydrous phono-tephritic melts. American Mineralogist 93(10):1493–1504

Sehlke A, Whittington AG, Robert B, Harris AJL, Gurioli L, Médard E (2014) Pahoehoe to `a`a transition of Hawaiian lavas: an experimental study. Bulletin of Volcanology, 76: 876, doi: 10.1007/s00445-014-0876-9

Wilson AD (1960) The micro-determination of ferrous iron in silicate minerals by a volumetric and a colorimetric method. Analyst 85(1016):823–827

6. Calorimetry

Method: About 20 mg of each sample was placed in a PtRh pan and heated at 30 K/min in a Netzsch® 404F1 Pegasus differential scanning calorimeter (DSC) under Ar atmosphere. Heat flow was converted to a quantitative measurement of isobaric heat capacity (C_P) by running a series of three experiments under identical temperature-time programs. The first experiment involved a blank (empty pan), the second a sapphire standard (Ditmars et al., 1982), and the third the material to be analyzed. Apparent heat capacity was measured using Netzsch® Proteus® software. Apparent heat capacity includes contributions from both sensible heat (heat capacity) and latent heat (enthalpies of transformation, e.g., crystallization and melting).

References:

Ditmars, D.A., Ishihara, S., Chang, S.S., Bernstein, G., and West, E.D., 1982, Enthalpy and heat capacity standard reference material: Synthetic sapphire (α-Al2O3) from 10 to 2250 K: Journal of Research of the National Bureau of Standards, v. 87, https://doi.org/10.6028/jres.087.012.

7. Viscosity

Method: Powdered sample was remelted a few grams at a time in a cylindrical $Pt_{90}Rh_{10}$ crucible, in an Orton RSV-1700 rotating spindle viscometer, in air. On achieving the desired temperature, a cylindrical $Pt_{90}Rh_{10}$ spindle with a hemispherical base was lowered 20 mm into the melt and rotated at speeds up to 80 rpm using a Brookfield LVDT2 viscometer head, which also measured the torque required. When possible, lower speeds were also used to verify Newtonian behavior (i.e., constant viscosity) across multiple strain rates. Temperatures were usually lowered in 50 °C intervals, with some temperatures repeated out of sequence to check for instrumental drift or sample crystallization below the liquidus. The apparatus was calibrated using NIST reference material NBS-710A soda lime silicate glass.

8. Thermal diffusivity of glass

Method: Remelted HQ glass was cored and then sliced into three disks 12.5 mm in diameter and 1–2.5 mm thickness, with parallel faces. The disks were spray-coated with graphite and their thermal diffusivity was measured in a Netzsch 467HT light-flash apparatus (LFA). The sample was held in a furnace in an Ar atmosphere, and heated from below by a light flash from a xenon lamp. As heat diffused from the bottom to the top of the sample, upward emissions were recorded as a function of time with a nitrogen-cooled InSb detector. The graphite coating blocked most light from traversing the sample directly, and enhanced absorption of the light flash. Data were obtained at 25 °C, 100 °C, and then at 100 °CC intervals up to 600 °C , then again at 300 °C and finally at 25 °C . Data consist of ~three acquisitions at each temperature, processed using the Netzsch software, which incorporates the algorithm of Mehling et al. (1998) to extract thermal diffusivity from the time-dependent emission data. Nine data for the Pyroceram reference material collected between 25 °C and 600 °C yielded results that are on average 0.05 mm^2s^{-1} lower than the certified values, although this is within the 2s uncertainty envelope for the certified equation (Salmon et al. 2010). After heating to 600 °C repeat measurements at 300 °C and 25 °C always agreed with the initial measurement to within 0.002 mm^2s^{-1}, well within the measurement precision, which is about 0.01 mm^2s^{-1}.

References:

Mehling H, Hautzinger G, Nilsson O, Fricke J, Hofmann R, and Hahn O (1998) Thermal diffusivity of semitransparent materials determined by the laser-flash method applying a new mathematical model. *International Journal of Thermophysics* 19: 941–949, DOI 10.1023/A:1022611527321

Salmon DR, Brandt R, Tye RP (2010) Pyroceram 9606, A Certified Ceramic Reference Material For High-Temperature Thermal Transport Properties: Part 2—Certification Measurements. *International Journal of Thermophysics* 31:355–373 DOI 10.1007/s10765-010-0710-3

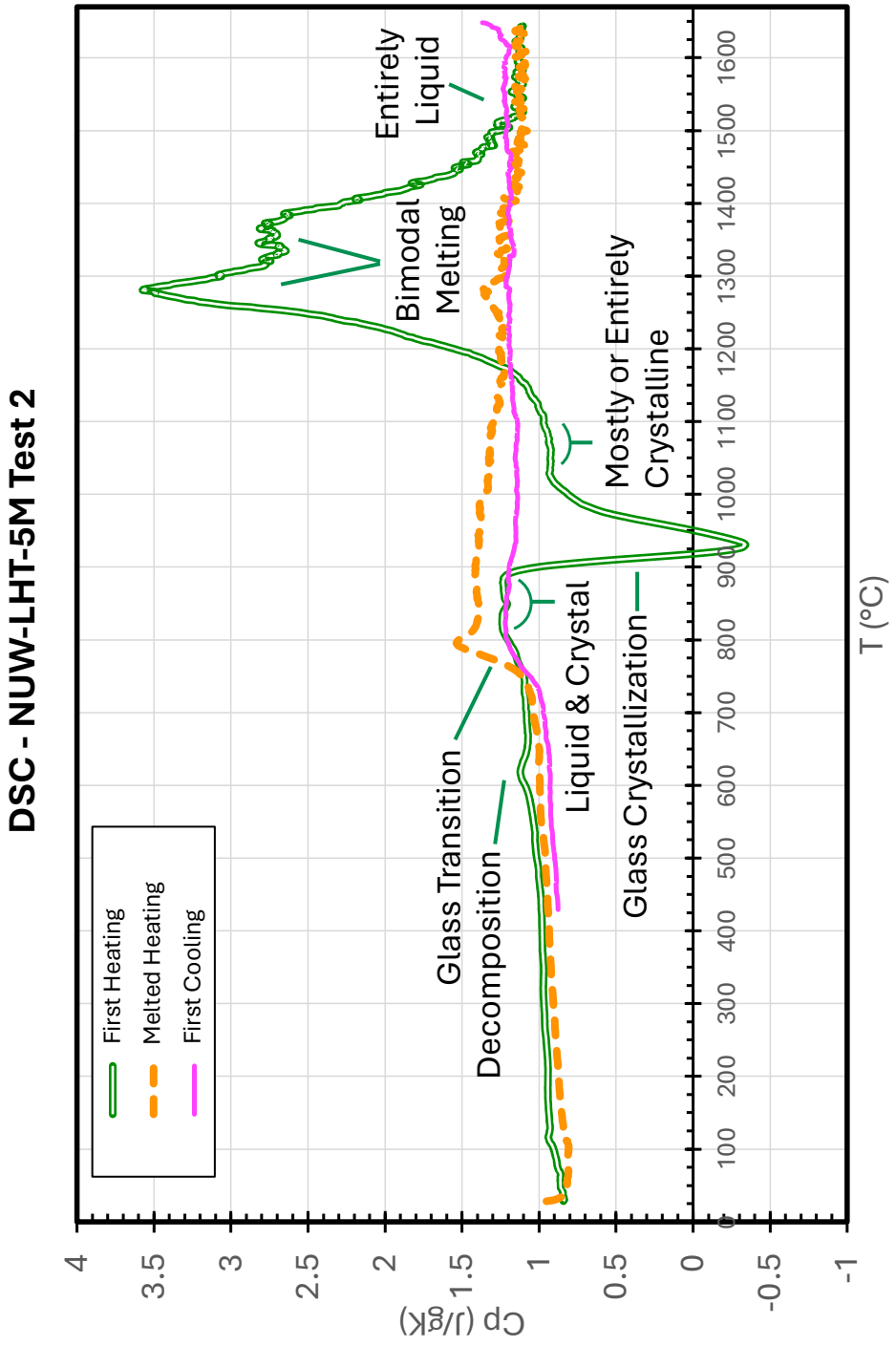

Figure J1. Differential Scanning Calorimetry of NUW-LHT-5M Test 2. The simulant as provided went through "First Heating" followed by "First Cooling". Heating was sufficient to assure total melting of all phases and the chill rate was fast enough to produce a pure glass. That glass was then heated to the final temperature used in the first heating. Endothermic processes are scaled with positive values and exothermic processes are scaled with negative values.

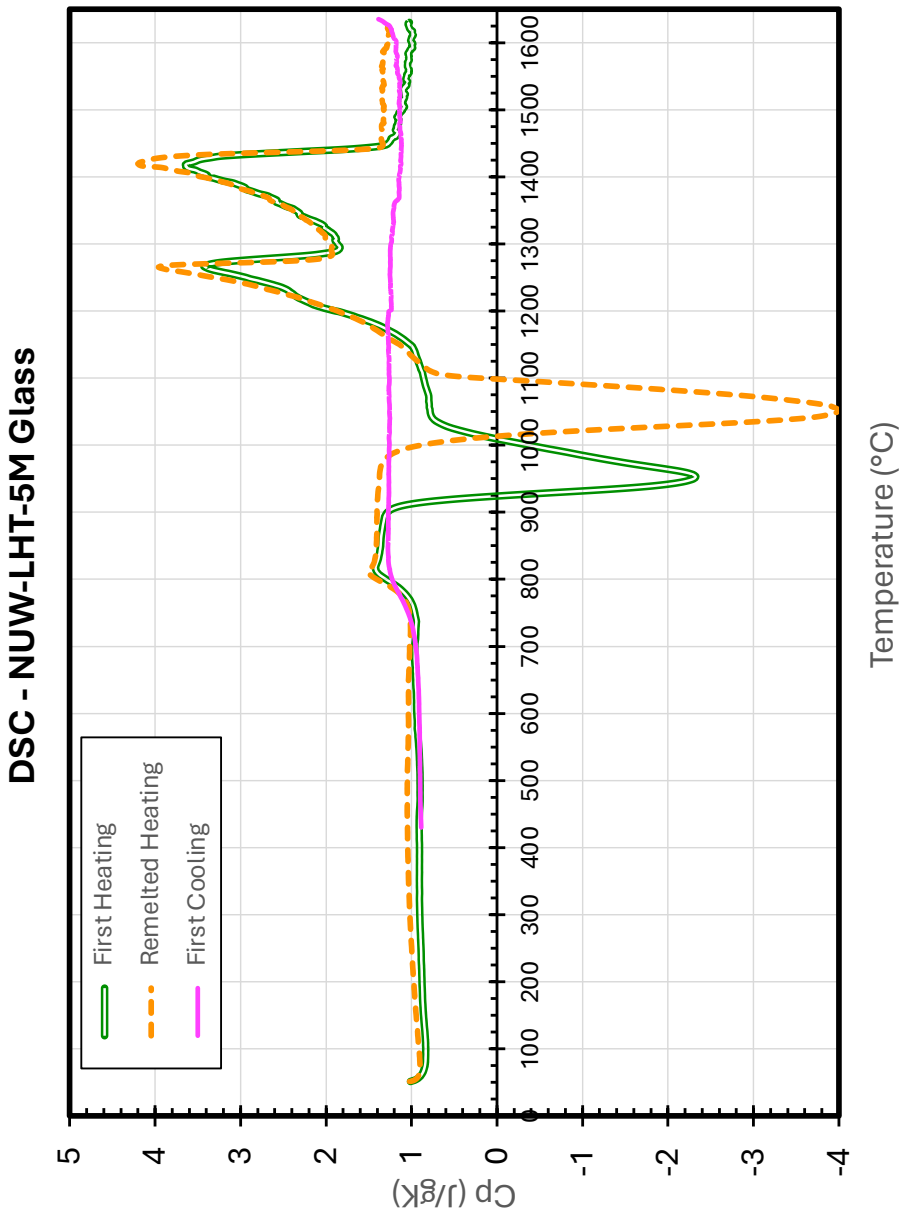

Figure J2. The synthetic glass used in NUW-LHT-5M went through "First Heating" followed by "First Cooling". Heating was sufficient to assure total melting of all phases and the chill rate was fast enough to produce a pure glass. That glass was then heated to the final temperature used in the first heating. Endothermic processes are scaled with positive values and exothermic processes are scaled with negative values. Note the displacement in the original glass's exothermic reaction in the remelted material. This displacement suggests there is at least one phase in the original glass that is acting as nucleation points. These points were eliminated in the first heating.

Appendix K Section 15 Supplemental Information

DSC AND EGA

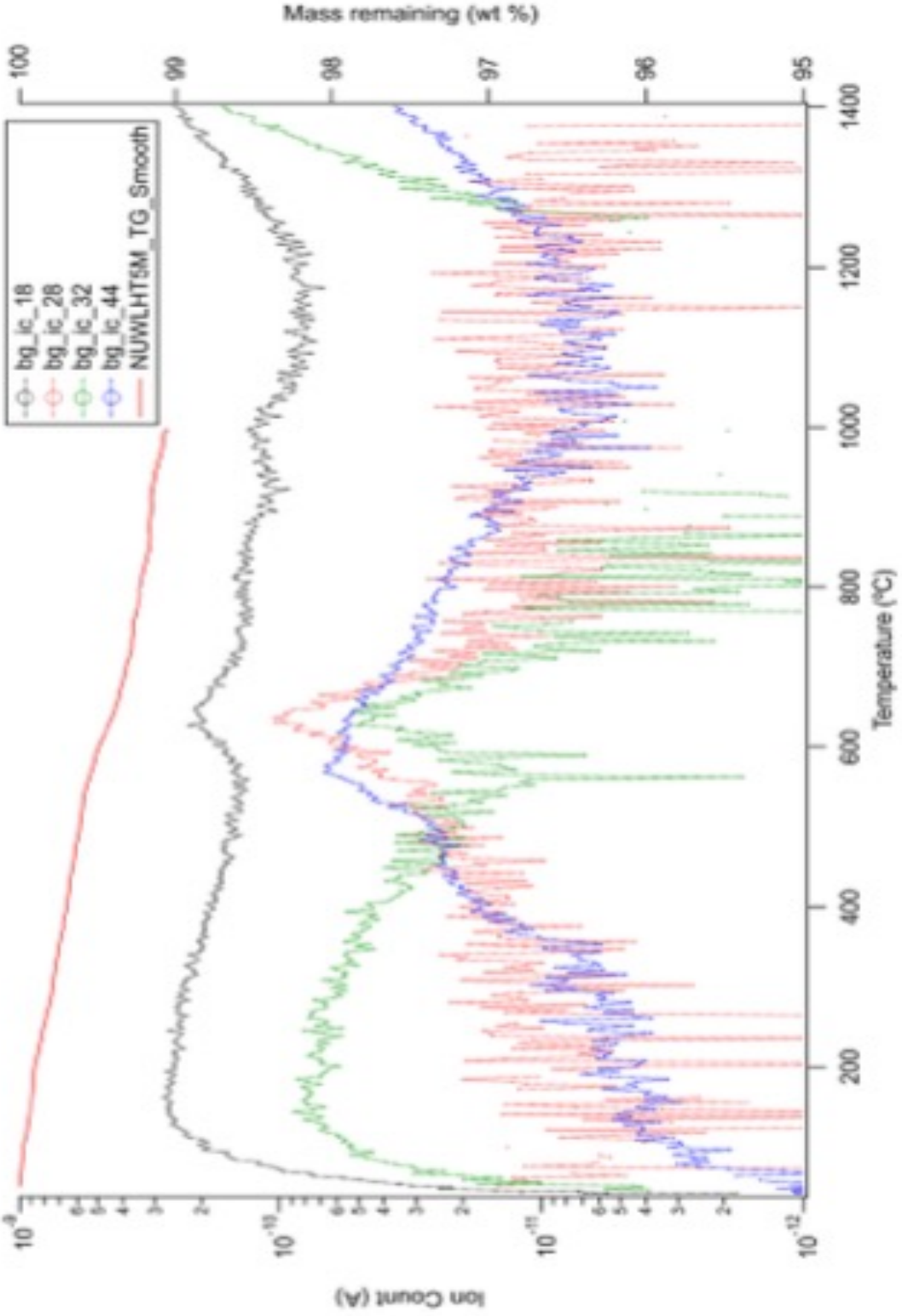

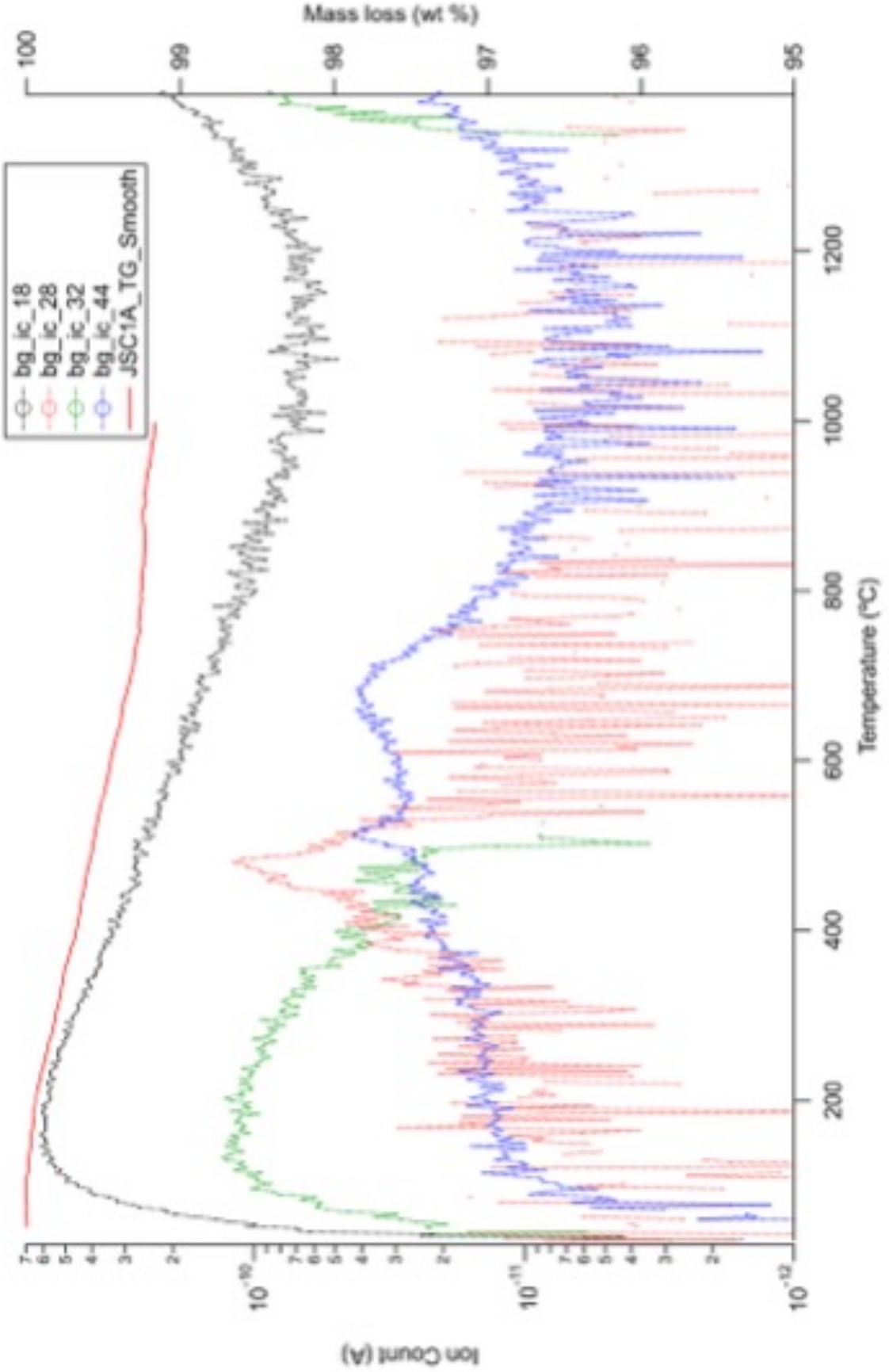
Mass loss (wt %)
100
99
98
97
96
95
bg_ic_18
bg_ic_28
bg_ic_32
bg_ic_44
JSC1A_TG_Smooth
200
400
600
800
1000
1200
Temperature (°C)
Ion Count (A)

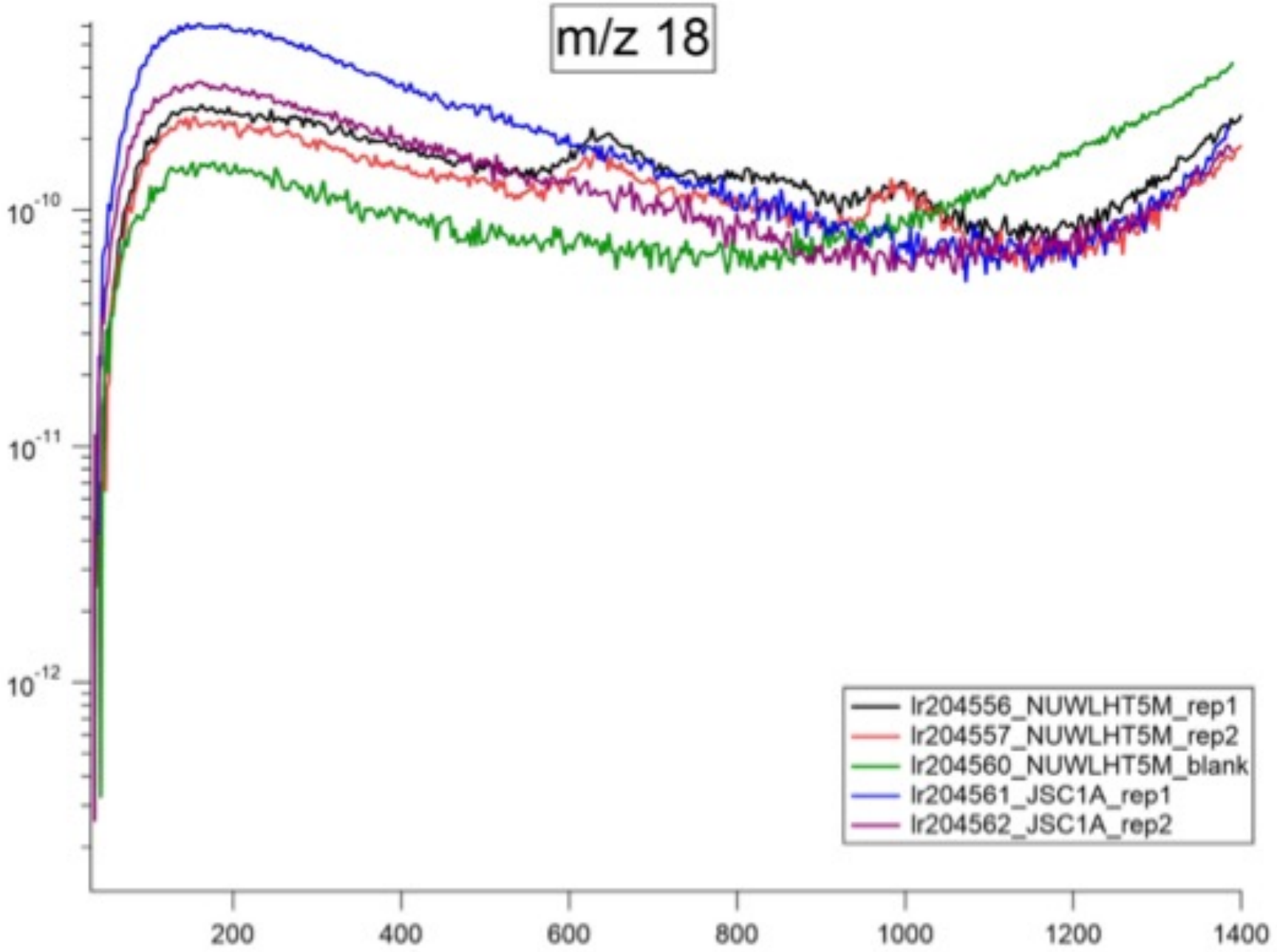
m/z 18
10-10
10-11
10-12
200
400
600
800
1000
1200
1400
Ir204556_NUWLHT5M_rep1
Ir204557_NUWLHT5M_rep2
Ir204560_NUWLHT5M_blank
Ir204561_JSC1A_rep1
Ir204562_JSC1A_rep2

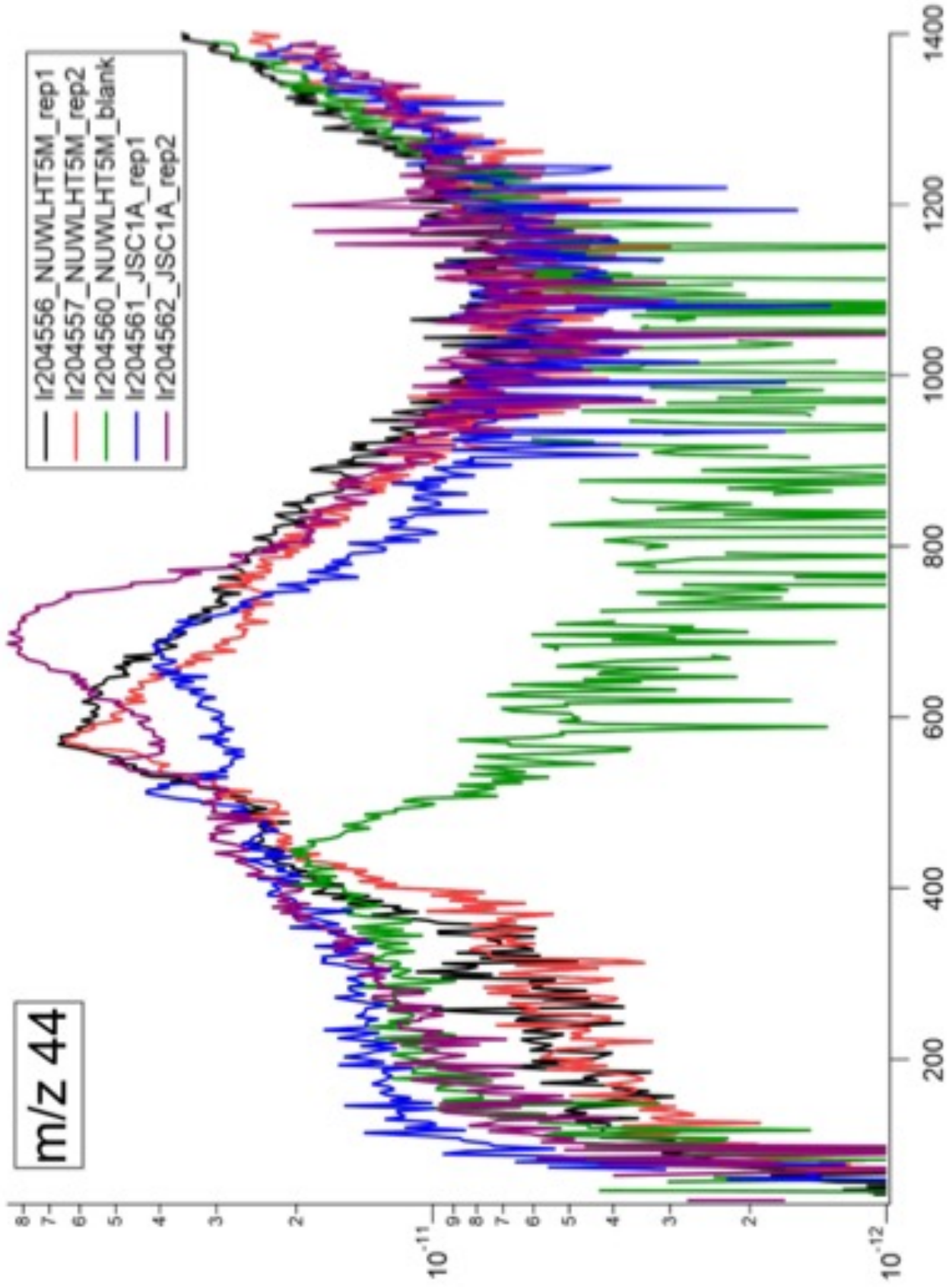
m/z 44
lr204556_NUWLHT5M_rep1
lr204557_NUWLHT5M_rep2
lr204560_NUWLHT5M_blank
lr204561_JSC1A_rep1
lr204562_JSC1A_rep2
200
400
600
800
1000
1200
1400
10^-11
10^-12

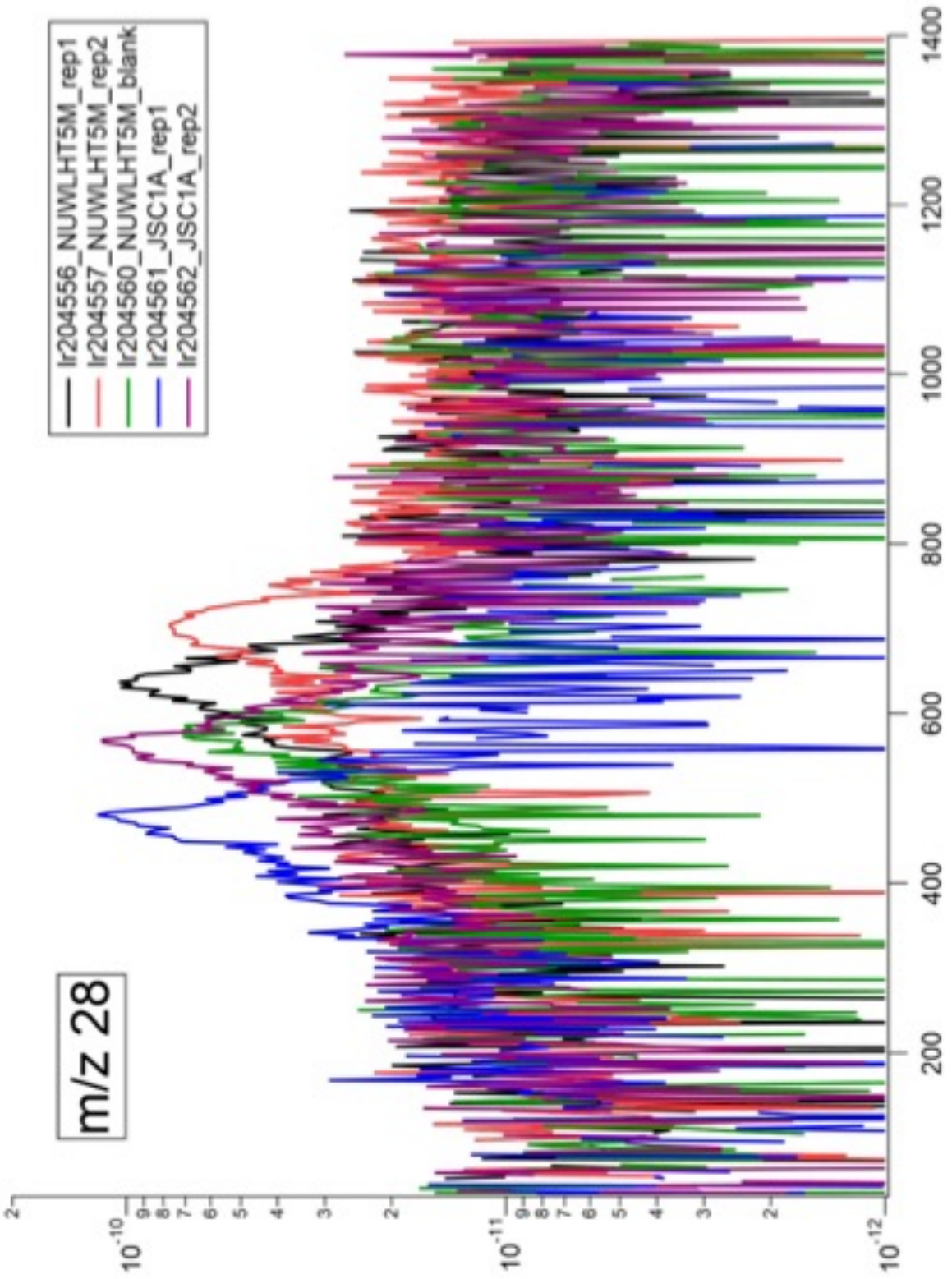
m/z 28
lr204556_NUWLHT5M_rep1
lr204557_NUWLHT5M_rep2
lr204560_NUWLHT5M_blank
lr204561_JSC1A_rep1
lr204562_JSC1A_rep2
200
400
600
800
1000
1200
1400

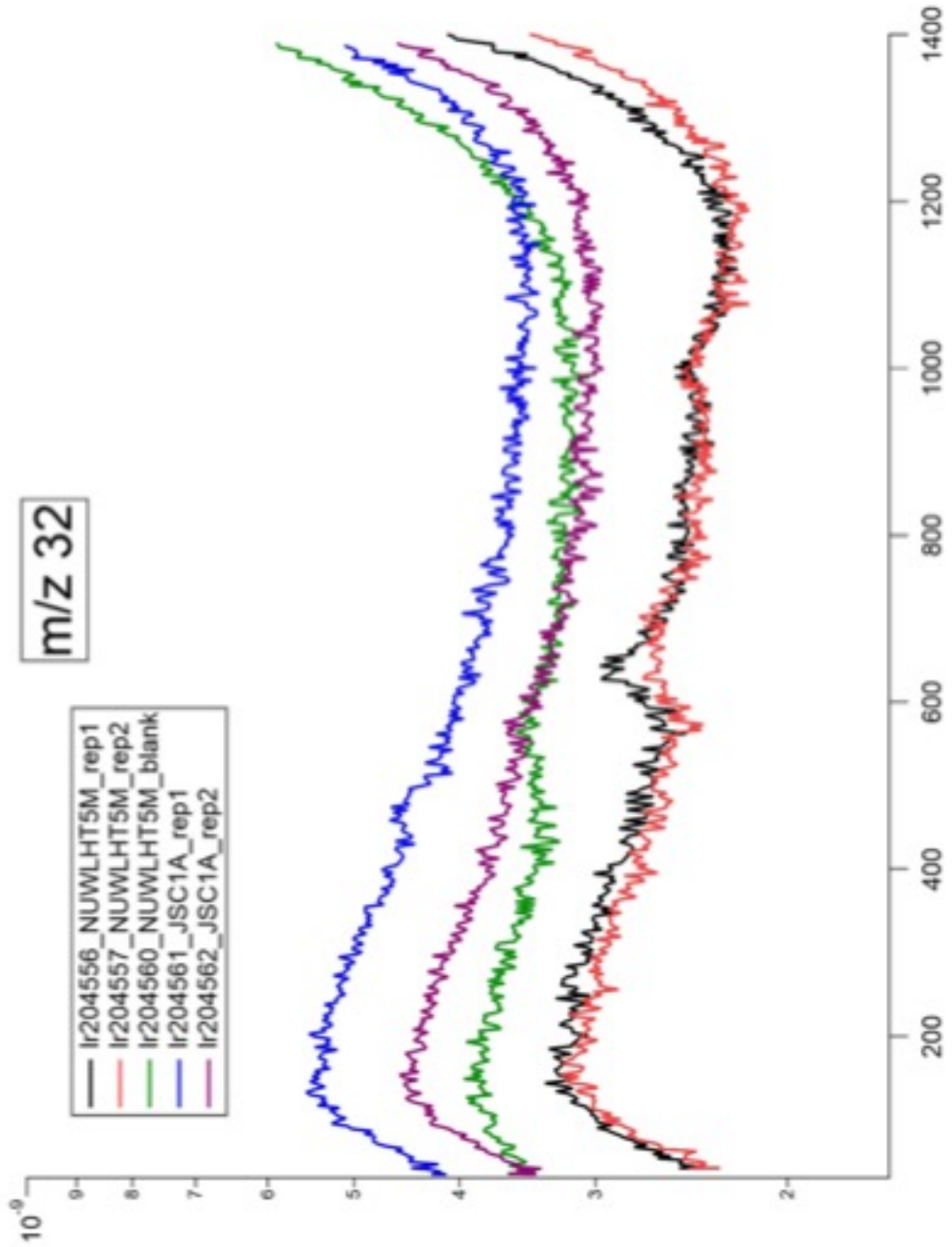
m/z 32
Ir204556_NUWLHT5M_rep1
Ir204557_NUWLHT5M_rep2
Ir204560_NUWLHT5M_blank
Ir204561_JSC1A_rep1
Ir204562_JSC1A_rep2
10^-9
9
8
7
6
5
4
3
2
200
400
600
800
1000
1200
1400

Appendix L Section 16 Supplemental Information

Spark Sintering

Spark Plasma Sintering (SPS) of Lunar Simulants: NUW-LHT-5M and JSC-1A

In Kyu Jeon[a], Yong-Rak Kim[a]

[a]Zachry Department of Civil and Environmental Engineering, Texas A&M University, College Station, TX, 77843, USA

The spark plasma sintering (SPS) method has been used to densify ceramic and metallic materials [1-3]. Unlike conventional sintering processes, SPS employs a pulse electric current, an applied uniaxial pressure, and a rapid heating rate in a vacuum atmosphere to sinter ceramic or metal powders [4]. It could provide many advantages due to the combined effect of electric field and applied pressure, such as high heating and cooling rates (as high as 1000 ºC /min) [5], short processing times (i.e., minutes) [6, 7], low sintering temperatures [8], and a high density of sintered products (nearly 100% theoretical density) [9, 10].

Figure K1 illustrates the schematic view of the SPS process. SPS has a good potential to apply to extraterrestrial conditions because it works well in a vacuum atmosphere to densify loose powders in a short time. As it is operated in a vacuum condition, it can also minimize oxidation issues. SPS for the lunar and martian regolith has been recently attempted. Several studies found the compelling physical, mechanical, and microstructure properties of sintered specimens [11-16].

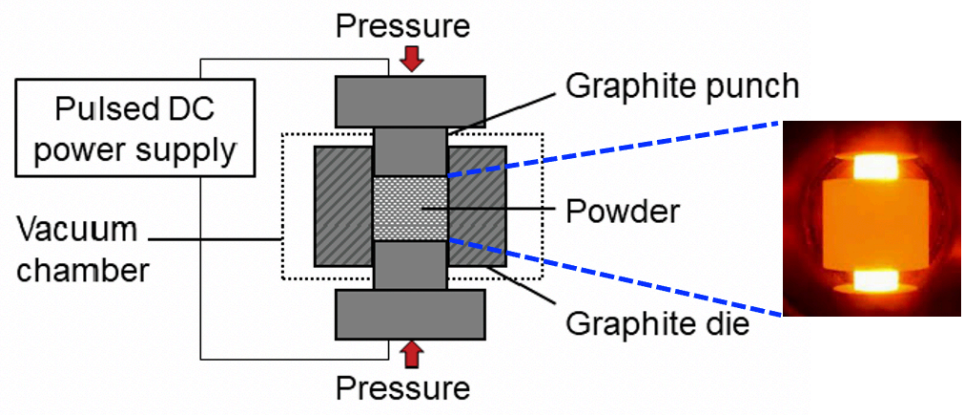

Figure L1. Schematic view of the SPS machine obtained from the previous study [11].

In the SPS procedure, pulsed direct current can be passed through the conductive die and sample, producing an electric field during the sintering process, resulting in possible heat from both outside and inside [17]. Therefore, high relative density can be obtained within a short time, which

prevents coarsening and grain growth effects during the sintering process. The SPS mechanism can be explained via micro-spark/plasma theory, and it is divided into three steps: 1) Plasma heating, 2) Joule heating, and 3) Plastic deformation [18]. When discharge occurs in the gaps between powder particles, high-temperature sparks are generated and the surface of the powder particles melts around the contact area between the particles to form necks. As a result, it allows for the flowing of electrical current through the necks, and the increment of neck growth by atomic diffusion in the necks generates Joule heating [19]. Under the uniaxial force, plastic deformation progresses during sintering, resulting in a sintered compact over 99% density, and particle growth can be controlled due to rapid self-heating of the surface temperature of particles [17].

This study used two different lunar simulants (JSC-1A as a Mare simulant and NUW-LHT-5M as a Highland simulant) for the SPS method. The SPS system (Model SPS 25-10, Thermal Technologies, Santa Rosa, USA) at Texas A&M University was used for this study. Table K1 summarizes the parameters used for operating the SPS. To avoid the adhesion and reaction between the simulant powder and graphite mold, thin (0.2 mm thickness) graphite paper was used.

Table K1. SPS parameters used in this study.

	NUW-LHT-5M	JSC-1A
Sintering Temperature	800 °C and 1000 °C	800 °C
External pressure	100 MPa	
Dwell time	20 min	
Heating Rate	200 °C/min	
Air pressure	Vacuum (2×10^{-2} torr)	

Figure L2 shows the SPSed specimens from each simulant and their resulting microstructure image using an optical microscope. Specimen names were denoted based on each simulant's first letter and sintering temperature. For example, N800 represents the specimen made by NUW-LHT-5M with a sintering temperature of 800 °C. Results indicate that NUW-LHT-5M sintered at 1000 °C and JSC-1A sintered at 800 °C show clean surface, and densification was successful, while the NUW-LHT-5M at 800 °C presents thin plate-shaped horizontal cracks normal to the direction of uniaxial pressure. Regarding NUW-LHT-5M cases, as the sintering temperature increased from 800 °C to 1000 °C, microscopic images indicate a more homogeneous matrix which might be related to phase changes. In addition, JSC-1A and NUW-LHT-5M specimens show different

microstructures related to the different mineralogical compositions. However, further analysis is needed to confirm the different sintering mechanisms between NUW-LHT-5M and JSC-1A. The SPS successfully sintered both simulants, and the resulting sintered specimens are sintering condition dependent.

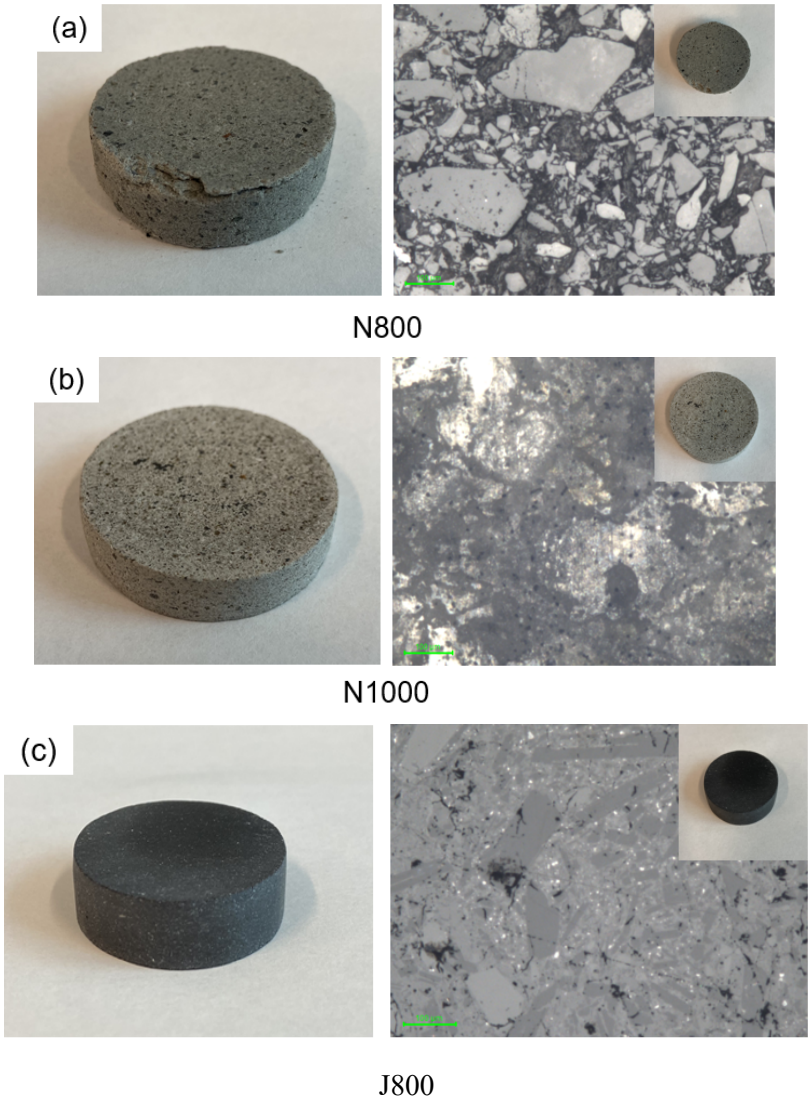

Figure L2. SPSed specimens and resulting optical microscope images.

Reference

1. Hayun, S., et al., *Microstructure and mechanical properties of silicon carbide processed by Spark Plasma Sintering (SPS).* Ceramics International, 2012. **38**(8): p. 6335-6340.
2. Yan, X., et al., *Fabrication of ODS austenitic steels and CoCrFeNi high-entropy alloys by spark plasma sintering for nuclear energy applications.* JOM, 2019. **71**: p. 2856-2867.
3. Long, Y., et al., *A fine-grained NbMoTaWVCr refractory high-entropy alloy with ultra-high strength: Microstructural evolution and mechanical properties.* Journal of Alloys and Compounds, 2019. **780**: p. 607-617.

4. Cui, B., *Microstructural evolution and oxidation behaviour of spark plasma sintered $M_{n+1}AX_n$ ceramics*. 2011, Imperial College London.
5. Guillon, O., et al., *Field-Assisted Sintering Technology/Spark Plasma Sintering: Mechanisms, Materials, and Technology Developments.* Advanced Engineering Materials, 2014. **16**(7): p. 830-849.
6. Munir, Z.A., U. Anselmi-Tamburini, and M. Ohyanagi, *The effect of electric field and pressure on the synthesis and consolidation of materials: A review of the spark plasma sintering method.* Journal of Materials Science, 2006. **41**(3): p. 763-777.
7. Santanach, J.G., et al., *Spark plasma sintering of alumina: Study of parameters, formal sintering analysis and hypotheses on the mechanism(s) involved in densification and grain growth.* Acta Materialia, 2011. **59**(4): p. 1400-1408.
8. Zhang, X., et al., *Mechanical properties and ablation behavior of ZrB_2–SiC ceramics fabricated by spark plasma sintering.* International Journal of Refractory Metals and Hard Materials, 2015. **48**: p. 120-125.
9. Yan, X., et al., *$(Hf_{0.2}Zr_{0.2}Ta_{0.2}Nb_{0.2}Ti_{0.2})$ C high-entropy ceramics with low thermal conductivity.* Journal of the American Ceramic Society, 2018. **101**(10): p. 4486-4491.
10. Cui, B., et al., *Microstructural evolution during high-temperature oxidation of spark plasma sintered Ti_2AlN ceramics.* Acta Materialia, 2012. **60**(3): p. 1079-1092.
11. Khedmati, M., et al., *Spark Plasma Sintering (SPS) for ISRU-Oriented Lunar Soil Simulant Densification: Microstructural Evolution and Mechanical Characteristics*, in *Earth and Space 2021*. 2021. p. 1409-1418.
12. Laot, M., et al., *Additive Manufacturing and Spark Plasma Sintering of Lunar Regolith for Functionally Graded Materials.* Spool. Journal of Architecture and the Built Environment, 2021. **8**(2# 4): p. 7-29.
13. Licheri, R., et al., *Spark plasma sintering and optical characterization of lunar regolith simulant.* Acta Astronautica, 2022. **201**: p. 164-171.
14. Zhang, X., et al., *Spark plasma sintering of a lunar regolith simulant: effects of parameters on microstructure evolution, phase transformation, and mechanical properties.* Ceramics International, 2021. **47**(4): p. 5209-5220.
15. Zhang, X., et al., *Microstructure evolution during spark plasma sintering of FJS-1 lunar soil simulant.* Journal of the American Ceramic Society, 2020. **103**(2): p. 899-911.
16. Phuah, X.L., et al., *Ceramic material processing towards future space habitat: Electric current-assisted sintering of lunar regolith simulant.* Materials, 2020. **13**(18): p. 4128.
17. Cavaliere, P., *Spark plasma sintering of materials: advances in processing and applications*. 2019: Springer.
18. Tamari, N., et al., *Effect of spark plasma sintering on densification and mechanical properties of silicon carbide.* Journal of the ceramic society of Japan, 1995. **103**(1199): p. 740-742.
19. German, R.M., *Sintering theory and practice*. 1996.